Physik-Department

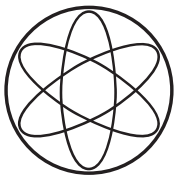

# Four Generations versus Left-Right Symmetry: A Comparative Numerical Analysis

Dissertation
von

**Tillmann J. Heidsieck**

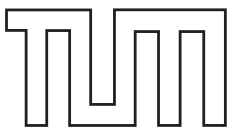

Technische Universität
München

TECHNISCHE UNIVERSITÄT MÜNCHEN

**T31 Lehrstuhl für theoretische Elementarteilchenphysik**
Physik Department

# Four Generations versus Left-Right Symmetry: A Comparative Numerical Analysis

**Tillmann J. Heidsieck**

Vollständiger Abdruck der von der Fakultät für Physik der Technischen Universität München zur Erlangung des akademischen Grades eines

**Doktors der Naturwissenschaften (Dr. rer. nat.)**

genehmigten Dissertation.

| | | |
|---|---|---|
| Vorsitzender: | | Univ.-Prof. Dr. Lothar Oberauer |
| Prüfer der Dissertation: | 1. | Univ.-Prof. Dr. Andrzej J. Buras |
| | 2. | Hon.-Prof. Dr. Wolfgang F. L. Hollik |

Die Dissertation wurde am 05.06.2012 bei der Technischen Universität München eingereicht und durch die Fakultät für Physik am 18.06.2012 angenommen.

## Abstract

In this work, we present a comparative numerical analysis of the Standard Model (SM) with a sequential fourth generation (SM4) and the left-right symmetric Standard model (LRM). We focus on the constraints induced by flavour violating $\Delta F = 2$ processes in the $K$ and $B$ system while the results of studies of collider bounds and electroweak precision tests are taken into account as external inputs. In contrast to many previous studies of both models considered in this work, we do make not any ad-hoc assumptions on the structure of the relevant mixing matrices. Therefore, we employ powerful Monte Carlo methods in order to approximate the viable parameter space of the models. In preparation of our numerical analysis, we present all relevant formulae and review the different numerical methods used in this work. In order to better understand the patterns of new effects in $\Delta F = 2$ processes, we perform a fit including all relevant $\Delta F = 2$ constraints in the context of the Standard Model. The result of this fit is then used in a general discussion on new effects in $\Delta F = 2$ processes in the context of generic extensions of the Standard Model. Our numerical analysis of the SM4 and the LRM demonstrates that in both models the existing anomalies in $\Delta F = 2$ processes can easily be resolved. We transparently show how the different observables are connected to each other by their dependence on combinations of mixing parameters. In our analysis of rare decays in the SM4, we establish patterns of flavour violation that could in principle be used to disprove this model on the basis of $\Delta F = 1$ processes alone. In the LRM, we discuss the importance of the contributions originating from the exchange of heavy, flavour changing, neutral Higgs bosons as well as the inability of the LRM to entirely solve the $V_{ub}$ problem.



## Zusammenfassung

In der vorliegenden Arbeit präsentieren wir eine vergleichende numerische Analyse zweier Modelle für Physik jenseits des Standard Modells (SM). Unsere Analyse des Standard Modells mit einer vierten Generation (SM4) und des links-rechts symmetrischen Standard Modells (LRM) konzentriert sich auf die Rolle Flavour verändernder Prozesse in Kaon und B-Mesonen Systemen. Hierbei gilt unsere Aufmerksamkeit besonders all jenen Observablen, für die vertrauenswürdige, experimentelle Daten vorliegen und bei denen die theoretische Vorhersagen möglichst zuverlässig sind. In Vorbereitung auf unsere numerische Analyse präsentieren wir ein Kompendium mit allen relevanten Formel sowie eine kurze Zusammenfassung der wichtigsten numerischen Methoden, die in dieser Arbeit Verwendung finden. Die Ergebnisse unserer Analyse stellen wir exemplarisch anhand verschiedener Korrelationen zwischen Observablen dar. Hierbei legen wir ein besonderes Augenmerk auf die transparente Darstellung von Zusammenhängen sowohl zwischen den jeweiligen Observablen als auch zwischen den verschiedenen Korrelationen. In unserer Analyse seltener Zerfälle von Kaonen und B-Mesonen im Rahmen des SM4 zeigen wir neben interessanten Korrelationen auch den globalen Zusammenhang zwischen den verschiedenen Zerfällen. Von besonderem Interesse sind in diesem Zusammenhang die seltenen Zerfälle von Kaonen, welche, wie sich herausstellt, von einer spezifischen Parameterkombination dominiert sind. Im Rahmen LRM spezifischer Themen zeigen wir die führende Rolle von Beiträgen, die durch den Austausch schwerer, Flavour verletzender, neutraler Higgs Bosonen vermittelt werden. Darüberhinaus diskutieren wir das bekannte $V_{ub}$ Problem und zeigen, dass wegen der unteren Grenze an die Masse von schweren $W'$ Bosonen das $V_{ub}$ Problem im Rahmen des LRM nicht mehr gelöst werden kann.

# Contents

# 1

# Introduction

After one year of data-taking at the LHC, the Standard Model (SM) of particle physics is in better shape than ever. First hints for a SM like Higgs particle at around 125 GeV have been found by Atlas [1], CMS [2] and the Tevatron experiments [3]. On the other hand, direct searches for heavy new particles have yet to reveal physics beyond the SM. The resulting lower limits on the masses of additional gauge bosons [4–8], quarks [9–12], scalars [13–15], exotics [16–18] or supersymmetric partners of SM particles [19–22] put stringent bounds on many extensions of the SM. Over the last years, certain anomalies in the flavour sector [23–34] gave rise to speculations on the 'demise of the CKM paradigm'. These anomalies triggered extensive research in the search for models that could explain them (for example see [35] and references therein). However, due to updated results from the B-factories [36, 37] and new LHCb data on the mixing induced CP asymmetry $S_{\psi\phi}$ [38] most of the flavour anomalies have vanished in the recent past. A small tension between $\varepsilon_K$ and $\sin 2\beta$ was left, which however has been defused by a recent calculation of next-to-next to leading order (NNLO) corrections [39] to the charm contribution to $\varepsilon_K$ where it was found that $\varepsilon_K$ suffers from uncertainties by far larger than previously assumed.

There are, however, some (long-standing) open questions surrounding the experimental status of the SM.

- The measurement of the anomalous magnetic moment of the muon [40] shows a 3.2 sigma deviation from the best SM prediction [41]. On the other hand, the calculation of this observable [41] requires a good understanding of hadronic effects [42] which diminishes the severity of this deviation. Moreover, the measurement [43–45] has not been confirmed by another experiment, yet.

- The measurement of $A_{\rm FB}(b)$ [46, 47] at LEP deviates by 2.3 sigma from the SM. The deviation of $A_{\rm FB}(b)$ from the SM expectation as measured at LEP was not verified by a similar measurement at SLD and therefore this tension is often ignored.

- The D0 measurement of $A_{\rm SL}(b)$ [48] exhibits a $3.2\sigma$ deviation from the SM prediction [49]. However, an enhanced value of this asymmetry contradicts a small value of $S_{\psi\phi}$ as found at the LHC [38].

- The different methods [50–54] for determining $|V_{ub}|$ and $|V_{cb}|$ are only consistent at roughly $2\sigma$. Interestingly, the tension in $|V_{ub}|$ and $|V_{cb}|$ is of a different nature for the two matrix elements. While the exclusive determinations of $|V_{ub}|$ give mutually different values which are also different from the inclusive value, the exclusive determinations of $|V_{cb}|$ are in good agreement with each other but prefer a different value compared to the

inclusive determination. There is still much debate on the issue of the determination of these matrix elements from inclusive and exclusive measurements. Therefore, this tension cannot unequivocally be understood as a problem of the SM.

- The direct CP violation $A_{\mathrm{CP}}(B \to K\pi)$ in $B \to K\pi$ decays deviates by nearly 4 sigma from the SM expectation [54–56]. Though the deviation appears to be a clear sign of physics beyond the SM, the calculation of $A_{\mathrm{CP}}(B \to K\pi)$ requires advanced techniques of handling non-perturbative QCD contributions [55, 56]. Therefore, it is still not understood whether the measured value of $A_{\mathrm{CP}}(B \to K\pi)$ can be explained in the SM or not.

- The existence of dark matter (DM) is firmly established by the means of astronomical observations [57]. However, the SM does not provide a DM candidate. This can be counted as irrefutable evidence for the existence of physics beyond the SM. However, in the absence of a direct detection of DM its nature remains unclear.

There are also a number of open questions on the theoretical side. Among the most popular of those are the hierarchy problem [58], the dynamics of electroweak symmetry breaking [47] and the inclusion of gravity. Since the early days of the SM, model builders have been busy trying to find models that on the one hand provide SM like phenomenology and on the other hand explain some or all of its problems.
The most popular models are supersymmetric extensions of the SM e.g. the Minimal Supersymmetric Standard Model (MSSM) [47, 59]. These models strive to solve the hierarchy problem but generically suffer from a huge number of additional parameters connected to the breaking of supersymmetry. Most supersymmetric extensions of the SM also provide one or more DM candidate(s). Another prized feature of such models is the possibility of gauge coupling unification at some high grand unification (GUT) scale $M_{\mathrm{GUT}} \sim 10^{15-16}$ GeV.
Other extensions of the SM include additional dimensions e.g. the Randall-Sundrum model [60–63] or universal extra dimensions [64]. In such models it is often possible to include gravity and to solve or to reformulate the hierarchy problem.
Yet other models are QCD like extensions called Technicolour models [47] and describe the electroweak symmetry breaking in the SM in terms of condensation phenomena. There are also models which are not viable up to the Plank scale but only up to $\mathcal{O}(10$ TeV). One example are little Higgs models which try to explain the SM electroweak symmetry breaking by the emergence of a pseudo-Goldstone Higgs particle [65–67].
In this work, we study two very well established extension of the SM. The Standard Model with a sequential fourth generation (SM4) [68,69] and the left-right symmetric Standard Model (LRM) [70–74].
The SM4, as studied in this work, does not solve any of the theoretical questions of the SM but introduces very interesting flavour violating effects. A possible fourth generation has profound consequences:

- SU(5) unification could be possible even without supersymmetry [75]. However, such models suffer from Landau poles well below the scale of unification which is an undesirable feature if one wants to stay in a well defined perturbative theory.

- Electroweak baryogenesis might be viable in the presence of a sequential fourth generation [76–78].

- The $\varepsilon_K$ – $\sin 2\beta$ anomaly can easily be resolved in the SM4 [79–82]. However, in the light of the recent NNLO calculation of corrections to the charm contribution in $\varepsilon_K$ [39] this anomaly is softened by large theoretical errors.
- A fourth generation of leptons introduces very interesting effects in flavour violating and flavour conserving processes. However, the anomalous magnetic moment of the muon cannot be explained in the SM4 as explicitly shown in [83].
- The lepton sector of the SM4 is very interesting from the theoretical point of view as the fourth generation neutrino has to be very heavy. On the other hand, the mixing between the fourth and the first three generations of leptons has to be tiny [83, 84] which suggests some sort of protection mechanism or symmetry.
- As the SM4 is a theory with purely left-handed (LH) charged currents and a very simple structure it can provide insights into more complex LH models.
- Going beyond perturbative Yukawa couplings, there are models where a fourth generation might trigger electroweak symmetry breaking [85–93]. Such models, however, defy by their very nature direct calculations of phenomenological quantities.

The SM4 has been studied extensively in the last years in the context of electroweak precision constraints [94–99] and flavour changing processes [79–83, 100–107]. Most recent studies focus on the interplay of collider bounds and electroweak precision constraints [99, 108–112]. In this work, we perform a numerical analysis of selected flavour changing processes in the SM4 using the results of electroweak precision analyses [96, 99] and direct searches [9–12] as external inputs. We focus in particular on the following points:

- We perform a full numerical analysis of the most important $\Delta S = 2$, $\Delta B = 2$, $\Delta S = 1$ and $\Delta B = 1$ processes. This includes $\varepsilon_K$, $S_{\psi K_S}$, $S_{\psi\phi}$, $\Delta M_{s,d}$, $B \to X_q\gamma$ as well as the rare decays $K_L \to \mu^+\mu^-$, $B_q \to \mu^+\mu^-$ and $K \to \pi\nu\bar{\nu}$.
- In our analysis we investigate the impact of different constraints on this model and highlight the most important constraints.
- We establish correlations between various observables. We transparently show how different correlations are connected through different combinations of CKM matrix elements.

The other model we are interested in is the LRM. In contrast to the SM4, this model is based on a simple extension of the gauge sector and does not introduce new fermions. Its main features are:

- The very symmetric gauge group $\mathrm{SU(2)_R \times SU(2)_L \times U(1)_X}$ allows for parity $P$ or charge-conjugation $C$ to be a symmetry of the model in some regions of the parameter space [74, 113–124].
- In [125–128], it was pointed out that right-handed (RH) currents could explain the discrepancy in the different determinations of $|V_{ub}|$.
- The symmetry group of the LRM automatically forces us to introduce right-handed neutrinos. Furthermore, choosing non-minimal representations [74, 129] for some of the Higgs fields naturally leads to a TeV See-Saw mechanism [130–133].

- The LRM might introduce a very interesting spectrum of heavy scalar and gauge particles within the reach of the LHC.

The main drawbacks of the LRM are a large number of additional parameters including mainly CP violating phases and a very complicated scalar sector. Moreover, it is known [134–136] that RH currents introduce huge corrections to $\Delta S = 2$ quantities, which puts stringent bounds on some combinations of couplings. Recent studies of many different observables can be found in [137–141]. The main highlights of our analysis of the LRM are:

- We perform a numerical analysis of all relevant constraints from $\Delta F = 2$ observables and $\mathrm{Br}(B \to X_q\gamma)$ in the context of the LRM. The electroweak precision constraints are included using the results of [140].
- Throughout this work, we do not assume any special form for the RH mixing matrix and do not impose a discrete symmetry i.e. $P$ or $C$ on the model.
- We study the impact of different constraints on the structure of the RH mixing matrix and comment on the fine-tuning problem of RH currents.

This thesis is organised as follows: In chapter 2, we introduce the SM4 and the LRM in a very compact fashion. We do not go into many details as both models are well established. In our short introduction of the models we give a brief overview of the most important features in the context of our analysis and fix the notation.

Chapters 3 and 4 are dedicated to $\Delta F = 2$ and $\Delta F = 1$ processes, respectively. The chapter on $\Delta F = 2$ processes includes a discussion of the NLO QCD corrections to the full operator basis as well as an introduction to all processes studied in this work. In order to facilitate the understanding of the new contributions, we always compare them to the SM formulae (also provided in this chapter). The section on $\Delta F = 2$ processes in the LRM is concluded by a discussion of the importance of Higgs effects and the derivation of bounds on the RH mixing matrix. Our discussion on $\Delta F = 1$ processes in chapter 4 is focused on presenting the necessary formulae needed for our numerical analysis. Our discussion is focused on the importance of different contributions and the interplay and connection between different observables.

In chapter 5, we review the numerical methods employed to study the SM and its extensions. We give a brief introduction to the statistical frameworks used in the SM fits and give an overview of the different methods used to analyse extensions of the SM numerically. In the last section of chapter 5, we present a proposal for an adaptive method for Monte Carlo scans.

Chapter 6 is dedicated to a discussion of the status quo of the SM fits and constraints on generic models of NP. Also discussed in chapter 6 are all non-flavour constraints used in our analysis e.g. tree-level determinations, electroweak precision constraints and collider bounds.

In chapter 7, we finally present the results of our numerical analysis of the SM4 and the LRM. We discuss the different measures of fine-tuning and show the impact of the combined constraints on the four-by-four mixing matrix and the RH mixing matrix in the SM4 and the LRM, respectively. We highlight the different correlations between selected $\Delta F = 1$ and $\Delta F = 2$ observables in both models and compare the results. Subsequently, we discuss LRM specific issues: The solution to the $V_{ub}$ problem and a lower bound on the mass of the flavour violating neutral Higgs. In the last section of chapter 7, we discuss our results for rare $B$ and

$K$ decays in the SM4. We show transparently how the different observables are connected and how the constraints affect the correlations.

We summarise our results in chapter 8. In the appendix, we provide some details on the structure of the LRM after symmetry breaking and give a list of all master functions needed in our numerical analysis.

# 2

# Introduction of the Models

In this chapter we introduce the Standard Model with a sequential fourth generation (SM4) and the left-right symmetric Standard Model (LRM). We keep the introductions short and do not go into too many details as both models are well established and more extensive introductions can for example be found in [68–74] and references therein.

## 2.1 The Standard Model with a Sequential Fourth Generation

This very short introduction of the SM4 serves to fix the notation and to introduce the main aspects of this model. For a more detailed discussion see [68] and references therein. Extending the three generations of quark and lepton of the SM by a fourth sequential one is arguably one of the most simple extensions of the SM. The new particles are

$$\begin{pmatrix} t'_L \\ b'_L \end{pmatrix}, b'_R, t'_R, \begin{pmatrix} (\nu_4)_L \\ E_L \end{pmatrix}, E_R, (\nu_4)_R, \tag{2.1}$$

where all the new particles are given in their $\mathrm{SU(2)_L}$ representations. If one decides to include a fourth generation of quarks then the addition of a fourth generation of leptons is necessary due to anomaly cancellation [142]. A fourth generation of leptons also introduces interesting lepton flavour violation (LFV) effects [83,84]. However, as this work focuses on the numerical analysis of the quark sector esp. the $K$ and $B_q$ system, we refrain from discussing the lepton sector of the SM4. The interested reader may find a study of LFV and non-LFV processes in [83, 84]. The simplest version of a model with a fourth generation does not introduce any changes to the scalar sector of the SM. The masses of the fourth generation quarks and leptons are generated through the vacuum-expectation-value (vev) of the SM Higgs field and are therefore bounded from above by perturbativety of the Yukawa couplings. As an alternative, models with a more complicated Higgs sector have been proposed in order to remove this upper limit on mass of the fourth generation quarks [143–145]. There are also ideas of a non-perturbative fourth generation [77, 86, 89, 90]. In those models electroweak symmetry breaking (EWSB) is supposed to be a dynamic effect triggered by the condensation of the fourth generation quarks. In such a model the lowest scalar resonance might provide a pseudo-Goldstone Higgs.

In the SM4, there are two new heavy quarks $b', t'$, one charged heavy lepton $E$ and a heavy neutrino $\nu_E$ in the particle spectrum after EWSB. As in the SM, rotating the quarks and leptons to their mass basis introduces mixing in the couplings of charged weak gauge bosons to quarks and leptons. In the SM4, the quark mixing matrix is a four-by-four unitary matrix with 6 angles and 3 phases. Adapting the standard notation, the CKM4 matrix takes the

form [146–148]

$$\begin{pmatrix} c_{12}c_{13}c_{14} & c_{13}c_{14}s_{12} & c_{14}s_{13}e^{-i\delta_{13}} & s_{14}e^{-i\delta_{14}} \\ -c_{23}c_{24}s_{12} - c_{12}c_{24}s_{13}s_{23}e^{i\delta_{13}} & c_{12}c_{23}c_{24} - c_{24}s_{12}s_{13}s_{23}e^{i\delta_{13}} & c_{13}c_{24}s_{23} & c_{14}s_{24}e^{-i\delta_{24}} \\ -c_{12}c_{13}s_{14}s_{24}e^{i(\delta_{14}-\delta_{24})} & -c_{13}s_{12}s_{14}s_{24}e^{i(\delta_{14}-\delta_{24})} & -s_{13}s_{14}s_{24}e^{-i(\delta_{13}+\delta_{24}-\delta_{14})} & \\ -c_{12}c_{23}c_{34}s_{13}e^{i\delta_{13}} + c_{34}s_{12}s_{23} & -c_{12}c_{34}s_{23} - c_{23}c_{34}s_{12}s_{13}e^{i\delta_{13}} & c_{13}c_{23}c_{34} & c_{14}c_{24}s_{34} \\ -c_{12}c_{13}c_{24}s_{14}s_{34}e^{i\delta_{14}} & -c_{12}c_{23}s_{24}s_{34}e^{i\delta_{24}} & -c_{13}s_{23}s_{24}s_{34}e^{i\delta_{24}} & \\ +c_{23}s_{12}s_{24}s_{34}e^{i\delta_{24}} & -c_{13}c_{24}s_{12}s_{14}s_{34}e^{i\delta_{14}} & -c_{24}s_{13}s_{14}s_{34}e^{i(\delta_{14}-\delta_{13})} & \\ +c_{12}s_{13}s_{23}s_{24}s_{34}e^{i(\delta_{13}+\delta_{24})} & +s_{12}s_{13}s_{23}s_{24}s_{34}e^{i(\delta_{13}+\delta_{24})} & & \\ -c_{12}c_{13}c_{24}c_{34}s_{14}e^{i\delta_{14}} & -c_{12}c_{23}c_{34}s_{24}e^{i\delta_{24}} + c_{12}s_{23}s_{34} & -c_{13}c_{23}s_{34} & c_{14}c_{24}c_{34} \\ +c_{12}c_{23}s_{13}s_{34}e^{i\delta_{13}} & -c_{13}c_{24}c_{34}s_{12}s_{14}e^{i\delta_{14}} & -c_{13}c_{34}s_{23}s_{24}e^{i\delta_{24}} & \\ +c_{23}c_{34}s_{12}s_{24}e^{i\delta_{24}} - s_{12}s_{23}s_{34} & +c_{23}s_{12}s_{13}s_{34}e^{i\delta_{13}} & -c_{24}c_{34}s_{13}s_{14}e^{i(\delta_{14}-\delta_{13})} & \\ +c_{12}c_{34}s_{13}s_{23}s_{24}e^{i(\delta_{13}+\delta_{24})} & +c_{34}s_{12}s_{13}s_{23}s_{24}e^{i(\delta_{13}+\delta_{24})} & & \end{pmatrix} . \tag{2.2}$$

In the case of no mixing between the first three and the fourth generation, the matrix in equation (2.2) reduces to a block-diagonal matrix with a three-by-three mixing matrix in the standard parametrisation [149] and a one. Though the form of the CKM matrix given in (2.2) is very complicated there are still some insight to be gained.

- All elements of the three-by-three sub-matrix directly receive corrections in the case of non-vanishing mixing with the fourth generation.
- The leading, new contribution to $\mathrm{Im}(V_{ts})$ is proportional to the leading contribution to $\mathrm{Im}(V_{t's})$.
- The leading correction to $V_{ts}$ and the leading correction to $V_{td}$ are proportional up to the ratio $s_{14}/s_{24}$.
- The correction to $V_{cb}$ can introduce an imaginary part of $\mathcal{O}(10^{-3})$, this corresponds to a possible enhancement by an order of magnitude.

In order to provide a more transparent form, we derived some approximate parametrisations of (2.2) which are provided in section 2, equations (2.29) - (2.32) of [105] and in equation (6.16) in section 6.3 of this work. The unitarity relations known from the SM are modified to

$$\lambda_u^{(M)} + \lambda_c^{(M)} + \lambda_t^{(M)} + \lambda_{t'}^{(M)} = 0\,, \tag{2.3}$$

in the SM4 with $M = K, B_d, B_s$, and $\lambda_i^{(M)}$ defined through

$$\lambda_i^{(K)} = V_{is}^{\mathrm{L}\,*} V_{id}^{\mathrm{L}}\,, \qquad\qquad \lambda_i^{(q)} = V_{ib}^{\mathrm{L}\,*} V_{iq}^{\mathrm{L}}\,, \tag{2.4}$$

where $q = d, s$. In equation (2.4), we introduced the short hand notation $\lambda_i^{(q)}$ for $\lambda_i^{(B_q)}$. The appearance of the fourth term in the unitarity relation (2.3) upgrades the unitarity triangle (see section 5.1) into an unitarity quadrangle. Furthermore, when adapting SM formulae one has to keep track of the places where three-by-three unitarity has been used and compensate by introducing additional terms. In [150], an alternative parametrisation for the CKM4 matrix was proposed. Although this alternative parametrisation makes the contributions to the observables in the $K$ and $B_q$ system more transparent in terms of model parameters e.g. $s_{14}, s_{24}$, we chose

to use the form provided in (2.2) as the parametrisation has no physical meaning. In our discussion we try to always use the physical CKM elements (or combinations thereof) and refrain from deriving bounds on the model parameters themselves. The bounds on the masses of the new particles as well as the constraints from the electroweak precision tests (EWPT) are discussed in section 6.3. Note that in the SM and SM4 we use $V$ and $V^{\mathrm{L}}$ synonymously for the CKM matrix.

## 2.2 The Left-Right Symmetric Standard Model

In this section, we give a brief description of the LRM. We restrict our discussion to the main features and provide formulae to introduce our notation. For a more detailed discussions on the LR symmetric and asymmetric models see [138, 139, 151] and references therein.

### The Gauge Group and the Fermion Content

A popular extension of the SM is the LRM. It is based on the extension of the gauge group to

$$\mathrm{SU}(3)_{\mathrm{QCD}} \times \mathrm{SU}(2)_{\mathrm{L}} \times \mathrm{SU}(2)_{\mathrm{R}} \times \mathrm{U}(1)_{\mathrm{B-L}} \,. \tag{2.5}$$

One of the reasons for the popularity of the LRM is the possible restoration of parity $P$ as a symmetry of the model. In models with spontaneous breaking of the $P$ symmetry [118–120] the restoration of $P$ takes place at scales of the order of the breaking of the gauge group. In more general models the restoration of $P$ as a symmetry might be achieved in some higher theory. In this work, we refrain from enforcing any additional discrete symmetries i.e. $P$, $C$. This has profound consequences for the model.

- The gauge couplings $g_L$ and $g_R$ for the $\mathrm{SU}(2)_{\mathrm{L}}$ and $\mathrm{SU}(2)_{\mathrm{R}}$ gauge group respectively are generally not equal.
- In general, the quark and lepton mixing matrices are not aligned. This introduces two independent RH mixing matrices to the model, one in the quark sector and one in the lepton sector.
- The Higgs potential (see Appendix 8) introduces a number of additional parameters compared to the $P$ or $C$ symmetric case. However, as the parameters of the Higgs sector enter our analysis only through the Higgs masses this does not further complicate our analysis.

Using the gauge group (2.5), the SM fermions can be embedded into multiplets in a very symmetric way

$$Q_L = \begin{pmatrix} u_L \\ d_L \end{pmatrix} \sim \left(\mathbf{3}, \mathbf{2}, \mathbf{1}, \frac{1}{3}\right) , \qquad Q_R = \begin{pmatrix} u_R \\ d_R \end{pmatrix} \sim \left(\mathbf{3}, \mathbf{1}, \mathbf{2}, \frac{1}{3}\right) , \tag{2.6}$$

$$L_L = \begin{pmatrix} \nu_L \\ e_L \end{pmatrix} \sim (\mathbf{1}, \mathbf{2}, \mathbf{1}, -1) , \qquad L_R = \begin{pmatrix} \nu_R \\ e_R \end{pmatrix} \sim (\mathbf{1}, \mathbf{1}, \mathbf{2}, -1) , \tag{2.7}$$

where the quantum numbers in the brackets correspond to the gauge group given in (2.5). The total fermion content is given by three replications of (2.6) and (2.7) for the three generations of quarks and leptons. In contrast to the SM embedding of the fermions, the RH quarks and

leptons are also organised in doublets. The assignment of the $B-L$ quantum numbers is due to the need for correct electromagnetic charges after symmetry breaking. The generator of the remaining group $\mathrm{U}(1)_Q$ is given by

$$Q = T_{3R} + T_{3L} + \frac{T_{B-L}}{2}\,. \tag{2.8}$$

The kinetic terms for the fermions are given by [138]

$$\mathcal{L}_{\text{ferm.kin.}} = i\sum_{i=1}^{3}\left[\bar{Q}_L^i\gamma_\mu D^\mu Q_L^i + \bar{Q}_R^i\gamma_\mu D^\mu Q_R^i + \bar{L}_L^i\gamma_\mu D^\mu L_L^i + \bar{L}_R^i\gamma_\mu D^\mu L_R^i\right]\,, \tag{2.9}$$

where $i = 1\ldots 3$ is the generation index and the covariant derivatives are given by

$$D^\mu Q_{L,R} = \partial^\mu Q_{L,R} - i\left(g_s G_a^\mu t^a Q_{L,R} + \frac{g_{L,R}}{2}\left(W_{L,R}^\mu\right)_a \tau^a Q_{L,R} + \frac{g'}{6}B^\mu Q_{L,R}\right)\,, \tag{2.10}$$

$$D^\mu L_{L,R} = \partial^\mu L_{L,R} - i\left(\frac{g_{L,R}}{2}\left(W_{L,R}^\mu\right)_a \tau^a L_{L,R} - \frac{g'}{2}B^\mu L_{L,R}\right)\,, \tag{2.11}$$

where $t^a$, $\tau^a$ are the generators of $\mathrm{SU}(3)_{\mathrm{QCD}}$ and $\mathrm{SU}(2)_{\mathrm{L,R}}$ respectively.

### The Higgs Sector and the Symmetry Breaking Pattern

In order to decouple the additional gauge bosons, the breaking of the LRM gauge group is done in two steps. The first step breaks (2.5) down to the SM gauge group while the second step emulates the EWSB of the SM. In order to illustrate this procedure, we show the breaking

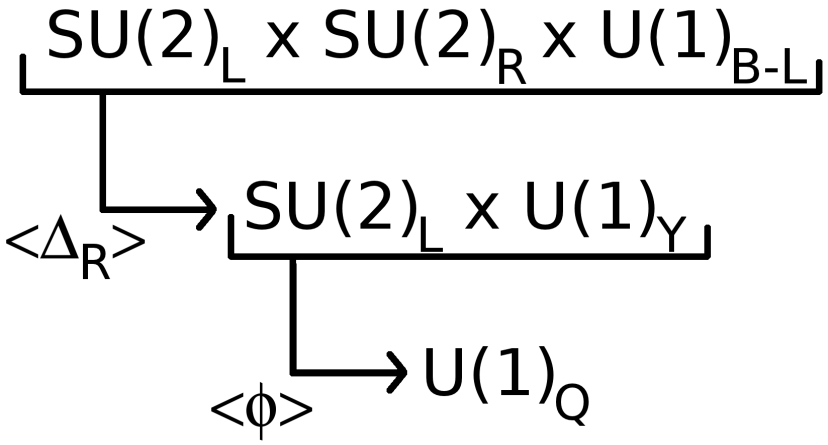


Figure 2.1: The LRM breaking pattern shown diagrammatically

pattern diagrammatically in figure 2.1. In the following, we leave aside the QCD gauge group, as it does not take part in the breaking.

**Step 1:** As the low energy spectrum of the model cannot include additional gauge bosons, we need to break the group (2.5) down to the SM one at some high scale $\kappa_R \sim \mathcal{O}(\,\mathrm{TeV})$. The

choice of TeV breaking of the gauge group is motivated by our hope for a discovery of NP at the LHC. In our work, we study models, with the pattern

$$\mathrm{SU(2)_R} \times \mathrm{U(1)_{B-L}} \xrightarrow[\langle\Delta\rangle]{} \mathrm{U(1)_Y}\,, \tag{2.12}$$

where the spontaneous breaking occurs due to the vacuum-expectation-value (vev) of a scalar field $\Delta$. This choice is not unique in models with a $\mathrm{SU(2)_1} \times \mathrm{SU(2)_2} \times \mathrm{U(1)}_X$ gauge group see [140] and references therein. However, in other cases the fundamental groups are not $\mathrm{SU(2)_L}$ and $\mathrm{SU(2)_R}$ which removes the intuitive embedding of the fermions. The most simple choice for the scalar field $\Delta$ would be a doublet under $\mathrm{SU(2)_R}$ [140]. However, as introducing a triplet $\Delta_R \sim (\mathbf{3},\mathbf{1},2)$ under $\mathrm{SU(2)_R}$ together with its $P$ symmetric partner $\Delta_L \sim (\mathbf{1},\mathbf{3},2)$ [74, 129] breaks the $\mathrm{SU(2)_R} \times \mathrm{U(1)}_X$ in the desired manner and provides a possible TeV See-Saw [130–133] mechanism, we chose the triplet representation for $\Delta_R$. The breaking given in (2.12) is thus mediated by

$$\Delta_R = \begin{pmatrix} \delta_R^+/\sqrt{2} & \delta_R^{++} \\ \delta_R^0 & -\delta_R^+/\sqrt{2} \end{pmatrix} \sim (\mathbf{3},\mathbf{1},2)\,, \tag{2.13}$$

which we assume to develop a vev

$$\langle\Delta_R\rangle = \begin{pmatrix} 0 & 0 \\ \kappa_R & 0 \end{pmatrix}. \tag{2.14}$$

The mass of the additional heavy gauge bosons as well as the remaining scalar degrees of freedom (d.o.f.) are therefore proportional to $\kappa_R \sim \mathcal{O}(\text{ TeV})$. Additionally to $\Delta_R$, we introduce

$$\Delta_L = \begin{pmatrix} \delta_L^+/\sqrt{2} & \delta_L^{++} \\ \delta_L^0 & -\delta_L^+/\sqrt{2} \end{pmatrix} \sim (\mathbf{1},\mathbf{3},2)\,, \tag{2.15}$$

which we assume to develop a vev

$$\langle\Delta_L\rangle = \begin{pmatrix} 0 & 0 \\ \kappa_L e^{i\theta_L} & 0 \end{pmatrix}. \tag{2.16}$$

In order not to prematurely break the $\mathrm{SU(2)_L}$ and for the purpose of a TeV See-Saw [130–133], we assume

$$\kappa_L \ll v \ll \kappa_R\,, \tag{2.17}$$

where $v$, given in equation (2.22), is at the scale of the SM EWSB. Each of the triplet Higgs fields has six degrees of freedom which are grouped into four fields, two neutral and two charged under $\mathrm{U(1)}_Q$. Two of the scalar fields (one neutral and one charged) of $\Delta_R$ are absorbed into the longitudinal components of the two massive gauge bosons which are in the spectrum after this step. This leaves us with one neutral and one doubly charged scalar originating from $\Delta_R$. The triplet $\Delta_L$ adds all of its degrees of freedom to the scalar sector.

**Step 2:** The SM like breaking of the remaining gauge group down to $\mathrm{U(1)_Q}$ is mediated by the vev of a scalar field $\phi$

$$\mathrm{SU(2)_L} \times U(1)_\mathrm{Y} \xrightarrow[\langle\phi\rangle]{} \mathrm{U(1)_Q}\,. \tag{2.18}$$

The choice for the embedding of $\phi$ is guided by its role in the breaking pattern as well as the need for the generation of fermion masses. The standard way is to choose $\phi \sim (\mathbf{2}, \mathbf{2}, 0)$ parametrised by [138]

$$\phi = \begin{pmatrix} \phi_1^0 & \phi_2^+ \\ \phi_1^- & \phi_2^0 \end{pmatrix} , \tag{2.19}$$

which is assumed to develop the vev

$$\langle \phi \rangle = \begin{pmatrix} \kappa & 0 \\ 0 & \kappa' e^{i\alpha} \end{pmatrix} . \tag{2.20}$$

In the absence of $\Delta_R$ the vev of $\phi$ would break $\mathrm{SU}(2)_\mathrm{R} \times \mathrm{SU}(2)_\mathrm{L}$ to its diagonal subgroup

$$\mathrm{SU}(2)_\mathrm{R} \times \mathrm{SU}(2)_\mathrm{L} \xrightarrow[\langle \phi \rangle]{} \mathrm{SU}(2)_V . \tag{2.21}$$

Together with the previous breaking discussed in 'Step 1' the vev of $\phi$ leads to EWSB. In order to simplify our notation we introduce

$$v = \sqrt{\kappa^2 + (\kappa')^2} = 174 \text{ GeV} , \tag{2.22}$$

which takes the role of the SM Higgs vev. We further introduce the notation

$$s = \frac{\kappa'}{v} , \qquad c = \frac{\kappa}{v} , \qquad \epsilon = \frac{v}{\kappa_R} . \tag{2.23}$$

As we assume $v \ll \kappa_R$, we know that $\epsilon \ll 1$ and therefore are able to expand in this small parameter. The Lagrangian for the scalar fields is given by

$$\begin{aligned} \mathcal{L}_\text{Higgs} = \mathrm{Tr}\left[ (D_\mu \Delta_R)^\dagger (D^\mu \Delta_R) \right] + \mathrm{Tr}\left[ (D_\mu \Delta_L)^\dagger (D^\mu \Delta_L) \right] + \\ \mathrm{Tr}\left[ (D_\mu \phi)^\dagger (D^\mu \phi) \right] + V(\Delta_L, \Delta_R, \phi) , \end{aligned} \tag{2.24}$$

where the covariant derivatives are given by

$$\begin{aligned} D^\mu \phi &= \partial^\mu \phi + i g_L \left( \vec{W}_L^\mu \cdot \vec{\tau} \right) \phi - i g_L \phi \left( \vec{W}_L^\mu \cdot \vec{\tau} \right) , \\ D^\mu \Delta_{L,R} &= \partial^\mu \Delta_{L,R} + i g_{L,R} \left[ \vec{W}_{L,R}^\mu \cdot \vec{\tau}, \Delta_{L,R} \right] + i g' B^\mu \Delta_{L,R} . \end{aligned} \tag{2.25}$$

The last term in (2.24) denotes the Higgs potential and is given in Appendix 8. The gauge sector after EWSB is discussed in Appendix 8. Of the eight d.o.f (grouped into six scalar fields) of $\phi$, three are absorbed into the longitudinal parts of $W^\pm$ and $Z$. This leaves us with one charged and three neutral scalar fields. After minimising the potential $V(\Delta_L, \Delta_R, \phi)$ one linear combination of neutral scalar fields takes the role of the SM Higgs particle, while the remaining two become additional heavy Higgs particles. The remaining charged field of $\phi$ is absorbed into heavy charged Higgs particles. To leading-order (LO), the masses of the Higgs particles relevant for our analysis are degenerate

$$M_H \equiv M_{H_1^0} = M_{H_2^0} = M_{H_1^\pm} = \frac{\sqrt{\alpha_3} \kappa_R}{1 - s^2} + \mathcal{O}(\varepsilon) , \tag{2.26}$$

where $\alpha_3$ is one of the couplings in the scalar potential given in Appendix 8 and $s$ is defined in equation (2.23).

### Yukawa Interactions, Fermion Masses and Mixing

By inspection of the quantum numbers for the fermions in equation (2.6) and in equation (2.7) and the scalar fields (2.13), (2.15) and (2.19), it is clear that only $\phi$ can couple to quarks due to the respective $B-L$ charges. The lepton doublets can couple to $\Delta_{L,R}$. These couplings could generate Majorana mass terms [130–133] for the neutrinos, which will introduce a TeV See-Saw mechanism. Concentrating on the quark sector, the most general renormalisable Yukawa coupling is given by

$$\mathcal{L}_{\text{Yuk.}} = -y_{ij}\bar{Q}^i_L \phi Q^j_R - \tilde{y}_{ij} Q^i_L \tilde{\phi} Q^j_R + \text{h.c.}\,, \tag{2.27}$$

where $\tilde{\phi} = \sigma_2 \phi^* \sigma_2$ and $i,j = 1\ldots 3$. After the scalar field $\phi$ develops its vev the quark mass matrices are given by

$$(M_u)_{ij} = v\left(c y_{ij} + s e^{-i\alpha}\tilde{y}_{ij}\right)\,, \qquad (M_d)_{ij} = v\left(s e^{i\alpha} y_{ij} + c\tilde{y}_{ij}\right)\,. \tag{2.28}$$

From (2.28), it is clear that setting $s \equiv c$ would align $|M_u|$ and $|M_d|$. This, however, stands in clear contradiction to the experimental data we have on the quark masses. In order to introduce the up-down mass splitting for the quarks, we chose $1 < \kappa/\kappa' < 10$. This allows for split fermion masses but not for a natural generation of the hierarchy $m_t/m_b$ as proposed in [123]. As we show explicitly in section 6.4, $\kappa/\kappa' \sim m_t/m_b$ is disfavoured by EWP data. Analogous to the SM, the quark mass matrices (2.28) can be diagonalised by means of bi-unitary transformations

$$M_u^{\text{diag.}} = U_L^\dagger M_u U_R\,, \tag{2.29}$$

$$M_d^{\text{diag.}} = D_L^\dagger M_d D_R\,, \tag{2.30}$$

where $U_{L,R}, D_{L,R}$ are unitary matrices connecting the flavour to the mass eigenstates. In the general case, the Yukawa matrices $y$ and $\tilde{y}$ are complex matrices, each having nine real parameters and nine phases. However, some of these 36 parameters are not physical and can be removed due to the flavour symmetry $\mathrm{SU(3)_L \times SU(3)_R}$. Finally we have nine quark masses and two unitary mixing matrices

$$V^{\text{L}} = U_L^\dagger D_L\,, \qquad V^{\text{R}} = U_R^\dagger D_R\,, \tag{2.31}$$

left. We chose to cast $V^{\text{L}}$ into the standard parametrisation [149] with three mixing angles and one complex phase

$$V^{\text{L}} = \begin{pmatrix} c_{12}c_{13} & s_{12}c_{13} & s_{13}e^{-i\delta_{13}} \\ -s_{12}c_{23} - c_{12}s_{23}s_{13}e^{i\delta_{13}} & c_{12}c_{23} - s_{12}s_{23}s_{13}e^{i\delta_{13}} & s_{23}c_{13} \\ s_{12}s_{23} - c_{12}c_{23}s_{13}e^{i\delta_{13}} & -s_{23}c_{12} - s_{12}c_{23}s_{13}e^{i\delta_{13}} & c_{23}c_{13} \end{pmatrix}\,. \tag{2.32}$$

In order to achieve this we have to use all redefinitions possible under the flavour symmetry and therefore $V^{\text{R}}$ has to be a unitary matrix with three angles and the full six phases. The standard way to parametrise $V^{\text{R}}$ is through

$$\tilde{V}^{\text{R}} = D_U V^0 D_D^\dagger\,, \tag{2.33}$$

where $V^0$ is a unitary matrix in the standard parametrisation of $V^{\text{L}}$ and the matrices $D_U$ and $D_D$ are given by

$$D_U = \text{diag}\left(1, e^{i\phi_2^u}, e^{i\phi_3^u}\right)\,, \qquad D_D = \text{diag}\left(e^{i\phi_1^d}, e^{i\phi_2^d}, e^{i\phi_3^d}\right)\,. \tag{2.34}$$

In this parametrisation, however, the elements $V_{td}^{\rm R}$ and $V_{ts}^{\rm R}$ take a complicated form. As we show explicitly in the last paragraph of section 3.4, having $|V_{td}^{\rm R}|$ as a complicated function of model parameters is not optimal due to the stringent bound on this element. In our numerical analysis we use $V^{\rm R}$ in the alternative parametrisation

$$V^{\rm R} = \begin{pmatrix} c_{12}c_{13}e^{i\delta_{ud}} & \begin{array}{c} -c_{23}s_{12}e^{i(-\delta_{td}+\delta_{ts}+\delta_{ud}-\phi)} \\ -c_{12}s_{13}s_{23}e^{i(-\delta_{td}+\delta_{ts}+\delta_{ud})} \end{array} & \begin{array}{c} s_{12}s_{23}e^{i(\delta_{tb}-\delta_{td}+\delta_{ud}-\phi)} \\ -c_{12}c_{23}s_{13}e^{i(\delta_{tb}-\delta_{td}+\delta_{ud})} \end{array} \\ c_{13}s_{12}e^{i\delta_{cd}} & \begin{array}{c} c_{12}c_{23}e^{i(\delta_{cd}-\delta_{td}+\delta_{ts}-\phi)} \\ -s_{12}s_{13}s_{23}e^{i(\delta_{cd}-\delta_{td}+\delta_{ts})} \end{array} & \begin{array}{c} -c_{23}s_{12}s_{13}e^{i(\delta_{cd}+\delta_{tb}-\delta_{td})} \\ -c_{12}s_{23}e^{i(\delta_{cd}+\delta_{tb}-\delta_{td}-\phi)} \end{array} \\ s_{13}e^{i\delta_{td}} & c_{13}s_{23e^{i\delta_{ts}}} & c_{13}c_{23}e^{i\delta_{tb}} \end{pmatrix}, \qquad (2.35)$$

which has the benefit of relating the bound on $|V_{td}^{\rm R}|$ directly to a bound on a model parameter e.g. $s_{13}$. Altogether, the LRM introduces nine new parameters in the quark mixing, six of those are phases. After EWSB, heavy Higgs particles including linear combinations of former $\phi$ fields couple to quarks in a flavour violating manner through the interactions given in (2.27). While the light neutral SM like Higgs has only $\mathcal{O}(\varepsilon^2)$ flavour violating couplings, there are heavy Higgs bosons with $\mathcal{O}(1)$ flavour violating couplings in the spectrum after EWSB. These Higgs particles, denoted by $H_1^0, H_2^0$ and $H^\pm$ (see Appendix 8) introduce important effects in $\Delta F = 1$ and $\Delta F = 2$ processes (see sections 3.4 and 4.1). In our numerical analysis, we ignore the phase $\alpha$, introduced through the vev of $\phi$, as it always multiplies $V^{\rm R}$ and can be therefore absorbed into a redefinition of $V^{\rm R}$. This does not change $V^{\rm R}$ in a physically meaningful way, as $V^{\rm R}$ is already an unitary matrix with six independent phases which is the maximal number possible.

# 3

# $\Delta F = 2$ Transitions

In this chapter, we provide formulae for the $\Delta F = 2$ processes studied in this work. We start this chapter with a brief discussion of the general effective Hamiltonian for $\Delta F = 2$ transitions including QCD corrections. Subsequently, we discuss the relevant observables $\varepsilon_K$, $S_{\psi K_s}$, $\Delta M_q$ $(q = d, s)$, $\Delta M_K$, $S_{\psi\phi}$, $\Delta\Gamma_q$ and $A_{\rm SL}^q$ both in the SM4 and in the LRM. Our notation and conventions are close to those used in [135, 152–155]. This facilitates an easy comparison between the $\Delta F = 2$ results for the SM4 and LRM, studied in this work, and other NP scenarios like the Randall-Sundrum scenario with custodial protection (RSc) [135], the Little Higgs model with T-parity (LHT) [152] or SUSY flavour models [156].

## 3.1 The General Effective Hamiltonian for $\Delta F = 2$ Transitions

The most general effective Hamiltonian for $\Delta F = 2$ processes at the high scale $\mu_{\rm in}$, at which the heavy degrees of freedom are integrated out, is given by

$$\mathcal{H}_{\rm eff}(\Delta F = 2) = \frac{G_F^2 M_W^2}{4\pi^2} \sum_i C_i(\mu_{\rm in}) Q_i(\mu_{\rm in})\,, \tag{3.1}$$

where the Wilson coefficients $C_i$ are model dependent. The eight local four-quark operators $Q_i$ are given by [157]

$$Q_1^{\rm VLL} = \left(\bar{b}^\alpha \gamma_\mu P_L q^\alpha\right)\left(\bar{b}^\beta \gamma^\mu P_L q^\beta\right)\,, \tag{3.2}$$

$$Q_1^{\rm LR} = \left(\bar{b}^\alpha \gamma_\mu P_L q^\alpha\right)\left(\bar{b}^\beta \gamma^\mu P_R q^\beta\right)\,, \tag{3.3}$$

$$Q_2^{\rm LR} = \left(\bar{b}^\alpha P_L q^\alpha\right)\left(\bar{b}^\beta P_R q^\beta\right)\,, \tag{3.4}$$

$$Q_1^{\rm SLL} = \left(\bar{b}^\alpha P_L q^\alpha\right)\left(\bar{b}^\beta P_L q^\beta\right)\,, \tag{3.5}$$

$$Q_2^{\rm SLL} = \left(\bar{b}^\alpha \sigma_{\mu\nu} P_L q^\alpha\right)\left(\bar{b}^\beta \sigma^{\mu\nu} P_L q^\beta\right)\,, \tag{3.6}$$

where, for definiteness, we restrict ourselves to the $B_q$ system. In our notation we have $\sigma_{\mu\nu} = \frac{1}{2}[\gamma_\mu, \gamma_\nu]$ and $P_{L,R} = \frac{1}{2}(1 \mp \gamma_5)$. The remaining three operators $Q_1^{\rm VRR}$ and $Q_{1,2}^{\rm SRR}$ can be derived from their LL counterparts by exchanging $P_L$ for $P_R$. In total, the $Q_i$ form a set of five independent sectors VLL, VRR, SLL, SRR and LR. While the operators of each subset mix due to renormalisation group (RG) effects, the different sectors stay independent even under RG running. The relevant operators for the $K$ system can be derived from (3.2) - (3.6) by

| | $K$ ($\mu_L = 2\,\text{GeV}$) | $B_d$ ($\mu_L = 4.6\,\text{GeV}$) | $B_s$ ($\mu_L = 4.6\,\text{GeV}$) |
|---|---|---|---|
| $B_1^{\text{VLL}}$ | 0.571(48)(30) | 0.88(4)(5) | 0.88(4)(5) |
| $B_1^{\text{LR}}$ | 0.562(39)(46) | 1.79(4)(18) | 1.79(4)(18) |
| $B_2^{\text{LR}}$ | 0.810(41)(31) | 1.14(3)(6) | 1.14(3)(6) |
| $B_1^{\text{SLL}}$ | 0.679(56)(27) | 0.79(2)(4) | 0.79(2)(4) |
| $B_2^{\text{SLL}}$ | 0.42(11)(11) | 0.70(5)(12) | 0.70(5)(12) |

Table 3.1: The hadronic matrix elements $B_i$ used for our calculation of the $P_i$ factors. The values for the $K$ system are taken from [161] while the values for the $B$ system from [162]. We already performed the transformation into our operator basis according to (3.10) - (3.12). The errors are divided into statistical and systematic ones.

performing the replacements $b \to s$ and $q \to d$. While the Wilson coefficients $C_i(\mu_{\text{in}})$ can be calculated in perturbation theory at the high scale $\mu_{\text{in}}$, the hadronic matrix elements

$$\mathcal{Q}_i = \langle \bar{B}_q^0 | Q_i(\mu_{\text{in}}) | B_q^0 \rangle \,, \tag{3.7}$$

depend crucially on the results of lattice QCD calculations which are usually given at the scale $\mu_L = 2$ GeV for the $K$ system and at the scale $\mu_L = \mu_b$ for the $B$ system. Connecting the high scale $\mu_{\text{in}}$ and the relevant lattice scale $\mu_L$ requires the calculation of short-distance (SD) QCD corrections and the evolution matrices $\hat{U}(\mu_{\text{in}}, \mu_m)$ [158–160]. Another complication arises in the case of a model with more than one high scale $\mu_{\text{in}}^{a=1\ldots n}$. As discussed in [158], this would require the calculation of QCD corrections in an effective theory below each scale $\mu_{\text{in}}^a$ successively. This is, on the one hand, beyond the scope of this work and, on the other hand, premature before the discovery of NP as well as in the light of the current precision of lattice results. Adapting the philosophy of [158], we can write the mixing amplitude for $\bar{B}_q^0 - B_q^0$ as

$$A(\bar{B}_q^0 \to B_q^0) = \langle \bar{B}_q^0 | \mathcal{H}_{\text{eff}}(\Delta F = 2) | B_q^0 \rangle = \frac{G_F^2 M_W^2}{4\pi^2} \sum_i C_i(\mu_{\text{in}}) \mathcal{Q}_i \,, \tag{3.8}$$

where $\mathcal{Q}_i$ is given by

$$\mathcal{Q}_i = \frac{2}{3} m_{B_q}^2 F_{B_q}^2 P_i(B_q) \,. \tag{3.9}$$

The decay constant $F_{B_q}$ has to be calculated by means of lattice methods, while the mass $m_{B_q}$ can be taken from experiment. The factors $P_i(B_q)$ [158] in (3.9) contain all the RG effects connected to the RG running from $\mu_{\text{in}}$ to $\mu_b$ as well as the hadronic matrix elements calculated by lattice methods. Since the Wilson coefficients $C_i(\mu_{\text{in}})$ can be calculated in perturbation theory and be expressed in terms of fundamental parameters, the SD effects of the model are displayed prominently, without being hidden by non-perturbative contributions. Therefore, the form of the amplitude given in (3.8) facilitates the understanding of the different contributions.

In this work, we calculate the coefficients $P_i$ with the help of the explicit formulae provided in [158] using the matrix elements given in [161] for the $K$ system and [162] for the $B$ system. Unfortunately those matrix elements are given in another operator basis [160] and we have to

| $\mu_{\rm in}$ | 200 GeV | 2.5 TeV | 10 TeV | 15 TeV |
|---|---|---|---|---|
| $P^{\rm VLL}$ | 0.448(38)(24) | 0.417(35)(22) | 0.404(34)(21) | 0.400(34)(21) |
| $P_1^{\rm LR}$ | -31(1)(2) | -45(2)(3) | -52(3)(4) | -55(3)(4) |
| $P_2^{\rm LR}$ | 52(3)(3) | 73(4)(5) | 84(4)(5) | 89(5)(6) |
| $P_1^{\rm SLL}$ | -22(2)(2) | -28(2)(2) | -30(3)(2) | -31(3)(2) |
| $P_2^{\rm SLL}$ | -39(3)(4) | -49(4)(4) | -54(4)(4) | -55(4)(4) |

Table 3.2: The values of $P_i$ in the $K$ system for different values of the high scale $\mu_{\rm in}$

| $\mu_{\rm in}$ | 200 GeV | 2.5 TeV | 10 TeV | 15 TeV |
|---|---|---|---|---|
| $P^{\rm VLL}$ | 0.74(3)(4) | 0.69(3)(4) | 0.67(3)(4) | 0.66(3)(4) |
| $P_1^{\rm LR}$ | -2.59(5)(20) | -3.42(7)(24) | -3.89(9)(27) | -4.03(9)(27) |
| $P_2^{\rm LR}$ | 3.23(9)(17) | 4.56(13)(24) | 5.30(15)(29) | 5.52(16)(30) |
| $P_1^{\rm SLL}$ | -1.32(4)(7) | -1.62(4)(9) | -1.78(5)(9) | -1.82(5)(10) |
| $P_2^{\rm SLL}$ | -2.55(8)(24) | -3.05(8)(24) | -3.32(9)(24) | -3.40(9)(25) |

Table 3.3: The values of $P_i$ in the $B$ system for different values of the high scale $\mu_{\rm in}$

use the conversion rules

$$B_1^{\rm VLL}(\mu_L) = B_1(\mu_L)\,, \qquad B_1^{\rm VRR}(\mu_L) = B_1(\mu_L)\,, \tag{3.10}$$

$$B_1^{\rm LR}(\mu_L) = B_5(\mu_L)\,, \qquad B_2^{\rm LR}(\mu_L) = B_4(\mu_L)\,, \tag{3.11}$$

$$B_1^{\rm SLL}(\mu_L) = B_2(\mu_L)\,, \qquad B_2^{\rm SLL}(\mu_L) = \frac{5}{3}B_2(\mu_L) - \frac{2}{3}B_3(\mu_L)\,, \tag{3.12}$$

before we can employ them in our calculations. We have collected the input parameters $B_i$ for the $K$ and the $B$ system in table 3.1. Using the input listed in table 7.1 we find the values given in table 3.2 ($K$ system) and in table 3.3 ($B$ system) for the $P_i$ factors. In table 3.4, we show, exemplary for the $B$ system and $\mu_{\rm in} = 2.5\,\text{TeV}$, the impact of the different input errors on the resulting uncertainty on $P_i$. Inspecting the different errors, we find a clear dominance of the errors stemming from the $B_i$ factors.

Because of their importance in SM calculations, the parameters $B_1^{\rm VLL}$ for the different meson systems are known to a much higher accuracy than the ones given in [161, 162] and collected in table 3.1. Moreover, in the context of the SM, one usually uses the RG invariant parameters $\hat\eta_q$ and $\hat B_q$ ($q = K, d, s$). Most recent lattice calculations [163–169] reach an impressive accuracy for $\hat B_q$. The averaged results read [170]

$$\hat B_K = 0.737(20)\,, \qquad \hat B_{B_d} = 1.26(11)\,, \qquad \hat B_{B_s} = 1.33(6)\,, \tag{3.13}$$

while the $\hat\eta$ factors have been calculated to a very high accuracy [39, 171–174] in perturbation theory. In this work we take advantage of the high accuracy of $\hat B_q$ by suitable redefinitions of $C_q^{\rm VLL}$ in the NP models studied here. This is shown explicitly in the discussion below. As

| | $P_i$ | $\sigma(\alpha_s(M_Z))$ | $\sigma(M_Z)$ | $\sigma(m_b)$ | $\sigma(m_d)$ | $\sigma(m_{B^0})$ | $\sigma(B_1^i)$ | $\sigma(B_2^i)$ |
|---|---|---|---|---|---|---|---|---|
| $P^{\rm VLL}$ | 0.69 | (1)(0) | (0)(0) | (0)(0) | (0)(0) | (0)(0) | (3)(4) | (0)(0) |
| $P_1^{\rm LR}$ | -3.42 | (3)(0) | (0)(0) | (3)(0) | (0)(0) | (0)(0) | (3)(13) | (6)(11) |
| $P_2^{\rm LR}$ | 4.56 | (4)(0) | (0)(0) | (4)(0) | (0)(0) | (0)(0) | (0)(1) | (12)(23) |
| $P_1^{\rm SLL}$ | -1.62 | (1)(0) | (0)(0) | (1)(0) | (0)(0) | (0)(0) | (4)(8) | (0)(0) |
| $P_2^{\rm SLL}$ | -3.05 | (2)(0) | (0)(0) | (2)(0) | (0)(0) | (0)(0) | (6)(12) | (5)(12) |

Table 3.4: The values of $P_i(B)$ for $\mu_{\rm in} = 2.5\,\text{TeV}$ and the induced errors seperated by source

QCD is not sensitive to the change of VLL, SLL $\to$ VRR, SRR, the results for the LL operators also apply to the respective RR operators.

## 3.2 $\Delta F = 2$ Processes in the Standard Model

The Standard Model effective Hamiltonian for $\Delta F = 2$ transitions is the most simple realisation of (3.1). As the SM $W^\pm$ boson has purely LH couplings and there are neither flavour changing charged scalars, charged bosons with RH couplings nor tree-level flavour changing neutral current (FCNC) mediating bosons, only the operator $Q_1^{\rm VLL}$ contributes. The effective Hamiltonians for the $K$ system and the $B$ system take the form [172]

$$\begin{aligned}\mathcal{H}_{\rm eff}^{\Delta S=2} = \frac{G_F^2 M_W^2}{4\pi^2}\left(\left(\lambda_c^{(K)}\right)^2\hat\eta_{cc}S_0(x_c) + \left(\lambda_t^{(K)}\right)^2\hat\eta_{tt}S_0(x_t) + 2\lambda_c^{(K)}\lambda_t^{(K)}\hat\eta_{ct}S_0(x_c,x_t)\right)\times \\ \times\left(\alpha_s^{(3)}(\mu)\right)^{-2/9}\left[1+\frac{\alpha_s^{(3)}(\mu)}{4\pi}J_3\right]Q_{\Delta S=2}^{\rm VLL}(\mu)\,,\end{aligned} \tag{3.14}$$

$$\mathcal{H}_{\rm eff}^{\Delta B=2} = \frac{G_F^2 M_W^2}{4\pi^2}\left(\lambda_t^{(q)}\right)^2\hat\eta_B S_0(x_t)\left(\alpha_s^{(5)}(\mu)\right)^{-6/23}\left[1+\frac{\alpha_s^{(5)}(\mu)}{4\pi}J_5\right]Q_{\Delta B=2}^{\rm VLL}(\mu)\,, \tag{3.15}$$

where we took all the relevant contributions into account and used the notation

$$\lambda_i^{(K)} = V_{is}^* V_{id}\,, \qquad\qquad \lambda_i^{(q)} = V_{ib}^* V_{iq}\,, \tag{3.16}$$

with $q = d, s$ in order to compactify the CKM dependence. The parameters $x_i$ for $i = u, c, t$ are defined as

$$x_i = \frac{\bar m_i(m_i)^2}{M_W^2}\,. \tag{3.17}$$

Note that in the $B$ system the charm contributions are neglected, while they are kept in the $K$ system. The importance of the charm contributions in the $K$ system is introduced by a CKM and QCD enhancement of the terms containing charm quarks. Additionally a CKM and QCD suppression of the top contribution to the $\bar K^0 - K^0$ mixing is found. In table 7.1, we provide numerical values for all inputs, e.g. the $\hat\eta$ factors. Let us introduce our notation [175]

by explicitly showing the definition of the mixing amplitude $M_{12}^q$ for the $B_q$ system

$$2m_{B_q}\,(M_{12}^q)^* = \langle \bar{B}_q^0 | \mathcal{H}_{\text{eff}}^{\Delta B=2} | B_q^0 \rangle\,, \tag{3.18}$$

where we defined

$$M_{12}^q = \frac{G_F^2 M_W^2}{12\pi^2} M_W^2 F_{B_q}^2 \hat{B}_{B_q} m_{B_q} \bar{M}_{12}^q\,, \tag{3.19}$$

with $\bar{M}_{12}^q$ given by

$$\bar{M}_{12}^q = \left(\lambda_t^{*(q)}\right)^2 \hat{\eta}_B S_0(x_t)\,, \tag{3.20}$$

where $\hat{\eta}_B$ summarises the SD QCD corrections. The RG invariant parameter $\hat{B}_{B_q}$ is defined as [173]

$$\hat{B}_{B_q} = \left(\alpha_s^{(5)}(\mu)\right)^{-6/23} \left[1 + \frac{\alpha_s^{(5)}(\mu)}{4\pi} J_5\right] B_{B_q}(\mu)\,. \tag{3.21}$$

In (3.20) we used the fact that $\hat{\eta}_B$ and $S_0$ are real-valued and therefore the complex conjugate in (3.18) only acts on $\lambda_t^{(q)}$. In the case of the $K$ system, the steps are analogous to (3.18) – (3.21) with a suitable replacements of the constants involved. For the definition of $\hat{B}_K$ the strong coupling for three active flavours has to be used as can be seen from (3.14).

### *B* System Observables in the Standard Model

Having the formulae for the mixing amplitude $M_{12}$ (3.18) - (3.20), we can give expressions for the mixing related observables in the context of the SM. For the $\bar{B}_q^0 - B_q^0$ mass difference we have [175]

$$\Delta M_q = 2\,|M_{12}^q| = \frac{G_F^2 M_W^2}{6\pi^2} M_W^2 F_{B_q}^2 \hat{B}_{B_q} m_{B_q} \hat{\eta}_B \left|\left(\lambda_t^{*(q)}\right)^2\right| S_0(x_t)\,. \tag{3.22}$$

The time dependent CP asymmetry in the decay of neutral $B$ mesons can be written as

$$\mathcal{A}(B_q \to f) = S_f \sin(\Delta M_q t) + C_f \cos(\delta M_q t)\,, \tag{3.23}$$

where the coefficients $S_{\psi K_s}$ and $S_{\psi\phi}$ for $B_d^0 \to \psi K_S$ and $B_s^0 \to \psi\phi$ respectively, are given by [47, 175]

$$S_{\psi K_s} = \sin(2\beta)\,, \qquad S_{\psi\phi} = -\sin(2\beta_s)\,, \tag{3.24}$$

where the phases $\beta$ and $\beta_s$ are defined as

$$\beta = -\arg(V_{td}^{\text{L}})\,, \qquad \beta_s = -\arg(-V_{ts}^{\text{L}})\,. \tag{3.25}$$

Equation (3.24) can be connected to the mixing amplitude by

$$S_f = \hat{\eta}_f \sin\left(\arg(M_{12}^q)\right)\,, \tag{3.26}$$

with $\hat{\eta}_f = 1(-1)$ for $f = \psi K_s(\psi\phi)$.

### $K$ System Observables in the Standard Model

The mixing amplitude $M_{12}^K$ for the $K$ system is, in the context of the SM, given by [172]

$$M_{12}^K = \frac{G_F^2 M_W^2 F_K^2 \hat{B}_K m_K}{12\pi^2} \left( \left(\lambda_c^{*(K)}\right)^2 \hat{\eta}_{cc} S_0(x_c) + \left(\lambda_t^{*(K)}\right)^2 \hat{\eta}_{tt} S_0(x_t) + 2\lambda_c^{*(K)} \lambda_t^{(K)} \hat{\eta}_{ct} S_0(x_c, x_t) \right) . \tag{3.27}$$

The short-distance (SD) part of the mass difference for $\bar{K}^0 - K^0$ is given by

$$\Delta M_K = 2\,\mathrm{Re}\left(M_{12}^K\right) , \tag{3.28}$$

Unfortunately, the constraining power of $\Delta M_K$ is diminished by sizeable unknown long-distance (LD) contributions [176]. However, the mixing induced CP asymmetry

$$\varepsilon_K = \frac{\kappa_\varepsilon e^{i\phi_\varepsilon}}{\sqrt{2}(\Delta M_K)_{\mathrm{exp}}} \mathrm{Im} M_{12}^K , \tag{3.29}$$

is theoretically clean and known to a high precision. The parameters $\kappa_\varepsilon = 0.94(2)$ and $\phi_\varepsilon = 43.51(5)^\circ$ include LD effects in $\mathrm{Im}\Gamma_{12}$ and $\mathrm{Im}M_{12}$ and have been studied by several authors [27,177,178]. It has also been shown that similar effects in the $B$ system [179] have no significant impact on our analysis.

## 3.3 $\Delta F = 2$ Processes in the SM4

In the SM4, the effective Hamiltonians for the $K$ and the $B$ system are only slightly modified compared to the SM. This can be traced back to the fact that the SM4 does not add any new operators from the basis given in (3.2) - (3.6) but only duplicates $Q_1^{\mathrm{VLL}}$ at a higher scale. This would in principle add further complications to the RG running, as below the scale $\mu_{t'}$ where the $t'$ particle is integrated out, the QCD corrections would have to be calculated in an effective theory. We believe that such a complicated analysis is premature for a hypothetical model and chose to integrate out all heavy degrees of freedom simultaneously at $\mu = \mathcal{O}(m_t, M_W)$. This adds a small irreducible error to our predictions but in view of the many new parameters this seems hardly problematic. This treatment is further encouraged by the slow the running of $\alpha_s$ above the weak scale as well as the smallness of the relevant anomalous dimensions. In the presence of a fourth generation, (3.14) and (3.15) receive the following corrections

$$\begin{aligned} \Delta\mathcal{H}_{\mathrm{eff}}^{\Delta S=2} = \frac{G_F^2 M_W^2}{4\pi^2} & \left( \left(\lambda_{t'}^{(K)}\right)^2 \hat{\eta}_{t't'} S_0(x_{t'}) + 2\lambda_t^{(K)} \lambda_{t'}^{(K)} \hat{\eta}_{tt'} S_0(x_t, x_{t'}) + \right. \\ & \left. + 2\lambda_c^{(K)} \lambda_{t'}^{(K)} \hat{\eta}_{ct'} S_0(x_c, x_{t'}) \right) \left(\alpha_s^{(3)}(\mu)\right)^{-2/9} \left[1 + \frac{\alpha_s^{(3)}(\mu)}{4\pi} J_3\right] Q_{\Delta S=2}^{\mathrm{VLL}}(\mu) , \end{aligned} \tag{3.30}$$

$$\begin{aligned} \Delta\mathcal{H}_{\mathrm{eff}}^{\Delta B=2} = \frac{G_F^2 M_W^2}{4\pi^2} & \left( \left(\lambda_{t'}^{(q)}\right)^2 \eta_B^{t't'} S_0(x_{t'}) + 2\lambda_t^{(q)} \lambda_{t'}^{(q)} \eta_B^{tt'} S_0(x_t, x_{t'}) \right) \times \\ & \times \left(\alpha_s^{(5)}(\mu)\right)^{-6/23} \left[1 + \frac{\alpha_s^{(5)}(\mu)}{4\pi} J_5\right] Q_{\Delta B=2}^{\mathrm{VLL}}(\mu) . \end{aligned} \tag{3.31}$$

Following the philosophy outlined in the beginning of this section, we approximate the QCD factors $\hat{\eta}$ by

$$\hat{\eta}_{t't'} \approx \hat{\eta}_{tt}\,, \qquad \hat{\eta}_{tt'} \approx \hat{\eta}_{tt}\,, \qquad \hat{\eta}_{ct'} \approx \hat{\eta}_{ct}\,, \tag{3.32}$$

$$\hat{\eta}_B^{t't'} \approx \hat{\eta}_B\,, \qquad \hat{\eta}_B^{tt'} \approx \hat{\eta}_B\,, \tag{3.33}$$

which is again justified by the slow running of $\alpha_s$ above $\mu_W$ as well as the very mild hierarchy between $m_t$ and $m_{t'}$.

### *B* System Observables in the SM4

In order to achieve a very compact form for the NP effects we follow the idea of [180] and absorb the new contributions into a redefinition of the masterfunction $S_0(x_t)$

$$S_0(x_t) \to S_q = S_0(x_t) + \left(\frac{\lambda_{t'}^{(q)}}{\lambda_t^{(q)}}\right)^2 S_0(x_{t'}) + 2\frac{\lambda_{t'}^{(q)}}{\lambda_t^{(q)}} S_0(x_t, x_{t'})\,, \tag{3.34}$$

which allows us to rewrite the model dependent part of the mixing amplitude in the following way

$$\bar{M}_{12}^q = \left(\lambda_t^{*(q)}\right)^2 \hat{\eta}_B S_q^*\,, \tag{3.35}$$

where $S_q$ is a complex valued non-universal function. This procedure allows us to reuse the SM expressions (3.22) and (3.26) by simply exchanging the universal function $S_0(x_t)$ through $S_q$. For convenience and later use we define the total phase of the mixing amplitude through

$$M_{12} = \frac{G_F^2 M_W^2}{12\pi^2} M_W^2 F_{B_q}^2 \hat{B}_{B_q} m_{B_q} \hat{\eta}_B \left(\lambda_t^{*(q)}\right)^2 S_q = |M_{12}| e^{2i\phi_q^{\rm tot}}\,. \tag{3.36}$$

Using equations (3.26) and (3.36), we find

$$S_{\psi K_s} = \sin(2\phi_d^{\rm tot})\,, \qquad S_{\psi\phi} = -\sin(2\phi_s^{\rm tot})\,, \tag{3.37}$$

for the time-dependent CP asymmetries. We further observe that

$$2\phi_d^{\rm tot} = 2\bar{\beta} - \arg(S_d) \qquad 2\phi_s^{\rm tot} = 2\bar{\beta}_s - \arg(S_s)\,, \tag{3.38}$$

with $\bar{\beta}$ and $\bar{\beta}_s$ defined like in (3.25) but generally different from their SM values $\beta \approx 21^\circ$ and $\beta_s \approx -1^\circ$ due to the changes in the CKM matrix discussed in section 2.1. The interference between the three terms in the mixing amplitude prohibits us from writing down an insightful formula for $\Delta M_q$ in terms of the relevant model parameters, in the sense that we cannot *a-priori* separate the terms by their relative importance. Moreover, we cannot separate the SM and NP contribution in in the spirit of [181] due to the fact that the SM4 introduces significant changes to the CKM matrix. We can however write down the very compact expression

$$\Delta M_q = \frac{G_F^2 M_W^2}{6\pi^2} M_W^2 F_{B_q}^2 \hat{B}_{B_q} m_{B_q} \hat{\eta}_B \left|\left(\lambda_t^{*(q)}\right)^2 S_q\right|\,, \tag{3.39}$$

for the mass differences, which has the benefit of looking like the SM one (3.22). We can parametrise the NP effects in the mixing amplitude by [134]

$$M_{12}^q = (M_{12}^q)_{\rm SM}\, C_{B_q} e^{2i\varphi_{B_q}}\,, \tag{3.40}$$

where we defined

$$\varphi_{B_q} = -\theta_q(S) + 2(\bar{\beta}_q - \beta_q^{\rm SM}) = \arg\left(\frac{M_{12}^{\rm tot}}{M_{12}^{\rm SM}}\right)\,, \tag{3.41}$$

with $\theta_q(S) = \arg(S_q)$. Using (3.40), we can follow [152] in order to calculate the width-difference $\Delta\Gamma_q$ and the semi-leptonic asymmetry $A_{\rm SL}^q$ in the SM4

$$\frac{\Delta\Gamma_q}{\Gamma_q} = -\left(\frac{\Delta M_q}{\Gamma_q}\right)^{\rm exp}\left[{\rm Re}\left(\frac{\Gamma_{12}^q}{M_{12}^q}\right)^{\rm SM}\frac{\cos(2\varphi_{B_q})}{C_{B_q}} + {\rm Im}\left(\frac{\Gamma_{12}^q}{M_{12}^q}\right)^{\rm SM}\frac{\sin(2\varphi_{B_q})}{C_{B_q}}\right]\,, \tag{3.42}$$

$$A_{\rm SL}^q = {\rm Im}\left(\frac{\Gamma_{12}^q}{M_{12}^q}\right)^{\rm SM}\frac{\cos(2\varphi_{B_q})}{C_{B_q}} - {\rm Re}\left(\frac{\Gamma_{12}^q}{M_{12}^q}\right)^{\rm SM}\frac{\sin(2\varphi_{B_q})}{C_{B_q}}\,, \tag{3.43}$$

where the SM predictions for $\Gamma_{12}^q$ and $M_{12}^q$ are taken from recent calculations [32, 49, 182–185] and are given by

$${\rm Re}\left(\frac{\Gamma_{12}^d}{M_{12}^d}\right)^{\rm SM} = -5.3(10)\cdot 10^{-3}\,, \qquad {\rm Re}\left(\frac{\Gamma_{12}^s}{M_{12}^s}\right)^{\rm SM} = -5.0(10)\cdot 10^{-3}\,, \tag{3.44}$$

$${\rm Im}\left(\frac{\Gamma_{12}^d}{M_{12}^d}\right)^{\rm SM} = -4.1(6)\cdot 10^{-4}\,, \qquad {\rm Im}\left(\frac{\Gamma_{12}^s}{M_{12}^s}\right)^{\rm SM} = 1.9(3)\cdot 10^{-5}\,. \tag{3.45}$$

Due to their sensitivity to NP effects, the observables $\Delta\Gamma_q$ and $A_{\rm SL}^q$ received a lot of attention in the recent past. This was mostly fueld by the D0 measurement of the di-muon asymmetry in $B$ decays [48] which is closely related to the semi-leptonic asymmetries [186]

$$A_{\rm SL}^B = 0.506 A_{\rm SL}^d + 0.494 A_{\rm SL}^s\,, \tag{3.46}$$

and shows a deviation of more than $2\sigma$ from the SM prediction. In table 3.5 we stake stock of the current experimental and theoretical situation. As can be seen from table 3.5 there are some interesting discrepancies between the different experiments on the determination of $\phi_s$, while the semi-leptonic asymmetries display some deviations from their SM prediction. The $2\sigma$ deviation of $\phi_s$ from its SM prediction found by the Tevatron experiments [187, 188] was another driving force for the study of NP effects in the $B_s$ system.

### $K$ System Observables in the SM4

For the $K$ system we follow the same procedure as for the $B$ system and absorb the new contributions (3.30) in a redefinition of $S_0(x_t)$

$$S_0(x_t) \to S_K = S_0(x_t) + \left(\frac{\lambda_{t'}^{(K)}}{\lambda_t^{(K)}}\right)^2 S_0(x_{t'}) + 2\frac{\lambda_{t'}^{(K)}}{\lambda_t^{(K)}} S_0(x_t, x_{t'}) + 2\frac{\lambda_c^{(K)}\lambda_{t'}^{(K)}}{\left(\lambda_t^{(K)}\right)^2}\frac{\hat{\eta}_{ct}}{\hat{\eta}_{tt}} S_0(x_c, x_{t'})\,. \tag{3.47}$$

| observable | experimental value | SM prediction |
|---|---|---|
| $\phi_s = -2(\beta_s + \phi_{B_s})$ | $\in [-1.04, -0.04]$ (CDF [187])<br>$-0.55^{+0.38}_{-0.36}$ (D0 [188])<br>$-0.002(83)(27)$ (LHCb [38]) | -0.0363(17) [189] |
| $\frac{\Delta\Gamma_d}{\Gamma_d}$ | 0.011(37) [54] | 0.0042(8) [32] |
| $\Delta\Gamma_s$ | $0.075(35)(1)\,\mathrm{ps}^{-1}$ (CDF [187])<br>$0.163^{+0.065}_{-0.064}\,\mathrm{ps}^{-1}$ (D0 [188])<br>$0.116(18)(6)\,\mathrm{ps}^{-1}$ (LHCb [190]) | $0.087(21)\,\mathrm{ps}^{-1}$ [32] |
| $A^d_{\mathrm{SL}}$ | $-0.12(52)\%$ [48] | $-0.041(6)\%$ [49] |
| $A^s_{\mathrm{SL}}$ | $-1.8(11)\%$ [48] | $0.0019(3)\%$ [49] |
| $A^b_{\mathrm{SL}}$ | $-0.79(20)\%$ [48] | $-0.020(3)\%$ [49] |

Table 3.5: Theoretical and experimental values of a number of observables related to $B_{s,d}-\bar{B}_{s,d}$ mixing

Using this replacement, the last factor in the mixing amplitude (3.19) reads

$$\bar{M}_{12}^K = \left(\lambda_c^{*(K)}\right)^2 \hat{\eta}_{cc} S_0(x_c) + \left(\lambda_t^{*(K)}\right)^2 \hat{\eta}_{tt} S_K^* + 2\lambda_c^{*(K)}\lambda_t^{*(K)}\hat{\eta}_{ct} S_0(x_c, x_t)\,, \tag{3.48}$$

where $S_0(x_c)$ and $S_0(x_c, x_t)$ are again real-valued functions while $S_K$ is not. The interesting $K$ system observables $\Delta M_K$ and $\varepsilon_K$ take the same form as in the SM with only a modified $\bar{M}_{12}^K$. While constraint on the mass-difference is less interesting due to its unknown LD contributions, the indirect CP violation $\varepsilon_K$ has a strong impact on the SM4 parameter space. Let us give the complete formula for $\varepsilon_K$ in the SM4 without the use of a compact notation

$$\begin{aligned}\varepsilon_K = \frac{\kappa_\varepsilon e^{i\varphi_\varepsilon}}{\sqrt{2}\,(\Delta M_K)^{\mathrm{exp}}} \Big[ & \mathrm{Im}\left(\lambda_c^{*(K)}\right)^2 \hat{\eta}_{cc} S_0(x_c) + \\ & + \mathrm{Im}\left(\lambda_t^{*(K)}\right)^2 \hat{\eta}_{tt} S_0(x_t) + 2\,\mathrm{Im}(\lambda_c^{*(K)}\lambda_t^{*(K)})\hat{\eta}_{ct} S_0(x_c, x_t) + \\ & + \mathrm{Im}\left(\lambda_{t'}^{*(K)}\right)^2 \hat{\eta}_{tt} S_0(x_{t'}) + 2\,\mathrm{Im}(\lambda_c^{*(K)}\lambda_{t'}^{*(K)})\hat{\eta}_{ct} S_0(x_c, x_{t'}) + \\ & + 2\,\mathrm{Im}(\lambda_t^{*(K)}\lambda_{t'}^{*(K)})\hat{\eta}_{tt} S_0(x_t, x_{t'})\Big]\,.\end{aligned} \tag{3.49}$$

The first three terms cannot be simply replaced by their SM numerical values as the SM4 introduces changes in all the elements of the CKM matrix. Especially the terms involving charm quarks get potentially large contributions relative to their SM value. Due to these contributions, $\varepsilon_K$ is not able to tightly constrain the value of $\mathrm{Im}\lambda_{t'}^{(K)}$ as one might naively suspect. In fact, the rare $K$ decays studied in chapter 4 provide much more stringent constraints on $\mathrm{Im}\lambda_{t'}^{(K)}$ for a significant part of the parameter space.

## 3.4 $\Delta F = 2$ Processes in LRM

The effective Hamiltonian for $\Delta F = 2$ transitions in the context of the LRM potentially includes all operators (3.2) - (3.6) as well as the RR counterparts for SLL and VLL. All the contributions in this model can be separated into three categories

1. Gauge boson contributions are introduced by box diagrams with the exchange of $W'^{\pm}$ and $W^{\pm}$ bosons in all possible combinations. Due to the small mixing between $W_L$ and $W_R$, or alternatively the high mass of $W'^{\pm}$, only boxes with $W^{\pm}W^{\pm}$ and $W^{\pm}W'^{\pm}$ contribute significantly. For illustration, the Feynman diagrams for these contributions are shown in figure 3.1. Note that the LRM does not introduce tree-level FCNCs through the exchange of gauge bosons, and therefore it does not generate $Q_1^{\mathrm{LR}}$ at LO in the gauge sector.

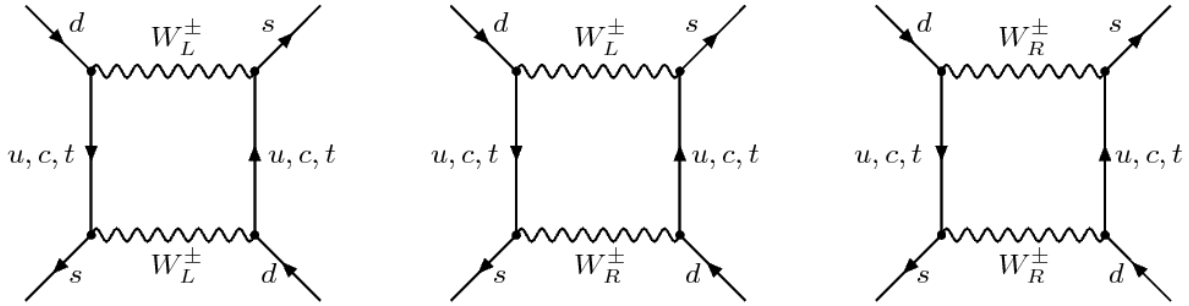


Figure 3.1: Feynman diagrams for the contributing gauge boson box diagrams

2. Charged Higgs contributions are introduced through box diagrams with the exchange of one (or two) charged Higgs bosons in conjunction with one (or zero) charged gauge bosons $W^{\pm}, W'^{\pm}$. As the mass of the charged Higgs in this class of models is at least in the multi TeV range, only diagrams with the exchange of one charged Higgs and one light $W^{\pm}$ gauge boson contribute here in an important manner. The relevant diagram is shown in the left panel of figure 3.2.

3. Neutral Higgs contributions are mediated by a flavour violating tree-level exchange of a heavy neutral Higgs boson. As the Higgs couples to quarks via their Yukawa couplings, the Higgs mass suppression is partially compensated by the top quark mass. More importantly, as the neutral Higgs contribution induce changes to the SLL, SRR or LR Wilson coefficients the QCD RG effects tend to enhance this contribution by more then a factor of ten in the $K$ system (see tables 3.3 and 3.2). The relevant diagram is shown in the right panel of figure 3.2.

In the following, we discuss the individual contributions separately, giving formulae for the Wilson coefficients and commenting on the QCD corrections. The Wilson coefficients can be written as

$$C_i = \Delta_{\mathrm{Box}} C_i + \Delta_{\mathrm{H}^{\pm}} C_i + \Delta_{\mathrm{H}^0} C_i \,, \tag{3.50}$$

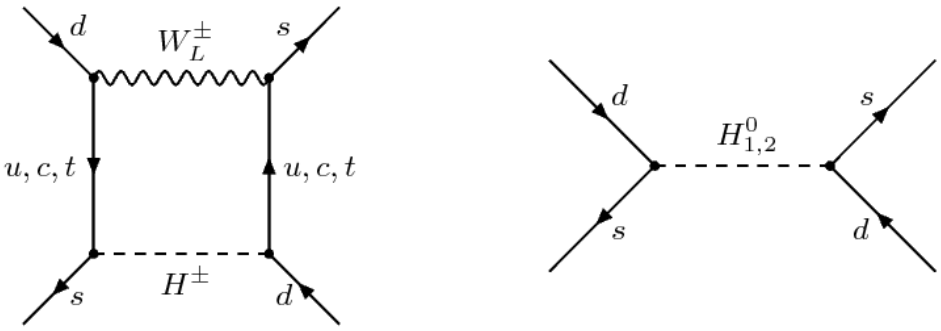


Figure 3.2: Feynman diagrams for charged Higgs box and the tree-level exchange of a neutral Higgs

where $i$ indicates the whole set of operators separately. The dependence on the mixing matrices $V^{\mathrm{L}}$ and $V^{\mathrm{R}}$ is always expressed in terms of [118]

$$\lambda_i^{AB}(K) = V_{is}^{A*} V_{id}^{B}\,, \qquad\qquad \lambda_i^{AB}(B_q) = V_{ib}^{A*} V_{iq}^{B}\,, \tag{3.51}$$

where $A, B = \mathrm{L}, \mathrm{R}$, $q = d, s$ and $i = u, c, t$.

**Gauge Boson Contributions**

The calculation of the Feynman diagrams in figure 3.1 and their symmetric partners yields the following contributions to the Wilson coefficients [118, 138, 191–193]

$$\Delta_{\mathrm{Box}} C_1^{\mathrm{VLL}}(\mu_W, q) = \sum_{i,j=c,t} \lambda_i^{\mathrm{LL}}(q) \lambda_j^{\mathrm{LL}}(q) S_{\mathrm{LL}}(x_i, x_j)\,, \tag{3.52}$$

$$\Delta_{\mathrm{Box}} C_2^{\mathrm{LR}}(\mu_R, q) = \sum_{i,j=u,c,t} \lambda_i^{\mathrm{LR}}(q) \lambda_j^{\mathrm{RL}}(q) S_{\mathrm{LR}}(x_i, x_j, \beta)\,, \tag{3.53}$$

$$\Delta_{\mathrm{Box}} C_1^{\mathrm{RR}}(\mu_R, q) = \sum_{i,j=c,t} \lambda_i^{\mathrm{RR}}(q) \lambda_j^{\mathrm{RR}}(q) S_{\mathrm{RR}}(\tilde{x}_i, \tilde{x}_j)\,, \tag{3.54}$$

with $q = K, B_d, B_s$ and $\lambda^{AB}$ defined in (3.51). The parameters $\tilde{x}_i$, $r$ and $\beta$ are defined as

$$\tilde{x}_i = \frac{m_i^2}{M_{W'}^2}\,, \qquad\qquad \beta = \frac{M_W^2}{M_{W'}^2}\,, \qquad\qquad r = \frac{s_W^2}{c_W^2 s_R^2} = \frac{g_R^2}{g_L^2}\,, \tag{3.55}$$

and the loop functions $S_{AB}$ are given in Appendix 8. The parameter $r$ describes the misalignment between $g_L$ and $g_R$ and thereby also the departure, in the gauge sector, from the (pseudo-)manifest models. Note that the LRM does not introduce $\mathcal{O}(\varepsilon^2)$ changes to the Wilson coefficient of the operator $Q_1^{\mathrm{VLL}}$ and consequently $\Delta_{\mathrm{Box}} C_1^{\mathrm{VLL}}(\mu_W, q)$ simplifies to the SM expression included in (3.14) and (3.15) respectively. In equation (3.52) and (3.54) the unitarity of the mixing matrices $V^{\mathrm{L}}$ and $V^{\mathrm{R}}$ or equivalently the GIM mechanism [194] was used in order to eliminate the up quark contribution. However, the GIM mechanism does not apply to the LR contribution given in (3.53) [138]. As pointed out in [191] the loop function $S_{\mathrm{LR}}$ is not gauge independent but as explicitly shown in [192, 193] the addition of the tree-level Higgs exchanges discussed below as well as the inclusion of vertex and self-energy corrections to the

tree-level Higgs exchange restores gauge invariance. It was also shown in [192, 193] that the restoration of gauge invariance does not significantly change our expression for $S_{\rm LR}$ given in the 't Hooft-Feynman gauge.

### Charged Higgs Contributions

The diagram for these contributions is shown in the left panel of figure 3.2. Note that at $\mathcal{O}(\varepsilon^2)$ the only contributing box diagrams are those with one charged Higgs and one light charged gauge boson. Box diagrams with two charged Higgs bosons or a charged Higgs boson and a heavy charged gauge boson are of higher order in $\varepsilon$ and can be neglected. Analogously, box diagrams with heavy neutral Higgs bosons have to also be excluded. The contribution to the Wilson coefficient $C_2^{\rm LR}$ due to the exchange of a charged Higgs particle is given by [118]

$$\Delta_{\rm H^\pm} C_2^{\rm LR}(\mu_H, q) = u(s) \sum_{i,j=u,c,t} \lambda_i^{\rm LR}(q) \lambda_j^{\rm RL}(q) S_{\rm LR}^{\rm H}(x_i, x_j, \beta_H)\,, \tag{3.56}$$

again with $q = K, B_d, B_s$, the master function $S_{\rm LR}^{\rm H}$ being given in Appendix 8 and $\beta_H = M_W^2/M_{H^\pm}^2$. The function $u(s)$, with $s$ defined in equation (2.23), is given by

$$u(s) = \left(\frac{1}{1-2s^2}\right)^2\,, \tag{3.57}$$

and can enhance the charged Higgs contribution drastically for $s \to 1/\sqrt{2}$. The quark masses in the first term of (51) have to be evaluated at $\mu_H$ as this factor arises from the Yukawa couplings of $H^\pm$ to quarks. In table 7.2, we provide values for the running quark masses at NLO for different high scales.

### Neutral Higgs Contributions

The tree-level exchange of a FCNC Higgs particle (right panel of figure 3.2) gives rise to only one correction term [138]

$$\Delta_{\rm H^0} C_2^{\rm LR}(\mu_H, q) = -\frac{16\pi^2}{\sqrt{2} M_H^2 G_F} u(s) \sum_{i,j=u,c,t} \lambda_i^{\rm LR}(q) \lambda_j^{\rm RL}(q) \sqrt{x_i(\mu_H) x_j(\mu_H)}\,, \tag{3.58}$$

as the contributions to the $C_{1,2}^{\rm SLL}$ and $C_{1,2}^{\rm SRR}$ cancel in the limit of $M_{H^0} = M_{H^1} = M_H$. Consequently, contributions due to the breaking of the degeneracy of masses are of higher order and can be neglected. Note that the quark masses have to be evaluated at the scale $\mu_H$ as the Higgs couples via the Yukawa couplings. In table 7.2, we provide values for the running quark masses at NLO for different high scales.

### Summary of LR Contributions to $\Delta F = 2$ Transitions

By comparing the contributions in equations (3.53), (3.56) and (3.58) we find that the sum (including QCD corrections for the running from $\mu_H$ to $\mu_R$)

$$C_2^{\rm LR}(\mu_R, q) = \Delta_{\rm Box} C_2^{\rm LR}(\mu_R, q) + \frac{P_2^{\rm LR}(\mu_H, q)}{P_2^{\rm LR}(\mu_R, q)} \left(\Delta_{\rm H^\pm} C_2^{\rm LR}(\mu_H, q) + \Delta_{\rm H^0} C_2^{\rm LR}(\mu_H, q)\right)\,, \tag{3.59}$$

can be rewritten into a form where the quark mixing related contributions are separated from the loop functions

$$C_2^{\rm LR}(\mu_R, q) = \sum_{i,j=u,c,t} \lambda_i^{\rm LR}(q)\lambda_j^{\rm RL}(q)\Bigg[S_{\rm LR}(x_i, x_j, \beta) + \\ + \frac{P_2^{\rm LR}(\mu_H, q)}{P_2^{\rm LR}(\mu_R, q)} u(s)\left(S_{\rm LR}^{\rm H}(x_i, x_j, \beta_H) - \frac{16\pi^2\sqrt{x_i(\mu_H)x_j(\mu_H)}}{\sqrt{2}M_H^2 G_F}\right)\Bigg] . \tag{3.60}$$

The second term in (3.60) is non-universal only due to the dependence on $P_2^{\rm LR}(\mu, q)$. In (3.59) and (3.60) we implicitly introduced the relevant scales for the QCD corrections, but let us do so more explicitly

- The SM contribution $\Delta_{\rm Box}C^{\rm VLL}$ is evaluated at $\mu = \mathcal{O}(\mu_t, \mu_W)$ [158]. As there are no new contributions aside from the SM ones we can use the RG invariant parameters $\hat{\eta}$ and $\hat{B}_q$ in the mixing amplitude without any further complications.
- For $\Delta_{\rm Box}C_2^{\rm LR}(\mu_R, q)$, we choose $\mu = \mu_R$ as the matching scale although as already mentioned the situation is in principle more complicated.
- For $\Delta_{\rm H^\pm}C_2^{\rm LR}(\mu_H, q)$, we choose $\mu = \mu_H$ with the same cautioning remarks valid as for $\Delta_{\rm Box}C_2^{\rm LR}(\mu_R, q)$.
- For tree-level Higgs exchanges the situation is again clear and $\mu = \mu_H$ has to be chosen at the current level in perturbation theory. Going beyond NLO for the QCD corrections should remove the scale dependence and render the choice of $\mu_H$ inconsequential.

### *B* System Observables in the LRM

In the LRM, the mixing amplitude $M_{12}^q$ can be written as

$$M_{12}^q = (M_{12}^q)_{\rm SM} + (M_{12}^q)_{\rm LR} , \tag{3.61}$$

where $(M_{12}^q)_{\rm SM}$ is given in (3.19). The RR contribution can be safely neglected as, for realistic $W_R^\pm$ masses, it is by orders of magnitude smaller than the SM one. The left-right contribution $(M_{12}^q)_{\rm LR}$ is given by

$$(M_{12}^q)_{\rm LR} = \frac{G_F^2 M_W^2}{12\pi^2} F_{B_q}^2 m_{B_q} \Big[P_2^{\rm LR}(\mu_R, q)\left(\Delta_{\rm Box}C_2^{\rm LR}(\mu_R, q)\right)^* + \\ + P_2^{\rm LR}(\mu_H, q)\left(\Delta_{\rm H^\pm}C_2^{\rm LR}(\mu_H, q) + \Delta_{\rm H^0}C_2^{\rm LR}(\mu_H, q)\right)^*\Big] . \tag{3.62}$$

Following the same procedure as for the SM4, we separate the SM and NP contributions through

$$M_{12}^q = (M_{12}^q)_{\rm SM}\, C_{B_q} e^{2i\varphi_{B_q}} , \tag{3.63}$$

where $(M_{12}^q)_{\rm SM}$ has to be evaluated for the best fit value of the CKM parameters. The mass-difference reads accordingly

$$\Delta M_q = (\Delta M_q)_{\rm SM}\, C_{B_q} . \tag{3.64}$$

The amplitudes of the time-dependent CP asymmetries are given by

$$S_{\psi K_s} = \sin(2\beta + 2\varphi_{B_d})\,, \qquad S_{\psi\phi} = -\sin(2\beta_s + 2\varphi_{B_s})\,. \tag{3.65}$$

For the calculation of the life-time difference $\Delta\Gamma_q$ and the semileptonic asymmetry we can use equations (3.42) and (3.43), using $C_{B_q}$ and $\varphi_{B_q}$ defined through (3.63).

### $K$ System Observables in the LRM

Neglecting the RR contributions as they are orders of magnitude smaller than the SM ones, the mixing amplitude for $\bar{K}^0 - K^0$ mixing can be written as

$$M_{12}^K = \left(M_{12}^K\right)_{\rm SM} + \left(M_{12}^K\right)_{\rm LR}\,, \tag{3.66}$$

where $\left(M_{12}^K\right)_{\rm SM}$ is given in (3.27) and the LR contributions are given by

$$\begin{aligned}\left(M_{12}^K\right)_{\rm LR} = \frac{G_F^2 M_W^2}{12\pi^2} F_K^2 m_{K^0} \Big[ & P_2^{\rm LR}(\mu_R, K)\left(\Delta_{\rm Box} C_2^{\rm LR}(\mu_R, K)\right)^* + \\ & + P_2^{\rm LR}(\mu_H, K)\left(\Delta_{\rm H^\pm} C_2^{\rm LR}(\mu_H, K) + \Delta_{\rm H^0} C_2^{\rm LR}(\mu_H, K)\right)^* \Big]\,.\end{aligned} \tag{3.67}$$

The indirect CP violation $\varepsilon_K$ and the mass difference $\Delta M_K$ are given by

$$\varepsilon_K = (\varepsilon_K)_{\rm SM} + (\varepsilon_K)_{\rm LR}\,, \qquad \Delta M_K = (\Delta M_K)_{\rm SM} + (\Delta M_K)_{\rm LR}\,, \tag{3.68}$$

where the contributions $(\varepsilon_K)_{\rm SM}$ and $(\Delta M_K)_{\rm SM}$ can be found in (3.29) and (3.28) and the LR contributions are given by

$$(\varepsilon_K)_{\rm LR} = \frac{\kappa_\varepsilon e^{i\phi_\varepsilon}}{\sqrt{2}\,(\Delta M_K)_{\rm exp}} \,{\rm Im}\left(M_{12}^K\right)_{\rm LR}\,, \qquad (\Delta M_K)_{\rm LR} = 2\,{\rm Re}\left(M_{12}^K\right)_{\rm LR}\,. \tag{3.69}$$

### Anatomy of LR Contributions to $\Delta F = 2$ Transitions

In order to better understand the importance of different contributions to the NP effects we follow (3.60) and rewrite the mixing amplitude $M_{12}^q$ ($q = K, B_d, B_s$) in order to separate the quark mixing matrix effects from the loop functions and the non-perturbative effects. Introducing $\Lambda_{ij}(q) = \lambda_i^{\rm LR}(q)\lambda_j^{\rm RL}(q)$, we find

$$\left(M_{12}^K\right)_{\rm LR} = \frac{G_F^2 M_W^2}{12\pi^2} F_K^2 m_{K^0} \sum_{i,j=u,c,t} \Lambda_{ij}(q) R_{ij}(q)\,, \tag{3.70}$$

where we collected the QCD running, the non-perturbative matrix elements and the SD effects from loop functions into one closed form

$$\begin{aligned}R_{ij}(q) = \; & P_2^{\rm LR}(\mu_R, q) S_{\rm LR}(x_i, x_j, \beta) + P_2^{\rm LR}(\mu_H, q) u(s) S_{\rm LR}^{\rm H}(x_i, x_j, \beta_H) - \\ & - P_2^{\rm LR}(\mu_H, q) \frac{16\pi^2}{\sqrt{2} M_H^2 G_F} \sqrt{x_i(\mu_H) x_j(\mu_H)}\,.\end{aligned} \tag{3.71}$$

As all contributions to $R_{ij}(q)$ are negative there is no possibility for accidental cancellations between the different terms in (3.71). The first issue we want to study is the importance of

the Higgs contributions to $R_{ij}(q)$. To this end we plot $R_{tt}^{\text{Higgs}}(q)/R_{tt}^{\text{tot}}(q)$ as a function of $M_H$ for different values of $M_{W'}$.
In figure 3.3 and figure 3.4, we show $R_{tt}^{\text{Higgs}}(q)/R_{tt}^{\text{tot}}(q)$ as a function of $M_H$ for different values of $M_{W'}$ for $s = 0.1$ and $s = 0.5$ respectively. From figure 3.3 it is evident that even for $s = 0.1$ and an already excluded mass of 500 GeV for $W'$, the Higgs contributions cannot be neglected for $M_H$ below 100 TeV. For a realistic $M_{W'} > 2$ TeV the Higgs contribution is even more dominant. For Higgs masses $M_H < 50$ TeV the Higgs contribution always accounts for more than 40% of the total value of $R_{tt}(q)$. For $s = 0.5$, the importance of the Higgs contributions is enhanced so that it accounts for more than 50% for $M_H < 50$ TeV and $M_{W'} > 2$ TeV. Furthermore, as both $M_H$ and $M_{W'}$ depend on $\kappa_R$ the Higgs mass is bounded from above by perturbativety for any given value of $M_{W'}$. The perturbativety bound is explicitly shown in figure 7.12. In Appendix 8, we give numerical values for $R_{ij}(q)$ for an exemplary choice of parameters.

As can be seen from the numeric values provided in Appendix 8, if we consider the matrix $\hat{R}(q)$ formed by the elements $R_{ij}$, $\hat{R}(q)$ exhibits a very strong and distinct hierarchy. For definiteness, we restrict the following discussion to the $K$ system, but similar arguments hold for the $B$ system as well. An order of magnitude approximation for the matrix $\hat{R}(K)$ is given by

$$\hat{R}(K) \sim (-1) \begin{pmatrix} 10^{-9} & 10^{-6} & 10^{-4} \\ 10^{-6} & 10^{-4} & 10^{-2} \\ 10^{-4} & 10^{-2} & 10^{1} \end{pmatrix}, \tag{3.72}$$

where we kept only the order of magnitude for the elements of $\hat{R}(K)$. We observe a wide spread of order of magnitude for the different elements of $\hat{R}(K)$ and a very strong hierarchy

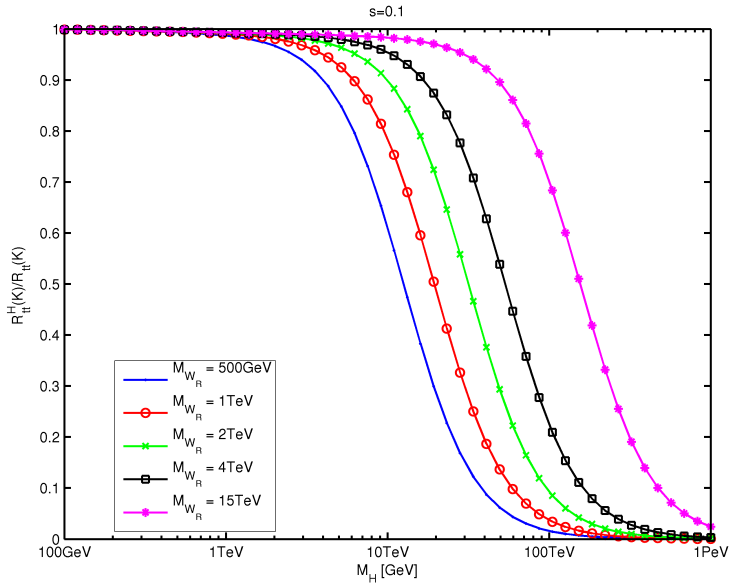


Figure 3.3: The relative importance of the Higgs contributions in $R_{tt}(q)$ for $s = 0.1$

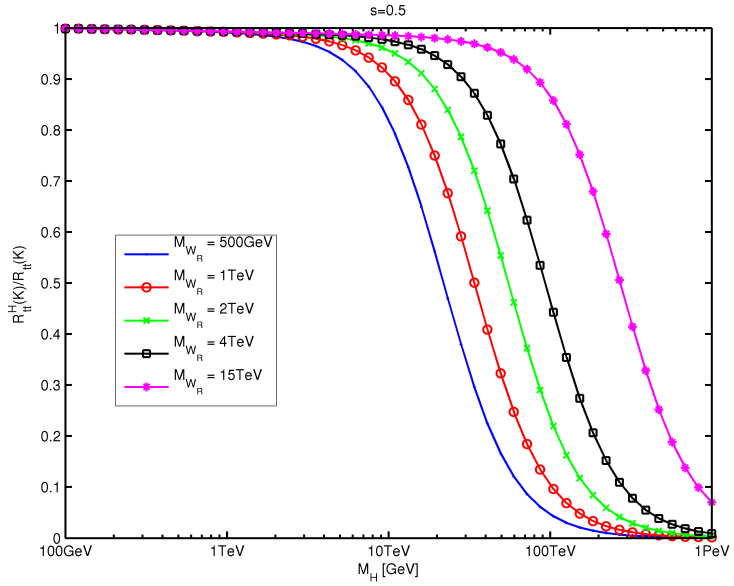


Figure 3.4: The relative importance of the Higgs contributions in $R_{tt}(q)$ for $s = 0.5$, the $s$ induced enhancement is clearly visible compared to the plot in figure 3.3

toward the third generation. As a rule of thumb, we find that changing a flavour index of $\hat{R}(K)$ by one changes the element by two-to-three orders of magnitude. Before summation the elements for $\hat{R}(K)$ are multiplied by the the elements $\Lambda_{ij}(K)$, compare equation (3.70). Barring any cancellations among the various contributions in equation (3.70), each of these LR contributions to $\Delta M_K$ and more importantly to $\varepsilon_K$ has to be suppressed well below the SM contributions $(\Delta M_K)_{\text{SM}}$ and $(\varepsilon_K)_{\text{SM}}$. For a compact notation, we define the operator $\otimes$ as the element-wise multiplication of two matrices $A$ and $B$

$$(A \otimes B)_{ij} = (A_{ij} B_{ij})_{ij} \,, \tag{3.73}$$

where no implicit summation over indices is assumed. Assuming no cancellations, we can write down the constraints in a very compact notation. Requiring the NP contribution to be below 10% of the SM one, we find

$$\left| \text{Im}\left(\hat{\Lambda} \otimes \hat{R}\right) \right| = \left| \text{Im} \begin{pmatrix} - & - & V_{ud}^{\text{R}} V_{ts}^{\text{R}*} 10^{-7} \\ - & V_{cd}^{\text{R}} V_{cs}^{\text{R}*} 10^{-8} & V_{cd}^{\text{R}} V_{ts}^{\text{R}*} 10^{-5} \\ V_{td}^{\text{R}} V_{us}^{\text{R}*} 10^{-7} & V_{td}^{\text{R}} V_{cs}^{\text{R}*} 10^{-6} & V_{td}^{\text{R}} V_{ts}^{\text{R}*} 10^{-3} \end{pmatrix} \right| \leq 10^{-8} \,, \tag{3.74}$$

using the constraint on $\varepsilon_K$. The constraint from $\Delta M_K$ is less stringent as the unknown LD contributions (see section 3.2) introduce an uncertainty of at least 30%. Furthermore, the SM prediction for $\Delta M_K$ is well below the experimental value. Nonetheless, as the LRM contribution potentially exceeds the SM one by orders of magnitude, we can write down the constraint from $\Delta M_K$ as

$$\left| \text{Re}\left(\hat{\Lambda} \otimes \hat{R}\right) \right| = \left| \text{Re} \begin{pmatrix} - & - & V_{ud}^{\text{R}} V_{ts}^{\text{R}*} 10^{-7} \\ - & V_{cd}^{\text{R}} V_{cs}^{\text{R}*} 10^{-5} & V_{cd}^{\text{R}} V_{ts}^{\text{R}*} 10^{-4} \\ V_{td}^{\text{R}} V_{us}^{\text{R}*} 10^{-6} & V_{td}^{\text{R}} V_{cs}^{\text{R}*} 10^{-4} & V_{td}^{\text{R}} V_{ts}^{\text{R}*} 10^{-3} \end{pmatrix} \right| \leq 5 \cdot 10^{-6} \,, \tag{3.75}$$

requiring the LRM contribution to be half the SM one at most. From equations (3.74) and (3.75), we can extract the most stringent bounds

$$\left|\operatorname{Im}\left(V_{td}^{\mathrm{R}} V_{ts}^{\mathrm{R}\,*}\right)\right| \leq \mathcal{O}(10^{-5})\,, \qquad \left|\operatorname{Re}\left(V_{td}^{\mathrm{R}} V_{ts}^{\mathrm{R}\,*}\right)\right| \leq \mathcal{O}(10^{-2})\,, \tag{3.76}$$

$$\left|\operatorname{Im}\left(V_{td}^{\mathrm{R}} V_{cs}^{\mathrm{R}\,*}\right)\right| \leq \mathcal{O}(10^{-2})\,, \qquad \left|\operatorname{Re}\left(V_{td}^{\mathrm{R}} V_{cs}^{\mathrm{R}\,*}\right)\right| \leq \mathcal{O}(10^{-1})\,, \tag{3.77}$$

$$\left|\operatorname{Im}\left(V_{cd}^{\mathrm{R}} V_{ts}^{\mathrm{R}\,*}\right)\right| \leq \mathcal{O}(10^{-3})\,, \qquad \left|\operatorname{Re}\left(V_{cd}^{\mathrm{R}} V_{ts}^{\mathrm{R}\,*}\right)\right| \leq \mathcal{O}(10^{-1})\,. \tag{3.78}$$

For further investigation we define two scenarios for the RH mixing matrix $V^{\mathrm{R}}$

1. the *normal hierarchy* scenario, where the hierarchy is similar to the one of $V^{\mathrm{L}}$ insofar as the diagonal terms are close to one and $1 \gg |V_{us}^{\mathrm{R}}| \gtrsim |V_{cb}^{\mathrm{R}}| \gtrsim |V_{ub}^{\mathrm{R}}|$.
2. the *inverted hierarchy* scenario, where the hierarchy of the $2-3$ sub-matrix in inverted. This entails $|V_{cs}^{\mathrm{R}}| \sim |V_{tb}^{\mathrm{R}}| \leq \mathcal{O}(10^{-1})$ and $|V_{ts}^{\mathrm{R}}| \sim |V_{cb}^{\mathrm{R}}| \sim \mathcal{O}(1)$.

In the first scenario, we find

$$\left|\operatorname{Im}(V_{td}^{\mathrm{R}})\right| \geq \mathcal{O}(10^{-2})\,, \qquad \left|\operatorname{Re}(V_{td}^{\mathrm{R}})\right| \geq \mathcal{O}(10^{-1})\,. \tag{3.79}$$

In the second scenario, we find

$$\left|\operatorname{Im}(V_{td}^{\mathrm{R}})\right| \leq \mathcal{O}(10^{-5})\,, \qquad \left|\operatorname{Re}(V_{td}^{\mathrm{R}})\right| \leq \mathcal{O}(10^{-2})\,, \tag{3.80}$$

$$\left|\operatorname{Im}(V_{cd}^{\mathrm{R}})\right| \leq \mathcal{O}(10^{-3})\,, \qquad \left|\operatorname{Re}(V_{cd}^{\mathrm{R}})\right| \leq \mathcal{O}(10^{-1})\,, \tag{3.81}$$

assuming $V_{ts}^{\mathrm{R}}$ is $\mathcal{O}(1)$ in its real and imaginary part. Performing similar steps for the $B_d$ and $B_s$ system we find

$$|V_{tb}^{\mathrm{R}\,*} V_{td}^{\mathrm{R}}| \leq 10^{-2}\,, \tag{3.82}$$

$$|V_{tb}^{\mathrm{R}\,*} V_{ts}^{\mathrm{R}}| \leq 10^{-2}\,, \tag{3.83}$$

$$|V_{cb}^{\mathrm{R}\,*} V_{ts}^{\mathrm{R}}| \leq 10^{-2}\,, \tag{3.84}$$

using the constraints from $\Delta M_d$ and $\Delta M_s$. While the constraint from $S_{\psi K_s}$ forces the imaginary part of to $\Delta^{\mathrm{LRM}} M_{12}^{(d)}$ to be below $10^{-5}$ there is no such constraint for the $B_s$ system[1]. Therefore, the constraint given in equation (3.83) and (3.84) have a loophole and are only binding in the case of a small LRM contribution to $\Delta M_s$. A discussion on this topic can be found in section 6.2. In conclusion to this discussion, the combined constraint on $V_{td}^{\mathrm{R}}$ is given by

$$|V_{td}^{\mathrm{R}}| \leq \mathcal{O}(10^{-2})\,, \tag{3.85}$$

in both scenarios assuming no cancellations. Interestingly this constraint holds even in the full analysis (see section 7.2) in the case of low fine-tuning.

[1] The new LHCb changes this to some extend as discussed in section 6.2.

# 4

# $\Delta F = 1$ Transitions

In this chapter, we provide formulae and notes on the treatment of the $\Delta F = 1$ processes studied in this work. Since most of these processes have not been measured up to date, they can only be used to put upper limits on predictions of NP models. Notable exceptions are the decay $B \to X_s\gamma$ and its close relatives $B \to X_d\gamma$ and $B \to X_s\ell^+\ell^-$. Consequently, this chapter starts with a short discussion of the decays $B \to X_s\gamma$ and $B \to X_d\gamma$ in the LRM and SM4. The other decays discussed in this chapter are only studied in the context of the SM4.

## 4.1 The Decay $B \to X_s\gamma$

The branching ratio $\mathrm{Br}(B \to X_s\gamma)$ can be used to put stringent bounds on many models of NP. On the one hand, this can be understood through the excellent agreement between NNLO SM prediction [195–197]

$$\mathrm{Br}(B \to X_s\gamma)_{\mathrm{SM}} = (3.15 \pm 0.23) \cdot 10^{-4}\,, \tag{4.1}$$

and the measured value [47]

$$\mathrm{Br}(B \to X_s\gamma)_{\mathrm{Exp}} = (3.55 \pm 0.24 \pm 0.09) \cdot 10^{-4}\,, \tag{4.2}$$

with their small errors. On the other hand, it is known that many NP models can cause large effects in this decay, see for example [198–202].

In the SM, the relevant effective Hamiltonian is given by [203]

$$\mathcal{H}_{\mathrm{eff}}^{\mathrm{SM}} = -\frac{G_F}{\sqrt{2}}\lambda_t^{(s)}\left[\sum_{i=1}^{6} C_i(\mu_b)Q_i + C_{7\gamma}(\mu_b)Q_{7\gamma} + C_{8G}(\mu_b)Q_{8G}\right]\,, \tag{4.3}$$

where the $Q_i$ denote the four quark operators given in [175], $Q_{7\gamma}$ and $Q_{8G}$ are the magnetic photon penguin operator and magnetic gluon penguin operator, respectively. The operators $Q_{7\gamma}$ and $Q_{8G}$ are given by [204]

$$Q_{7\gamma}(\mu_W) = \frac{e}{16\pi^2} m_b \bar{s}_\alpha \sigma^{\mu\nu} P_R b_\alpha F_{\mu\nu}\,, \qquad Q_{8G} = \frac{e}{16\pi^2} m_b \bar{s}_\alpha \sigma^{\mu\nu} P_R T^a_{\alpha\beta} b_\alpha G^a_{\mu\nu}\,. \tag{4.4}$$

In the presence of NP, equation (4.3) is modified by the following replacements [204]

$$C_{7\gamma}(\mu_b) \to C_{7\gamma}^{\mathrm{SM}}(\mu_b) + \Delta C_{7\gamma}(\mu_b)\,, \qquad C_{8G}(\mu_b) \to C_{8G}^{\mathrm{SM}}(\mu_b) + \Delta C_{8G}(\mu_b)\,, \tag{4.5}$$

where the NNLO result for $C_{7\gamma}^{\rm SM}(\mu_b)$ is given by [195–197]

$$C_{7\gamma}^{\rm SM}(\mu_b) = -0.3523\,, \tag{4.6}$$

and $C_{8G}^{\rm SM}$ does only contribute via RG induced mixing. In principle, one also has to add the primed operators $Q'_{7\gamma}$ and $Q'_{8G}$ to (4.3). The primed operators are derived from $Q_{7\gamma}$ and $Q_{8G}$ by replacing $P_R$ by $P_L$. In the SM, the primed operators are suppressed by a factor $m_s/m_b$ and can be neglected at the current level of precision. Later in this section, we discuss why they are also negligible in the LRM and SM4. The branching ratio of $B \to X_s\gamma$ is given by the simple formula [204]

$$\begin{aligned}\mathrm{Br}(B \to X_s\gamma) &= R \left( |C_{7\gamma}(\mu_b) + \Delta C_{7\gamma}|^2 + \underbrace{\left|C'_{7\gamma}(\mu_b)\right|^2}_{\approx\mathcal{O}(m_s^2/m_b^2,\varepsilon^4)} + N(E_\gamma) \right) , \\ &= \mathrm{Br}(B \to X_s\gamma)_{\rm SM} + \Delta\mathrm{Br}(B \to X_s\gamma)\,,\end{aligned} \tag{4.7}$$

with $R = 2.47 \cdot 10^{-3}$ [195–197] and a small correction $N(E_\gamma) = (3.6 \pm 0.6) \cdot 10^{-3}$ corresponding to the photon-energy cut-off $E_\gamma > 1.6\,\mathrm{GeV}$ in the $B$ meson rest frame [196]. The corrections $\Delta C_{7\gamma}(\mu_b)$ and $\Delta C_{8\gamma}(\mu_b)$ are of course model dependent. A more general discussion on this topic can be found in [204]. Here, we will only discuss the cases relevant for our analysis. Note that

- in the following we set $\mu_b$ to the value used in the SM calculations [195–197]

$$\mu_b = 2.5\,\mathrm{GeV}\,; \tag{4.8}$$

- in case $V^{\rm L}$ differs from its SM fit, the coefficient $R$ in (4.7) has to be replaced by $r_{bs\gamma}R$, with $r_{bs\gamma}$ defined as

$$r_{bs\gamma} = \frac{|V_{cb}^{\rm L}|^2_{\rm SM}}{|V_{cb}^{\rm L}|^2} \frac{|\lambda_t^{(s)}|^2}{|\lambda_t^{(s)}|^2_{\rm SM}}\,. \tag{4.9}$$

### $\mathrm{Br}(B \to X_s\gamma)$ in the SM4

The addition of a fourth generation does not change the overall structure of the calculation for the decay $b \to s\gamma$. At LO, the addition of a heavier top-like quark and its appearance in the loop adds a SM top like contribution at a higher scale. Consequently, the LO correction is given by

$$\Delta C_{7\gamma}(\mu_b) = -\frac{1}{2}\frac{\lambda_{t'}^{(s)}}{\lambda_t^{(s)}} \left(\kappa_7 D'_0(x_{t'}) + \kappa_8 E'_0(x_{t'})\right)\,, \tag{4.10}$$

where the magic numbers $\kappa_{7,8}$ describe the RG evolution from $\mu_{t'}$ down to $\mu_b$ and are given in table 4.1. The master-functions $E'_0$ and $D'_0$ are given in Appendix 8. Substituting (4.10) into equation (4.7), we find

$$\mathrm{Br}(B \to X_s\gamma) = r_{bs\gamma}\mathrm{Br}(B \to X_s\gamma)_{\rm SM} + r_{bs\gamma}R\left(2C_{7\gamma}^{\rm SM}(\mu_b)\,\mathrm{Re}\left(\Delta C_{7\gamma}(\mu_b)\right) + |\Delta C_{7\gamma}(\mu_b)|^2\right)\,. \tag{4.11}$$

From (4.11), we can immediately conclude that

| $\mu_R$ | 200 GeV | 1 TeV | 2.5 TeV | 10 TeV | 15 TeV |
|---|---|---|---|---|---|
| $\kappa_7$ | 0.524 | 0.457 | 0.427 | 0.390 | 0.380 |
| $\kappa_8$ | 0.118 | 0.125 | 0.128 1 | 0.130 | 0.130 |
| $\kappa_{\rm LR}$ | 0.473 | 0.665 | 0.778 | 0.953 | 1.005 |
| $\rho_8$ | 0.568 | 0.504 | 0.475 | 0.439 | 0.429 |
| $\rho_{\rm LR}$ | -0.064 | -0.052 | -0.043 | -0.025 | -0.019 |
| $\tilde{\kappa}_7$ | 0.981 | 0.857 | 0.801 | 0.731 | 0.712 |
| $\tilde{\kappa}_8$ | 0.006 | 0.044 | 0.060 | 0.078 | 0.082 |
| $\tilde{\kappa}_{\rm LR}$ | 0.006 | 0.063 | 0.099 | 0.156 | 0.175 |
| $\tilde{\rho}_8$ | 0.984 | 0.874 | 0.824 | 0.760 | 0.743 |
| $\tilde{\rho}_{\rm LR}$ | -0.005 | -0.033 | -0.044 | -0.056 | -0.058 |

Table 4.1: *The NP magic numbers for* $\Delta C_{7\gamma}^{\rm LR}$ *and* $\Delta C_{8G}^{\rm LR}$ *at* $\mu_b = 2.5\,\text{GeV}$ *and* $\mu_t(m_t)$.

- the strictly positive contribution $|\Delta C_{7\gamma}(\mu_b)|^2$ is small in most cases, because $\kappa_{7,8}$, $D_0'$ and $E_0'$ are all smaller than 1, while $|\lambda_{t'}^{(s)}/\lambda_t^{(s)}|$ is at least of the order $\mathcal{O}(\lambda)$. The parameter $\lambda$ denotes the Wolfenstein [205] parameter $\lambda$ defined in equation (5.1).

- the sign and size of the dominant correction is determined by the sign and size of $\text{Re}\left(\lambda_{t'}^{(s)}/\lambda_t^{(s)}\right)$.

- only a logarithmic enhancement in dependence on the mass $m_{t'}$ is possible. This is dictated by the behaviour of $D_0'$ and $E_0'$ as functions of $m_{t'}$. For $m_{t'} < 1\,\text{TeV}$, this enhancement is partly cancelled by the dependence of $\kappa_{7,8}$ on the high mass scale, while for $m_{t'} > 1\,\text{TeV}$ the suppression from $\kappa_{7,8}$ becomes equally large as the enhancement through the master functions and $\Delta C_{7\gamma}(\mu_b)$ as a function of $m_{t'}$ shows an asymptotic behaviour.

- the coefficient $r_{bs\gamma}$ can modify the SM part of the branching ratio as well as the NP part. However, $r_{bs\gamma}$ is correlated with $\lambda_{t'}^{(s)}$ through the $\Delta F = 2$ constraints and there are no direct insights to be gained.

Concerning primed operators, it is clear from the above that the addition of a fourth family will not change the SM suppression mechanism in this case. The SM4 introduces no new couplings of SM quarks to gauge bosons and thereby no way to enhance the primed operators.

Our approach, as outlined above, is very different to the existing calculations present in the literature [100, 150, 206–211]. We chose to employ the improved SM predictions and treat the SM4 effects as perturbations, while traditionally all contributions have been treated equally. However, in most studies the SM prediction was not as precise as it is today and even more importantly the possible 3 – 4 mixing was not known to be as constrained as found in [96,98,99] and section 6.3.

### $\mathbf{Br}(\boldsymbol{B \to X_s\gamma})$ in the LRM

Changing the gauge structure of the model introduces various new effects in the decay $b \to s\gamma$. Many authors have studied the decay $B \to X_s\gamma$ in the context of models with a $\text{SU}(2)_\text{L} \times$

$\mathrm{SU}(2)_\mathrm{R} \times \mathrm{U}(1)_\mathrm{X}$ gauge symmetry in the past [212–223] and we will use their findings in this analysis. The new contributions in the LRM can be divided into two distinct classes.

1. Gauge contribution: This is the contribution traditionally studied in the literature [215, 222]. In the SM, the LH structure of the $W^\pm$ couplings to quarks requires the necessary chirality flip, for the transition $b \to s\gamma$, to occur via the mass of the initial or the final state quark. Consequently the amplitude is proportional to either $m_b$ or $m_s$. In models with charged gauge bosons with both LH and RH couplings, the chirality flip can occur on the internal top quark line resulting in an enhancement factor $m_t/m_b$ of the NP contribution relative to the SM one at the level of the amplitude.

2. Higgs contribution: This contribution is mediated by the exchange of charged Higgs bosons instead of weak gauge bosons. Although the Higgs mass is of the order of $\kappa_R$ and usually larger then 10 TeV, the Higgs effects cannot be neglected. The relative importance of the Higgs contributions is, on the one hand, founded by an $m_t/m_b$ enhancement of the resulting amplitude [216–219, 221]. And on the other hand by the fact that, in contrast to the gauge contributions, the Higgs contributions do not suffer from small $W_L$–$W_R$-mixing-induced couplings. We show that, even for Higgs masses above 10 TeV, the Higgs contribution cannot be neglected and can in fact be dominant for certain ranges of the relevant parameters.

In the following, we keep the phase $\alpha$. However, as already pointed out in section 2.2 this phase is redundant in the case of a general RH mixing matrix $V^\mathrm{R}$.

### The Gauge Contribution

As described in the beginning of this section, we collect all new contributions into one correction $\Delta C_{7\gamma}$. The gauge boson contribution at the scale $\mu_b$ is given by [215]

$$\Delta C_{7\gamma}(\mu_b) = \kappa_7(\mu_R)\Delta^\mathrm{LR} C_{7\gamma}(\mu_R) + \kappa_8(\mu_R)\Delta^\mathrm{LR} C_{8G}(\mu_R) + \kappa_\mathrm{LR}(\mu_R) A^{cb}\,, \tag{4.12}$$

where the QCD factors $\kappa_{7,8}$, connected to the RG evolution from $\mu_R$ down to $\mu_b$, are given in table 4.1. The corrections to $\Delta^\mathrm{LR} C_{7\gamma}$ and $\Delta^\mathrm{LR} C_{8G}$ are given by [215]

$$\Delta^\mathrm{LR} C_{7\gamma}(\mu_R) = -\frac{1}{2} A^{tb} \tilde{D}'_0(x_t)\,, \qquad \Delta^\mathrm{LR} C_{8G}(\mu_R) = -\frac{1}{2} A^{tb} \tilde{E}'_0(x_t)\,, \tag{4.13}$$

where the master-functions $\tilde{D}'_0$ and $\tilde{E}'_0$ are given in Appendix 8. The factors $A^{ib}$ $(i = u, c, t)$ read

$$A^{ib} = \frac{m_i}{m_b} sc\epsilon^2 e^{i\alpha} \left(\frac{V^\mathrm{R}_{ib}}{V^L_{tb}}\right)\,, \tag{4.14}$$

and include the aforementioned enhancement factor $m_t/m_b$ in the case of $i \equiv t$. In equation (4.14), the $\overline{\mathrm{MS}}$ masses $\bar{m}_i(\mu)$ and $\bar{m}_b(\mu)$ have to be evaluated at $\mu = m_i$ and $\mu = \mu_b$ respectively. Note that traditionally $A^{tb}$ is expressed in terms of the left–right mixing angle $\zeta$ and the misalignment $r$ of $g_L$ and $g_R$. This notation can be recovered by replacing $sc\epsilon^2 e^{i\alpha}$ by $\sqrt{r}\zeta$ with $\zeta$ and $r$ defined in (7) and (3.55). The last term in equation (4.12) is related to the

non-vanishing initial condition $C_{10}(\mu_R) = A^{cb}$ for the Wilson coefficient $C_{10}$ corresponding to the new operator [215]

$$O_{10} = \frac{m_b}{m_c} (\bar{s}_\alpha \gamma_\mu P_L c_\alpha) (c_\beta \gamma^\mu P_R b_\beta) \,. \tag{4.15}$$

This is similar to the term induced by the non-vanishing Wilson coefficient $C_2(\mu_W) = 1$ in the SM. Note there is a small correction to $\Delta C_{7\gamma}(\mu_b)$ related to the charm contribution in $\Delta^{\mathrm{LR}} C_{7\gamma}(\mu_R)$ which has been neglected in [215] (and derived work). This correction reads

$$\Delta^{\mathrm{LR,charm}} C_{7\gamma}(\mu_R) \approx -\frac{5}{3} A^{cb} \,, \tag{4.16}$$

where the factor $5/3$ arises from taking the limit $x_c \to 0$ in $-\frac{1}{2}\tilde{D}'_0(x_c)$. This contribution introduces a small correction of the same order as the last term in equation (4.12).

### The Higgs Contribution

The charged Higgs contribution to $\mathrm{Br}(B \to X_s\gamma)$ has been calculated in [216, 221]. We use the results given in [216, 221], adapting their formulae to match our notation and overall normalisation conventions. Neglecting the charged Higgs contributions to $C_{8G}(\mu_H)$ we have [216, 221]

$$\Delta^{\mathrm{H}^\pm} C_{7\gamma}(\mu_R) = -u(s) \frac{\kappa_7(\mu_H)}{\kappa_7(\mu_R)} \left[ \frac{m_t}{m_b} sc e^{i\alpha} \left( \frac{V_{tb}^{\mathrm{R}}}{V_{tb}^{\mathrm{L}}} \right) A_H^{(1)}(y) + 2s^2 c^2 A_H^{(2)}(y) \right] \,, \tag{4.17}$$

where the function $u(s)$ has been defined in (3.57). The parameter $y$ is given by $y = m_t^2/M_H^2$ and the functions $A_H^i$ by [221]

$$A_H^{(1)}(y) = \frac{3y^2 - 2y}{3(1-y)^3} \ln(y) + \frac{5y^2 - 3y}{6(1-y)^2} \,, \tag{4.18}$$

$$A_H^{(2)}(y) = \frac{1}{3} D'_0(y) - A_H^{(1)}(y) \,. \tag{4.19}$$

The master-function $D'_0$ can again be found in Appendix 8. Let us come to some comments on the charged Higgs contribution given in equation (4.17):

- In the above we have to use $m_t = m_t(\mu_H)$, because the scale is set by the heavy charged Higgs.
- The charged Higgs contribution can be subject to a very strong enhancement in the case of $s \to 1/\sqrt{2}$. This is similar to the $\tan(\beta)$ enhancement in common SUSY models [200,201] or the 2HDM [198].
- The full contribution $\Delta^{\mathrm{LRM}} C_{7\gamma}(\mu_R)$ can be found by adding (4.17) and (4.13). The result can be inserted in (4.12) without further modifications.
- For $M_H > 10\,\mathrm{TeV}$, the term proportional to $D'_0(y)$ in equation (4.17) is smaller than $A_H^1(y)$ by at least two orders of magnitude. We can therefore approximate the Higgs contribution for $M_H > 10\,\mathrm{TeV}$ to be

$$\Delta^{H^\pm} C_{7\gamma}(\mu_R) \approx -u(s) sc \frac{\kappa_7(\mu_H)}{\kappa_7(\mu_R)} \left[ \frac{m_t}{m_b} e^{i\alpha} \left( \frac{V_{tb}^{\mathrm{R}}}{V_{tb}^{L}} \right) - 2sc \right] A_H^1(y) \,. \tag{4.20}$$

  As long as $\mathrm{Re}(V_{tb}^{\mathrm{R}}) \sim \mathcal{O}(1)$, the first term in (4.20) dominates this expression due to its $m_t/m_b$ enhancement.

### Primed Operators and other Contributions

In the LRM we potentially have several additional contributions to the amplitude.

- New LL and RR contributions: At the order $\epsilon^2$, the LRM does not introduce new LL contributions to the coupling of $W^\pm$ to quarks. It does, however, introduce RR contributions through the exchange of heavy $W'^\pm$ bosons. These new contributions, in contrast to the ones discussed up to now, are not $m_t/m_b$ enhanced. They are also governed by the SM master functions $D'_0$ and $E'_0$ which are strongly suppressed if $x_t = m_t^2/M_W^2$ is replaced by $\tilde{x}_t = m_t^2/M_{W'}^2$. This is similar to our arguments leading to (4.20).

- Primed operators: The LR corrections to $C'_{7\gamma}$ and $C'_{8G}$ are $m_t/m_b$ enhanced like the unprimed ones and also present at order $\epsilon^2$ in the amplitude. However, since the SM contribution to $C'_{7\gamma}$ and $C'_{8G}$ is very small, interference between the LRM contribution and the SM contribution does not introduce $\mathcal{O}(\varepsilon^2)$ terms and therefore $C'_{7\gamma}$ and $C'_{8G}$ appear only at $\mathcal{O}(\epsilon^4)$ in the branching ratio.

### The Full LRM Contributions to Br($B \to X_s\gamma$)

In conclusion to this section we present the full NP contribution to $\mathrm{Br}(B \to X_s\gamma)$ in the LRM

$$\begin{aligned}\Delta^{\mathrm{LRM}} C_{7\gamma}(\mu_b) = \kappa_7(\mu_R) \left[\Delta^{\mathrm{LR}} C_{7\gamma}(\mu_R) + \Delta^{H^\pm} C_{7\gamma}(\mu_R)\right] \\ + \kappa_8(\mu_R)\Delta^{\mathrm{LR}} C_{8G}(\mu_R) + \kappa_{\mathrm{LR}}(\mu_R) A^{cb}\,.\end{aligned} \tag{4.21}$$

In the case of the LRM, the correction factor $r_{bs\gamma}$ deviates from unity by only $\pm 2\%$. As this is below the precision of the theoretical prediction and mostly accounted for by the parametric uncertainty therein, we neglect the correction introduced by $r_{bs\gamma}$ in the context of the LRM. Consequently, the full correction to the branching ratio is given by

$$\Delta\mathrm{Br}(B \to X_s\gamma) = 2RC_{7\gamma}^{\mathrm{SM}}(\mu_b)\ \mathrm{Re}(\Delta C_{7\gamma}(\mu_b)) + \mathcal{O}(\varepsilon^4)\,. \tag{4.22}$$

From equation (4.22), by inspecting (4.12), (4.13), and (4.17), we can deduce that:

- The sign of $\Delta\mathrm{Br}(B \to X_s\gamma)$ is equal to the sign of $\mathrm{Re}V_{tb}^{\mathrm{R}}$ and thereby closely related to the phase $\phi_{tb}$ of $V_{tb}^{\mathrm{R}}$. This holds true as long as the RH mixing matrix has no 'exotic' structure, e.g $|V_{tb}^{\mathrm{R}}| \ll 1$ where the sign of $\mathrm{Re}V_{cb}^{\mathrm{R}}$ would become more important. In case of $\mathrm{Im}(V_{tb}^{\mathrm{R}}) \sim 1$, the last term in the charged Higgs contribution (4.17) introduces effects in dependence on $s$ (see figure 4.2 for a more detailed picture). Note that the phase $\alpha$ can be absorbed into the RH mixing matrix as discussed in section 2.2.

- the relative importance of the gauge and charged Higgs contribution depends on $s$ and the Higgs mass $M_H$. In figure 4.1, we show this behaviour for $V_{tb}^{\mathrm{R}} = 1$ as a function of $M_H$ and of different values of $s$ and $M_{W'}$. We can see that the charged Higgs contribution is important for $M_H < 10\,\mathrm{TeV}$ even for $s = 0.1$. For $M_H > 10\,\mathrm{TeV}$ and a realistic mass $M_{W'} > 2\,\mathrm{TeV}$, the charged Higgs contribution is even more important over a large range of values for $M_H$. For $s = 0.5$, the charged Higgs contribution is visibly enhanced, as can be seen from the plot in the right panel of figure 4.1.

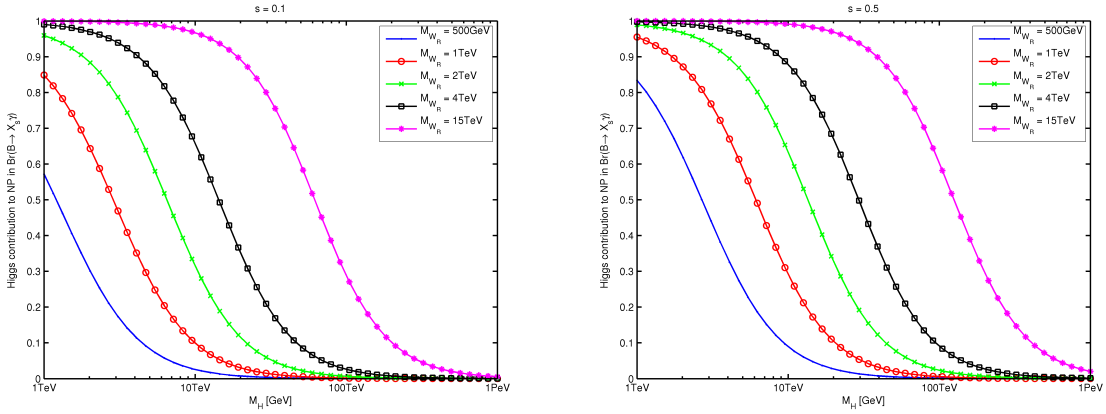


Figure 4.1: The relative importance of the charged Higgs contribution to $\mathrm{Br}(B \to X_s\gamma)$ in the LRM as a function of $M_H$, in the left panel we show the situation for $s = 0.1$ while the same plot is shown for $s = 0.5$ in the right panel.

- The size of the new contributions relative to the SM one can be used to put bounds on the electroweak parameter $s$ as well as the Higgs mass $M_H$. In figure 4.2, we show $|\Delta\mathrm{Br}(B \to X_s\gamma)|/\mathrm{Br}(B \to X_s\gamma)_{\mathrm{SM}}$ as a function of $M_H$ for different values of $V_{tb}^{\mathrm{R}}$ and $s$. We can see that $s = 0.7$, for $M_H < 40\,\mathrm{TeV}$, can be excluded by $\mathrm{Br}(B \to X_s\gamma)$ alone. It is also evident from figure 4.2 that for $s = 0.1$ the LRM effect on $\mathrm{Br}(B \to X_s\gamma)$ cannot exceed a few percent for $M_H > 10\,\mathrm{TeV}$. Furthermore, only in the case of a big and mostly real $V_{tb}^{\mathrm{R}}$ the effects can exceed 20% for $M_H$ of the order of a few times 10 TeV and $s \leq 0.6$.

## 4.2 The CP Averaged Branching Ratio $\langle \mathrm{Br}(B \to X_d\gamma)\rangle$

While the decay $B \to X_s\gamma$ is a well established benchmark for any NP model, the decay $B \to X_d\gamma$ has only recently been recognised as a promising constraint. This can be easily understood because only recently it has been shown that the CP averaged branching ratio of $b \to d\gamma$ is subject to only small hadronic uncertainties [224]. Furthermore, the experimental data has become more reliable. The measurement of the CP-averaged branching ratio yields [54]

$$\langle \mathrm{Br}(B \to X_d\gamma)\rangle = (1.41 \pm 0.49) \cdot 10^{-5}\,, \tag{4.23}$$

which has to be compared with the most recent next-to-leading-logarithm (NLL) SM prediction [141]

$$\langle \mathrm{Br}(B \to X_d\gamma)\rangle_{\mathrm{SM}} = (1.54^{+0.26}_{-0.31}) \cdot 10^{-5}\,. \tag{4.24}$$

From (4.23) and (4.24), it is clear that the calculations for $\langle \mathrm{Br}(B \to X_d\gamma)\rangle$ have a long way to go until the precision of $B \to X_s\gamma$ is reached. On the experimental side there is also much room for improvement. However, as has been shown in [141], the current data and prediction still yield some interesting constraints on extensions of the SM. For our treatment of $\langle \mathrm{Br}(B \to X_d\gamma)\rangle$, we

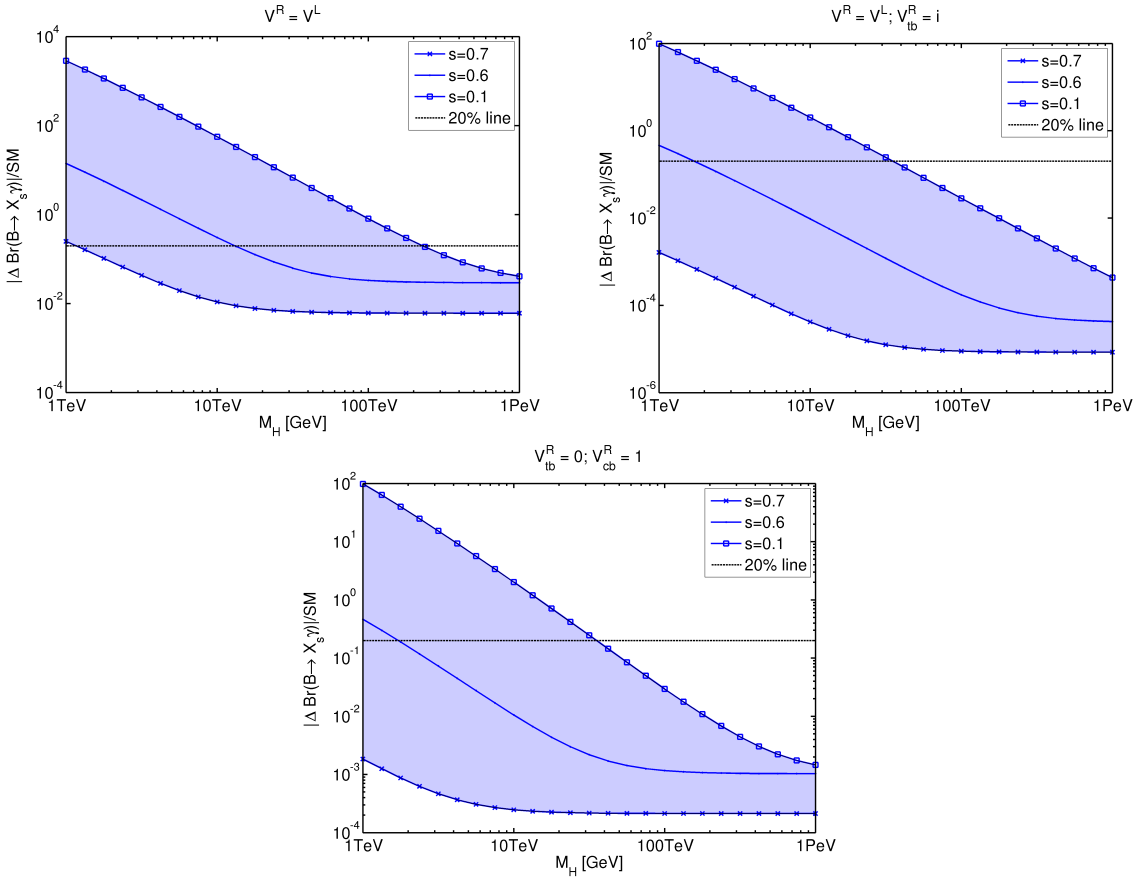


Figure 4.2: The normalised NP contribution $|\Delta\mathrm{Br}(B \to X_s\gamma)|/\mathrm{Br}(B \to X_s\gamma)_{\mathrm{SM}}$ as a function of $M_H$ for different values of $V_{tb}^{\mathrm{R}}$ and $s$. In the top panel we show, on the left the case for $V_{tb}^{\mathrm{R}} = 1$ and on the right the case for $V_{tb}^{\mathrm{R}} = i$. In the bottom panel we show the case for $V_{tb}^{\mathrm{R}} = 0$. The dashed black line in all plots indicates the 20% contribution. In all plots three different values of $s$ are shown explicitly while the shaded area depicts all values of $s = 0.1 \ldots 0.7$

closely follow [225]. In the presence of NP, the branching ratio $\langle \mathrm{Br}(B \to X_d\gamma)\rangle$ can be written as [225]

$$\langle \mathrm{Br}(B \to X_d\gamma)\rangle = \frac{\mathcal{N}}{100}\left|\frac{(V_{td}^{\mathrm{L}})^* V_{tb}^{\mathrm{L}}}{V_{cb}^{\mathrm{L}}}\right|^2 (\tilde{a} + P_7 + P_8 + P_{78})\,, \tag{4.25}$$

where $\mathcal{N} \approx 2.6 \cdot 10^{-31}$ and

$$\tilde{a} = a + a_{\epsilon\epsilon} + a_\epsilon^r\ \mathrm{Re}(\epsilon_d)\,, \tag{4.26a}$$
$$P_7 = a_{77}\ |R_7|^2 + a_7^r\ \mathrm{Re}(R_7) + a_{7\epsilon}^r\ \mathrm{Re}(R_7\epsilon_d^*)\,, \tag{4.26b}$$
$$P_8 = a_{88}\ |R_8|^2 + a_8^r\ \mathrm{Re}(R_8) + a_{8\epsilon}^r\ \mathrm{Re}(R_8\epsilon_d^*)\,, \tag{4.26c}$$
$$P_{78} = a_{78}^r\ \mathrm{Re}(R_8 R_7^*)\,. \tag{4.26d}$$

[1] In principle we have to replace $\mathcal{N}$ by $\mathcal{N}|V_{cb}^{\mathrm{L}}/V_{ub}^{\mathrm{L}}|^2|V_{ub}^{\mathrm{L}}/V_{cb}^{\mathrm{L}}|_{\mathrm{SM}}^2$. However, the changes in $V_{ub}^{\mathrm{L}}$ and $V_{cb}^{\mathrm{L}}$ are directly constrained by the tree-level determinations and we can therefore neglect this subtlety as the error on $V_{ub}^{\mathrm{L}}/V_{cb}^{\mathrm{L}}$ is already included in the uncertainty on $\mathcal{N}$.

| $a$ | $a_{\epsilon\epsilon}$ | $a_\epsilon^r$ | $a_{77}$ | $a_7^r$ | $a_{7\epsilon}^r$ | $a_{88}$ | $a_8^r$ |
|---|---|---|---|---|---|---|---|
| 7.8221 | 0.4384 | −1.6981 | 0.8161 | 4.8802 | −0.7827 | 0.0197 | 0.5680 |

| $a_{8\epsilon}^r$ | $a_{87}^r$ | $a_7^i$ | $a_8^i$ | $a_\epsilon^i$ | $a_{87}^i$ | $a_{7\epsilon}^i$ | $a_{8\epsilon}^i$ |
|---|---|---|---|---|---|---|---|
| −0.0601 | 0.1923 | 0.3546 | −0.0987 | 2.4997 | −0.0487 | −0.9067 | −0.0661 |

Table 4.2: *The relevant $a_i^j$ parameters from [225].*

The values of the parameters $a_i$ can be found in table 4.2 and $R_{7,8}$ are defined as

$$R_7 = \frac{C_{7\gamma}^{\mathrm{tot}}(\mu_t)}{C_{7\gamma}^{\mathrm{SM}}(\mu_t)}\,, \qquad\qquad R_8 = \frac{C_{8G}^{\mathrm{tot}}(\mu_t)}{C_{8\gamma}^{\mathrm{SM}}(\mu_t)}\,, \tag{4.27}$$

where $C_{7\gamma}^{\mathrm{tot}}(\mu_t)$ and $C_{8G}^{\mathrm{tot}}(\mu_t)$ are the total Wilson coefficients, including the SM contribution, evaluated at $\mu_t$. The coefficient $\epsilon_d$ is defined as

$$\epsilon_d = \frac{(V_{ud}^{\mathrm{L}})^* V_{ub}^{\mathrm{L}}}{(V_{td}^{\mathrm{L}})^* V_{tb}^{\mathrm{L}}}\,. \tag{4.28}$$

The CP averaged branching ratio for $b \to s\gamma$ can easily be found by replacing $d \to s$ in (4.25), (4.28), and (4.26a) - (4.26d).

### $\langle \mathbf{Br}(\boldsymbol{B \to X_d\gamma})\rangle$ in the SM4

In the SM4, the contributions to $C_{7\gamma}$ and $C_{8G}$ can again be derived from the SM LO formulae. Including the QCD running from $\mu_{t'}$ to $\mu_t$, the corrections to the Wilson coefficients read

$$\Delta C_{7\gamma} = -\frac{1}{2}\frac{\lambda_{t'}^{(d)}}{\lambda_t^{(d)}}\left(\tilde\kappa_7(\mu_{t'})D_0'(x_{t'}) + \tilde\kappa_8(\mu_{t'})E_0'(x_{t'})\right)\,, \tag{4.29}$$

$$\Delta C_{8G} = -\frac{1}{2}\frac{\lambda_{t'}^{(d)}}{\lambda_t^{(d)}}\tilde\rho_8(\mu_{t'})E_0'(x_{t'})\,, \tag{4.30}$$

where the QCD factors $\tilde\kappa_{7,8}$ and $\tilde\rho_8$ describe the running from $\mu_{t'}$ to $\mu_t$ and can be found in table 4.1. The master functions $D_0'$ and $E_0'$ are already known from our discussion on $b \to s\gamma$ and given in Appendix 8. If we divide the expression in equation (4.25) into a SM and one NP part

$$\langle \mathrm{Br}(B \to X_d\gamma)\rangle = \langle \mathrm{Br}(B \to X_d\gamma)\rangle_{\mathrm{SM}} + \Delta\langle \mathrm{Br}(B \to X_d\gamma)\rangle\,, \tag{4.31}$$

we find that the leading contribution to $\Delta\langle \mathrm{Br}(B \to X_d\gamma)\rangle$ can be written as

$$\Delta\langle \mathrm{Br}(B \to X_d\gamma)\rangle = \frac{\mathcal{N}\, a_7^r}{100}\left|\frac{\lambda_t^{(d)}}{V_{cb}^{\mathrm{L}}}\right|^2 \frac{\tilde\kappa_7(\mu_{t'})D_0'(x_{t'}) + \tilde\kappa_8(\mu_{t'})E_0'(x_{t'})}{D_0'(x_t)}\,\mathrm{Re}\left(\frac{\lambda_{t'}^{(d)}}{\lambda_t^{(d)}}\right)\,. \tag{4.32}$$

The sign of the leading, new contribution, given in (4.32), is governed by the sign of $\mathrm{Re}\left(\lambda_{t'}^{(d)}/\lambda_t^{(d)}\right)$. While equation (4.32) is only an approximation, we can expect a correlation between $\Delta\langle \mathrm{Br}(B \to X_d\gamma)\rangle$ and $\mathrm{Re}\left(\lambda_{t'}^{(d)}/\lambda_t^{(d)}\right)$. However, as long as $\lambda_{t'}^{(d)}/\lambda_t^{(d)}$ and $\lambda_{t'}^{(s)}/\lambda_t^{(s)}$ are not or only mildly correlated, we would not expect to find a correlation between the corrections to the branching ratios $\mathrm{Br}(B \to X_s\gamma)$ and $\mathrm{Br}(B \to X_d\gamma)$.

### $\langle \mathrm{Br}(B \to X_d\gamma)\rangle$ in the LRM

Similar to the discussion of $\Delta\mathrm{Br}(B \to X_s\gamma)$ in the LRM, the corrections to $\Delta\langle\mathrm{Br}(B \to X_d\gamma)\rangle$ originate from two different sources:

1. The $W_L$–$W_R$ mixing induced LR contributions
2. The contributions due to the exchange of a heavy charged Higgs particle

Following [225], we have to evaluate $C_{7\gamma}$ and $C_{8G}$ at $\mu_t$. This can be achieved by replacing $\kappa_{7,8,\mathrm{LR}}$ in (4.12) and (4.17) by $\tilde{\kappa}_{7,8,\mathrm{LR}}$ given in table 4.1. The missing correction to $C_{8G}$ is given by

$$\Delta^{\mathrm{LR}} C_{8G}(\mu_t) = \tilde{\rho}_8(\mu_t)\Delta C_{8G}(\mu_R) + \tilde{\rho}_{\mathrm{LR}} A^{cb}\,, \tag{4.33}$$

where the QCD factors $\tilde{\rho}_{8,\mathrm{LR}}$ can be found in table 4.1 and $\Delta C_{8G}(\mu_R)$ is defined in (4.13). As both corrections $\Delta\mathrm{Br}(B \to X_s\gamma)$ and $\Delta\mathrm{Br}(B \to X_d\gamma)$ are proportional to the same RH mixing matrix elements, we expect a correlation between the predictions for both branching ratios. *Crivellin et al.* [141] argued that primed operators in models with RH currents could help constrain the RH $t$–$d$ coupling. They found a bound approximately 3.5 times stronger as what was found for a 'best-fit' solution in [128] where this constraint was not taken into account. In this work we argue that primed operators do not contribute (see section 4.1). This does not contradict [141] as their bound can be expressed as

$$sc\epsilon^2 \left|V_{tb}^{\mathrm{R}}\right| \leq 1.4 \cdot 10^{-4}\,, \tag{4.34}$$

in our notation. Our numerical analysis shows that $sc\epsilon^2 \lesssim 10^{-3}$ which translates (4.34) into the bound

$$|V_{tb}^{\mathrm{R}}| \simeq 0.14\,, \tag{4.35}$$

not taking into account the charged Higgs contributions. A naive estimate (3.85) as well as our numerical analysis show that this bound must be always fulfilled due to the very important constraint from $\varepsilon_K$. Furthermore, the constraints on $sc\epsilon^2$ and $|V_{tb}^{\mathrm{R}}|$ are not independent as with increasing $s$ the effects in $\varepsilon_K$ are increased as well. In turn, $|V_{tb}^{\mathrm{R}}|$ is even stronger constrained for large $s$.

## 4.3 CP Asymmetries in $B \to X_{s,d}\gamma$

The direct CP asymmetries in the decays $b \to q\gamma$, i.e. $A_{\mathrm{CP}}(b \to q\gamma)$ [226], are very sensitive to NP CP violating effects. In particular, the SM prediction $A_{\mathrm{CP}}(b \to s\gamma)_{\mathrm{SD}} \simeq +0.5\%$ [225] is very close to zero and could, similar to $S_{\psi\phi}$, provide conclusive proof of CP violation beyond the SM if large deviations from the SM predictions were found. The corresponding asymmetry in $b \to d\gamma$ is predicted to be much larger in the SM [225] but could provide an interesting cross-check. These asymmetries are defined as ($q = s, d$)

$$A_{\mathrm{CP}}(b \to q\gamma) \equiv \frac{\Gamma(\overline{B} \to X_{\bar{q}}\gamma) - \Gamma(B \to X_q\gamma)}{\Gamma(\overline{B} \to X_{\bar{q}}\gamma) + \Gamma(B \to X_q\gamma)}\,, \tag{4.36}$$

and have been studied by several authors in the past [227, 228] and more recently in [225]. Unfortunately, as pointed out in [229], these asymmetries, similar to other direct CP asymmetries like e.g. $A_{\mathrm{CP}}(B \to K\pi)$, suffer from hadronic uncertainties. Of course, this reduces the predictive power of the asymmetries $A_{\mathrm{CP}}(b \to q\gamma)$. In [229], it has been pointed out that $A_{\mathrm{CP}}(b \to s\gamma) < -2\%$ could be considered a signal of NP. In this work we investigate whether the SD part of the asymmetries could be strongly effected by the models in question. In the following we use the formulae provided in [225], which are compatible with [227, 228]. The general formula for the direct CP asymmetry in $b \to q\gamma$ is given by [225]

$$A_{\mathrm{CP}}(b \to q\gamma) = \frac{\mathcal{N}}{100} \left| \frac{(V_{tq}^{\mathrm{L}})^* V_{tb}^{\mathrm{L}}}{V_{cb}^{\mathrm{L}}} \right|^2 \frac{\mathrm{Im}\left(a_7^i R_7 + a_8^i R_8 + a_\epsilon^i \epsilon_q + a_{78}^i R_8 R_7^* + a_{7\epsilon}^i R_7 \epsilon_q^* + a_{8\epsilon}^i R_8 \epsilon_q^*\right)}{\langle \mathrm{Br}(B \to X_q\gamma)\rangle}\,, \tag{4.37}$$

where the coefficients $a_j^i$ can be found in table 4.2 and $R_7$, $R_8$ are defined in (4.27). The corrections $\Delta C_{7\gamma}$ and $\Delta C_{8G}$ can be found in the previous sections 4.1 and 4.2.

These CP asymmetries have been studied in the past in the context of the SM4 [230] as well as in the LRM [219].

## 4.4 The Inclusive Semi-Leptonic Rate $\mathbf{Br}(B \to X_s \ell^+ \ell^-)$

The decay $b \to s\ell^+\ell^-$ is obviously closely related to the decay $b \to s\gamma$. As already mentioned in the beginning of this chapter, we calculate this and the observables discussed below only in the SM4. The relevant effective Hamiltonian is given by [203, 231, 232]

$$\mathcal{H}_{\mathrm{eff}}(b \to s\ell^+\ell^-) = \frac{G_F}{\sqrt{2}} \lambda_t^{(s)} \left[ \sum_{i=1}^{10} C_i(\mu_b) Q_i \right], \tag{4.38}$$

where the operators $Q_i$ can be found in [231,232]. The NLO calculation yields the differential branching fraction [231, 232]

$$\begin{aligned} R(\hat{s}) = \frac{\alpha^2}{4\pi^2} \left| \frac{\lambda_t^{(s)}}{\lambda_c^{(s)}} \right|^2 \frac{(1-\hat{s})^2}{f(z)\kappa(z)} \Bigg[ (1+2\hat{s}) \left( \left| \bar{C}_9^{\mathrm{eff}} \right|^2 + \left| \bar{C}_{10}^{\mathrm{eff}} \right|^2 \right) + \\ 4 \left( 1 + \frac{2}{\hat{s}} \right) \left| C_7^{(0)\mathrm{eff}} \right|^2 + 12\,\mathrm{Re}\left( \bar{C}_9^{\mathrm{eff}} \left( C_7^{(0)\mathrm{eff}} \right)^* \right) \Bigg], \end{aligned} \tag{4.39}$$

where $\hat{s} = (q/m_b^{\mathrm{pole}})^2$. The functions $\kappa(z), f(z), C_7^{(0)\mathrm{eff}}, \bar{C}_9^{\mathrm{eff}}$ and $\bar{C}_{10}$ are given in [232]. For the integrated branching ratio the HFAG group [54] quotes

$$\mathrm{Br}(B \to X_s \ell^+ \ell^-)_{M(\ell^+\ell^-) > 0.2\,\mathrm{GeV}} = 3.66^{+0.77}_{-0.76} \cdot 10^{-6}\,. \tag{4.40}$$

However, due to the presence of resonances there is no rigorous theoretical prediction for the whole $q^2$ range. Instead, theory and experiment are compared for a high $q^2$ cut, $q^2 > 14.4\,\mathrm{GeV}^2$, and a low $q^2$ range, $1\,\mathrm{GeV}^2 < q^2 < 6\,\mathrm{GeV}^2$. The experimental measurements from BaBar [233]

and Belle [234] for both ranges are given by

$$\mathrm{Br}(B \to X_s \ell^+ \ell^-)_{1\,\mathrm{GeV}^2 < q^2 < 6\,\mathrm{GeV}^2} = \begin{cases} \left(1.493 \pm 0.504^{+0.411}_{-0.321}\right) \cdot 10^{-6} & \text{Belle} \\ (1.8 \pm 0.7 \pm 0.5) \cdot 10^{-6} & \text{BaBar} \\ (1.6 \pm 0.5) \cdot 10^{-6} & \text{Average} \end{cases} \tag{4.41}$$

$$\mathrm{Br}(B \to X_s \ell^+ \ell^-)_{q^2 > 14.4\,\mathrm{GeV}^2} = \begin{cases} \left(0.418 \pm 0.117^{+0.061}_{-0.068}\right) \cdot 10^{-6} & \text{Belle} \\ \left(0.5 \pm 0.25^{+0.08}_{-0.07}\right) \cdot 10^{-6} & \text{BaBar} \\ (0.44 \pm 0.12) \cdot 10^{-6} & \text{Average} \end{cases} \tag{4.42}$$

We use the averaged measurement for our numerical analysis. In the SM, the decay $b \to s\ell^+\ell^-$ has been studied at the NNLO level by various authors [235–240]. Furthermore, there are extensive studies on non-perturbative effects [241–244]. The NNLO SM prediction is given by [239]

$$\mathrm{Br}(B \to X_s \ell^+ \ell^-)_{\mathrm{SM}} = \begin{cases} (1.63 \pm 0.20) \cdot 10^{-6}\,, & 1\,\mathrm{GeV}^2 < q^2 < 6\,\mathrm{GeV}^2 \\ (0.404 \pm 0.078) \cdot 10^{-6}\,, & q^2 > 14.4\,\mathrm{GeV}^2 \end{cases} \tag{4.43}$$

which agrees quite well with the experimental averages. Of particular interest is the zero of the forward-backward asymmetry $A_{\mathrm{FB}}(b \to s\ell^+\ell^-)$ as a function of $\hat{s}$. The SM prediction, for $\hat{s}_0$, at the NNLO is given by [245]

$$\hat{s}_0 = 0.162 \pm 0.008\,. \tag{4.44}$$

We have checked numerically that the changes in $\hat{s}_0$ due to SM4 corrections are below 10% and thereby below the accuracy of the NLO calculation employed here. Our procedure to include effects from the fourth generation is straight forward. Using the formulae given in [180, 232], we replace

$$F(x_t) \to F(x_t) + \frac{\lambda_{t'}^{(s)}}{\lambda_t^{(s)}} F(x_{t'})\,, \tag{4.45}$$

with $F_0 = Y_0, Z_0, E_0, E_0', D_0'$. This procedure is also outlined in [180]. However, in doing so the slow running of $\alpha_s$ between $\mu_{t'}$ and $M_W$ is neglected. In our numerical analysis we included this effect for the sake of completeness. Furthermore, the NNLO contribution is known to be sizeable and negative [245]. In fact, this shift cannot be accommodated by shifting $\mu_b$ as can be done in the case of $b \to s\gamma$. Therefore, we rescale our NLO result to match the NNLO result [245] in the low and high $q^2$ region respectively.

In the context of the SM4 this decay has been studied by several authors [100, 211, 246–248]. Our ansatz, however, is to include all constraints while not introducing any assumptions on the particular form of the SM4 CKM matrix.

Some authors tried to estimate $\mathrm{Br}(B \to X_s\ell^+\ell^-)$ in the LRM [249,250] by taking only corrections to $C_7^{\mathrm{eff}}$ into account. However, we think this oversimplifies the situation as there is no clear dominance of $C_7^{\mathrm{eff}}$ even for low $q^2$. This is clear from equation (4.39). The leading term in (4.39) is $\mathcal{O}(1/\hat{s})$ but the next to leading term is $\mathcal{O}(1)$ and not $\mathcal{O}(\hat{s})$. Therefore, we cannot, *a-priori*, conclude a dominance of $C_7^{\mathrm{eff}}$.

## 4.5 The Inclusive Semi-Leptonic rate $\mathbf{Br}(B \to X_s \nu\bar{\nu})$

The decay of $B$ mesons into hadrons containing s-quarks and neutrinos provides a very interesting test of modified effective $Z^0$ couplings [251, 252]. However, the measurement of the branching ratio $\mathrm{Br}(B \to X_s \nu\bar{\nu})$ and its exclusive modes e.g. $\mathrm{Br}(B \to K^{(*)} \nu\bar{\nu})$ proves to be an experimental challenge. In fact, one of the arguments in favour of building Super-B factories is the prospect [253–255] of measuring $\mathrm{Br}(B \to X_s \nu\bar{\nu})$. Due to this, and its all around interesting features, $\mathrm{Br}(B \to X_s \nu\bar{\nu})$ and $\mathrm{Br}(B \to K^{(*)} \nu\bar{\nu})$ have been studied recently in great detail in the SM and beyond [256, 257]. In our analysis, we focus on the theoretically clean decays $B \to X_{s,d} \nu\bar{\nu}$. The SM prediction for the branching ratio of $B \to X_s \nu\bar{\nu}$ reads [257]

$$\mathrm{Br}(B \to X_s \nu\bar{\nu}) = (2.7 \pm 0.2) \cdot 10^{-5} \,. \tag{4.46}$$

In the SM, the relevant effective Hamiltonian for this decay is given by [203]

$$\mathcal{H}_{\text{eff}} = \frac{G_F}{\sqrt{2}} \frac{\alpha}{2\pi \sin^2 \theta_W} \sum_{\ell=e,\mu,\tau} \lambda_t^{(q)} X_0(x_t) \left(\bar{b} q\right)_{V-A} \left(\bar{\nu}_\ell \nu_\ell\right)_{V-A} \,, \tag{4.47}$$

with $q = s, d$ and the master function $X_0(x_t)$ given in Appendix 8. The SM4 introduces new contributions through the heavy $t'$ particle as well as the heavy charged 4G lepton $E$. These contributions can again be absorbed into a redefinition of the relevant master function.

$$X_0(x_t) \to X_q^\ell = X_0(x_t) + \frac{\lambda_{t'}^{(q)}}{\lambda_t^{(q)}} X_0(x_{t'}) + 4 \left|U_{\ell 4}\right|^2 \left( F^{\nu\bar{\nu}}(x_t, z_4) + \frac{\lambda_{t'}^{(q)}}{\lambda_t^{(q)}} F^{\nu\bar{\nu}}(x_{t'}, z_4) \right) \,, \tag{4.48}$$

where $z_\ell = \left(m_4^\ell\right)^2 / M_W^2$ is the lepton-sector equivalent of $x_i$ and the box function $F^{\nu\bar{\nu}}(x, z)$ is given in Appendix 8. In equation (4.47) and (4.48), we neglected the charm and $\tau$ contributions, which give only small corrections in the $B$ system. The elements $U_{\ell 4}$ of the lepton mixing matrix have to be small [84, 105] in order to fulfill all constraints in the lepton sector. Therefore we will drop the terms proportional to $|U_{\ell 4}|$ as well. As the improvements in the SM calculations [256, 257] also apply to the SM4, we consider the ratio

$$\frac{\mathrm{Br}(B \to X_s \nu\bar{\nu})}{\mathrm{Br}(B \to X_s \nu\bar{\nu})_{\text{SM}}} = \frac{1}{3} \frac{\sum_{\ell=1,2,3} \left|X_q^\ell\right|^2}{\left|X_0(x_t)\right|^2} \frac{\left|\lambda_t^{(q)}\right|^2}{\left|\lambda_t^{(q)}\right|^2_{\text{SM}}} \,. \tag{4.49}$$

The branching ratio is defined to include all three light neutrinos in the final state, as can be seen explicitly from equation (4.49). The last factor in (4.49) has to be introduced due to the fact that, in the SM4, $V_{tq}^{\text{L}}$ usually deviates from the SM value $\left(V_{\text{SM}}^{\text{L}}\right)_{tq}$. Furthermore, as the SM4 is a non MFV theory, as has been discussed in [105], the ratio

$$\frac{\mathrm{Br}(B \to X_d \nu\bar{\nu})}{\mathrm{Br}(B \to X_s \nu\bar{\nu})} = \frac{\sum_{\ell=1,2,3} \left|X_d^\ell\right|^2}{\sum_{\ell=1,2,3} \left|X_s^\ell\right|^2} \frac{\left|\lambda_t^{(d)}\right|^2}{\left|\lambda_t^{(s)}\right|^2} \frac{\left|\lambda_t^{(s)}\right|^2_{\text{SM}}}{\left|\lambda_t^{(d)}\right|^2_{\text{SM}}} \,, \tag{4.50}$$

does not measure $\left|V_{td}^{\text{L}} / V_{ts}^{\text{L}}\right|$ as it would in the SM. However, the ratio in equation (4.50) can be used to measure the departure from the MFV hypothesis. In the absence of RH couplings the relative change in the branching ratio as defined in (4.49) is also valid for the exclusive modes [256, 257].

## 4.6 The Leptonic Decay $B_{s,d} \to \mu^+\mu^-$

Currently, the most exciting rare decay, due to its experimental prospects at the LHC, is $B_s \to \mu^+\mu^-$. The projected sensitivity of the LHCb experiment is expected to reach the SM prediction within the near future. The current experimental upper limit [258]

$$\mathrm{Br}(B_s \to \mu^+\mu^-) < 4.5 \cdot 10^{-9} \qquad (95\%\ \mathrm{C.L.})\,, \tag{4.51}$$

is only slightly above our SM prediction (which has also been reported in [259])

$$\mathrm{Br}(B_s \to \mu^+\mu^-)_{\mathrm{SM}} = 3.33(17) \cdot 10^{-9}\,, \tag{4.52}$$

and its measurement is expected to provide another benchmark for any model of NP, as well as a sophisticated cross-check for the integrity of the SM. The even more suppressed decay $B_d \to \mu^+\mu^-$ remains out of the experimental reach in the near future, but will hopefully be discovered in this decade. The current upper limit [258]

$$\mathrm{Br}(B_d \to \mu^+\mu^-) < 1.03 \cdot 10^{-9} \qquad (95\%\ \mathrm{C.L.})\,, \tag{4.53}$$

is a factor of ten above our SM prediction

$$\mathrm{Br}(B_d \to \mu^+\mu^-)_{\mathrm{SM}} = 1.03(9) \cdot 10^{-10}\,. \tag{4.54}$$

Starting from the relevant effective Hamiltonian [203]

$$\mathcal{H}_{\mathrm{eff}}(B_q \to \mu^+\mu^-) = -\frac{G_F}{\sqrt{2}}\frac{\alpha}{2\pi \sin^2\theta_W}\lambda_t^{(q)} Y_0(x_t)\left(\bar{b}q\right)_{V-A}\left(\bar{\mu}\mu\right)_{V-A}\,, \tag{4.55}$$

we follow the same procedure as before and absorb the SM4 contributions in a redefinition of the master function $Y_0$ (which can be found in the Appendix 8). Including the effects of the heavy fourth generation neutrino $\nu_4$, we have

$$Y_0(x_t) \to Y_q = Y_0(x_t) + \frac{\lambda_{t'}^{(q)}}{\lambda_t^{(q)}} Y_0(x_{t'}) + |U_{4\mu}|^2 \left( F^{\mu\bar{\mu}}(x_t, y_4) + \frac{\lambda_{t'}^{(q)}}{\lambda_t^{(q)}} F^{\mu\bar{\mu}}(x_{t'}, y_4) \right)\,, \tag{4.56}$$

with $y_i = (m_i^\nu)^2/M_W^2$ and $F^{\mu\bar{\mu}}$ given in Appendix 8. The charm contribution and the term proportional to $|U_{4\mu}|^2$ can be safely neglected, as already discussed in section 4.5. Adapting the SM formula for the branching ratio $\mathrm{Br}(B_q \to \mu^+\mu^-)$ [203], we find

$$\mathrm{Br}(B_q \to \mu^+\mu^-) = \tau_{B_q} \frac{G_F^2 \alpha^2 \eta_Y^2}{16\pi^3 \sin^4\theta_W} F_{B_q}^2 m_\mu^2 m_{B_q} \sqrt{1 - \left(2\frac{m_\mu}{m_{B_q}}\right)^2} \left|\lambda_t^{(q)} Y_q\right|^2\,, \tag{4.57}$$

where $F_{B_q}$ is the $B_q$ meson decay constant and $\eta_Y$ the short distance QCD correction evaluated at $m_t = \bar{m}_t(m_t)$. In equation (4.57), we assumed $\eta_Y(m_t) \simeq \eta_Y(m_{t'})$. In [260], it was pointed out that in certain models (i.e. MFV based models) the uncertainty on the branching ratio can be substantially reduced by eliminating $F_{B_q}$. This can be achieved by exchanging the parameter $F_{B_q}$ for the measured value $\Delta M_q$. Although the SM4 is a non-MFV model this procedure can also be applied here. Eliminating $F_{B_q}$ in favour of $(\Delta M_q)_{\mathrm{exp}}$, we find

$$\mathrm{Br}(B_q \to \mu^+\mu^-) = C \frac{\tau_{B_q}}{\hat{B}_{B_q}} \frac{|Y_q|^2}{|S_q|} \left(\Delta M_q\right)_{\mathrm{exp}}\,, \tag{4.58}$$

where $(\Delta M_q)_{\rm exp}$ is given in table 7.1 and $\hat{B}_{B_q}$ is the RG invariant bag parameter related to the hadronic matrix element already discussed in section 3.1. The pre-factor $C$ is defined as

$$C = 6\pi \frac{\eta_Y^2}{\eta_B} \left( \frac{\alpha}{4\pi \sin^2 \theta_W} \right)^2 \frac{m_\mu^2}{M_W^2} = 4.39 \cdot 10^{-10}. \tag{4.59}$$

Both methods for calculating the branching ratio yield only slightly different results. Using equation (4.57), we find

$$\mathrm{Br}(B_d \to \mu^+\mu^-) = 1.07(8) \cdot 10^{-10}\,, \tag{4.60}$$

$$\mathrm{Br}(B_s \to \mu^+\mu^-) = 3.29(24) \cdot 10^{-9}\,, \tag{4.61}$$

which has to be compared with (4.52) and (4.54). Both determinations give very similar results in both the central value and the error. In the direct calculation the errors are dominated by the error on $F_{B_q}$ and the parametric errors introduced by $\lambda_t^{(q)}$, while in the result derived through (4.58) the error is dominated by the errors on $\tau_{B_q}$, $\eta_B$ and most importantly $\hat{B}_{B_q}$. From equations (4.57) and (4.58), it is obvious that the golden relation between $\mathrm{Br}(B_q \to \mu^+\mu^-)$ and $\Delta M_d/\Delta M_s$, valid in MFV models [261], gets modified by a factor

$$r = \left| \frac{Y_d}{Y_s} \right|^2 \left| \frac{S_s}{S_d} \right|\,, \tag{4.62}$$

which is generally different from unity. The golden relation now reads

$$\frac{\mathrm{Br}(B_d \to \mu^+\mu^-)}{\mathrm{Br}(B_s \to \mu^+\mu^-)} = \frac{\hat{B}_{B_s}}{\hat{B}_{B_d}} \frac{\tau_{B_d}}{\tau_{B_s}} \frac{\Delta M_d}{\Delta M_s} r\,. \tag{4.63}$$

This can be used to further distinguish the SM4 from (C)MFV models in our numerical analysis. This decay was also studied in [82] in the context of the SM4.

## 4.7 Time-Dependent CP Violation in $B \to \phi K_s$ and $B \to \eta' K_s$

The time-dependent CP asymmetry in the the decays of neutral $B_d^0$ mesons into final CP eigenstates $f$ can be written as

$$\mathcal{A}_f = S_f \sin(\Delta M\, t) + C_f \cos(\Delta M\, t)\,. \tag{4.64}$$

In the SM the the parameters $|S_f|$ and $C_f$ are predicted to be universal to a good accuracy for the transitions $\bar{b} \to \bar{q}q\bar{s}$ (with $q = c, s, d, u$). In terms of SM parameters, this implies

$$-\eta_f S_f \simeq \sin(2\beta)\,, \tag{4.65}$$

where $\eta_f = \pm 1$ is the CP eigenvalue of the final state $f$. Furthermore, the SM also predicts $C_f \simeq 0$. In this work, we closely follow [262] using their results for hadronic elements as well as their notation. Turning to models of NP, there are two different places NP effects can contribute[2]

[2] Assuming no significant contribution to the asymmetry in the tree-level transition $\bar{b} \to \bar{c}c\bar{s}$

1. in the $B_d$ mixing amplitude;
2. in the decay amplitudes $\bar{b} \to \bar{q}q\bar{s}$ [262–264].

In the first case all asymmetries are shifted away from $\sin 2\beta$ in a universal manner, while the $C_f$ parameters still vanish. In the second case $S_f$ and $C_f$ are generally different from their SM expectation in a non-universal way. In the following, we outline how we use [262] for our treatment of the SM4 contributions. Using [262], we can calculate the CP asymmetries $S_f$ and $C_f$ as

$$S_f = \frac{2\,\mathrm{Im}\left(\frac{\bar{A}_f}{A_f} e^{-2i\phi_{B_d}^{\mathrm{tot}}}\right)}{1 + \left|\frac{\bar{A}_f}{A_f}\right|^2}, \qquad C_f = \frac{1 - \left|\frac{\bar{A}_f}{A_f}\right|^2}{1 + \left|\frac{\bar{A}_f}{A_f}\right|^2}, \tag{4.66}$$

where $A_f$ and $\bar{A}_f$ are the relevant decay amplitudes and $\phi_{B_d}^{\mathrm{tot}}$ is the phase in the $B_d$ mixing amplitude as defined in (3.63). The decay amplitude $A_f$ ($\bar{A}_f$) can be calculated from the effective Hamiltonian relevant for non-leptonic $\Delta B = 1$ decays [262]

$$A_f = \langle f\,|\mathcal{H}_{\mathrm{eff}}|\,B_d\rangle\,, \qquad \bar{A}_f = \langle f\,|\mathcal{H}_{\mathrm{eff}}|\,\bar{B}_d\rangle\,, \tag{4.67}$$

where the Wilson coefficients can be calculated from electroweak theory and the corresponding hadronic matrix elements $\langle f|O_i|B_d(\bar{B}_d)\rangle$ can be estimated in QCD factorisation [55, 56], for example. In the presence of NP contribution the amplitude $A_f$ [262] is given by

$$A_f = A_f^c \left[1 + a_f^u e^{i\gamma} + \sum_i \left(b_{f\,i}^c + b_{f\,i}^u e^{i\gamma}\right) C_i^{\mathrm{NP}}(\mu_W)\right], \tag{4.68}$$

where the coefficient $A_f^c \propto (V_{cb}^{\mathrm{L}})^* V_{cs}^{\mathrm{L}}$ is almost real, the parameters $b_{f\,i}^{c,u}$ are given in table 4.3, and $a_f^u$ is defined as

$$a_f^u \equiv e^{-i\gamma}\frac{A_f^u}{A_f^c}\,, \tag{4.69}$$

with $A_f^u \propto (V_{ub}^{\mathrm{L}})^* V_{us}^{\mathrm{L}}$. The parameter $a_f^u$ has been evaluated in the QCD factorisation approach in [262] and found to be 0.019(0.007) for $f = \phi K_s\,(\eta' K_s)$. The NP contribution to the Wilson coefficients $C_i = C_i^{\mathrm{SM}} + C_i^{\mathrm{NP}}$ in the SM4 are given by

$$C_3^{\mathrm{NP}}(\mu_W) = \frac{\alpha}{6\pi}\frac{1}{\sin^2\theta_W}\frac{\lambda_{t'}^{(s)}}{\lambda_t^{(s)}}\left(2Y_0(x_{t'}) - X_0(x_{t'})\right), \tag{4.70}$$

$$C_7^{\mathrm{NP}}(\mu_W) = \frac{4\alpha}{6\pi}\frac{\lambda_{t'}^{(s)}}{\lambda_t^{(s)}} Z_0(x_{t'})\,, \tag{4.71}$$

$$C_9^{\mathrm{NP}}(\mu_W) = \frac{\alpha}{6\pi}\frac{\lambda_{t'}^{(s)}}{\lambda_t^{(s)}}\left(4Z_0(x_{t'}) - \frac{2}{\sin^2\theta_W}(Y_0(x_{t'}) + X_0(x_{t'}))\right), \tag{4.72}$$

$$C_{7\gamma}^{\mathrm{NP}}(\mu_W) = -\frac{1}{2}\frac{\lambda_{t'}^{(s)}}{\lambda_t^{(s)}} D_0'(x_{t'})\,, \tag{4.73}$$

$$C_{8G}^{\mathrm{NP}}(\mu_W) = -\frac{1}{2}\frac{\lambda_{t'}^{(s)}}{\lambda_t^{(s)}} E_0'(x_{t'})\,. \tag{4.74}$$

| $f$ | $\phi K_s$ | $\eta' K_s$ |
|---|---|---|
| $b^c_{f3}$ | $-46$ | $-26$ |
| $b^c_{f7}$ | 22 | 3.8 |
| $b^c_{f9}$ | 23 | 3.5 |
| $b^c_{f8G}$ | 1.4 | 0.86 |

Table 4.3: Hadronic parameters at $\mu = m_b$ taken from [262]. The parameters $b^u_{fi}$ can be obtained via $b^u_{fi} = (|V_{ub}V^*_{us}|/|V_{cb}V^*_{cs}|)b^c_{fi}$.

Following [262], we will drop the $C^{\rm NP}_{7\gamma}(\mu_W)$ contribution due to only small effects in $\bar{b} \to \bar{s}\gamma$. To a good accuracy the amplitude $A_f$ can now be approximated as

$$A_f \approx A^c_f \left[1 + \sum_i b^c_{f\,i} C^{\rm NP}_i(\mu_W)\right] = A^c_f \left[1 + r_f \frac{\lambda^{(s)}_{t'}}{\lambda^{(s)}_t}\right] , \tag{4.75}$$

with $r_f$ given by

$$r_{\phi K_S} = +0.004\, X_0(x_{t'}) - 0.248\, Y_0(x_{t'}) + 0.075\, Z_0(x_{t'}) - 0.7\, E'_0(x_{t'}) , \tag{4.76}$$

$$r_{\eta' K_S} = +0.034\, X_0(x_{t'}) - 0.106\, Y_0(x_{t'}) + 0.012\, Z_0(x_{t'}) - 0.43\, E'_0(x_{t'}) . \tag{4.77}$$

The departure of $S_f$ from $S_{\psi K_s}$ is governed by the common phase of $\lambda^{(s)}_{t'}/\lambda^{(s)}_t$. From (4.76) and (4.77), it is clear that the effect is larger for $f = \phi K_s$ than for $f = \eta' K_s$. Using (4.66) and defining the phase $\phi_f$ of $A_f$, we find

$$-\eta_f S_f = \sin\left(2\phi^{\rm tot}_{B_d} + 2\phi_f\right) , \tag{4.78}$$

for the CP asymmetry. We conclude this section with a few comments.

- The parameters $a^u_f$ and $b^c_{f\,i}$ given in [262] have been derived using QCD factorisation taking leading-order terms in $\alpha_s$ into account and neglecting $\Lambda/m_b$ corrections except for so-called chirally enhanced terms.
- It is known that by going beyond LO in the calculation of the parameters $b_f$ one would introduce potentially substantial strong phases, which cannot be calculated from first principles and have to be fitted to the data. While the hadronic matrix elements for the decays in question are known to NLO [55, 56], a full fit of the free parameters to the existing B-factory data is clearly beyond the scope of this work.

In the context of the SM4, the CP violation in $B \to f$ decays has been studied in several publications [81, 82, 265, 266]. The great interest in $S_{\phi K_s}$ and $S_{\eta' K_s}$ was due to a slight tension between the experimental data and the theoretical prediction. However, this tension has been resolved by updated results from BaBar and Belle.

## 4.8 The Short Distance Contribution to the Leptonic Decay $K_L \to \mu^+\mu^-$

Turning to the $K$ system, we first discuss the decay $K_L \to \mu^+\mu^-$. There are three contributions to the amplitude of this decay [267]

- the absorptive LD contribution, which is dominated by the two-photon exchange;
- the dispersive LD contribution, which is also mediated by the two-photon exchange;
- the dispersive SD contribution, which is induced by $Z$ penguin and box diagrams.

While the SD contribution can be calculated directly in perturbation theory, the LD contributions have to be extracted from experiments or estimated using complicated non-perturbative calculations. In the case of $K_L \to \mu^+\mu^-$, the absorptive LD contribution can be estimated through $K_L \to \gamma\gamma$ to a good accuracy. The dispersive LD contribution can be estimated using chiral perturbation theory together with experimental input on various $K$ decays. However, as there are sizeable uncertainties on the extraction of a limit on the dispersive contribution [267], one can only give a very conservative upper limit on the SD contribution. The SD contribution to the branching ratio can be calculated within the SM4. The constraint [267]

$$\mathrm{Br}(K_L \to \mu^+\mu^-)_{\mathrm{SD}} \leq 2.5 \cdot 10^{-9}\,, \tag{4.79}$$

derived from the experimental input [268], is very important in this model, as we show explicitly in section 7.5. The SM prediction for the sort distance part of $K_L \to \mu^+\mu^-$ is given by [269]

$$\mathrm{Br}(K_L \to \mu^+\mu^-)_{\mathrm{SD}}^{\mathrm{SM}} = (0.79 \pm 0.12) \cdot 10^{-9}\,, \tag{4.80}$$

which only leaves room for a factor 3 enhancement by NP. Starting from the relevant effective Hamiltonian [267, 269]

$$\mathcal{H}_{\mathrm{eff}}(K_L \to \mu^+\mu^-) = -\frac{G_F}{\sqrt{2}}\frac{\alpha}{2\pi\sin^2\theta_W}\left(\lambda_c^{(K)}Y_0(x_c) + \lambda_t^{(K)}Y_0(x_t)\right)(\bar{s}d)_{V-A}\,(\bar{\mu}\mu)_{V-A}\,, \tag{4.81}$$

which is of course closely related to the effective Hamiltonian for $B_q \to \mu^+\mu^-$ given in (4.55). We use the replacement given in (4.56) for $q = K$ and introduce the second replacement

$$Y_0(x_c) \to Y_0(x_c) + |U_{4\mu}|^2 F^{\bar{\mu}\mu}(x_c, y_4)\,, \tag{4.82}$$

where $y_4$ has been defined in section 4.6 and $F^{\bar{\mu}\mu}$ is given in Appendix 8. The contributions involving the fourth generation of leptons can again be dropped due to a very small mixing angle $|U_{4\mu}|^2$. However, the charm contribution cannot be neglected in the $K$ system. The branching ratio is than given by [269]

$$\mathrm{Br}(K_L \to \mu^+\mu^-)_{\mathrm{SD}} = \kappa_\mu \left(\frac{\mathrm{Re}\lambda_c^{(K)}}{|V_{us}^{\mathrm{L}}|}P_c(Y_K) + \frac{\mathrm{Re}(\lambda_t^{(K)}Y_K)}{|V_{us}^{\mathrm{L}}|^5}\right)^2\,, \tag{4.83}$$

where $P_c(Y_K) = 0.113 \pm 0.017$ [269], and the numerical pre-factor can be calculated using

$$\kappa_\mu = \frac{\alpha^2\,\mathrm{Br}(K^+ \to \mu^+\nu_\mu)}{\pi^2\sin^4\theta_W}\frac{\tau(K_L)}{\tau(K^+)}\left|V_{us}^{\mathrm{L}}\right|^8 = 2.08 \cdot 10^{-9}\,. \tag{4.84}$$

The NNLO QCD corrections [269] to the charm contribution in (4.81) are included in (4.83) through $P_c(Y_K)$ and remain unchanged as long as the mixing $U_{4\mu}$ is small enough to be neglected.

## 4.9 The Semi-Leptonic Decays $K^+ \to \pi^+\nu\bar{\nu}$ and $K_L \to \pi^0\nu\bar{\nu}$

Within the SM, the semi-leptonic branching ratios of $\mathrm{Br}(K_L \to \pi^0\nu\bar{\nu})$, $\mathrm{Br}(K^+ \to \pi^+\nu\bar{\nu})$ provide a theoretically clean cross check for the determination of $\lambda_t^{(K)}$. In the context of models beyond the Standard Model (BSM), these decays can be used as stringent constraints once the branching ratios are measured. The current experimental situation [47, 270, 271]

$$\mathrm{Br}(K^+ \to \pi^+\nu\bar{\nu}) = \left(17.3^{+11.5}_{-10.5}\right) \cdot 10^{-11}\,, \tag{4.85}$$

$$\mathrm{Br}(K_L \to \pi^0\nu\bar{\nu}) \leq 2.6 \cdot 10^{-8}\,, \tag{4.86}$$

clearly leaves room for improvements on the experimental side and hypothetical NP effects on the theoretical side. The branching ratio $\mathrm{Br}(K^+ \to \pi^+\nu\bar{\nu})$ is expected to be measured with an accuracy of about 10%, by the NA62 experiment [272] at the CERN SPS, within the next decade. The theoretical predictions read [273]

$$\mathrm{Br}(K^+ \to \pi^+\nu\bar{\nu})_{\mathrm{SM}} = (8.5 \pm 0.7) \cdot 10^{-11}\,, \tag{4.87}$$

$$\mathrm{Br}(K_L \to \pi^0\nu\bar{\nu})_{\mathrm{SM}} = (2.8 \pm 0.6) \cdot 10^{-11}\,, \tag{4.88}$$

where the errors are dominated by parametrical uncertainties, in particular by the ones introduced by the dependence on the CKM parameters. In the context of the SM, the effective Hamiltonian for these decays is given by [203]

$$\mathcal{H}_{\mathrm{eff}} = \frac{G_F}{\sqrt{2}} \frac{\alpha}{2\pi \sin^2\theta_W} \sum_{\ell=e,\mu,\tau} \left(\lambda_c^{(K)} X_0(x_c, z_\ell) + \lambda_t^{(K)} X_0(x_t)\right) (\bar{s}d)_{V-A} \, (\bar{\nu}_\ell \nu_\ell)_{V-A}\,, \tag{4.89}$$

where $z_\ell = m_\ell^2/M_W^2$ and $X_0(x_c, 0) = X_0(x_c)$. The charm contribution has been calculated to high accuracy in [273–275]. In the SM4, the effective Hamiltonian (4.89) is derived by using the redefinitions of the $X_0$ functions

$$X_0(x_c, z_\ell) \to X_0(x_c, z_\ell) + \frac{1}{\lambda_c^{(K)}} \left(4|U_{\ell\tau}|^2 F^{\nu\bar{\nu}}(x_c, z_\tau) + 4|U_{\ell 4}|^2 F^{\nu\bar{\nu}}(x_c, z_4)\right)\,, \tag{4.90}$$

and (4.48). The charm contribution remains unchanged as long as the mixing between the first three and the fourth lepton generation $|U_{\ell 4}|^2$ is negligible. As already pointed out, this is always true as the constraints on the lepton mixing matrix are very stringent [84, 105]. Using (4.89) together with the redefinitions (4.48) and (4.90), the formulae for the branching ratios are given by [203, 276]

$$\mathrm{Br}(K^+ \to \pi^+\nu\bar{\nu}) = \kappa_+ \left[\left(\frac{\mathrm{Im}(\lambda_t^{(K)} X_K)}{|V_{us}^{\mathrm{L}}|^5}\right)^2 + \left(\frac{\mathrm{Re}(\lambda_c^{(K)})}{|V_{us}^{\mathrm{L}}|} P_c(X) + \frac{\mathrm{Re}(\lambda_t^{(K)} X_K)}{|V_{us}^{\mathrm{L}}|^5}\right)^2\right]\,, \tag{4.91}$$

$$\mathrm{Br}(K_L \to \pi^0\nu\bar{\nu}) = \kappa_L \left(\frac{\mathrm{Im}(\lambda_t^{(K)} X_K))}{|V_{us}^{\mathrm{L}}|^5}\right)^2\,, \tag{4.92}$$

where we already evaluated the summation over the light neutrino flavours in the final state. In the absence of new contributions from heavy leptons, the charm contribution $P_c(X)$ remains unchanged and we use the value calculated within the SM [273]

$$P_c(X) = 0.372(15)\,. \tag{4.93}$$

This value of $P_c(X)$ includes NNLO QCD corrections [275], electroweak corrections [273], and LD contributions [274]. The small parametric error of $P_c(X)$ can be attributed to a large extend to the improved value of the charm quark mass $m_c(m_c)$ [170, 277, 278]. The hadronic matrix elements $\kappa_L$ and $\kappa_+$ can be determined from tree-level $K$ decays and read [279]

$$\kappa_+ = (5.36 \pm 0.026) \cdot 10^{-11}\,, \qquad \kappa_L = (2.31 \pm 0.01) \cdot 10^{-10}\,. \tag{4.94}$$

The analytic formulae for the determination of $\kappa_{L,+}$ are given by [175, 279]

$$\kappa_+ = r_{K^+} \frac{3\alpha^2 \mathrm{Br}(K^+ \to \pi^0 e^+ \nu)}{2\pi^2 \sin^4 \theta_W} \left|V_{us}^{\mathrm{L}}\right|^8\,, \tag{4.95}$$

$$\kappa_L = \frac{r_{K_L}}{r_{K^+}} \frac{\tau(K_L)}{\tau(K^+)} \kappa_+\,, \tag{4.96}$$

where $r_{K^+} = 0.901$ and $r_{K_L} = 0.944$ summarise the isospin breaking corrections in relating $K^+(K_L) \to \pi^{+(0)}\nu\bar{\nu}$ to $K^+ \to \pi^0 e^+ \nu$ [280]. From the comparison of equations (4.91) and (4.92), we can deduce that the branching ratios of $K^+ \to \pi^+\nu\bar{\nu}$ and $K_L \to \pi^0\nu\bar{\nu}$ are clearly related. In fact, the first term in (4.91) is directly proportional to $\mathrm{Br}(K_L \to \pi^0\nu\bar{\nu})$, which gives rise to the Grossman-Nir bound [281] in the correlation of $\mathrm{Br}(K_L \to \pi^0\nu\bar{\nu})$ and $\mathrm{Br}(K^+ \to \pi^+\nu\bar{\nu})$. Writing $\mathrm{Br}(K_L \to \pi^0\nu\bar{\nu})$ as a function of $\mathrm{Br}(K^+ \to \pi^+\nu\bar{\nu})$, we find

$$\mathrm{Br}(K_L \to \pi^0\nu\bar{\nu}) = \frac{\kappa_L}{\kappa_+} \mathrm{Br}(K^+ \to \pi^+\nu\bar{\nu}) - \kappa_L \left( \frac{\mathrm{Re}(\lambda_c^{(K)})}{|V_{us}^{\mathrm{L}}|} P_c(X) + \frac{\mathrm{Re}(\lambda_t^{(K)} X_K)}{|V_{us}^{\mathrm{L}}|^5} \right)^2\,, \tag{4.97}$$

which is important for our discussion of $\varepsilon'/\varepsilon$. Note that, as the second term in (4.97) is strictly positive, this provides an upper bound on $\mathrm{Br}(K_L \to \pi^0\nu\bar{\nu})$ as a function of $\mathrm{Br}(K^+ \to \pi^+\nu\bar{\nu})$. Furthermore, the second term in (4.91), and thereby the second term in (4.97), is closely related to the branching ratio $\mathrm{Br}(K_L \to \mu^+\mu^-)_{\mathrm{SD}}$. This allows us to constrain the CP conserving part of $\mathrm{Br}(K^+ \to \pi^+\nu\bar{\nu})$ through $\mathrm{Br}(K_L \to \mu^+\mu^-)_{\mathrm{SD}}$ as discussed in section 7.5.

The branching ratios $\mathrm{Br}(K^+ \to \pi\nu\bar{\nu})$ and $\mathrm{Br}(K_L \to \pi\nu\bar{\nu})$ have also been studied in [82].

## 4.10 The Semi-Leptonic Decays $K_L \to \pi\ell^+\ell^-$

The rare decays $K_L \to \pi\ell^+\ell^-$ are dominated by CP violation and therefore provide another interesting laboratory for verifying the SM or constraining NP models. While the branching ratios are relatively clean theoretically, the experimental studies of this decay suffer from various background processes [282, 283], which can mimic the decays studied here. However, the present experimental bounds [47, 282, 283]

$$\mathrm{Br}(K_L \to \pi e^+ e^-) \leq 28 \cdot 10^{-11}\,, \tag{4.98}$$

$$\mathrm{Br}(K_L \to \pi\mu^+\mu^-) \leq 38 \cdot 10^{-11}\,, \tag{4.99}$$

can still be used to constrain a possible enhancement of the branching ratios. The theoretical predictions within the SM read [284]

$$\mathrm{Br}(K_L \to \pi e^+ e^-) = 3.54^{+0.98}_{-0.85} \left(1.56^{+0.62}_{-0.49}\right) \cdot 10^{-11}\,, \tag{4.100}$$

$$\mathrm{Br}(K_L \to \pi\mu^+\mu^-) = 1.41^{0.28}_{-0.26} \left(0.95^{+0.22}_{-0.21}\right) \cdot 10^{-11}\,, \tag{4.101}$$

where the two different values are related to a sign ambiguity in the branching ratio, as explicitly shown below. Comparing the experimental bound and the SM prediction, we observe that enhancements of more than an order of magnitude in the branching ratios are disfavoured. We are therefore able to use the decays $K_L \to \pi\ell^+\ell^-$ to help constrain the SM4 in our analysis. The leading effective Hamiltonian for these decays is given by [203, 284]

$$\mathcal{H}_{\text{eff}}^{V,A} = -\frac{G_F}{\sqrt{2}}\alpha\lambda_t^{(K)}\left[y_{7V}\,(\bar{s}\gamma_\mu d)\left(\bar{\ell}\gamma^\mu\ell\right) + y_{7A}\,(\bar{s}\gamma_\mu d)\left(\bar{\ell}\gamma^\mu\gamma_5\ell\right)\right] + \text{h.c.}\,, \tag{4.102}$$

where $\alpha = \alpha(M_Z)$, and the four-quark operators $Q_1 \ldots Q_6$ are suppressed. After including all relevant effects [284], the branching ratio reads [284–287]

$$\text{Br}(K_L \to \pi\ell^+\ell^-) = 10^{-12}\left(C_{\text{dir}}^\ell \pm C_{\text{int}}^\ell|a_s| + C_{\text{mix}}^\ell|a_s|^2 + C_{\text{CPC}}^\ell\right)\,, \tag{4.103}$$

where the sign ambiguity is made explicit and the contributions $C^\ell$ are given by [284]

$$C_{\text{dir}}^e = (4.62 \pm 0.24)\left(w_{7V}^2 + w_{7A}^2\right)\,, \qquad C_{\text{dir}}^\mu = (1.09 \pm 0.05)\left(w_{7V}^2 + 2.32 w_{7A}^2\right)\,, \tag{4.104}$$

$$C_{\text{int}}^e = (11.3 \pm 0.3)\,w_{7V}\,, \qquad C_{\text{int}}^\mu = (2.63 \pm 0.06)\,w_{7V}\,, \tag{4.105}$$

$$C_{\text{mix}}^e = (14.5 \pm 0.5)\,, \qquad C_{\text{mix}}^\mu = (3.36 \pm 0.2)\,, \tag{4.106}$$

$$C_{\text{CPC}}^e \simeq 0\,, \qquad C_{\text{CPC}}^\mu = (5.2 \pm 1.6)\,. \tag{4.107}$$

In the above, we followed the notation of [284]. The coefficient $|a_s|$ is given by $|a_s| = 1.2 \pm 0.2$ with hints of being negative [285, 286]. The Wilson coefficients [284]

$$w_{7A,7V} = \frac{\text{Im}(\lambda_t^{(K)} y_{7A,7V})}{\text{Im}(\lambda_t^{(K)})_{\text{SM}}}\,, \tag{4.108}$$

are given by

$$w_{7V} = \frac{10^4}{2.8\pi}\left[P_0 + \frac{\text{Im}(\lambda_t^{(K)} Y_K)}{\sin^2\theta_W} - 4\,\text{Im}(\lambda_t^{(K)} Z_K)\right]\,, \tag{4.109}$$

$$w_{7A} = -\frac{10^4}{2.8\pi}\frac{\text{Im}(\lambda_t^{(K)} Y_K)}{\sin^2\theta_W}\,, \tag{4.110}$$

where we already used $\text{Im}(\lambda_t^{(K)})_{\text{SM}} \simeq 1.4 \cdot 10^{-4}$ [284]. The charm contribution encoded in $P_0$ is given by $P_0 = 2.88 \pm 0.06$ [288]. The master functions $Y_q$ and $Z_q$ are again given by

$$F_q = F_0(x_t) + \frac{\lambda_{t'}^{(q)}}{\lambda_t^{(q)}} F_0(x_{t'})\,, \tag{4.111}$$

with $q = K, d, s$ and $F = Y, Z$. In the SM4, the NP effects are mainly felt in $w_{7A}$, as the NP contributions in $w_{7V}$ cancel each other to a large extend. By comparing (4.92) and (4.110), it is clear that the constraint from $K_L \to \pi\ell^+\ell^-$ is only interesting as long as the experimental bound on $\text{Br}(K_L \to \pi\nu\bar{\nu})$ is not improved.

| | $\Lambda_{\overline{\rm MS}}(m_c) = 310\,{\rm MeV}$ | | | $\Lambda_{\overline{\rm MS}}(m_c) = 340\,{\rm MeV}$ | | | $\Lambda_{\overline{\rm MS}}(m_c) = 370\,{\rm MeV}$ | | |
|---|---|---|---|---|---|---|---|---|---|
| $i$ | $r_i^{(0)}$ | $r_i^{(6)}$ | $r_i^{(8)}$ | $r_i^{(0)}$ | $r_i^{(6)}$ | $r_i^{(8)}$ | $r_i^{(0)}$ | $r_i^{(6)}$ | $r_i^{(8)}$ |
| 0 | -3.574 | 16.552 | 1.805 | -3.602 | 17.887 | 1.677 | -3.629 | 19.346 | 1.538 |
| X | 0.574 | 0.030 | 0 | 0.564 | 0.033 | 0 | 0.554 | 0.036 | 0 |
| Y | 0.403 | 0.119 | 0 | 0.392 | 0.127 | 0 | 0.382 | 0.134 | 0 |
| Z | 0.714 | -0.023 | -12.510 | 0.766 | -0.024 | -13.158 | 0.822 | 0.026 | -13.855 |
| E | 0.213 | -1.909 | 0.550 | 0.202 | -2.017 | 0.589 | 0.190 | -2.131 | 0.631 |

Table 4.4: The magic numbers $r_i$ as given in [293]

## 4.11 Direct CP Violation in $K \to \pi\pi$ ($\varepsilon'/\varepsilon$)

The direct CP violation $\varepsilon'$ [289–293] in the decay $K \to \pi\pi$ compared to the mixing induced (indirect) CP violation $\varepsilon_K$ provides a very interesting observable. The experimental situation for $\varepsilon'/\varepsilon$ is very good thanks to the concentrated efforts by the collaborations NA48 [294] and KTeV [295]. The current world average reads [47]

$$\frac{\varepsilon'}{\varepsilon} = (16.8 \pm 1.4) \cdot 10^{-4}\,, \tag{4.112}$$

which could have significant impact on any NP model. However, as we discuss in the following, the theoretical prediction of $\varepsilon'/\varepsilon$ suffers from large hadronic uncertainties. Due to this unfortunate fact, the observable $\varepsilon'/\varepsilon$ is often ignored. In our numerical analysis we show that, in spite of the large uncertainties, $\varepsilon'/\varepsilon$ could provide an interesting constraint. To this end, one has to make assumptions on the non-perturbative contributions.

Using [293, 296], $\varepsilon'/\varepsilon$ can be written in the form

$$\frac{\varepsilon'}{\varepsilon} = P_0\,{\rm Im}\lambda_t^{(K)} + P_X\,{\rm Im}(\lambda_t^{(K)} X_K) + P_Y\,{\rm Im}(\lambda_t^{(K)} Y_K) + P_Z\,{\rm Im}(\lambda_t^{(K)} Z_K) + P_E\,{\rm Im}(\lambda_t^{(K)} E_K)\,, \tag{4.113}$$

where the master functions $X_K, Y_K, Z_K, E_K$ are defined as in the previous sections and the coefficients $P_i$ summarise the NLO short distance effects as well as the non-perturbative ones. The $P_i$ coefficients are given in terms of the short distance contributions $r_i$ and non-perturbative parameters $R_{6,8}$

$$P_i = r_i^{(0)} + r_i^{(6)} R_6 + r_i^{(8)} R_8\,, \tag{4.114}$$

where the $r_i$ are given in table 4.4 and $R_{6,8}$ are defined as

$$R_6 \equiv B_6^{(1/2)} \left[\frac{121\,{\rm MeV}}{m_s(m_c) + m_d(m_c)}\right]^2\,, \qquad R_8 \equiv B_8^{(3/2)} \left[\frac{121\,{\rm MeV}}{m_s(m_c) + m_d(m_c)}\right]^2\,. \tag{4.115}$$

The matrix elements $B_6^{(1/2)}$ and $B_8^{(3/2)}$ have to be calculated using lattice methods. However this calculation proves to be very challenging as more than a decade of research can attest to. From equation (4.113), we can see a clear connection to the rare $K$ decays discussed in the previous sections. More specifically, the term ${\rm Im}(\lambda_t^{(K)} X_K)$ is proportional to ${\rm Br}(K_L \to \pi\nu\bar{\nu})$ [297, 298] discussed in section 4.9, and correlated with ${\rm Br}(K_L \to \pi\ell^+\ell^-)$ [297] discussed in

| | I | II | III | IV |
|---|---|---|---|---|
| $R_6$ | 1 | 1.2 | 2.0 | 1.5 |
| $R_8$ | 1 | 0.8 | 1.0 | 0.5 |

Table 4.5: The scenarios for $(R_6, R_8)$ we will use in our numerical analysis

section 4.10. The correlation of $\varepsilon'/\varepsilon$ with $\mathrm{Br}(K_L \to \pi\ell^+\ell^-)$ through the term $\mathrm{Im}(\lambda_t^{(K)} Z_K)$ is mostly cancelled due to the cancellation of NP effects in $w_{7V}$ (see equation (4.109)). The decays $K \to \pi\nu\bar{\nu}$ are also closely correlated with the $\mathrm{Im}(\lambda_t^{(K)} Z_K)$ contribution to $\varepsilon'/\varepsilon$. The only difference is the different behaviour of $Z_0$ and $X_0$ as functions of $m_{t'}$. The close connection between $\varepsilon'/\varepsilon$ and some rare $K$ decays has been used by several authors [297, 298] to constrain $K \to \pi\nu\bar{\nu}$ decays in model independent studies. From (4.114) and by comparing the values for different $r_i$ in table 4.4, we can clearly see that terms proportional to $R_6$ will give the dominant contribution to $P_0$ and $P_E$ while terms proportional to $R_8$ dominate $P_Z$. It is also clear that $P_Z$ and $P_0$ dominate the final value of $\varepsilon'/\varepsilon$. We come back to this during the numerical analysis in section 7.5.

We conclude this section by outlining our treatment of the non-perturbative parameters $R_6$ and $R_8$. From lattice [178] and large-N calculations [289], we can require

$$0.2 \leq R_8 \leq 2\,, \tag{4.116}$$

without restricting ourselves. The situation for $R_6$ is even worse. While large-N calculations [289] predict $R_6 = R_8$, the lattice community has yet to come up with a reliable result. Therefore, we restrict ourselves to

$$0.3 \leq R_6 \leq 3\,, \tag{4.117}$$

to be on the conservative side. We chose the exemplary scenarios for $(R_6, R_8)$, collected in table 4.5, to show the impact of $\varepsilon'/\varepsilon$. Recent lattice determinations [178] give

$$\mathrm{Re}(\varepsilon'/\varepsilon)_{\mathrm{EWP}} = (-6.52 \pm 0.49_{stat} \pm 1.24_{syst}) \cdot 10^{-4}, \tag{4.118}$$

for the electroweak penguin contribution in the SM. Using their result, we find

$$R_8 = 0.80 \pm 0.05_{\mathrm{stat}} \pm 0.12_{\mathrm{syst}} \pm 0.05_{R_6} \pm 0.04_{\mathrm{CKM}}\,, \tag{4.119}$$

which is compatible with our conservative range given in (4.116). In deriving the error from $R_6$, we assumed $R_6 = 0 \ldots 2$. Further, we assumed the uncertainty on $\mathrm{Im}\lambda_t^{(K)}$ to be 7%. Combining the errors in (4.119) in quadrature, we arrive at

$$R_8 = 0.80 \pm 0.14\,, \tag{4.120}$$

which is more convenient for our purposes. Note that our result (4.119) is only valid in the SM. Staying within the SM for a moment we can even deduce $R_6$ by combining the measured value for $\varepsilon'/\varepsilon$ and the lattice determination (4.118). Assuming no or only mild correlations between the inputs, we write down the $\chi^2$ function for this situation. The result of this procedure is shown in figure 4.3. From figure 4.3, we can deduce approximate values for $R_6$ and $R_8$ and even get a hint of the correlation between the two. The best fit, according to figure 4.3, can

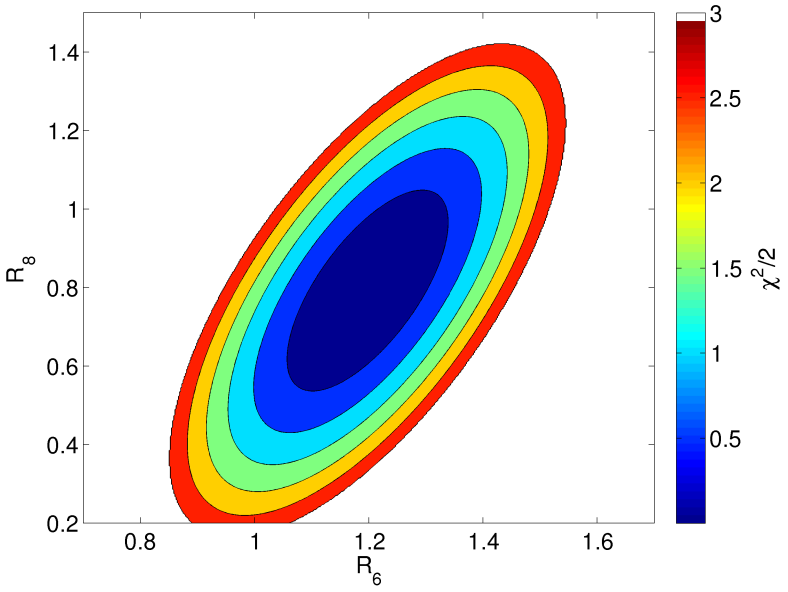


Figure 4.3: The quality of a simultaneous fit to $\mathrm{Re}(\varepsilon'/\varepsilon)_{\mathrm{EWP}}$ and $(\varepsilon'/\varepsilon)_{\mathrm{exp}}$ is shown as a function of $R_6$ and $R_8$. The quality of the fit is indicated as the colour.

be found for $R_8 \approx 0.8$ and $R_6 \approx 1.2$. As is clear from the slant of the ellipses the errors are correlated. However, as the plot shows only the qualitative features, we cannot directly determine the size of the errors. We might use the $\chi^2/2 = 1$ ellipse as a hint on the size. In this analysis we did not use a rigorous error treatment and only estimate uncertainties using an educated guess. Therefore, it is clear that we cannot make any quantitative statements about our result. Interestingly, our result is very close to the one found in [293] nearly 10 years ago.

# 5

# Numerical Methods

In this chapter we review different numerical methods available for analysing the SM and its extensions. We focus our discussion on the flavour sector, but the general ideas are also applicable to other problems. The first section is dedicated to the discussion of the unitarity fits in the SM. Subsequently, we discuss the different ideas on how to tackle the vastly increased parameter space in NP models.

## 5.1 Unitarity Fits in the Standard Model

In the SM, we can use the strong hierarchy of the CKM matrix to derive a more transparent but approximate form [205]. Let us follow the standard convention [205, 288, 299] and define the parameters $(\lambda, A, \eta, \rho)$ through

$$s_{12} = \lambda\,, \qquad s_{23} = A\lambda^2\,, \qquad s_{13}e^{-i\delta_{13}} = A\lambda^3(\rho - i\eta)\,. \tag{5.1}$$

Using the definitions in (5.1), the CKM matrix can be expanded in the small parameter $\lambda$. At LO, this procedure yields

$$V = \begin{pmatrix} 1-\frac{\lambda^2}{2} & \lambda & A\lambda^3(\rho - i\eta) \\ -\lambda & 1-\frac{\lambda^2}{2} & A\lambda^2 \\ A\lambda^3(1-\rho-i\eta) & -A\lambda^2 & 1 \end{pmatrix} + \mathcal{O}(\lambda^4)\,. \tag{5.2}$$

Going beyond LO in this expansion, we again follow the established procedure and introduce the relation between $V_{ub}/V_{cb}$ and the apex $\bar\rho + i\bar\eta$ of the unitarity triangle

$$\begin{aligned} \bar\rho + i\bar\eta \equiv \frac{V_{ud}V_{ub}^*}{V_{cd}V_{cb}^*} &= -\frac{c_{12}s_{13}e^{i\delta}}{c_{23}s_{12}s_{23} + c_{12}s_{23}s_{13}e^{i\delta}} \\ &= (\rho + i\eta)\left(1 - \frac{\lambda^2}{2}\right) + \mathcal{O}(\lambda^4)\,. \end{aligned} \tag{5.3}$$

Changing variables $(\eta, \rho) \to (\bar\rho, \bar\eta)$ preserves the form of $V_{td}$ in (5.2) to higher order in $\lambda$. Expressing the factors $\lambda_i^{(q)}$ defined in (3.16) in terms of the Wolfenstein parameters (5.1) and (5.3) yields [288, 299]

$$\mathrm{Im}\lambda_t^{(K)} = -\,\mathrm{Im}\lambda_c^{(K)} = \eta A^2\lambda^5 = |V_{ub}||V_{cb}|\sin\delta_{13}\,, \tag{5.4}$$

$$\mathrm{Re}\lambda_c^{(K)} = -\lambda\left(1 - \frac{\lambda^2}{2}\right)\,, \tag{5.5}$$

$$\mathrm{Re}\lambda_t^{(K)} = -\left(1 - \frac{\lambda^2}{2}\right)A^2\lambda^5\,(1-\bar\rho)\,. \tag{5.6}$$

The factors $\lambda_t^{(q)}$ $(q = d, s)$ for the $B_q$ system can be read off (5.2) for the LO approximation. To higher accuracy, we find

$$V_{tb} = 1 - \frac{1}{2}A^2\lambda^4 + \mathcal{O}(\lambda^6)\,, \tag{5.7}$$

which changes the LO expressions only at order $\lambda^7$ when taking into account the definition of $\bar{\eta}$ and $\bar{\rho}$ given in (5.3). Keeping only leading order terms, the factors relevant for the $B$ system are given by

$$\lambda_t^{(d)} = A\lambda^3(1 - \bar{\rho} - i\bar{\eta})\,, \tag{5.8}$$

$$\lambda_t^{(s)} = -A\lambda^2 + \frac{1}{2}A(1 - 2\bar{\rho} - 2i\bar{\eta})\lambda^4\,. \tag{5.9}$$

From (5.9), it is immediately clear that CP violation in the $B_s$ system is highly suppressed compared to the $B_d$ system (5.8). After substitution of equations (5.4) - (5.6), (5.8), and (5.9) into the SM formulae for the $\Delta F = 2$ processes given in section 3.2, we can use the experimental data on these observables in order to constrain the values of $\bar{\eta}$ and $\bar{\rho}$. The parameters $\lambda$ and $A$ can be determined from tree-level processes. Using the unitarity constraint

$$\lambda_u^{(d)} + \lambda_c^{(d)} + \lambda_t^{(d)} = 0\,, \tag{5.10}$$

we can introduce the unitarity triangle (UT) [175,288]. Expressing $\lambda_i^{(d)}$ in terms of $(\lambda, A, \bar{\rho}, \bar{\eta})$, one finds that (5.10) can be depicted as a triangle in the $(\bar{\rho}, \bar{\eta})$ plane with its corners at $(0, 0)$, $(1, 0)$ and $(\bar{\rho}, \bar{\eta})$. We are not going into more details on the construction of the UT as this is discussed in detail for example in [175, 288]. In the remainder of this section we discuss the different methods for the determination of the apex $(\bar{\rho}, \bar{\eta})$ of the UT. The procedures used in the attempt to estimate $(\bar{\rho}, \bar{\eta})$ are centred around the treatment of the statistics involved. The correct and consistent treatment of the statistical problems involved in the fit becomes more and more important as the precision of the experimental data and esp. of the lattice inputs increases.

### Frequentist View: The CKMfitter Approach

The *CKMfitter* approach to the SM fits [300] is based on the frequentist view of statistics. Given experimental observations $x^i_{\text{exp}}$ and theoretical predictions $x^i_{\text{theo}}(\vec{y}; \vec{x}_0)$ the $\chi^2$ function is defined as a function of the model parameters $\vec{y}$

$$\chi^2(\vec{y}) = \sum_{i=1}^{n_{\text{obs}}} \left( \frac{x^i_{\text{exp}} - x^i_{\text{theo}}(\vec{y}; \vec{x}_0)}{\sigma_i} \right)^2 - \sum_{j=1}^{n_{\text{param}}} 2 \ln \mathcal{L}_{\text{syst.}}(x_0^j, \kappa, \zeta)\,, \tag{5.11}$$

with $i$ running over all observables included in the fit. The theoretical inputs in $\vec{x}_0$ are treated differently from the experimental inputs even if both exhibit systematic errors. The index $j$ runs over all theoretical inputs and all measurements with systematic errors. The likelihood function due to the systematic errors is defined as

$$-2 \ln \mathcal{L}_{\text{syst.}}(x_0^i, \kappa, \zeta) = \begin{cases} 0 & x_0^i \in [\bar{x}_0^i \pm \zeta\sigma^i] \\ \left( \frac{\bar{x}_0^i - x_0^i}{\kappa\sigma_0^i} \right)^2 & x_0^i \notin [\bar{x}_0^i \pm \zeta\sigma^i] \end{cases} \tag{5.12}$$

where $\bar{x}_0^i$ defines the central value of the parameter e.g. $\hat{B}_K$, $F_K$ or measurement and $\sigma_0^i$ its uncertainty. For $\kappa = 0$ and $\zeta > 0$, we find the so-called *RFit* scheme [300], where parameters are only allowed to fall within a certain range but without any preference therein. For $\zeta = 0$ and $\kappa = 1$, we find the standard $\chi^2$ formulation. The CKMfitter group assigns $\kappa = 0, \zeta > 0$ for most of the lattice inputs while using $(\kappa, \zeta) = (1, 0)$ for experimental systematic errors. See [300] for a more detailed discussion of this treatment. The best value for $(\bar{\rho}, \bar{\eta})$ is found by minimizing $\chi^2(\bar{\rho}, \bar{\eta})$.

### Bayesian View: The UTfit Approach

The *UTfit* group [301–303] bases their approach on the Bayesian treatment of statistics. The following is based on [303, 304] and is only a very short repetition. The Bayesian approach to statistics is founded on the theorem of Bayes

$$P(H|E) = \frac{P(E|H)P(H)}{P(E)}\,, \tag{5.13}$$

which reads: *The probability of H given E is equal to the probability of E given H times the ratio of the (a-priori) probabilities of H and E.* Bayes' theorem (5.13) can be extended to include multiple mutually exclusive hypotheses $H_i$

$$P(H_i|E) = \frac{P(E|H_i)P(H_i)}{\sum\limits_j P(E|H_j)P(H_j)}\,. \tag{5.14}$$

In our applications, the hypotheses $H_i$ become a continuous variable, as do the events $E$. In this case, we can write Bayes' theorem as

$$f(\mu|x) = \frac{\int f(x|\mu, h) f_0(\mu, h) dh}{\int\int f(x|\mu, h) f_0(\mu, h)\, d\mu\, dh}\,, \tag{5.15}$$

where $\mu$ is a vector of parameters e.g. $(\bar{\rho}, \bar{\eta})$, $x$ describes all the experimental observables, and $h$ is a vector of all the (model) parameters we are currently not interested in e.g. $A$, $\lambda$, $\hat{B}_K$ etc.. The function $f(x|\mu, h)$ is the probability density function (PDF) for $x$ *given* $\mu$ *and* $h$, and $f_0$ is the a-priori PDF for $\mu$ and $h$. The explicit appearance of the a-priori probabilities in Bayes' theorem is sometimes taken as a hint that results, derived by this methods, are arbitrary. However, as discussed in [304]

- all the different statistical methods make at least implicit use of a prior PDF;
- the choice of the prior does not necessarily influence the result, as long as one makes a 'sane' choice.

Furthermore, the formulation (5.15) gives us a very intuitive way to include new measurements. Assume we have calculated $f(\mu|x)$ at some point and now want to include another observation. This new observation is assumed to be uncorrelated with all the observations we used in our previous calculation for the sake of simplicity. In this case, we have some prior knowledge on $\mu$ and we can use our previously calculated PDF $f(\mu|x)$ to create our prior distribution for $\mu$.
In their SM fit, the UTfit group uses the experimental likelihood functions if they are provided by the experimental collaborations. The theoretical parameters are treated in the same way

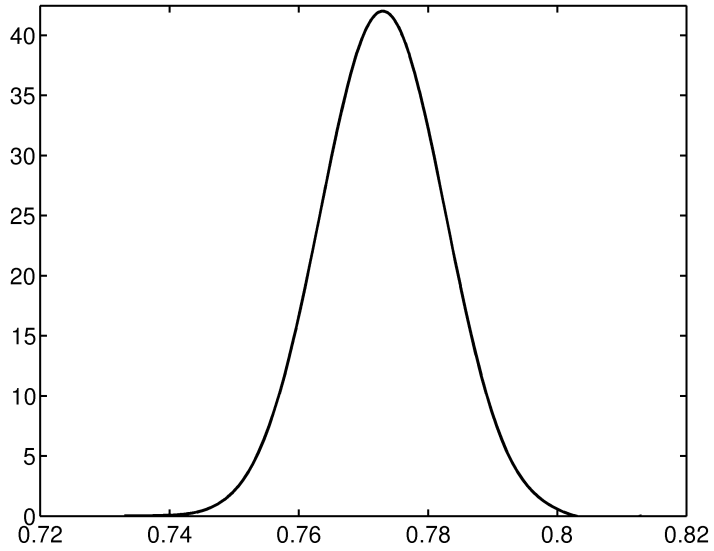


Figure 5.1: The joint PDF for $\hat{B}_K^{\mathrm{BMW'11}}$ as a function of $\hat{B}_K$

as the experimental inputs. This treatment is founded in the fact that the Bayesian formalism makes no distinction between different errors. For example, the PDF for $\hat{B}_K$ as determined by the BMW collaboration [163]

$$\hat{B}_K^{\mathrm{BMW'11}} = 0.773(8)_{\mathrm{stat.}}(3)_{\mathrm{sys.}}(8)_{\chi\mathrm{PT}}(45)_{\mathrm{renorm.}} \tag{5.16}$$

can be determined as the convolution of a Gaussian with three uniform distributions. In figure 5.1, we show the resulting PDF as a function of $\hat{B}_K$, this PDF can be approximated by a Gaussian distribution to a very good accuracy. Interestingly, fitting a Gaussian distribution to the joint PDF gives

$$\hat{B}_K^{\mathrm{BMW'11,comb.}} = 0.773(13)\,, \tag{5.17}$$

which exhibits a slightly larger error than naively expected by adding all uncertainties in quadrature

$$\hat{B}_K^{\mathrm{BMW'11,naive}} = 0.773(11)\,. \tag{5.18}$$

The joint PDF is not necessarily Gaussian as can be seen from $\hat{B}_K$ as determined by the Laiho and van de Water [165]

$$\hat{B}_K^{\mathrm{L\&dW'11}} = 0.7623(38)_{\mathrm{stat.}}(62)_{\chi\mathrm{PT}}(53)_{\mathrm{r_1,m_q}}(45)_{\mathrm{FV}}(183)_{\mathrm{renorm.}}(8)_{\mathrm{EM}}\,. \tag{5.19}$$

Its joint PDF is shown in figure 5.2 in blue. It does clearly not match a Gaussian distinction with a similar width. This is shown by the green curve in figure 5.2.

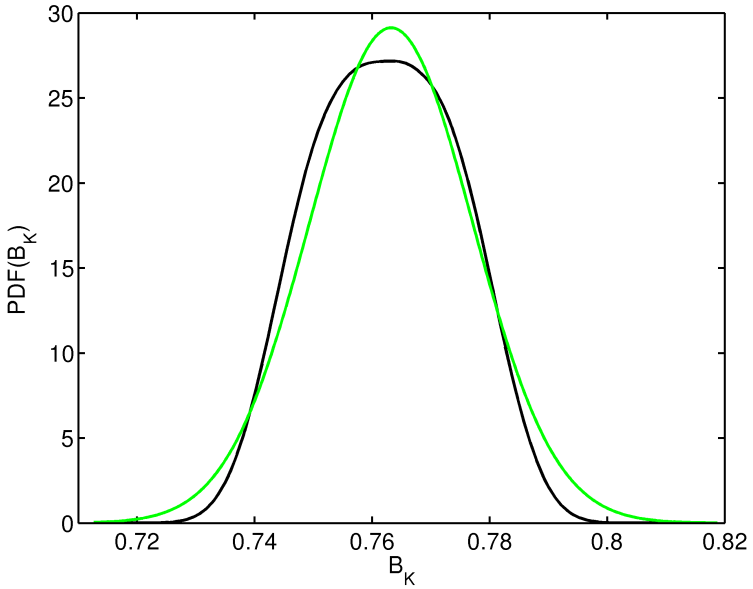


Figure 5.2: The joint PDF for $\hat{B}_K^{\mathrm{L\&dW'11}}$ as a function of $\hat{B}_K$ (in blue). The green line shows the result of the attempt to fit a Gaussian to this distribution.

## 5.2 Analysing Models Beyond the SM

When going beyond the SM, one encounters a number of problems when attempting to do a numerical analysis. The list of potential problems includes but is not limited to the following points:

- The number of inputs e.g. observations is small compared to the number of parameters.
- The complexity of the formulae generally increases with the number of parameters. If a formula has to be evaluated $\mathcal{O}(10^8-10^{10})$ times, even a very small increase in computation time can be disastrous.
- The chosen parametrisation is usually optimised for analytical considerations but might not be optimal for numerical applications. For example there might be a strong constraint on a very complicated combination of parameters but not on the individual ones. This could, in the worst case, render fitting procedures unstable or reduce the efficiency of MC methods by orders of magnitude.
- Due to the large number of parameters, fits might not converge because
  - the gradient of $\chi^2$ or any other measure of the likelihood for a given point can be very small around local minima/maxima, which in many cases spoils the convergence of the numerical algorithm;
  - the gradient of the likelihood estimator might be large in regions with very low likelihood which tends to cause numerical algorithms 'overshoot' the minima/maxima.

- Monte Carlo scans use uniform random numbers which do not respect regions of interest (ROI). This in turn means that a large number of valid points has to be found. With a ratio of e.g. $1:1000$ or worse of valid points per number of tries, the computing time needed for a sufficient number of valid points is quite large.

Concentrating on the flavour sector, our main concern becomes the number of parameters. The minimal SM with neutrino masses has

$$N_{\text{param}} = 4_{\text{CKM}} + 9_{\text{ferm.masses}} + 2_{\alpha,\alpha_s} + 3_{G_F,M_Z,m_H} + 3_{\nu-\text{masses}} + 4_{\text{PNMS}} = 25 \tag{5.20}$$

parameters (SM + $\nu$-masses and PNMS). In the case of Majorana neutrinos and a See-Saw [130–133] mechanism, the number of parameters is increased by

$$N_{\text{param}}^{\text{See-Saw}} = 3_{\text{N masses}} + 2_{\text{Majoranaphase}}\,. \tag{5.21}$$

Of these 25(30) parameters, 10 are associated with the quark masses and mixing while another 10(15) parametrise the masses and mixing angles in the lepton sector. Models beyond the SM can introduce easily $\mathcal{O}(100)$ additional ones. As the number of experimental constraints does not increase, the viable parameter space is potentially huge. Our second problem is the parametrisation. This problem however cannot be solved in a general form, because the optimal parametrisation might differ for individual regions in the parameter space. The problem related to the number of parameters is usually alleviated in several steps:

- The first step is reducing the number of parameters. One usually tries to find theoretical arguments (symmetries) which help define relation between parameters. The most common ansatz in the flavour sector is to assume some form of a MFV.

- The second step is to find and eliminate the portions of the parameter space that would lead to a non-perturbative behaviour of the theory. Though this is not strictly necessary, not doing so would leave us with very little predictive power.

- At this point, one could start with a numerical analysis by applying all constraints from EWPO and flavour data. However, some theorists want to further restrict the parameter space and define 'naturalness' criteria for the parameters. This has become common practice among physicists. However, we refrain from doing so as this procedure is again not invariant under re-parametrisation of the model and thereby has no direct physical meaning.

After having reduced the number of additional model parameters to a manageable number $N_{\text{add.param}} \sim \mathcal{O}(10)$, one has to decide on a procedure for the numerical analysis. There is a number of very different general strategies which we review briefly.

- Fitting: This is by far the most ambitious numerical strategy. Performing fits for models of NP only yields meaningful results in very specific cases where there is
  - only a small number of additional parameters;
  - a direct impact of the parameters on measured observables;
  - preferably no or only small cancellations between new contributions and the known SM ones.

Additionally, one would prefer some non trivial deviations of the SM predictions from the measured values or equivalently a bad SM fit. If these requirements are met, performing a fit can be worthwhile as only a fit can give qualitative as well as quantitative results.

- Monte Carlo (MC) Scans [305]: The strategy we want to follow in this work is a Monte Carlo scan of the parameter space in order to estimate viable regions. The resulting hypervolume of the parameter space can only be understood as the minimally allowed one. In contrast to a fit, this method cannot give information on preferred regions and cannot exclude parameters. However, in spite if its shortcomings in quantifying results, this method can provide interesting insights into models of NP without requiring an untenable effort. For a very large number of sampled points, the resulting hypervolume will in fact converge to the maximally allowed one. However, in practice this seldom happens.

- Markov-Chain Monte Carlo Methods (MCMC): Markov-Chains [305–308] can either be used as a numerical device for fits or in order to improve the performance of Monte Carlo scans. In either case, one defines a likelihood estimator and tries to minimise (maximise) it. Each 'link' or state of the Markov-Chain is derived from the previous one by changing one (or multiple) parameter(s) randomly. If the likelihood is improved the change is accepted instantly and the next link is found. If the likelihood is not improved the change is still accepted but only with a certain probability. This enables the Markov-Chain to 'jump fences', i.e. leave local minima. The application of MCMC methods in the analysis of NP models crucially depends on the likelihood estimator. Using $\chi^2$ for example tends to yield poor results due to very steep changes of $\chi^2$ and wide local minima.

- Scenarios: The least expensive method in terms of computing power is to fix all but a very few parameters. This is usually done by defining a number of scenarios for the fixed parameters in order to show their impact. The remaining free parameters can be scanned directly i.e. on a fixed grid or can be fitted using standard methods. This procedure allows quick insights into the behaviour of a model and can be used for exploratory studies. However, as with a Monte Carlo scan, the results obtained cannot be quantified. Moreover, while the results of Monte Carlo methods do eventually converge to the maximally allowed region for a large number of sampled points, the method of choosing scenarios can never give anything more than exemplary results.

## 5.3 An Improved Monte Carlo Scan Method

In this section, we want to propose an improved method for MC scans. Inspired by adaptive methods in Monte Carlo integration, e.g. VEGAS [309,310], this method refines the search for valid points in the N-dimensional parameter space in each step. But first, we want to discuss the problem we are facing in more detail.

### The Problem

The problem we are facing when performing Monte Carlo scans is the non-linearity of the constraints in terms of the model parameters. This is made worse by possible interference between SM and NP contributions as well as cancellations and interference between different

NP contributions. Take for example our discussion on $\varepsilon_K$ in the SM4 (section 3.3) or the more general considerations concerning the suppression of LRM effects (section 3.4). In the case of $\varepsilon_K$ in the SM4, we found that the constraint on $\lambda_{t'}^{(K)}$ was far milder than naively suspected. This was due to cancellations between changed SM contributions and the NP contributions induced by the presence of the $t'$ in the loop. In the case of the LRM, we found that we could restrict certain combinations of elements of the RH mixing matrix to be below some bounds. However, in both cases the dependence on the model parameters was non trivial as the CKM elements are (complicated) functions of the model parameters.
The first improvement one could introduce is a more suitable parametrisation of the CKM matrix. In the case of the LRM for example, it turns out that a RH matrix with transposed (compared to the LH matrix) structure is more suitable. This is mainly due to the strict upper limit on $|V_{td}^{\mathrm{R}}|$. Choosing a general but improved parametrisation might improve the performance of the Monte Carlo scan over large regions of the parameter space. However, we are very interested in specific regions of the parameter space, for example regions with large $|V_{ub}^{\mathrm{R}}|$ in the LRM. If we are willing to invest a lot of computer power, the Monte Carlo scan can find these regions. Having $\mathcal{O}(10-100)$ points in such a region, we could proceed in the following way:

1. Identify the points in an interesting region.

2. Try to find correlations between the parameters of these points.

3. Improve the Monte Carlo scan by enforcing these correlations.

This procedure can be expected to find valid points in the interesting regions much faster than a general scan. However, finding correlations between parameters requires a certain amount of points to start with. Furthermore, the efficiency of this method depends on how strongly the correlations are enforced. Allowing even small perturbations from the correlations can decrease the efficiency drastically but might be desired in order to further investigate the region of interest.

### Proposal: An Adaptive Monte Carlo Scan

In order to improve the efficiency of Monte Carlo scans we want to propose an adaptive method inspired by the VEGAS algorithm [309, 310]. First of all we have to specify the setup. We assume a P-dimensional parameters space with N constraints. Our task is to find the maximally allowed hypervolume in the P-dimensional parameter space. The general procedure follows the steps described below:

1. Generate a number of valid points using a general Monte Carlo Scan.

2. Select any number of combinations of observables with direct constraining power or not. These are grouped into pairs or triples. Due to memory constraints on the computer, the groups should not be much larger.

3. Generate a fixed grid for each of these pairs or triples and count the number of points in each box. The grid can can either be imposed on the whole allowed range for the selected observables in each set, or it can be imposed on the ranges spanned by the values of the selected observables for the initial points.

4. Try to find new points in the neighbourhood of existing points. The number of tries is inverse to the number of points in the box. This reflects the point that we are interested in regions not easily accessible by a general scan.

We have implemented the general idea outline above and show the results after a more detailed description of the algorithm. We conclude this section with a short discussion on the problems and possible improvements of our algorithm.

**The Algorithm**

Starting from a number of initial points, the following steps are performed repeatedly until the desired point density in the the regions of interest is reached.

1. Create a grid with maximal 100 filled boxes for each pair or triple of observables.
2. Select one point $x$ randomly from each filled box in (1).
3. Generate $q$ tries for each point $x$, where $q$ is calculated according to equation (5.22). Each try is an independent and random variation of all $N$ components of $x$. We found that in order to improve the performance of the algorithm using Gaussian-distributed random numbers for these variations is advisable.
4. Calculate all observables and apply all constraints to the new points and add the valid points passing all constraints to the pool of valid/initial points for the next iteration.

The number of tries per box is given by

$$q = 1 + \frac{10^6}{N_P^4}\,, \tag{5.22}$$

where $N_P$ denotes the number of points in the corresponding box. For more than 32 points in one box equation (5.22) allows for only one new point in this box per iteration. The constraint of at most 100 filled boxes prevents the algorithm from requiring exponential execution time.

**Results**

As a test setup we chose the LRM for large $s = 0.6$. In this case, our global analysis shows (see section 7.2) only a few points for a large $|V_{ub}^{\mathrm{R}}|$. The point density is especially low for points with low fine tuning (see section 7.2). In figure 5.3, we show the correlation of $|V_{ub}^{\mathrm{R}}|$ and $|V_{cb}^{\mathrm{R}}|$ in the LRM for $s = 0.6$. The black crosses are the initial set while the blue points are found by our algorithm. The time required to arrive at this result was approximately 2 h and the computation was performed on a single computer. Achieving a similar result using enforced correlations between several parameters would take more than a day on a cluster with $\mathcal{O}(100)$ CPUs. However, as our initial points show a large fine-tuning so do our new points. The reason for this is twofold:

1. We can assume that in the vicinity of points with high/low fine-tuning there are again points with high/low fine-tuning. This is basically the definition of fine-tuning.
2. If we find points in new boxes these potentially have a large fine-tuning. This is clear from the definition of fine-tuning, as a point near another point in the parameter space but not near it in the space of observables is fine-tuned by the Athron-Miller criterion of fine-tuning (see section 7.1).

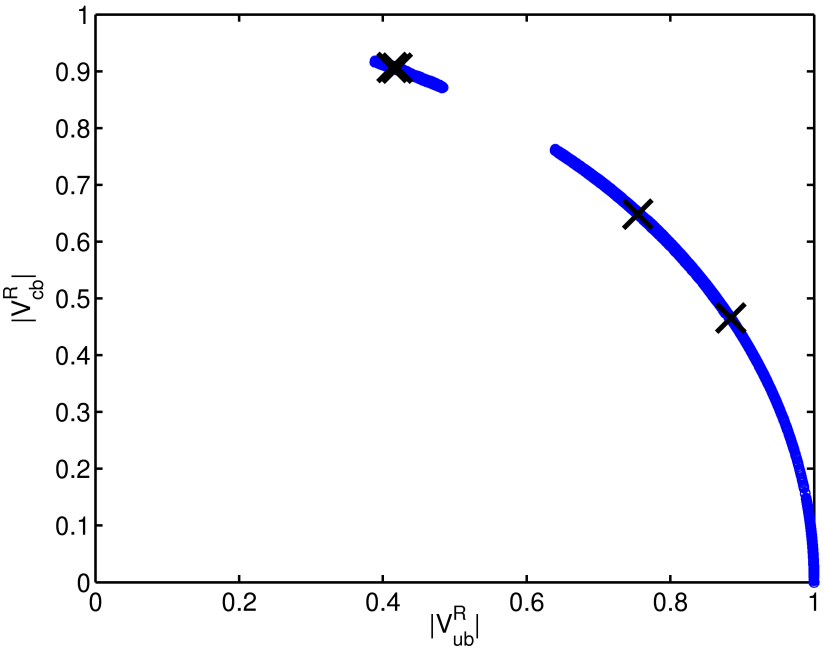


Figure 5.3: The correlation of $|V_{ub}^{\mathrm{R}}|$ and $|V_{cb}^{\mathrm{R}}$ in the LRM for $s = 0.6$. The black crosses represent the initial set used for our algorithm and the blue points show the additional points found by our method.

### Discussion and Improvements

We have shown that the general idea for our improved MC scan works quite well as discussed above. However, there are a series of problems still to be addressed in the concrete application of our idea. The main drawbacks of the algorithm currently are:

- A strong dependence on the initial set of points. If for example the initial set of points exhibits a large amount of fine-tuning, the algorithm most likely finds points with large fine-tuning. This is true even if there are regions in the parameters space that have low fine-tuning and are mapped to the region of interest.

- The solution to the problem of exponential computing time is far from perfect. In our approach, keeping the number of filled bins below 100, the grid can get very coarse which would negate some of the benefits of the algorithm.

- The size of the variations has to be tuned by hand and is common for the whole parameter space. On the one hand, this forces us to optimize the algorithm for each setup by hand. On the other hand, this ignores the fact that the sensitivity on different parameters varies for different regions of the parameter space.

We close this discussion by addressing some of the issues raised above. Possible improvements of the algorithm are:

- Making the grid more adaptive could improve the performance of the algorithm. The grid for each pair (triple) of observables could be adapted in each step of the iteration.

While keeping the number of boxes constant the size of different boxes could be allowed to vary as long as there is no overlap. This would allow for a finer grid in regions with few points and a more coarse grid in regions with a very high or zero point density.

- One might also choose to use a non-regular grid e.g. using triangular shaped cells. This would be inspired by finite-element-methods (FEM) for solving partial differential equations (PDE) [311–313].
- The size of the variation could be adapted in each step to increase the number of valid points. This could improve the algorithm because the sensitivity on different parameters can be expected to vary. The best result could probably be achieved by adapting the variation size for each individual box and parameter separately. However, as this would increase the required memory drastically, we suggest to use the same variation size for groups of boxes.
- Combining the MC scan aspect of this algorithm with MCMC methods could in principle increase the performance as well. In this case the likelihood function would have to be chosen with great care. Using MCMC methods could, however, mitigate some of the problems related to the strong dependence on the initial set of points.

However, implementing even one of these points would require some effort in redesigning the algorithm.

# 6

# General Constraints and Non-Flavour Bounds

Before we can turn to constraints on models of NP, we have to take stock of the SM. To this end, we revisit the SM fits and show a rough fit to the most important inputs. Subsequently, we discuss the constraints from $\Delta F = 2$ observables on general NP contributions. In the last two sections we discuss the constraints from collider searches, electroweak precision tests and tree-level constraints on the SM4 and the LRM respectively.

## 6.1 The SM Fit

In this section we discuss the SM fits. We present the $\Delta F = 2$ constraints in the Wolfenstein parametrisation and perform a simplified fit to the existing data. In the end of this section we compare our result to the ones given by the CKMfitter and UTfit collaborations.

In section 5.1, we have introduced the Wolfenstein parametrisation for the CKM matrix. Using this parametrisation, we can give approximate expression for the SM observables introduced in section 3.2

$$\begin{aligned}\varepsilon_K = 2A^2\lambda^6\bar{\eta}C_\varepsilon \Bigg[&\hat{\eta}_{ct}S_{ct}\left(1-\left(\frac{3}{4}+A^2\right)\frac{\lambda^4}{2}\right)\\ &-\hat{\eta}_{cc}S_{cc}\left(1-\lambda^2-A^2\lambda^4\right)+\hat{\eta}_{tt}S_{tt}A^2\lambda^4(1-\bar{\rho})\Big]\,,\end{aligned} \tag{6.1}$$

$$\Delta M_d = C_d\hat{\eta}_B S_{tt}A^2\lambda^6\left(1-\frac{1}{2}A^2\lambda^4\right)\left(\bar{\eta}^2+(\bar{\rho}-1)^2\right)\,, \tag{6.2}$$

$$\Delta M_s = C_s\hat{\eta}_B S_{tt}A^2\lambda^4\left(1-(1-2\bar{\rho})\lambda^2\right)\,, \tag{6.3}$$

$$\Delta M_d/\Delta M_s = \frac{m_{B_d}}{m_{B_s}}\xi^{-2}\lambda^2\left(1+(1-2\bar{\rho})\lambda^2\right)\left(\bar{\eta}^2+(\bar{\rho}-1)^2\right)\,, \tag{6.4}$$

$$S_{\psi K_s} = \sin\left[\arctan\left(\frac{2\bar{\eta}(1-\bar{\rho})}{(1-\bar{\rho})^2-\bar{\eta}^2}\right)\right]\,, \tag{6.5}$$

where we used the abbreviation $S_{ij}$ for $S_0(x_i, x_j)$ and defined

$$C_\varepsilon = \frac{G_F^2M_W^2F_K^2\hat{B}_K m_K}{6\sqrt{2}\pi^2\Delta M_K}\,, \qquad C_q = \frac{G_FM_W^2\left(F_{B_q}\sqrt{\hat{B}_{B_q}}\right)^2 m_{B_q}}{6\pi^2}\,. \tag{6.6}$$

In figure 6.1, we show the constraints from $\varepsilon_K$, $\Delta M_d/\Delta M_s$, $|V_{ub}/V_{cb}|$, $S_{\psi K_s}$ and $\gamma$ in the $(\bar{\rho},\bar{\eta})$ plane evaluated for $(\lambda, A) = (0.2252, 0.782)$. The plot in figure 6.1 illustrates how the interference of the different constraints work. If two constraints overlap the colour changes and the likelihood increases in such regions. The colour code is in more detail given by:

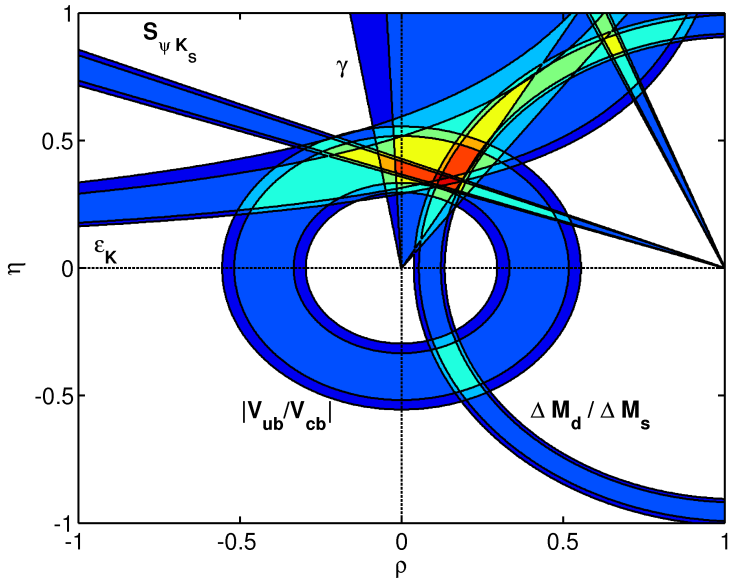


Figure 6.1: The constraints on the $(\bar{\rho}, \bar{\eta})$ plane from $\Delta M_d/\Delta M_s$, $\sin 2\beta$, $\varepsilon_K$, $|V_{ub}/V_{cb}|$ and $\gamma$

- Dark blue, blue regions indicate roughly the two and one sigma regions for the observables.
- Light blue and green regions indicate that two or three constraints overlap at two or one sigma.
- Yellow and orange regions indicate that three or four constraints overlap at two sigma or one sigma.
- Red and dark red regions indicate that four or five constraints overlap at two sigma or one sigma.

We have performed three very simple fits using different constraints. In these simple fits we ignore the subtleties introduced by the errors on theoretical parameters and include them in a very simple, straightforward manner (6.9). This clearly makes our results non-quantifiable. However, this procedure can serve to get a qualitative picture on how the constraints act on the parameters. The first fit uses all $\Delta F = 2$ constraints together with $|V_{us}|$ and $|V_{ub}/V_{cb}|$. In our second and third fit we concentrate on different inputs and perform a fit using only $\Delta F = 2$ constraints (together with $|V_{us}|$) or only tree-level constraints together with $\sin(2\beta)$. All our fits treat $\varepsilon_K$ as an output, this would allow us to identify potential tensions [23–25, 27, 179]. However, as the error on $\hat{\eta}_{cc}$ was drastically increased in the recent NNLO calculation [39], our very rudimentary fit is not able to find such a tension. As can be seen from figure 6.1, decreasing the error on $\varepsilon_K$ would introduce a tension between $\varepsilon_K$ and the other constraints. The results of our fits are given in table 6.1, while the inputs are listed in tables 6.3 and 7.1. In our analysis, we use the result of the first fit as our reference point for the SM.

However, our simple fit neglects some of the points already outlined in section 5.1. A complete and rigorous analysis of the UT and the general SM fit is clearly beyond the scope of this work.

| | $\bar{\rho}$ | $\bar{\eta}$ | $\lambda$ | $A$ |
|---|---|---|---|---|
| $\Delta F = 2 + \lvert V_{ub}/V_{cb}\rvert$ | 0.152 | 0.334 | 0.2252 | 0.782 |
| only $\Delta F = 2$ | 0.143 | 0.324 | 0.2250 | 0.780 |
| tree-level + $\sin(2\beta)$ | 0.137 | 0.346 | 0.2258 | 0.797 |

Table 6.1: The result of the three simple fits, $\varepsilon_K$ is treated as an output

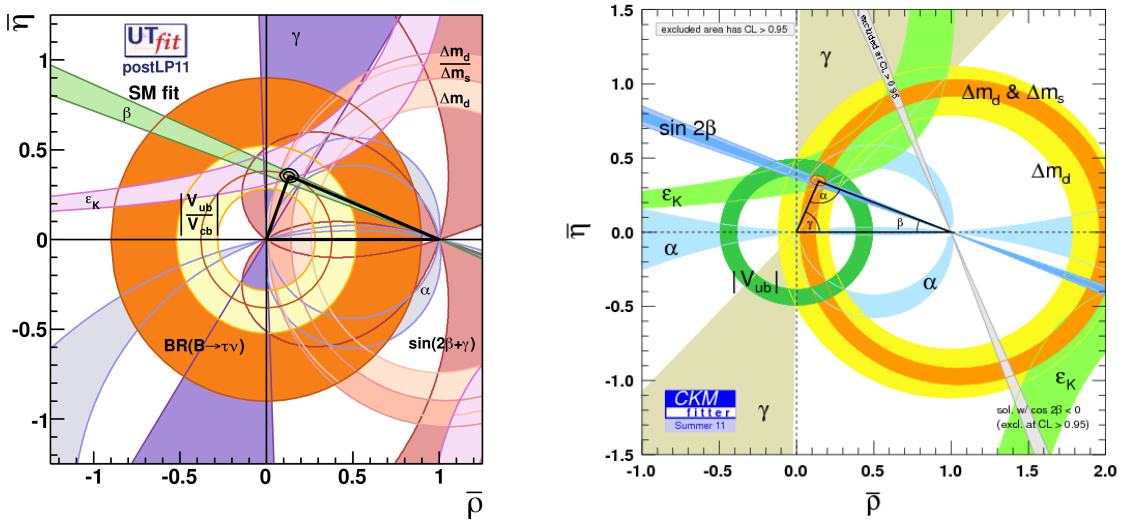


Figure 6.2: The results of the full SM fit given as constraints in the $(\bar{\rho}, \bar{\eta})$ plane. The left panel shows the result published by the UTfit collaboration [314], while the right panel shows the result given by the CKMfitter collaboration [189]

| | $\bar{\rho}$ | $\bar{\eta}$ | $\lambda$ | $A$ |
|---|---|---|---|---|
| UTfit | 0.131(22) | 0.354(15) | 0.2252(1) | 0.817(15) |
| CKMfitter | $0.144^{+0.023}_{-0.026}$ | $0.343^{+0.015}_{-0.014}$ | $0.22539^{+0.00062}_{-0.00095}$ | $0.801^{+0.026}_{-0.014}$ |

Table 6.2: The result of the global SM fit from the UTfit group [314] and the CKMfitter group [189]

We conclude this section by showing the state-of-the-art results for the global SM fit. In figure 6.2, we show the most recent UT fits by the CKMfitter [189] and UTfit [314] collaborations. The results for the CKM parameters derived by both groups are given in table 6.2. The results of both groups are compatible within errors. However, the result of the UTfit group has slightly smaller errors due to their more consistent treatment of the theoretical uncertainties (see [315] for a more detailed discussion of the differences between the Bayesian and the frequentist approach). Furthermore, the CKMfitter result exhibits strongly asymmetric errors, which introduces difficulties in interpreting the numbers as no shape functions for the errors are

provided (see [316] for a critical discussion on asymmetric errors).

## 6.2 $\Delta F = 2$ Constraints on NP Models

In this section, we discuss the impact of the constraints from $\Delta M_d$, $\Delta M_s$, $S_{\psi K_s}$, $S_{\psi\phi}$ and $\Delta\Gamma_s$ on general extensions of the SM. To this end we parametrise $M_{12}^{(q)}$ in the following way [181]

$$M_{12}^{(q)} = \left(M_{12}^{(q)}\right)_{\rm SM}\left[1 + h_q e^{i\phi_q}\right] . \tag{6.7}$$

This parametrisation encompasses most of the models of NP including the LRM. The SM4 contributions, however, cannot be cast into this form due to the changes in the 3-by-3 CKM matrix. In order to find out how the constrains affect $h_q$ and $\phi_q$ we use

$$\chi^2 = \sum_{i=1}^{N_{\rm obs}} \left(\frac{o_i^{\rm exp} - o_i^{\rm theo}}{\sigma_i^{\rm tot}}\right)^2 , \tag{6.8}$$

where $o_i^{\rm exp}$ and $o_i^{\rm theo}$ are the experimental and theoretical value of a given observable, $N_{\rm obs}$ is the number of observables considered. The total uncertainty

$$\sigma_i^{\rm tot} = \sqrt{(\sigma_i^{\rm exp})^2 + (\sigma_i^{\rm theo})^2}\,, \tag{6.9}$$

serves as a short-cut for the introduction of the theoretical uncertainties. This treatment is justified in our current discussion as we are only interested in qualitative results. Note that our simplified treatment of the theoretical uncertainties implicitly assumes Gaussian PDFs for the theoretical parameters. The correct treatment would be to use one of the methods outlined in section 5.1. However, using the correct treatment would require unwarranted effort in this case. Using equation (6.8), we generate plots of $\phi_q$ versus $h_q$ with $\chi^2/n_{\rm d.o.f.}$ shown in colour. This allows us understand the impact of different constraints in a very intuitive way. For transparency, we chose to plot the area with $\chi^2/n_{\rm d.o.f.} \geq 7$ in white and regions with $\chi^2/n_{\rm d.o.f.} < 1$ in the same colour as $\chi^2/n_{\rm d.o.f.} = 1$. In figure 6.3, we show the constraint on $h_s$ and $\phi_s$ from $\Delta M_s$ alone (left panel) and from $\Delta M_s$, $S_{\psi\phi}$ and $\Delta\Gamma_s$ together (right panel). The plot in the left panel of figure 6.3 shows that mostly real new contributions to $M_{12}^{(s)}$ are forbidden for $h_s \sim 1$ while dominantly imaginary ones are not. This is clear from equations (6.7) and (3.22). The constraint from $\Delta M_s$ alone allows also for $h_s \sim 2$ together with a marginal phase $\phi_s$, which serves as a loophole in NP studies, as already pointed out in [181]. In March of 2012 the LHCb collaboration released updated values for $S_{\psi\phi}$ and $\Delta\Gamma_s$ [38, 190]. Adding these new constraints to $\chi^2$ we find the plot in the right panel of figure 6.3. This plot shows a drastically different picture, the interplay of $\Delta\Gamma_s$ and $S_{\psi\phi}$ eliminated most of the formerly allowed regions. In particular, adding the new constraints closes the aforementioned loophole. The allowed region, taking into account the new data, is strongly constrained to NP having a small amplitude when compared to the SM. The amplitude $h_s$ is allowed to be slightly larger only for $|\phi_s| \sim \pi/2$. This is in contrast to the situation in the $B_d$ system, where a real NP contribution is allowed to be larger only at very sharp peaks around $\phi_d \sim 0$ and $\phi_d \sim \pm\pi$.

In figure 6.4, we show the constraints on $(h_d, \phi_d)$ on the left hand side and ( Re($h_K$), Im($h_K$)) on the right hand side. The constraints on $(h_d, \phi_d)$ are comparable in strength to the new

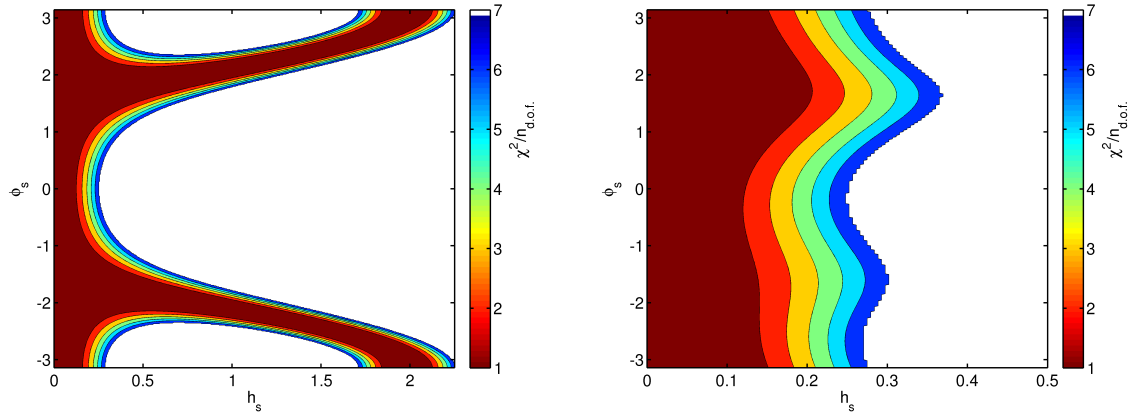


Figure 6.3: $\chi^2/n_{\text{d.o.f.}}$ in dependence of the parameters $\phi_s$ and $h_s$. In the left panel only the constraint from $\Delta M_s$ is used, while in the right panel all available data was taken into account.

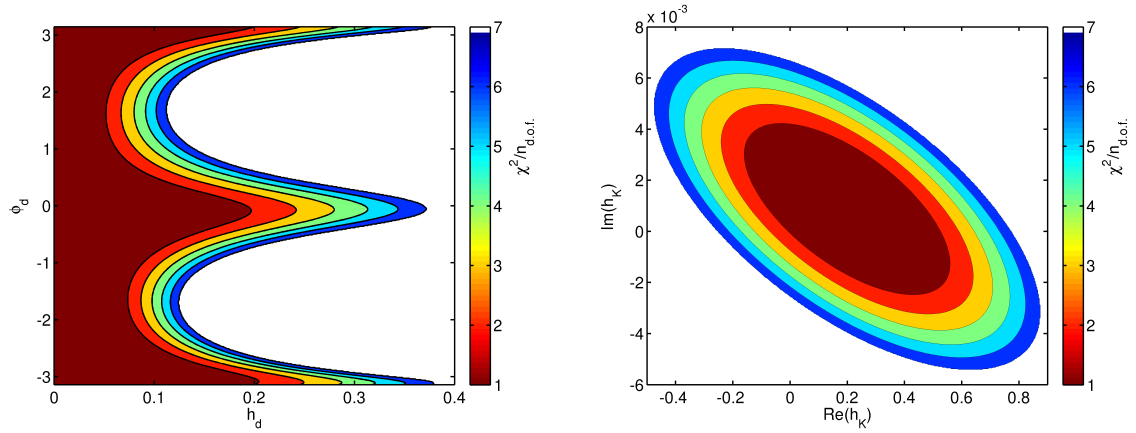


Figure 6.4: The parameters $\phi_d$ and $h_d$ as functions of each other with $\chi^2/n_{\text{d.o.f.}}$ as the colour (left panel), and the real and imaginary part of $h_K$ with $\chi^2/n_{\text{d.o.f.}}$ as the colour (right panel)

constraints on $(h_s, \phi_s)$. However, the contour exhibits a completely different structure. While the new constraint on $(h_s, \phi_s)$ is the weakest in the region around $\phi_s \sim \pi/2$, the preferred region of $(h_d, \phi_d)$ has sharp peaks at $\phi_d \sim \pm\pi, 0$. This indicates the good agreement between theory and experiment in $S_{\psi K_s}$ as well as the small error on the measurement and the prediction. The plot in the right panel of figure 6.4 shows the constraint from $\varepsilon_K$ and $\Delta M_K$ on $h_K$, where we defined the complex parameter $h_K$ as

$$M_{12}^{(K)} = \left(M_{12}^{(K)}\right)_{\text{SM}} [1 + h_K] \ . \tag{6.10}$$

We can clearly see that the imaginary part of $h_K$ is tightly constrained by $\varepsilon_K$ while the uncertainty on the LD contribution to $\Delta M_K$ allows for large effects in the real part of $h_K$. As can be seen from the plot in the right panel of figure 6.4, the SM point $(0, 0)$ is at the edge of the $\chi^2/2 \equiv 1$ ellipsis. This shows the minimal tension in $\varepsilon_K$ which could become important if the error on $\hat{\eta}_{cc}$ could be reduced.

## 6.3 Tree-Level, EWP and Collider Bounds on the SM4

The experimental situation is becoming increasingly dire for the SM4. While direct searches at the LHC pushed the lower limits on the masses up to the perturbativety limit [9–12, 317], the Higgs searches indicate a low mass Higgs [1–3] which puts the SM4 further under pressure. Most recent studies of the LHC data in the context of the SM4 include the data on potential Higgs decays which can help to put very stringent bounds on the SM4 [99, 110–112].

### The Collider Bounds

The current lower limits on the masses of the heavy quarks are given by [11, 12]

$$557\,\text{GeV} \leq m_{t'} \qquad (95\%\text{CL})\,, \qquad\qquad 611\,\text{GeV} \leq m_{b'} \qquad (95\%\text{CL})\,. \tag{6.11}$$

Though the bounds given in (6.11) put very strong constraints on the SM4, they have to be used with caution. As in many studies, this experimental search was performed assuming the total dominance of one decay channel

$$t' \to Wb\,, \qquad\qquad b' \to Wt\,, \tag{6.12}$$

respectively. In [110, 318], the effects of non-vanishing mixing between the fourth and the first two generations were studied in the context of such exclusion limits. Though the mass limits studied in [110, 318] are somewhat lower than the ones available today, their reasoning remains solid. Assuming a more general scenario, the authors of [110, 318] were able to find general limits on the masses which were by $40\,\text{GeV} - 100\,\text{GeV}$ weaker than the ones given by the experimental groups. In our study we do not investigate this subtlety further and fix the masses to

$$m_{t'} = 600\,\text{GeV}\,, \qquad\qquad m_{b'} = 650\,\text{GeV}\,, \tag{6.13}$$

though the mass of the $b'$ is not important for our study. Interchanging the masses in (6.13) would be allowed, as the mass limits can be weakened by opening other decay channels. In [95], it has been shown that a mass splitting of roughly 50 GeV is preferred by electroweak precision tests.

### The Electroweak Precision Tests in the Context of the SM4

The impact of a fourth generation on the EWPT has been studied by several authors [96,98,99]. In fact, the EWPT were cited as a clear sign for the SM4 to be ruled out [47]. However, this holds only for a very specific region in the parameter space of the SM4 i.e. no mixing and degenerate masses of the fourth generation fermions. Allowing for mixing between all four generations as well as a mass splitting of the fourth generation fermions allows to circumvent the strict bounds introduced by the $S$ and $T$ parameters [319] as well as the bound from $\Gamma(Z \to \bar{b}b)$ [47]. As the analysis of the electroweak precision observables (EWPO) in the context of the SM4 requires great effort, we use the results provided by [96]. For a light Higgs as indicated by Tevatron [3], ATLAS [1] and CMS [2] and a large $t'$ mass, the upper limit on $|V_{tb'}|$ is very strict. Using [96], we find the approximate bound

$$|V_{tb'}| \leq 0.07\,, \tag{6.14}$$

| | | | |
|---|---|---|---|
| $\|V_{ud}\|$ | 0.97425(22) | $\|V_{cd}\|$ | 0.230(11) |
| $\|V_{us}\|$ | 0.2252(9) | $\|V_{cs}\|$ | 1.023(36) |
| $\|V_{ub}\|$ | $3.89(44)\cdot 10^{-3}$ | $\|V_{cb}\|$ | $40.6(13)\cdot 10^{-3}$ |
| $\|V_{tb}\|$ | 0.95(2) | $\gamma$ | $77(11)^\circ$ |

Table 6.3: The tree level constraints on a model without RH couplings of charged gauge bosons. The values are averages over different measurements and given in [47]. $V_{tb}$ was determined by D0 [320]

which is still very optimistic. In the derivation of this bound, recent studies of possible enhancements of Higgs decays [99, 110–112] have not yet been included. However, we checked whether the bound is in drastic contradiction to the constraints studied in [99]. Using figure 4 of [99], one can see that (6.14) does respect the new constraints discussed there.

### Tree-Level Constraints on the CKM4 Matrix

The SM4 does not introduce couplings of $W^\pm$ bosons to right handed currents. Therefore, we can use the extensive studies of tree-level decays in the context of the SM in order to determine some of the CKM4 elements directly. In table 6.3, we have collected the available constraints [47]. It includes a value of $|V_{ub}|$ and $|V_{cb}|$ where the results of the inclusive and exclusive determinations have been averaged (see section 6.4 for more information). Using the values given in table 6.3, we can restrict the matrix elements $|V_{ub'}|$ and $|V_{cb'}|$ by using the unitarity of the CKM4 matrix. On the other hand, the bound on $|V_{tb'}|$ derived this way is much weaker than the one given in (6.14), therefore we neglect it in favour of (6.14). Using the tree-level constraints given in table 6.3, we find

$$|V_{ub'}| \leq 0.042\,, \qquad\qquad |V_{cb'}| \leq 0.1\,, \tag{6.15}$$

where we increased the errors on $|V_{tb}|$ and $|V_{cs}|$ by a factor of two and taking all constraints at $2\sigma$ assuming uniform distributions. Increasing the errors of $|V_{tb}|$ and $|V_{cs}|$ restores the SM[1] as a valid point in the SM4 parameter space. From a comparison of the upper bounds given in (6.14) and (6.15) it is clear that the usual assumption of a one channel dominance in $t'$ and in $b'$ decays is generally not justified. The assumption of one channel dominance is of course still valid though the mixing elements $|V_{t'b}|$ and $|V_{tb'}|$ are tightly constrained which could drastically increase the lifetime of the $t'$ and $b'$ quarks. Putting the constraints on the CKM4 matrix together, we find the following approximate form

$$V = \begin{pmatrix} 1-\frac{\lambda^2}{2} & \lambda & \lambda^3\sigma^* & \lambda^2\xi^* \\ \lambda^3\left(\frac{d^2}{2}-\xi\kappa^*\right)-\lambda & \left(-\frac{d^2}{2}-\frac{1}{2}\right)\lambda^2+1 & a\lambda^2 & \kappa\lambda \\ \lambda^3(a-\sigma) & -a\lambda^2-e\kappa\lambda^3 & 1 & e\lambda^2 \\ \lambda^2(\kappa-\xi) & \lambda^3\left(\frac{\kappa}{2}-\xi\right)-\kappa\lambda & -a\kappa\lambda^3-e\lambda^2 & 1-\frac{d^2\lambda^2}{2} \end{pmatrix} + \mathcal{O}(\lambda^4)\,. \tag{6.16}$$

[1] In the limit of vanishing mixing between the fourth and the first three generations, we find the SM when only concentrating on the flavour sector.

In order to derive the expression given in equation (6.16) we used the following replacement rules:

$$s_{12} \to \lambda\,, \qquad s_{23} \to a\lambda^2\,, \qquad s_{13} \to b\lambda^3\,, \quad s_{14} \to c\lambda^2\,, \quad s_{24} \to d\lambda\,, \quad s_{34} \to e\lambda^2\,,$$
$$be^{i\delta_{13}} \to \sigma\,, \quad ce^{i\delta_{14}} \to \xi\,, \qquad de^{i\delta_{24}} \to \kappa\,. \tag{6.17}$$

For the maximal allowed mixing scenario, the coefficients $a, b, c, d, e$ are of $\mathcal{O}(1)$.

## 6.4 Tree-Level, EWP and Collider Bounds on the LRM

In this section we review the current bounds on the LRM including limits from direct searches, EWPO and tree-level decays. In contrast to the SM4, the bounds on the LRM are not threatening to exclude the model. This can be easily understood: While the SM4 is a non-decoupling theory and therefore has upper limits on the masses of the additional quarks, the LRM does not introduce upper limits on the additional gauge bosons. Therefore, the heavy degrees of freedom can in principle be decoupled. In turn, the LRM can only be excluded for certain masses but never entirely, while the SM4 is nearly excluded already.

### Collider Bounds

The LHC experiments ATLAS and CMS as well as the Tevatron experiments CDF and D0 provide direct limits on the mass of additional heavy gauge bosons $W'$ and $Z'$. Assuming RH couplings of the $W'^{\pm}$ boson equal to the LH couplings of the $W^{\pm}$ boson (or making similar assumptions for the couplings of the $Z'$ boson), the experimental groups find [4–8]

$$2.5\,\text{TeV} \leq M_{W'} \qquad (95\%\text{CL})\,, \qquad\qquad 1.12\,\text{TeV} \leq M_{Z'} \qquad (95\%\text{CL})\,. \tag{6.18}$$

However, all searches assumed $g_L \equiv g_R$ which implies weaker bounds in the case of $g_R < g_L$ and even stronger bounds otherwise. In our analysis, we use the relaxed bound

$$2\,\text{TeV} \leq M_{W'}\,, \tag{6.19}$$

while always assuming $g_R < g_L$. The $Z'$ in the LRM is always heavier than the $W'$ (see Appendix 8). As the constraint on the mass of the $W'$ is stronger than the constraint on the mass of the $Z'$, the constraint on the mass of the $Z'$ has no impact on our analysis. The search for anomalous couplings of the $W$ boson to top quarks also sets potential bounds on the LRM. However, the most stringent bound [321]

$$|f_R^V|^2 \leq 0.3\,, \tag{6.20}$$

is not competitive with the other bounds outlined in this section.

The TWIST collaboration [322] analyses the decays of polarised muons at a very high accuracy. Their goal is to provide data on the left-right asymmetry of the SM, which in turn allows for bounds on RH couplings of the $W$ boson and the mass and coupling of a new heavy $W'$ boson with dominantly RH couplings. In terms of our parameters and to LO in $\varepsilon$, their bounds [322] can be written as

$$sc\varepsilon^2 < 0.020\,, \qquad\qquad \frac{e}{s_W}\kappa_R > 578\,\text{GeV}\,. \tag{6.21}$$

Currently these bounds are not competitive with the ones provided by direct searches. However, updated results could exclude regions of the parameter space that are not easily excluded by direct searches.

| | Experiment | SM prediction |
|---|---|---|
| $\sigma_{\rm had}$ | 41.541(16) | 41.484(8) |
| $A_{\rm FB}(b)$ | 0.0992(16) | 0.1034(7) |
| $Q_W(\mathrm{Cs})$ | −73.20(35) | −73.15(2) |
| $(g_L^{N\nu})^2$ | 0.3027(18) | 0.30399(17) |
| $M_W$ | 80.420(31) GeV | 80.384(14) GeV |

Table 6.4: The experimental and theoretical inputs [47] used in our analysis of selected EWPO

**The Electroweak Precision Constraints**

The electroweak precision tests put stringent bounds on basically any model of NP. The combination of about forty precision observables from high and low energy experiments [47,323–330] provides an extensive test of the SM and its extensions. A full analysis, combining all available data, is clearly beyond the scope of this work. In our analysis we take advantage of [140], where the authors performed an extensive analysis of EWPO in the context of so-called $G(221)$ models. $G(221)$ models are models of NP based on an underlying $\mathrm{SU}(2)_1 \times \mathrm{SU}(2)_2 \times U(1)_{\rm X}$ gauge group. The model we consider in this work is denoted by LR-T in [140]. The authors of [140] provide approximate expressions for the LRM contributions to the four most important observables in their analysis. The approximate LRM contributions read

$$\delta\sigma_{\rm had}/\sigma_{\rm had,SM} = \left(-1.13\frac{c_R^2}{4} - 0.142\frac{c_R^4}{4} + 0.0432(2s^2c^2)\right)\varepsilon^2\,, \tag{6.22}$$

$$\delta A_{\rm FB}(b)/A_{\rm FB,SM}(b) = \left(-30.0\frac{c_R^2}{4} + 67.6\frac{c_R^4}{4} - 20.6(2s^2c^2)\right)\varepsilon^2\,, \tag{6.23}$$

$$\delta Q_W(\mathrm{Cs})/Q_{W,\rm SM}(\mathrm{Cs}) = \left(-0.855\frac{c_R^4}{4} - 0.145(2s^2c^2)\right)\varepsilon^2\,, \tag{6.24}$$

$$\delta(g_L^{N\nu})^2/(g_L^{N\nu})^2_{\rm SM} = \left(-0.0219 + 0.478c_R^2 + 0.210c_R^4 - 1.42(4s^2c^2)\right)\varepsilon^2\,, \tag{6.25}$$

where we already changed the results of [140] in order to match our notation. For completeness sake, we also give the translation rules

$$\tilde{x} = \frac{1}{\varepsilon^2}\,, \qquad c_{\tilde{\phi}} = c_R\,, \qquad \sin 2\bar{\beta} = 2sc\,. \tag{6.26}$$

In table 6.4, we provide the experimental and SM values for the constraints used in our analysis. Our inputs are taken from [47] where one can also find a review of all the observables considered as well as a general discussion of the SM fit to the electroweak precision data. In addition to the constraints listed above, we further use

$$\left(\delta M_W\right)^{\rm NP}/M_W^{\rm SM} = \frac{M_Z}{2M_W^{\rm SM}}\frac{c_W^3}{c_W^2 - s_W^2}\left(\frac{c_R^4}{4} - 2s^2c^2\right)\varepsilon^2\,. \tag{6.27}$$

As already discussed in section 4.1, $s$ is bounded from above by $\mathrm{Br}(B \to X_s\gamma)$. We take this into account by enforcing

$$s \leq 0.64\,, \tag{6.28}$$

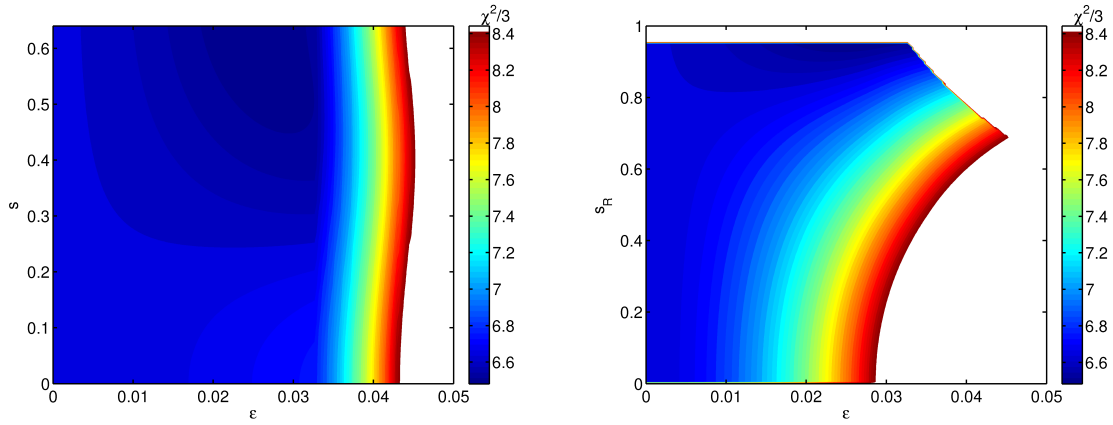


Figure 6.5: The combined constraints from EWPT and collider data on the correlations of $\varepsilon$ and $s$ (left panel) and $\varepsilon$ and $s_R$ (right panel). The colour corresponds to the minimal $\chi^2/n_{\text{d.o.f.}}$ for any given point.

in our analysis. Apart from this bound, the electroweak parameters of the LRM are basically independent of the $\Delta F = 2$ and $\Delta F = 1$ constraints. This allows us to separate our analysis of flavour violating effects from the EWP constraints discussed in this section.

In figure 6.5, we show the impact of selected EWPO and collider constraints in the $\varepsilon - s$ plane (left panel) and $\varepsilon - s_R$ plane (right panel). The colour in figure 6.5 refers to the minimal $\chi^2/n_{\text{d.o.f.}}$ when projecting onto the corresponding plane. The strongest constraints are those from $\sigma_{\text{had}}, (g_L^{N\nu})^2$ and the lower limit on $M_{W'}$. The darkest region in both plots of figure 6.5 represents a softening of the discrepancy between $A_{\text{FB}}^{\text{SM}}(b)$ and $A_{\text{FB}}^{\text{exp}}(b)$. This requires the simultaneous fulfilment of the conditions

$$0.01 \leq \varepsilon\,, \qquad 0.3 \leq s\,, \qquad 0.85 \leq s_R\,, \tag{6.29}$$

which in turn put an upper limit on the mass of the new gauge bosons, as $\kappa_R$ is bounded from above if there is a lower limit on $\varepsilon$. Note that because of the strict upper limit on $\varepsilon$, the $A_{\text{FB}}(b)$ tension can only be softened to below $2\sigma$. Disregarding the softening of the $A_{\text{FB}}(b)$ tension, we find only a minimal preference for $s \sim 0.4$ for large values $\varepsilon$. The correlation between $\varepsilon$ and $s_R$ is much stronger than the one between $s$ and $\varepsilon$. We find that either $\varepsilon < 0.03$ and $s_R$ only bounded by perturbativety, or $s_R \sim 0.7$ in which case $\varepsilon$ is allowed to be as large as roughly 0.045. In our analysis of flavour violating effects, we fix the parameters $\varepsilon$ and $s_R$ to

$$s_R = 0.80\,, \qquad \varepsilon = 0.03\,. \tag{6.30}$$

As the parameter $s$ has a very strong influence on the coupling of neutral and charged Higgs bosons (see section 3.4) through $u(s)$ given in equation (3.57), we chose to vary $s$ in our analysis

$$0.1 \leq s \leq 0.6\,. \tag{6.31}$$

Translating this choice of EW parameters into more tangible quantities we have

$$M_{W'} = 2.6\,\text{TeV}\,, \qquad M_H = \frac{16}{\sqrt{1-2s^2}}\,\text{TeV}\,, \tag{6.32}$$

where the mass of the heavy $W'$ boson would change when changing our reference point for $s_R$ and $\varepsilon$ (6.30). The strong dependence of the Higgs mass $M_H$ on $s$ has profound consequences on the upper limit of the $M_H$ due to perturbativety of the Higgs couplings. For $s = 0$ and to LO in $\varepsilon$, we find $M_H$ to depend only on $\kappa_R$ and one dimensionless parameter $\alpha_3$ (see Appendix 8). This allows us to set a rough upper limit on $M_H$

$$M_H(s \equiv 0) = \sqrt{\alpha_3}\frac{v}{\varepsilon} \lesssim 16\,\text{TeV}\,, \tag{6.33}$$

where we required that $\alpha_3 < 4\pi$.

### Tree-Level Constraints on the LH and RH Mixing Matrices

The appearance of new gauge bosons with RH couplings and the addition of RH couplings to the light $W$ boson has a huge impact on the analysis of tree-level decays. We keep our discussion very short and follow the treatment of [128] concerning the necessary modifications to the (differential) branching ratios studied in this context. In table 6.5, we give a short list with all the necessary inputs. In the LRM, the leptonic or semi-leptonic tree-level decays studied in this context can be potentially modified by several different mechanisms:

| | | | |
|---|---|---|---|
| $\text{Br}(\pi \to \mu\nu) = 0.9998770(4)$ | [331] | $f_\pi = 129.5(17)\,\text{MeV}$ | |
| $f_+(0)\lvert V_{us}\rvert^{K\to\pi\ell\nu} = 0.2163(5)$ | | $f_+(0) = 0.9584(44)$ | |
| $f_K/f_\pi\lvert V_{us}/V_{ud}\rvert^{K\to\mu\nu} = 0.2758(5)$ | [332] | $f_K/f_\pi = 1.1931(53)$ | |
| $\text{Br}(D_s \to \tau\nu) = 0.0529(28)$ | | $f_{D_s} = 248.9(39)\,\text{MeV}$ | |
| $\text{Br}(B \to \tau\nu) = 1.64(34)\cdot 10^{-4}$ | | $f_B = 205(12)\,\text{MeV}$ | [170] |
| $F(1)\lvert V_{cb}\rvert^{B\to D^*\ell\nu} = 0.03604(52)$ | | $F(1) = 0.908(17)$ | [333] |
| $G(1)\lvert V_{cb}\rvert^{B\to D\ell\nu} = 0.0423(15)$ | [54] | $G(1) = 1.074(24)$ | [334] |

Table 6.5: Values of the most important experimental and theoretical quantities used as input parameters for the constraints on tree level charged currents.

1. RH couplings of the light $W$ boson: The new RH coupling of the light $W$ boson in the particular model introduces changes to the predictions for tree-level amplitudes. Depending on RH interactions, the relevant tree-level diagram contributes at $\mathcal{O}(1)$, $\mathcal{O}(\varepsilon)$ or $\mathcal{O}(\varepsilon^2)$.

2. A heavy $W'$ in the intermediate state: The heavy $W'$ could in principle appear in the intermediate state, this introduces a suppression factor $1/M^2_{W'} \lesssim \mathcal{O}(\varepsilon^2)$ through the propagator. However, as the heavy $W'$ couples to light (mostly left-handed) neutrinos only at $\mathcal{O}(\varepsilon)$, the total contribution of $W'$ is at least $\mathcal{O}(\varepsilon^3)$ and can be neglected.

3. A heavy charged Higgs boson in the intermediate state: As for the $W'$ the exchange of a heavy Higgs introduces a suppression of $1/M^2_H \lesssim \mathcal{O}(\varepsilon^2)$. The coupling of the charged Higgs boson is proportional to the Yukawa coupling of the participating fermions and therefore the charged Higgs contribution is negligible for processes involving light quarks. The only possible exception to this rule is the decay $B^+ \to \tau^+\nu_\tau$ due to the

chiral suppression of the $W^+$ contribution. However, as the charged Higgs diagram is suppressed by $m_B^2/M_H^2$ the contribution is still negligible compared to the RH coupling of the light $W$ boson.

4. The mixing of left and right-handed neutrinos: This effect can be neglected as for realistic neutrino masses the mixing of RH and LH neutrinos is below $\mathcal{O}(10^{-6})$ [133], which is well below the leading effects in $\varepsilon$.

5. Corrections to $G_F$: The corrections to the total decay width of the muon are of $\mathcal{O}(\varepsilon^4)$ and therefore negligible.

As only the RH coupling of the light $W$ boson introduces non-negligible corrections to the tree-level processes, we can introduce the following notation for the mixing entering the vector and axial couplings respectively. In particular we have

$$|V_{ij}|_V = \left|V_{ij}^{\mathrm{L}} + sc\varepsilon^2 V_{ij}^{\mathrm{R}}\right| , \qquad |V_{ij}|_A = \left|V_{ij}^{\mathrm{L}} - sc\varepsilon^2 V_{ij}^{\mathrm{R}}\right| . \tag{6.34}$$

Following [128], we can now use the inputs listed in table 6.5 in order to constrain the axial and vector mixing matrices and thereby $V^{\mathrm{L}}$ and $V^{\mathrm{R}}$. In table 6.6, we show the constraints on the different mixing elements. From table 6.6, it is clear that the elements $|V_{ub}|$ and $|V_{cb}|$ both

| | | |
|---|---|---|
| $\|V_{ud}\|_V = 0.97425(22)$<br>$\|V_{ud}\|_A = 0.981(13)$ | $\|V_{us}\|_V = 0.2257(12)$<br>$\|V_{us}\|_A = 0.2268(22)$ | $\|V_{ub}\|_V = 3.38(36)\cdot 10^{-3}$<br>$\|V_{ub}\|_A = 4.70(56)\cdot 10^{-3}$<br>$\|V_{ub}\|_{\mathrm{L}} = 4.27(38)\cdot 10^{-3}$ |
| $\|V_{cd}\|_V = 0.229(25)$<br>$\|V_{cd}\|_L = 0.230(11)$ | $\|V_{cs}\|_V = 0.98(10)$<br>$\|V_{cs}\|_A = 0.978(31)$ | $\|V_{cb}\|_V = 39.4(17)\cdot 10^{-3}$<br>$\|V_{cb}\|_A = 39.70(92)\cdot 10^{-3}$<br>$\|V_{cb}\|_L = 41.54(73)\cdot 10^{-3}$ |
| – | – | $\|V_{tb}\| = 0.95(2)$ |

Table 6.6: The constraints on the different mixing elements. The values are taken from [54, 320, 331–335].

exhibit a tension between the various determinations. Interestingly, the tension in $|V_{ub}|$ can be potentially explained through RH currents [125–128]. This is due to the fact that $|V_{ub}|_{\mathrm{L}}$ is in between $|V_{ub}|_A$ and $|V_{ub}|_V$. By inspecting equation (6.34) we find that in this case the effects from RH currents can explain (or soften) the tension. In the case of $|V_{cb}|$, on the other hand, RH currents cannot resolve the tension as both exclusive determinations $|V_{cb}|_{V,A}$ are in good agreement while the inclusive value displays a tension of slightly more than $1\sigma$ with the exclusive values. The $2\sigma$ tension in $|V_{tb}|_{\mathrm{L}}$ cannot be explained in the LRM. We ignore this constraint for the moment and wait for the LHC experiments to verify the existence of a tension in $|V_{tb}|_{\mathrm{L}}$.

# 7

# Numerical Results

In this chapter, we present the numerical results of our global MC scan analysis of the LRM and the SM4. Our scan was performed using the theoretical and experimental inputs listed in table 7.1. All constraints are enforced at $2\sigma$ assuming a uniform distribution of the experimental uncertainty and of the uncertainty on our prediction.

We start the discussion of the numerical results with a short overview of the different measures of fine-tuning. Subsequently, we discuss the structure of the additional flavour mixing in the SM4 and the LRM highlighting the impact of the different constraints. This discussion is related to the general constraints discussed in section 6.2. After discussing the structure of the additional mixing, we present selected results for the $\Delta F = 2$ observables and $\mathrm{Br}(B \to X_q\gamma)$ in the context of the SM4 and LRM. We focus our discussion on the impact of constraints and connect our results to our analytical considerations in chapters 3 and 4 and on the dependence of the observables on the elements of the mixing matrices. In the last section of this chapter,

| | |
|---|---|
| $G_\mu = 1.16637(1) \cdot 10^{-5}\,\mathrm{GeV}^{-2}$ | $\eta_1 = 1.87(76)$ [39] |
| $M_W = 80.399(23)\,\mathrm{GeV}$ | $\eta_3 = 0.496(47)$ [171, 172] |
| $\alpha(M_Z) = 1/127.9$ | $\eta_2 = 0.5765(65)$ [173] |
| $\alpha_s(M_Z) = 0.1184(7)$ | $\eta_B = 0.55(1)$ [173, 174] |
| $\sin^2\hat{\theta}_W = 0.23116(13)$ | $F_K = 156.0(11)\,\mathrm{MeV}$ |
| $m_K^0 = 497.614(24)\,\mathrm{MeV}$ | $\hat{B}_K = 0.737(20)$ |
| $\Delta M_K = 0.5292(9) \cdot 10^{-2}\,\mathrm{ps}^{-1}$ | $F_{B_d} = 205(12)\,\mathrm{MeV}$ |
| $\lvert\varepsilon_K\rvert = 2.228(11) \cdot 10^{-3}$ | $F_{B_s} = 250(12)\,\mathrm{MeV}$ |
| $m_{B_d} = 5279.5(3)\,\mathrm{MeV}$ | $\hat{B}_{B_d} = 1.26(11)$ |
| $m_{B_s} = 5366.3(6)\,\mathrm{MeV}$ [331] | $\hat{B}_{B_s} = 1.33(6)$ |
| $\Delta M_d = 0.507(4)\,\mathrm{ps}^{-1}$ | $F_{B_d}\sqrt{\hat{B}_{B_d}} = 233(14)\,\mathrm{MeV}$ |
| $\Delta M_s = 17.77(12)\,\mathrm{ps}^{-1}$ | $F_{B_s}\sqrt{\hat{B}_{B_s}} = 288(15)\,\mathrm{MeV}$ |
| $\tau_{B_s} = 1.471(25)\,\mathrm{ps}$ | $\hat{B}_{B_s}/\hat{B}_{B_d} = 1.05(7)$ |
| $\tau_{B_d} = 1.519(7)\,\mathrm{ps}$ | $\xi = 1.237(32)$ [170] |
| $\sin(2\beta)_{b\to c\bar{c}s} = 0.679(20)$ [54] | |
| $m_c(m_c) = 1.268(9)\,\mathrm{GeV}$ [170, 278] | |
| $m_t(m_t) = 163(1)\,\mathrm{GeV}$ | |
| $m_b(2.5\,\mathrm{GeV}) = 4.60(3)\,\mathrm{GeV}$ | |

Table 7.1: Values of the experimental and theoretical quantities used as input parameters.

| | 2GeV | 4.6GeV | 172GeV | 2.5TeV | 15TeV |
|---|---|---|---|---|---|
| $m_u(\mu)$(MeV) | 2.09(0)(9) | 1.74(6)(7) | 1.15(8)(5) | 0.97(8)(4) | 0.88(8)(4) |
| $m_d(\mu)$(MeV) | 4.73(0)(11) | 3.94(1)(9) | 2.61(2)(6) | 2.19(2)(5) | 2.00(2)(5) |
| $m_s(\mu)$(MeV) | 93.6(2)(11) | 77.9(3)(9) | 51.6(4)(6) | 43.4(4)(5) | 39.5(4)(5) |
| $m_c(\mu)$(MeV) | 1089(7)(0) | 907(6)(0) | 601(5)(0) | 505(4)(0) | 460(4)(0) |
| $m_b(\mu)$(GeV) | – | 4.074(19)(0) | 2.702(14)(0) | 2.268(12)(0) | 2.068(12)(0) |
| $m_t(\mu)$(GeV) | – | – | 162.3(10)(0) | 136.3(9)(0) | 124.2(8)(0) |

Table 7.2: The NLO running quark masses at different scales. The first and the second parenthesis shows the statistical and systematic error, respectively.

we focus on predictions for $\Delta F = 1$ observables in the SM4 discussing important correlations and constraints.

The plots in this chapter exhibit a very different colour codes. The colour code is chosen in such a way as to facilitate the understanding of the model. In plots with a black cross, the black cross is always used to indicate the SM value. If not otherwise indicated, a wide, dashed, horizontal or vertical line indicates the experimental central value. Other symbols and lines are explained in the plot descriptions.

## 7.1 A Fine-Tuning Study

The idea of fine-tuning is to introduce a measure to quantify how artificial a model is. Though the concept of fine-tuning is a very old one, it was revived in [336] in order to evaluate the effectiveness of the solution to the hierarchy problem in different SUSY models. The idea of quantifying models or at least regions of the parameter space of a given model is appealing enough that the fine-tuning idea spread to other types of models as well. There are many different measures and philosophies of fine-tuning on the market and we restrict ourselves to a short list of the most common one and its competitors. A critical review on this topic can be found in [337, 338].

- Barbieri-Giudice (BG): Motivated by the fine-tuning idea of Wilson [336], Barbieri and Giudice [339, 340] proposed a fine-tuning measure that could quantify the sensitivity of an observable on the model parameters. The BG fine-tuning measure is defined as

$$\Delta_{\rm BG}(O_i) = \max_{\rm j} \left| \frac{p_j}{O_i(p_j)} \frac{\partial O_i(p_j)}{\partial p_j} \right| , \tag{7.1}$$

  where $p_j$ denotes the model parameters and $O_i$ an observable. Barbieri and Giudice chose 10 as a 'natural' upper limit on $\Delta_{\rm BG}(O_i)$. However, this fine-tuning measure has serious drawbacks. The most obvious problem is that terms linear in a parameter can introduce a large irreducible fine-tuning over the whole parameter space. Another important problem with this fine-tuning definition is that there is no way to quantitatively compare the fine-tuning of two different models or even two different parametrisations of the same model. This of course makes the 'natural' upper limit of 10 very ad-hoc and probably not applicable in every model. The BG fine-tuning takes into account only

one observable though there might be fine-tuning in several observables. Furthermore, studying the dependence on each parameter separately could mask interesting collective effects. There are a number of ways to ameliorate some of these problems [341–350], but they are all based on modifications of the BG fine-tuning. A more detailed review of the problems of the BG fine-tuning measure can be found in [337, 351].

- Athron-Miller (AM): In an attempt to remedy most of the drawbacks of the BG fine-tuning measure, Athron and Miller [351] proposed an alternative fine-tuning measure. The idea of Athron and Miller was to construct a fine-tuning measure which includes all observables and all parameters simultaneously. Their idea is based on selecting small areas of the whole parameter space with volume $F$ and calculating the variance of an observable in this area. The fine-tuning is than defined as the ratio $F/G$, where $G$ is the volume spanned by the variance of the considered observable. This localised measure can be upgraded to a quantitative measure over the whole parameter space by including a normalisation depending on the volume of the whole parameter space. However, the AM fine-tuning measure (as all the others) is inherently dependent on the parametrisation. As the parametrisation has no physical meaning, i.e. it is not measurable and can be changed without changing the observables, there has to be some doubt whether results derived from such an un-physical construct are indeed reliable.

- 't Hooft: A completely different idea of fine-tuning was introduced by 't Hooft. He states [352]:

  *The naturalness criterion states that one such [dimensionless and measured in units of the cut-off] parameter is allowed to be much smaller than unity only if setting it to zero increases the symmetry of the theory. If this does not happen, the theory is unnatural.*

  However, this idea of fine-tuning is not applicable to a large number of problems we are facing and has therefore been disregarded in favour of other more direct measures.

In [134–136], it has been pointed out that the chirally enhanced LR $\Delta F = 2$ operators could introduce substantial effects in $\varepsilon_K$ and $\Delta M_K$. Thereforem it was argued that LR operators introduce a fine-tuning 'problem'. As the LRM also introduces LR operators, we have to comment on this and study the fine-tuning of the LRM. As the practical application of the AM fine-tuning is very cost intensive in terms of computing power and the results can be approximated by a modified version of the BG fine-tuning, we introduce our own fine-tuning measure

$$\Delta_{\mathrm{BG}}^{\mathrm{mod}} = \frac{1}{N_{\mathrm{obs}}} \sum_{i=1}^{N_{\mathrm{obs}}} \Delta_{\mathrm{BG}}(O_i)\,. \tag{7.2}$$

Our definition (7.2) has to be used in a sensible manner as introducing a large number of un-tuned observables would artificially decrease the fine-tuning. However, we are only including $\varepsilon_K$, $\Delta M_K$ and $\Delta M_s$ as they may exhibit fine-tuning in the BG sense. In our study, we show the fine-tuning as the colour code in some plots as we do not want to enforce artificial bounds on the fine-tuning. Bounds are also given for various levels of fine-tuning leaving the interpretation of the fine-tuning open.

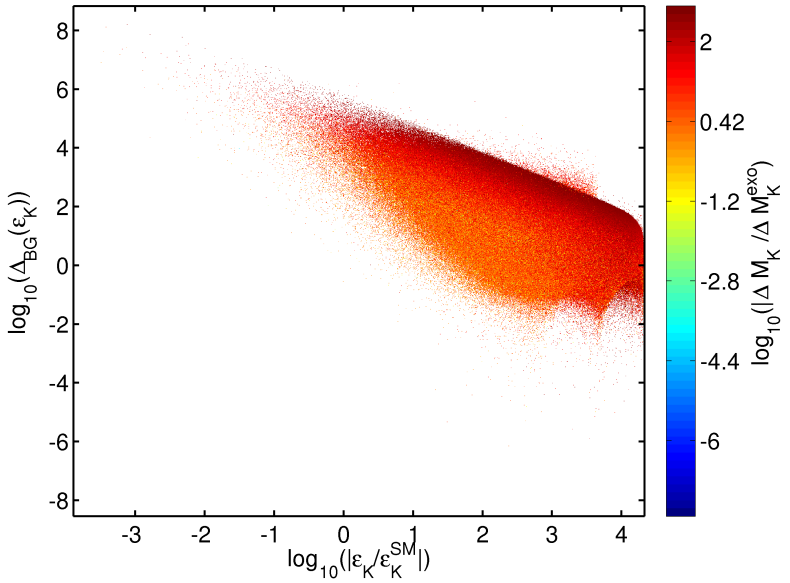


Figure 7.1: The fine-tuning in $\varepsilon_K$ as a function of $|\varepsilon_K/\varepsilon_K^{\rm exp}|$, the value of $|\Delta M_K/\Delta M_K^{\rm exp}|$ is indicated by the colour of the points

We conclude this section with a comment on the so-called 'fine-tuning problem'. In figure 7.1, we show the fine-tuning in $\varepsilon_K$ as a function of $|\varepsilon_K/\varepsilon_K^{\rm SM}|$ in the LRM. For this plot we set the LH mixing matrix to the SM fit value and allowed for arbitrary parameters in the RH mixing matrix. The colour code in figure 7.1 indicates the dependence on $\Delta M_K/\Delta M_K^{\rm SM}$. We find no correlation between $\varepsilon_K$ and $\Delta M_K$ for an arbitrary structure of the RH mixing matrix. The maximal enhancement of $|\Delta M_K|$ compared to the SM value is roughly two orders of magnitude and thereby much smaller than the potential effects in $\varepsilon_K$. From figure 7.1, it is clear that the value of $\varepsilon_K$ can deviate by up to four orders of magnitude from its experimental value. This is not surprising as arbitrary parameters in the RH mixing matrix are obviously in contradiction to the bounds derived in section 3.4. The drastic increase of the upper limit of the fine-tuning together with the low point density for low fine-tuning in the region of $\varepsilon_K$ close to its experimental value led to the idea of a fine-tuning problem. While there might be some debate on the first point, the second point is clearly not valid. Due to the fundamental mechanics of a MC scan, we cannot assign any meaning to the point density. The only information we can derive from the distribution of points in the $\Delta_{\rm BG}(\varepsilon_K) - \varepsilon_K$ plane is that uniformly distributed random numbers are not natural to the model in the sense that they mostly ignore the region of $\varepsilon_K$ close to its experimental value and low fine-tuning.

## 7.2 The Structure of Additional Mixing

### The RH Mixing Matrix

The structure of the RH mixing matrix in the LRM can be very different from the one of the LH mixing matrix. In figure 7.2, we show the correlation between the elements $|V_{us}^{\rm R}|$, $|V_{ub}^{\rm R}|$ and $|V_{cb}^{\rm R}|$ of the RH mixing matrix. The fine-tuning is included in this plot as the colour

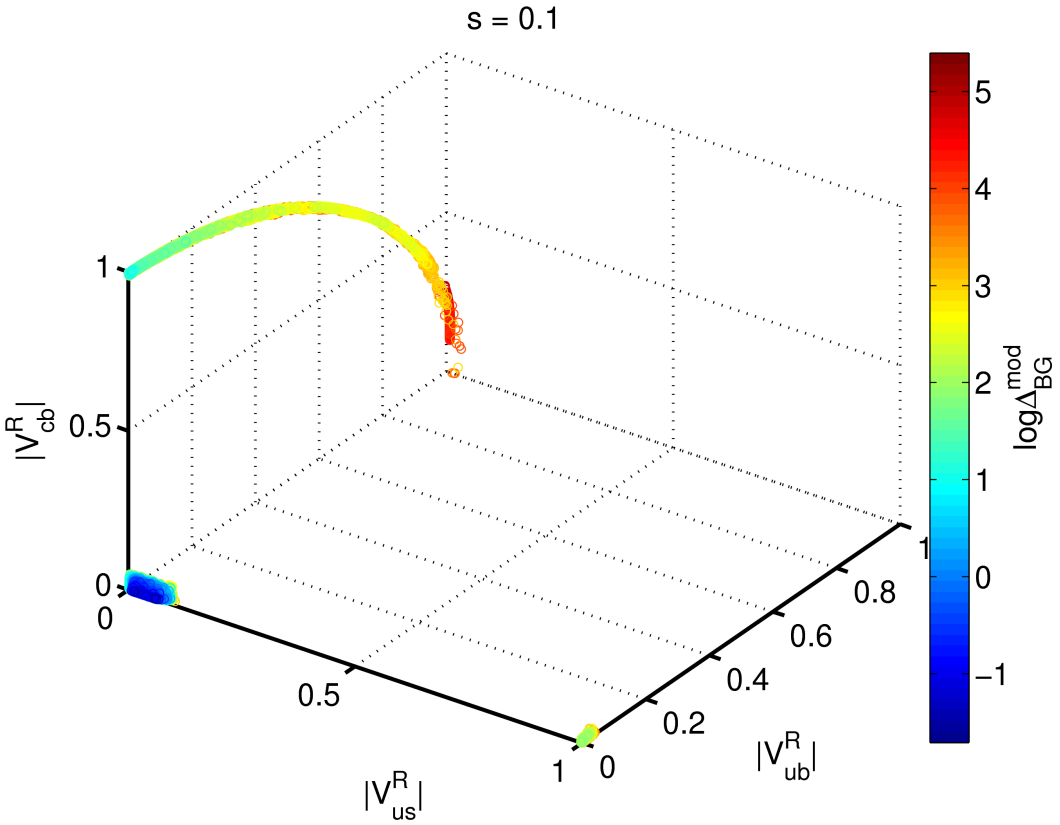


Figure 7.2: The correlation between the elements $|V^R_{us}|$, $|V^R_{ub}|$ and $|V^R_{cb}|$ of the RH mixing matrix in the LRM, the fine-tuning is included in colour.

of the points. Note that points with low fine-tuning are plotted in front of points with high fine-tuning. From figure 7.2, we can see that there are three very distinct scenarios of RH mixing.

- Normal Hierarchy: A matrix with the points in the lower left corner close to $(0, 0, 0)$ in figure 7.2 exhibits a hierarchy similar to the hierarchy of $V^L$. In this case the fine-tuning is potentially very low.

- Inverted 2–3 hierarchy: For $|V^R_{cb}| \sim 1$, $|V^R_{tb}| \ll 1$ is required by unitarity. In this case the RH mixing matrix exhibits an inverted hierarchy in the 2–3 mixing compared to $V^L$. For the limited number of points we have in this scenario we find a moderate to high fine-tuning. However, as already pointed out in section 5.2, the result of a MC scan can only be used to estimate the minimal possible effect. In this scenario it is also possible to shift the big value of $|V^R_{cb}|$ into a big value of $|V^R_{ub}|$ while $|V^R_{us}|$ is required to stay close to zero.

- Inverted 1–2 hierarchy: For $|V^R_{us}| \sim 1$, $|V^R_{cs}| \ll 1$ is required by unitarity. In this case the fine-tuning is moderate to high. The elements $|V^R_{ub}|$ and $|V^R_{cb}|$ have to be close to zero in this scenario.

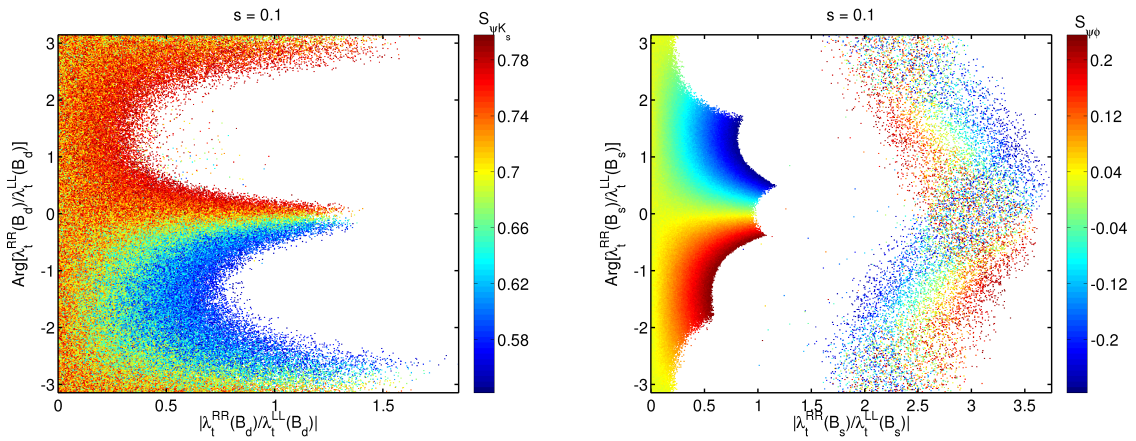


Figure 7.3: The phase as a function of the absolute value of the ratio $\mathcal{F}_t$ in the $B_d$ system (left panel) and the $B_s$ (right panel). The colour code corresponds to the value of $S_{\psi K_s}$ in the left and the value of $S_{\psi\phi}$ in the right panel, respectively.

It is interesting to revisit the possible effect in the $B_d$ and $B_s$ system. To this end we define

$$\mathcal{F}_i(M) = \frac{\lambda_i^{\mathrm{RR}}(M)}{\lambda_i^{\mathrm{LL}}(M)}\,, \tag{7.3}$$

for $i = u, c, t$ and $M = K, B_d, B_s$. In figure 7.3, we show the phase of $\mathcal{F}_t(B_{d,s})$ as a function of $|\mathcal{F}_t(B_{d,s})|$ in the left and right panel, respectively. The colour code represents $S_{\psi K_s}$ in the left panel and $S_{\psi\phi}$ in the right panel. We observe a close relation between the time-dependent CP violation in the respective $B$ system and the ratio $\mathcal{F}_t(B_{d,s})$. In the left panel of figure 7.3, we find a structure very similar to the one shown in the left panel of 6.4. From this structure it is clear that in the case of the $B_d$ system the parametrisation (6.7) is valid for each scenario for the RH mixing matrix with $h_d e^{i\phi_d} \sim \mathcal{F}_t(B_d)$. We can furthermore deduce a clear dominance of the $R_{tt}$ element in this system. The relative enhancement of $\lambda_{tt}^{\mathrm{RR}}(B_d)$ over its LL counterpart cannot exceed roughly 1.5. For a relative phase below zero the changes in $S_{\psi K_s}$ are either small or negative while for a positive relative phase the changes in $S_{\psi K_s}$ are either small or positive. The correlation between $S_{\psi K_S}$ and $\mathcal{F}_t(B_d)$ is diluted for some values of $\mathcal{F}_t(B_d)$. In these cases other elements of $\hat{R}$ and $\hat{\Lambda}$ (as defined in equations (3.71) and (3.70)) are competetive with $R_{tt}\Lambda_{tt}$.

In the right panel of figure 7.3, we show $S_{\psi\phi}$ in dependence on $|\mathcal{F}_t(B_s)|$ and $\arg(\mathcal{F}_t(B_s))$. We find the structure to be only partly similar to the one derived for general extensions of the SM. Up to reparametrisations of the phase of $\mathcal{F}_t(B_s)$, the region with $|\mathcal{F}_t(B_s)| \lesssim 1$ resembles the plot in the right panel of figure 6.3. In this case the RH mixing matrix is in the normal hierarchy scenario and we can parametrise the effects in the $B_s$ system by (6.7) with $h_s e^{i\phi_s} \sim \mathcal{F}_t(B_s)$. The dominant contribution to $M_{12}^{B_s}$ is proportional to $\lambda_i^{\mathrm{RR}}(B_s)$. The cloud of points around $|\mathcal{F}_t(B_s)| \sim 2.5$ represents points from the inverted hierarchy scenario of the RH mixing matrix. In this case we cannot establish a clear dominance of the top-top contribution. In order to better understand this situation, we first introduce an approximate form of the RH mixing

matrix in the inverted hierarchy scenario

$$\begin{pmatrix} e^{i\phi_{ud}}\left(1-\frac{1}{2}\tilde{\lambda}^2\right) & e^{i\phi_{us}}\tilde{\lambda} & Ae^{i\phi_{ub}}\tilde{\lambda}^2 \\ e^{i(\phi_{cb}+\phi_{ud})}\left(-e^{-i\phi_{ub}}A - Be^{-i(\phi_{tb}-\phi_{ts}+\phi_{us})}\right)\tilde{\lambda}^2 & Be^{i(\phi_{cb}-\phi_{tb}+\phi_{ts})}\tilde{\lambda} & e^{i\phi_{cb}}\left(1-\frac{1}{2}B^2\tilde{\lambda}^2\right) \\ e^{i(\phi_{ts}+\phi_{ud}-\phi_{us})}\tilde{\lambda} & e^{i\phi_{ts}}\left(\frac{1}{2}\left(B^2+1\right)\tilde{\lambda}^2-1\right) & Be^{i\phi_{tb}}\tilde{\lambda} \end{pmatrix}, \tag{7.4}$$

where $\tilde{\lambda} \sim \mathcal{O}(10^{-1})$ and $A, B \sim \mathcal{O}(1)$. From equation (7.4), it is clear that the combination $|V_{cb}^{\mathrm{R}*}V_{ts}^{\mathrm{R}}|$ is more important than the combination $|V_{ts}^{\mathrm{R}*}V_{tb}^{\mathrm{R}}|$ in the scenario with inverted 2–3 hierarchy. In this scenario, the leading order terms are given by

$$|V_{ts}^{\mathrm{R}*}V_{tb}^{\mathrm{R}}| \sim \tilde{\lambda}B\,, \tag{7.5}$$

$$|V_{ts}^{\mathrm{R}*}V_{cb}^{\mathrm{R}}| \sim 1\,. \tag{7.6}$$

Taking into account the suppression from the LH mixing matrix and the relative importance due to $\hat{R}$ defined in equation (3.71), we find the LR contribution to $M_{12}^{B_s}$

$$\Delta^{\mathrm{LR}}\bar{M}_{12}^{B_s} = e^{-i\phi_{ts}}\left(2.6\cdot 10^{-3}e^{i\phi_{cb}} - 0.57B\tilde{\lambda}e^{i\phi_{tb}}\lambda_t^{\mathrm{LL}}(B_s)\right)\,, \tag{7.7}$$

Together with $\lambda_t^{\mathrm{LL}}(B_s) \sim 10^{-2} + 10^{-5}i$, we can safely assume dominance of the first term in equation (7.7). As the term proportional to $|V_{ts}^{\mathrm{R}*}V_{cb}^{\mathrm{R}}|$ dominates, the $|V_{ts}^{\mathrm{R}*}V_{tb}^{\mathrm{R}}|$ contribution to $M_{12}^{B_s}$ is not directly constrained in this scenario and therefore $\lambda_t^{\mathrm{RR}}$ can be enhanced in this scenario compared to the normal hierarchy scenario.

In the $K$ system, we cannot establish the dominance of one contribution to $M_{12}^{K}$. Therefore, the relative size of $\lambda_t^{\mathrm{RR}}$ can be up to $\mathcal{O}(100)$ when compared to its LL counterpart. Comparing the constraint on $|V_{td}^{\mathrm{R}}|$ for different levels of fine-tuning, we find

$$|V_{td}^{\mathrm{R}}| \leq \begin{cases} 1.2\cdot 10^{-2} & (\Delta_{\mathrm{BG}}^{\mathrm{mod.}} \leq 10) \\ 0.11 & (\text{no constraint on } \Delta_{\mathrm{BG}}^{\mathrm{mod.}}) \end{cases} \tag{7.8}$$

which coincides with the result of our discussion in the last part of section 3.4 if we enforce $\Delta_{\mathrm{BG}}^{\mathrm{mod.}} \leq 10$. This shows the weakness of the measures of fine-tuning we introduced in the beginning of this chapter. As we have argued in section 3.4, the corrections to $\varepsilon_K$ and $\Delta M_{d,s}$ are one order below the SM value for $|V_{td}^{\mathrm{R}}| \lesssim 10^{-2}$. This tells us that a low fine-tuning automatically prefers regions in the parameter space which naturally introduce only small effects in the observables considered for the determination of the fine-tuning.

### The CKM4 Matrix

The SM4 introduces changes to the CKM elements of the three-by-three sub-matrix for the first three generations as well as new mixing elements. In the $K$ system, the new $t'$ contributions turn out to be very important and the constraints from the rare $K$ decays together with $\varepsilon_K$ shape the structure of $B_d$ – $B_s$ correlations. In figure 7.4, we show the correlation of $|V_{ub'}|$ and $|V_{cb'}|$ together with $\mathrm{Br}(K_L \to \mu^+\mu^-)$ in colour. We observe that the constraints put stringent bounds on this correlation and force the new mixing elements into nearly linear correlations. Either $|V_{cb'}|$ is below 0.02 or it is a linear function of $|V_{ub'}|$ which is limited to be below 0.025. Alternatively, $|V_{ub'}|$ can reach its upper limit of 0.04 while $|V_{cb'}|$ is below 0.02.

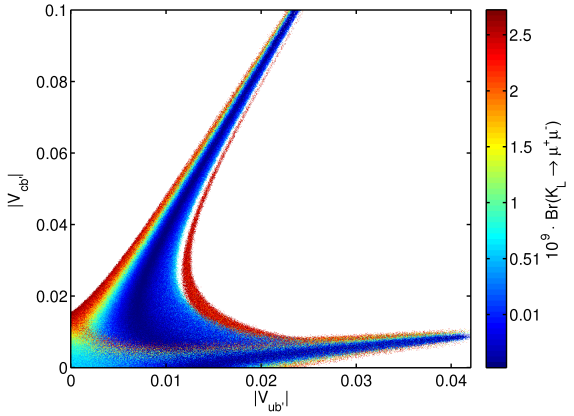


Figure 7.4: The correlation of $|V_{ub'}|$ and $|V_{cb'}|$, showing $\mathrm{Br}(K_L \to \mu^+\mu^-)$ in colour

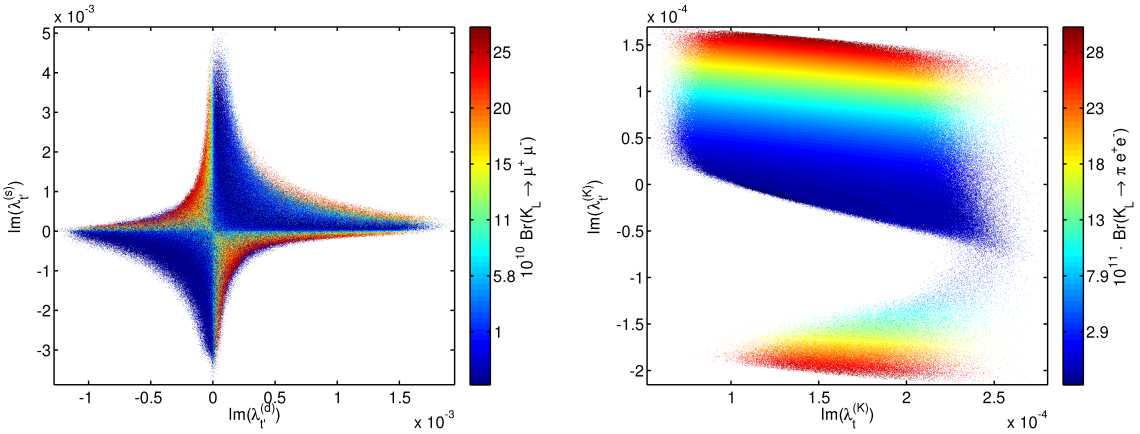


Figure 7.5: The correlation of $\mathrm{Im}(\lambda_{t'}^{(d)})$ and $\mathrm{Im}(\lambda_{t'}^{(s)})$ showing the $\mathrm{Br}(K_L \to \mu^+\mu^-)$ dependence in colour in the left panel, and the correlation of $\mathrm{Im}(\lambda_{t'}^{(K)})$ and $\mathrm{Im}(\lambda_{t}^{(K)})$ showing the $\mathrm{Br}(K_L \to \pi\ell^+\ell^-)$ in colour in the right panel

This anti-correlation can also be found in the elements $V_{t'd}$ and $V_{t's}$ as we show explicitly in the following. From figure 7.4, it is clear that the correlation between $|V_{ub'}|$ and $|V_{cb'}|$ is at least in part due to the constraint from $\mathrm{Br}(K_L \to \mu^+\mu^-)$.

In figure 7.5, we show the correlation of $\mathrm{Im}(\lambda_{t'}^{(d)})$ and $\mathrm{Im}(\lambda_{t'}^{(s)})$ in the left panel. In this plot we illustrate the impact of the $K$ decays on this correlation by explicitly showing the $\mathrm{Br}(K_L \to \mu^+\mu^-)$ dependence in colour. It is clear that at least a part of the strong anti-correlation observed in this plot is due to the constraint from $\mathrm{Br}(K_L \to \mu^+\mu^-)$. Other rare decays such as $K_L \to \pi^0\ell^+\ell^-$ also constrain the correlation of $\mathrm{Im}(\lambda_{t'}^{(d)})$ and $\mathrm{Im}(\lambda_{t'}^{(s)})$ or more generally: The rare $K$ decays constrain the combination $V_{t'd}V_{t's}^*$ of CKM4 elements.

In the right panel of figure 7.5, we show the correlation of $\mathrm{Im}(\lambda_{t'}^{(K)})$ and $\mathrm{Im}(\lambda_{t}^{(K)})$ with the branching ratio $\mathrm{Br}(K_L \to \pi^0 e^+ e^-)$ encoded in colour. From this plot we can see that the

branching ratio is dominated by $\mathrm{Im}(\lambda_{t'}^{(K)})$, which in turn puts limits on the allowed rage of $\mathrm{Im}(\lambda_{t'}^{(K)})$. However, even though $\mathrm{Im}(\lambda_t^{(K)})$ seems less important in this case, we observe interesting changes compared to the SM value $\mathrm{Im}(\lambda_t^{(K)})_{\mathrm{SM}} \approx 1.2{\cdot}10^{-4}$. The 'gap' in the plot in the right panel of figure 7.5 is at least partially introduced by the bound on $\mathrm{Br}(K_L \to \mu^+\mu^-)_{\mathrm{SD}}$.

## 7.3 $\Delta F = 2$ and $\mathrm{Br}(B \to X_q\gamma)$ in the SM4 and LRM

In this section, we show and discuss highlights of the correlations between selected observables. We investigate whether our analytical considerations are correct and provide insights into the structure of both models. In particular, we find interesting differences between the two models studied in this work.

### $\langle \mathrm{Br}(B \to X_d\gamma)\rangle$ and $\mathrm{Br}(B \to X_s\gamma)$

As already discussed in section 4.1, the decays of $\mathrm{Br}(B \to X_s\gamma)$ and $\langle \mathrm{Br}(B \to X_d\gamma)\rangle$ are expected to exhibit a very strong dependence on different model parameters. In the LRM a strong dependence on $s$ and $\mathrm{Re}(V_{tb}^{\mathrm{R}})$ is expected. Furthermore from inspecting the formulae (4.22) and (4.25) one suspects a correlation between the two branching ratios as well. In

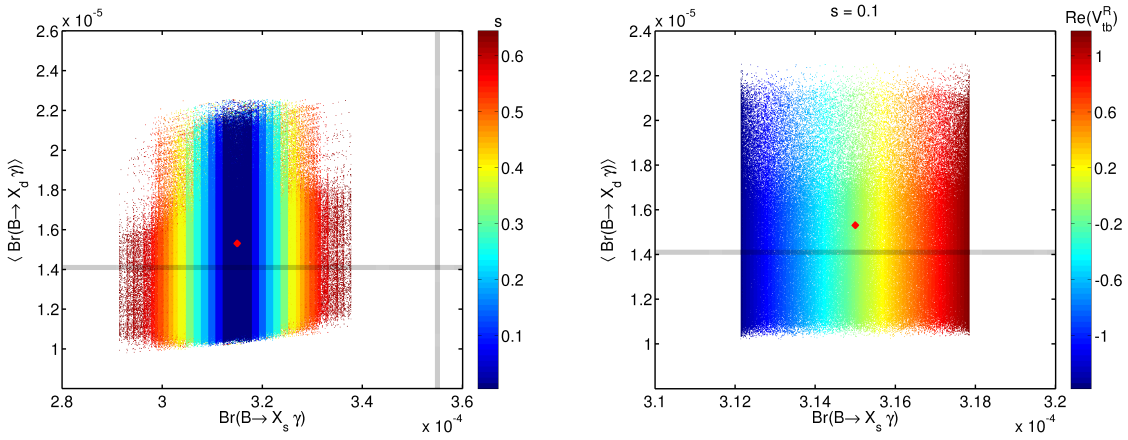


Figure 7.6: The correlation of $\mathrm{Br}(B \to X_s\gamma)$ and $\langle \mathrm{Br}(B \to X_d\gamma)\rangle$ in the LRM. The plot in the left panel shows the $s$ dependence in colour, while the plot in the right panel shows the dependence on $\mathrm{Re}(V_{tb}^{\mathrm{R}})$.

figure 7.6 we show the correlation of $\mathrm{Br}(B \to X_s\gamma)$ and $\langle \mathrm{Br}(B \to X_d\gamma)\rangle$. In the left panel, we show the $s$ dependence in colour, while in the right panel the dependence on $\mathrm{Re}(V_{tb}^{\mathrm{R}})$ is indicated through the colour code. As can be seen in the plot in the left panel of figure 7.6, the allowed range for $\mathrm{Br}(B \to X_s\gamma)$ is enlarged by more than a factor of ten for increasing $s$. This is in accordance with the anticipated strong $s$ dependence found in equation (4.20). The dependence of $\langle \mathrm{Br}(B \to X_d\gamma)\rangle$ on $\mathrm{Br}(B \to X_s\gamma)$ is not very prominent although the leading LRM contributions in both cases are proportional to $\mathrm{Re}(V_{tb}^{\mathrm{R}})$. From this we can conclude that in contrast to the SM4, the leading contribution[1] to $\langle \mathrm{Br}(B \to X_d\gamma)\rangle$ is not the dominant one. This is clear from the plot in the right panel of figure 7.6, where we do not see any

[1] The contribution with the largest coefficient.

dependence of $\langle \mathrm{Br}(B \to X_d\gamma)\rangle$ on $\mathrm{Re}(V_{tb}^{\mathrm{R}})$ and only a very small dependence on $\mathrm{Br}(B \to X_s\gamma)$.

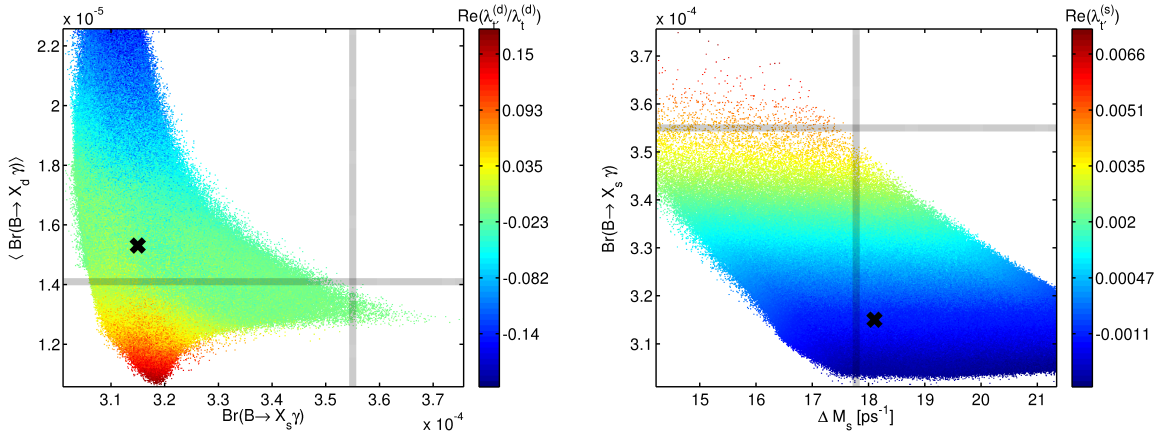


Figure 7.7: The correlation of $\mathrm{Br}(B \to X_s\gamma)$ and $\langle \mathrm{Br}(B \to X_d\gamma)\rangle$ in the SM4 (left panel) showing the dependence on $\mathrm{Re}(\lambda_{t'}^{(d)})$ in colour. The correlation of $\mathrm{Br}(B \to X_s\gamma)$ with $\Delta M_s$ in the SM4 (right panel) showing the dependence on $\mathrm{Re}(\lambda_{t'}^{(s)})$ in colour.

In the left panel of figure 7.7, we show the correlation of $\mathrm{Br}(B \to X_s\gamma)$ and $\langle \mathrm{Br}(B \to X_d\gamma)\rangle$ together with the dependence on $\mathrm{Re}(\lambda_{t'}^{(d)}/\lambda_t^{(d)})$ in colour. In the right panel of figure 7.7, we show the correlation of $\Delta M_s$ and $\mathrm{Br}(B \to X_s\gamma)$ together with the dependence on $\mathrm{Re}(\lambda_{t'}^{(s)})$ in colour. In contrast to the LRM, the correlation between $\mathrm{Br}(B \to X_s\gamma)$ and $\langle \mathrm{Br}(B \to X_d\gamma)\rangle$ exhibits a strongly non-linear behaviour in the SM4. As already discussed in section 4.2, we find a very strong dependence of $\langle \mathrm{Br}(B \to X_d\gamma)\rangle$ on $\mathrm{Re}(\lambda_{t'}^{(d)}/\lambda_t^{(d)})$ while $\mathrm{Br}(B \to X_s\gamma)$ is almost independent of this quantity. For an enhanced $\mathrm{Br}(B \to X_s\gamma)$ the value of $\langle \mathrm{Br}(B \to X_d\gamma)\rangle$ approaches an asymptotic value below the experimental central value while the allowed range for $\langle \mathrm{Br}(B \to X_d\gamma)\rangle$ is strongly constrained. In the case of $\mathrm{Br}(B \to X_s\gamma)$ close to its SM value, the range for $\langle \mathrm{Br}(B \to X_d\gamma)\rangle$ is enlarged to encompass a sizeable enhancement while a suppression below $1.1 \cdot 10^{-5}$ is not allowed by the constraints. As can be seen from the colour code, the suppression of $\langle \mathrm{Br}(B \to X_d\gamma)\rangle$ requires a substantial $\mathrm{Re}(\lambda_{t'}^{(d)}/\lambda_t^{(d)}) > 0.17$. Finding that the real part of $\lambda_{t'}^{(d)}/\lambda_t^{(d)}$ is constrained to be below roughly 20% is in accordance with our discussion on the impact of $\Delta M_d$ and $S_{\psi K_s}$ on general models of NP in section 6.2. The lower limit on $\mathrm{Br}(B \to X_s\gamma)$ is due to the upper limit on $\mathrm{Br}(B_s \to \mu^+\mu^-)$. The anti-correlation between $b \to d$ and $b \to s$ processes is a general feature of the SM4. The elements $\lambda_{t'}^{(d)}$ and $\lambda_{t'}^{(s)}$ are constrained by the rare $K$ decays as we have shown explicitly in section 7.2.

In the right panel of figure 7.7, we show the correlation of $\Delta M_s$ and $\mathrm{Br}(B \to X_s\gamma)$ together with the dependence on $\mathrm{Re}(\lambda_{t'}^{(s)})$ in colour. From this plot we find an almost linear correlation between $\Delta M_s$ and $\mathrm{Br}(B \to X_s\gamma)$, and $\mathrm{Br}(B \to X_s\gamma)$ and $\mathrm{Re}(\lambda_{t'}^{(s)})$. However, the horizontal range is larger than $2\,\mathrm{ps}^{-1}$ and shows a widening for lower values of $\mathrm{Br}(B \to X_s\gamma)$. As $\mathrm{Br}(B \to X_s\gamma)$ is directly proportional to $\mathrm{Re}(\lambda_{t'}^{(s)})$, we conclude that $\Delta M_s$ is correlated with $\mathrm{Re}(\lambda_{t'}^{(s)})$. Inspecting equation (3.39), we find that, as there is no direct dependence of $\Delta M_s$

on $\lambda_{t'}^{(s)}$, the dependence has to be introduced by the changes of the SM contribution, e.g. $\lambda_t^{(s)}$. The experimental central value of $\Delta M_s$ and $\mathrm{Br}(B \to X_s\gamma)$ cannot be reached simultaneously for the current value of $F_{B_s}\sqrt{\hat{B}_{B_s}}$. However, as the lattice values are prone to change within their error as new lattice determinations are included in the average, this cannot be viewed as a tension, yet. However, for $F_{B_s}\sqrt{\hat{B}_{B_s}} \lesssim 250\,\mathrm{GeV}$, the experimental value of $\mathrm{Br}(B \to X_s\gamma)$ would not be reachable, for $\Delta M_s$ close to its experimental value, in such a manner as to constitute a real tension once the error on $\mathrm{Br}(B \to X_s\gamma)$ is reduced.

### CP Violation $B_s$ System

Although the recent LHCb data puts $S_{\psi\phi}$ close to zero, the CP violation in $B_s$ system might still prove to give insights into possible physics beyond the SM. In figure 7.8, we show the direct CP violation in $b \to q\gamma$ as a function of the branching ratio for $q = s$ and $q = d$ in the the SM4 in the left and right panel, respectively. The colour code in figure 7.8 shows the dependence on $S_{\psi\phi}$ and $S_{\psi K_s}$ in the left and right panel, respectively. The direct CP violation

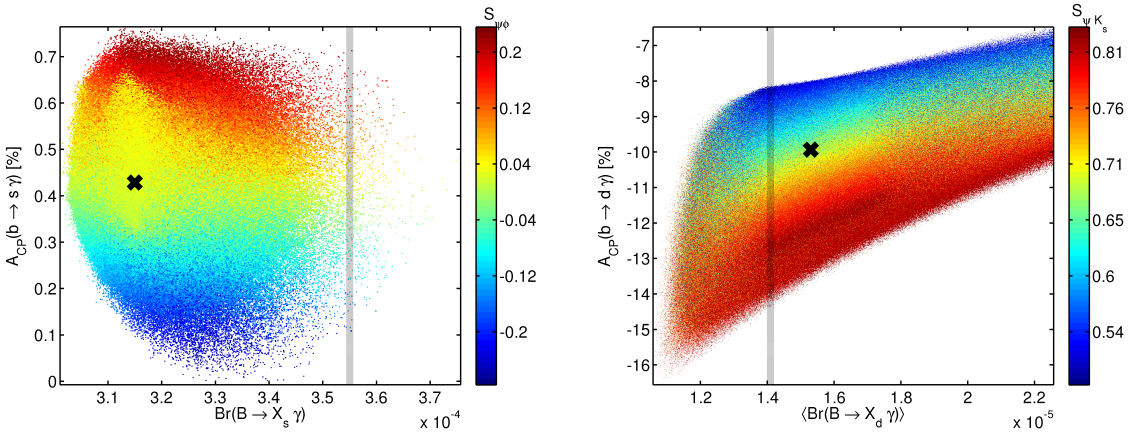


Figure 7.8: The correlations of $\mathrm{Br}(B \to X_s\gamma)$ and $A_{\mathrm{CP}}(b \to s\gamma)$ together with the dependence on $S_{\psi\phi}$ (left panel) and the correlation of $\langle \mathrm{Br}(B \to X_d\gamma)\rangle$ and $A_{\mathrm{CP}}(b \to d\gamma)$ together with the dependence on $S_{\psi K_s}$ (right panel), both in the SM4

in the decay $b \to s\gamma$ is of great interest due to its very small SM prediction. Unfortunately, as already discussed in section 4.3, this observable suffers from large hadronic uncertainties. However, as pointed out in [229], $A_{\mathrm{CP}}(b \to s\gamma) < -2\%$ could be interpreted as a clear sign for new physics. In the left panel of figure 7.8, we show in (the context of the SM4) the correlation of $\mathrm{Br}(B \to X_s\gamma)$ and $A_{\mathrm{CP}}(b \to s\gamma)$ including the $S_{\psi\phi}$ dependence in colour. We observe that the CP violation in $b \to s\gamma$ is closely related to the mixing induced CP violation $S_{\psi\phi}$. Therefore only small changes of $A_{\mathrm{CP}}(b \to s\gamma)$ compared to its SM value are allowed due to the increasingly tight constraint on $S_{\psi\phi}$. In the SM4, the CP violation $A_{\mathrm{CP}}(b \to s\gamma)$ and the branching ratio $\mathrm{Br}(B \to X_s\gamma)$ are mostly uncorrelated.

In the right panel of figure 7.8, we show the correlation between $\langle \mathrm{Br}(B \to X_d\gamma)\rangle$ and the corresponding direct CP asymmetry $A_{\mathrm{CP}}(b \to d\gamma)$ in the SM4. In this plot, the time-dependent CP asymmetry $S_{\psi K_s}$ is encoded in colour. We find an increasingly sharp correlation with an

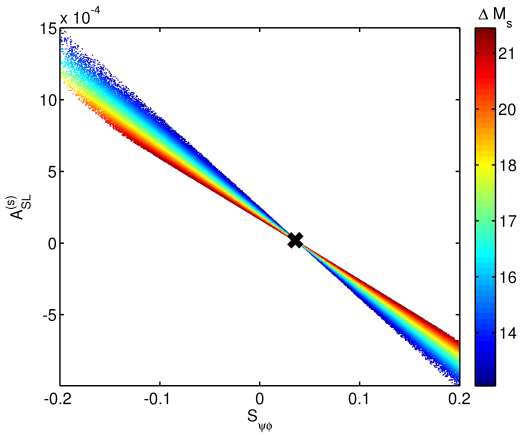


Figure 7.9: The model independent correlation between $S_{\psi\phi}$ and $A_{\rm SL}^{(s)}$. The colour code corresponds to $\Delta M_s$ and transparently shows how this correlation is enforced.

increasing value of $\langle \mathrm{Br}(B \to X_d\gamma)\rangle$. While the lower limit on $A_{\rm CP}(b \to d\gamma)$ is directly correlated to $\langle \mathrm{Br}(B \to X_d\gamma)\rangle$ over the full range, the upper limit shows only a moderate dependence on the branching ratio. The correlation between direct and indirect CP violation is very clear for the range $1.4 \cdot 10^{-5} \leq \langle \mathrm{Br}(B \to X_d\gamma)\rangle \leq 1.8 \cdot 10^{-5}$ but gets diluted for a branching ratio outside of this window.

In figure 7.9, we show the model-independent correlation of $S_{\psi\phi}$ and $A_{\rm SL}^{(s)}$ encoding the $\Delta M_s$ dependence in colour. From this plot it is clear that the $\Delta M_s$ constraint is responsible for this clear correlation. The semi-leptonic asymmetry $A_{\rm SL}^{(s)}$ is very interesting, as it contributes to the di-muon asymmetry $A_{\rm SL}(b)$ measured at the Tevatron [48] (see section 3.3 for more details). The data currently exhibits a $3.2\sigma$ deviation from the SM prediction (see table 3.5). From our plot it is clear that an order of magnitude enhancement of $A_{\rm SL}^{(s)}$ is only possible for negative $S_{\psi\phi}$. However, in this case $A_{\rm SL}^{(s)}$ would have the wrong sign. Thus, we can conclude, that although moderate enhancements are still possible in $A_{\rm SL}^{(s)}$, the Tevatron di-muon asymmetry anomaly can only be slightly softened.

In figure 7.10 we show the correlations of $\mathrm{Br}(B \to X_q\gamma)$ and the respective direct CP violation $A_{\rm CP}(b \to q\gamma)$ in the LRM. The colour code indicates the dependence on $\mathrm{Re}(V_{tb}^{\rm R})$ in the left panel and on $S_{\psi K_s}$ in the right panel. Both plots exhibit a very different structure when compared to the SM4 plots in figure 7.8. In the left panel of figure 7.10, we show $A_{\rm CP}(b \to s\gamma)$ as a function of $\mathrm{Br}(B \to X_s\gamma)$ for $s = 0.5$ in the LRM. We find a very curious ring shaped structure centered around a small area close to the SM point. As anticipated, the dependence on $\mathrm{Re}(V_{tb}^{\rm R})$ is linear in $\mathrm{Br}(B \to X_s\gamma)$, while the size of the CP violation is not linked to $\mathrm{Re}(V_{tb}^{\rm R})$. Overall, we find only very small deviations of $A_{\rm CP}(b \to s\gamma)$ from its SM value. Such small deviations have to be compared with the sizeable hadronic uncertainties in this observable, which leads us to conclude that the LRM as well as the SM4 cannot be found experimentally in this channel. Furthermore, we checked for a $S_{\psi\phi}$ dependence of $A_{\rm CP}(b \to s\gamma)$ but were not able to identify any correlation between those two observables.

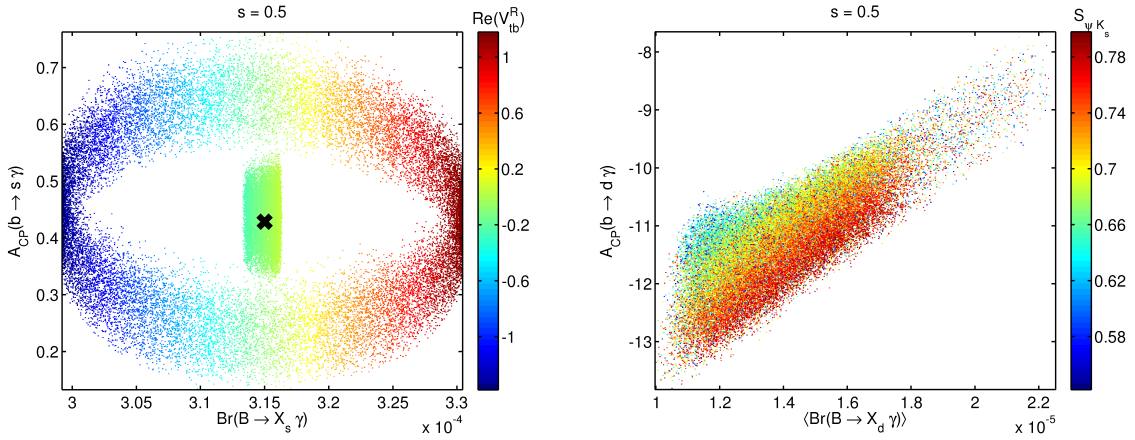


Figure 7.10: The correlations of $\mathrm{Br}(B \to X_s\gamma)$ and $A_{\mathrm{CP}}(b \to s\gamma)$ (left panel) and $\mathrm{Br}(B \to X_d\gamma)$ and $A_{\mathrm{CP}}(b \to d\gamma)$ (right panel) both in the LRM. The colour code represents the dependence on $\mathrm{Re}(V_{tb}^{\mathrm{R}})$ in the left panel and $S_{\psi K_s}$ in the right panel.

In the right panel of figure 7.10, we show $A_{\mathrm{CP}}(b \to d\gamma)$ as a function of $\mathrm{Br}(B \to X_d\gamma)$ for $s = 0.5$ in the LRM. The colour code in this plot shows the dependence on $S_{\psi K_s}$. We find that similar to the SM4 the branching ratio and the CP violation are correlated in a linear manner. However, in contrast to the SM4 the correlation in the LRM is much more pronounced. Interestingly, we observe only a very washed-out correlation of $A_{\mathrm{CP}}(b \to d\gamma)$ and $S_{\psi K_s}$. This is a quite general observation in the LRM. Due to the huge number of new parameters and in particular the new phases, we seldom observe any correlation between the different observables.

## 7.4 LRM Specific Considerations

In this section, we discuss two LRM specific topics, namely the proposed solution to the $V_{ub}$ problem [125–128] and the lower limit on the mass of the FCNC Higgs bosons.

### The $|V_{ub}|$ Problem

In [125, 126, 128], it was proposed that in the presence of RH currents the apparent problem between the various determinations of $|V_{ub}|$ could be resolved. Based on our brief discussion in section 6.4, we find that

$$|V_{ub}^{\mathrm{L}}|^2_{\mathrm{exp}} - \left(|V_{ub}|^2_{\mathrm{V,A}}\right)_{\mathrm{exp}} = \pm 2sc\varepsilon^2\,\mathrm{Re}(V_{ub}^{\mathrm{L}}V_{ub}^{\mathrm{R}})\,. \tag{7.9}$$

Using the experimental data, this allows us to find a lower limit for $sc\varepsilon^2|V_{ub}^{\mathrm{R}}|$ if we want to shift the values of $|V_{ub}|_{\mathrm{V,A}}$ close to their respective experimental central values

$$sc\varepsilon^2|V_{ub}^{\mathrm{R}}| \geq \begin{cases} 8\cdot 10^{-4} \\ 5\cdot 10^{-4} \end{cases} \approx 6.5\cdot 10^{-4}\,. \tag{7.10}$$

In figure 7.11, we show $sc\varepsilon^2|V_{ub}^{\mathrm{R}}|$ as a function of $s$ for $\varepsilon = 0.03$ and different levels of fine-tuning. The dashed, horizontal, black line on top indicates the value (7.10) at which the $|V_{ub}|$ problem would be solved. From figure 7.11, it is clear that, even without enforcing any constraints on

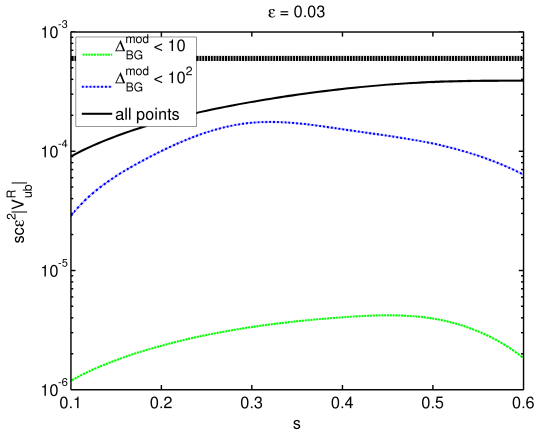


Figure 7.11: The dependence of $sc\varepsilon^2|V_{ub}^{\mathrm{R}}|$ on s for different levels of fine-tuning in the LRM. The dashed, black line indicates the value required to 'solve' the $|V_{ub}|$ problem.

the fine-tuning, the $|V_{ub}|$ problem cannot be solved in this model. This is mainly due to the improved bound on the mass of $W'$ which gives an indirect bound on $\varepsilon$. In the absence of the direct limit on the mass of $W'$ the EWPT and FCNC constraints would still put stringent limits on $\varepsilon$ due to the good agreement between theory and experiment. In our numerical analysis, we were not able to find points with large $|V_{ub}^{\mathrm{R}}|$ and low fine-tuning simultaneously. As already discussed in section 5.2, this does not preclude such points from existing and therefore the curves for low fine-tuning in figure 7.11 have to be understood as the minimal allowed ones.

### Limits on the Mass of the Heavy Higgs

In most of our analysis we have set the Higgs mass $M_H$ to its maximal allowed value

$$M_H^{\max} = \frac{\sqrt{\alpha_3^{\max}}\kappa_R}{\sqrt{1-2s^2}} = \frac{16\ \mathrm{TeV}}{\sqrt{1-2s^2}}\,, \tag{7.11}$$

for our nominal point $\kappa_R = 5.8\,\mathrm{TeV}$ and $s_R = 0.8$. This choice was guided by the aim to soften the impact of the FCNC Higgs exchange in $\Delta F = 2$ processes while keeping the Higgs sector perturbative. In this section we reverse our philosophy and investigate whether common wisdom holds and the FCNC Higgs really needs to be as heavy as possible. To this end we proceed as follows:

- We select a number of values for $s$ in the range $s = 0.1 \ldots 0.6$.
- For each value of $s$, we go through our set of valid points and search for the minimal $\alpha_3$ for which we still have points left after re-evaluating the constraints.

This procedure is valid as we can expect our set of points to encompass the viable parameter space for a lower Higgs mass as well. In figure 7.12, we show the result of our search for the minimal allowed Higgs mass as a function of $s$. For our nominal point with $\kappa_R \approx 5.8$ TeV we

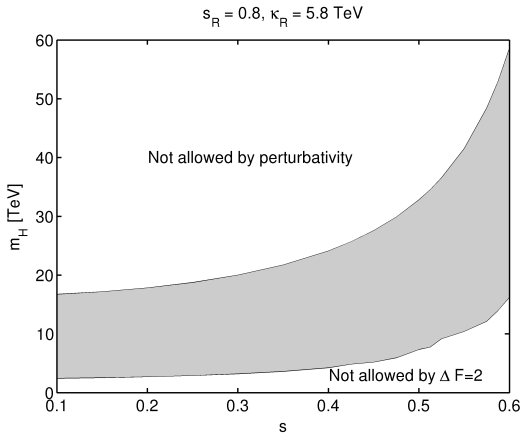


Figure 7.12: The allowed range of the heavy Higgs mass as a function of $s$ in the LRM. The mass is bound by unitarity from above and by FCNC processes from below.

find a soft[2] lower limit on the heavy Higgs mass

$$M_H \geq \begin{cases} 2.4 \text{ TeV}\,, & (s = 0.1) \\ 7.3 \text{ TeV}\,, & (s = 0.5) \\ 16.2 \text{ TeV}\,. & (s = 0.6) \end{cases} \tag{7.12}$$

One might suspect that such low Higgs masses would lead to a very high fine-tuning but this is not the case. We observe that points with a high fine-tuning are even more fine-tuned after lowering the Higgs mass if they survive the constraints at all. However, points with a low initial fine-tuning get only a small additional amount of fine-tuning in the low Higgs mass scenario. This is reassuring as it shows that our idea of fine-tuning is not totally misbehaved: If a point is valid regardless of the Higgs mass, we do not want to have a large amount of fine-tuning assigned to it, as intuitively it seems to be very stable. However, the structure of $V^{\mathrm{R}}$, in such an extreme case for the Higgs mass, is very hierarchical. In equation (7.13) we have collected two exemplary results for $V^{\mathrm{R}}$

$$|V^{\mathrm{R}}| \sim \begin{pmatrix} 1 & 10^{-2} & 10^{-4} \\ 10^{-2} & 1 & 10^{-3} \\ 10^{-3} & 10^{-3} & 1 \end{pmatrix}, \qquad |V^{\mathrm{R}}| \sim \begin{pmatrix} 1 & 10^{-5} & 10^{-2} \\ 10^{-2} & 10^{-1} & 1 \\ 10^{-3} & 1 & 10^{-1} \end{pmatrix}, \tag{7.13}$$

keeping only an order of magnitude approximation of the elements. As can be seen from (7.13), the inverted 2–3 hierarchy is not excluded by a low Higgs mass, which makes this scenario quite interesting. Moreover, one could imagine a scenario where the heavy $W$ boson is much heavier than the FCNC Higgs boson. This would have profound implications for the direct searches at the LHC.

## 7.5 $\Delta F = 1$ Processes in the SM4

In this section, we show our results for selected rare $B$ and $K$ decays in the context of the SM4. The undoubtedly most interesting observables at the moment are the branching ratio

[2] In the sense that we cannot exclude even lower Higgs masses because of our MC scan analysis.

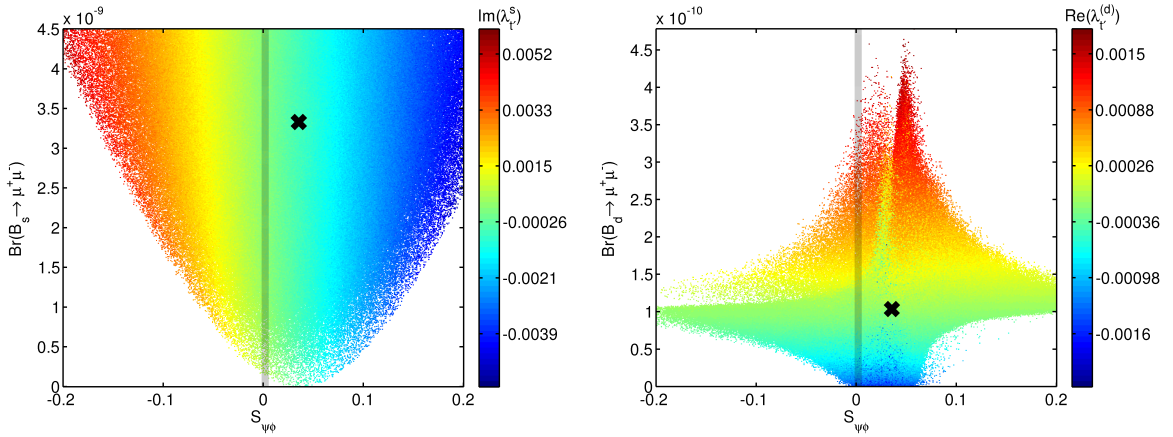


Figure 7.13: The branching ratio $\mathrm{Br}(B_s \to \mu^+\mu^-)$ and $\mathrm{Br}(B_d \to \mu^+\mu^-)$ as functions of the time-dependent CP asymmetry $S_{\psi\phi}$ in the SM4 in the left and right panel respectively. The colour code corresponds to $\mathrm{Im}(\lambda_{t'}^{(s)})$ and $\mathrm{Re}(\lambda_{t'}^{(d)})$, respectively.

$\mathrm{Br}(B_s \to \mu^+\mu^-)$ and the mixing induced, time-dependent CP asymmetry $S_{\psi\phi}$. The more suppressed branching ratio $\mathrm{Br}(B_d \to \mu^+\mu^-)$ comes as a close third in the list of the most interesting flavour observables in the next years. In section 3.3 and 4.6, we have already shown the current experimental situation together with the SM predictions.

### Rare $B$ Decays

Having identified the most interesting observables, we start our discussion with the correlations of $\mathrm{Br}(B_q \to \mu^+\mu^-)$ and $S_{\psi\phi}$. In figure 7.13, we show the branching ratios $\mathrm{Br}(B_s \to \mu^+\mu^-)$ and $\mathrm{Br}(B_d \to \mu^+\mu^-)$ as functions of the time-dependent CP asymmetry $S_{\psi\phi}$ in the SM4 in the left and right panel, respectively. In order to better understand the importance of the new contributions, we show the imaginary part of $\lambda_{t'}^{(s)}$ and the real part of $\lambda_{t'}^{(d)}$ in colour, respectively. In the left panel of figure 7.13, we show $\mathrm{Br}(B_s \to \mu^+\mu^-)$ as a function of $S_{\psi\phi}$ with $\mathrm{Im}(\lambda_{t'}^{(s)})$ encoded in colour. First, we observe the direct correlation of $S_{\psi\phi}$ with $\mathrm{Im}(\lambda_{t'}^{(s)})$ which leads us the conclude that while the CKM3 element $V_{ts}$ can be changed relative to its SM value, the new contribution through $V_{t's}$ is important. Interestingly, we find the change in $\lambda_t^{(s)}$ to be of the same order as $\lambda_{t'}^{(s)}$, for the largest possible mixing between the fourth and the first three generations (see equation (6.3) for an approximate form of the CKM4 matrix in this case). Therefore we conclude that the new contribution through $t'$ and the change in the three-by-three mixing matrix can be equally important. The second observation is the overall shape of the correlation, which looks like a filled parabola. From figure 7.14, we know that the branching ratio $\mathrm{Br}(B_s \to \mu^+\mu^-)$ is directly correlated with the real part of $\lambda_{t'}^{(s)}$. We further know that the absolute value of $\lambda_{t'}^{(s)}$ is constrained by the constrains on $|V_{ub'}|$ and $|V_{cb'}|$. Together with the correlation of $S_{\psi\phi}$ and $\mathrm{Im}(\lambda_{t'}^{(s)})$ the correlation in the left panel of figure 7.13 can be easily understood.

- For a suppression of the branching ratio $\mathrm{Br}(B_s \to \mu^+\mu^-)$, we need to suppress the SM contributions which is mostly negative and real, therefore we need a positive and real

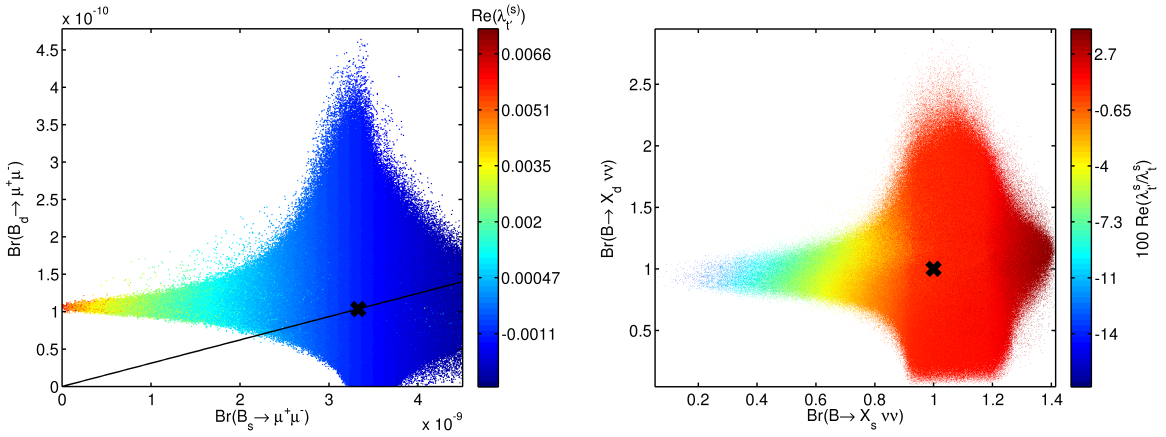


Figure 7.14: The correlation of $\mathrm{Br}(B_d \to \mu^+\mu^-)$ and $\mathrm{Br}(B_s \to \mu^+\mu^-)$ together with $\mathrm{Re}(\lambda_{t'}^{(s)})$ encoded in colour (left panel). The straight black line indicates the CMFV prediction for this correlation. The correlation between $\mathrm{Br}(B \to X_d\nu\bar{\nu})$ and $\mathrm{Br}(B \to X_s\nu\bar{\nu})$ in dependence on $\mathrm{Re}(\lambda_{t'}^{(s)}/\lambda_t^{(s)})$ in colour (right panel)

$\lambda_{t'}^{(s)}$. As the absolute value of $\lambda_{t'}^{(s)}$ is constrained through the product of $|V_{ub'}|$ and $|V_{cb'}|$, the imaginary part of $\lambda_{t'}^{(s)}$ is automatically reduced when increasing the real part.

- In [82, 105] before the new LHCb data, the correlation of $\mathrm{Br}(B_s \to \mu^+\mu^-)$ and $S_{\psi\phi}$ did show a very distinct structure, where big $S_{\psi\phi}$ would require an enhanced branching ratio. In this case, the enhancement of the branching ratio was due to a substantial imaginary part of $\lambda_{t'}^{(s)}$. The region with enhanced branching ratio and SM like $S_{\psi\phi}$, though excluded by the direct limit on $\mathrm{Br}(B_s \to \mu^+\mu^-)$, is also forbidden by a combination of rare $K$ decays. This is due to the fact that a positive real part of $\lambda_{t'}^{(K)}$ is tightly constrained by e.g. $\mathrm{Br}(K_L \to \mu^+\mu^-)$.

In the right panel of figure 7.13, we show the correlation of $\mathrm{Br}(B_d \to \mu^+\mu^-)$ and $S_{\psi\phi}$ together with $\mathrm{Re}(\lambda_{t'}^{(d)})$ encoded in colour. This plot exhibits the anticipated anti-correlation between $B_d$ and $B_s$ system as already found in figure 7.5, figure 7.7 and the relevant discussion in section 7.2. However, as this correlation probes the correlation between $\mathrm{Re}(\lambda_{t'}^{(d)})$ and $\mathrm{Im}(\lambda_{t'}^{(s)})$ there obviously is a loophole. This loophole can be seen from the points for $S_{\psi\phi} < S_{\psi\phi}^{\mathrm{SM}}$ and $\mathrm{Br}(B_d \to \mu^+\mu^-) > \mathrm{Br}(B_d \to \mu^+\mu^-)_{\mathrm{SM}}$. Furthermore, we observe a moderate possible enhancement of the branching ratio compared to the SM. As for the branching ratio $\mathrm{Br}(B_s \to \mu^+\mu^-)$, a suppression of the branching ratio $\mathrm{Br}(B_d \to \mu^+\mu^-)$ is also clearly possible. Analogous to the $B_s$ system, we find a strong correlation between $\mathrm{Br}(B_d \to \mu^+\mu^-)$ and $\mathrm{Re}(\lambda_{t'}^{(d)})$. Note that in contrast to the $B_s$ system, $\mathrm{Re}(\lambda_{t'}^{(d)})$ is allowed to lie in a symmetric range. This shows that the experimental limit on $\mathrm{Br}(B_d \to \mu^+\mu^-)$ does currently not pose a constraint on the SM4.

In figure 7.14, we show $\mathrm{Br}(B_d \to \mu^+\mu^-)$ as a function of $\mathrm{Br}(B_s \to \mu^+\mu^-)$. The colour code corresponds to $\mathrm{Re}(\lambda_{t'}^{(s)})$ and the straight black line though the SM point indicates the (C)MFV prediction for this correlation. Together with figure 7.13, we know that the correlation in the left panel of figure 7.14 is directly related to the anti-correlation found in figure 7.5. As dis-

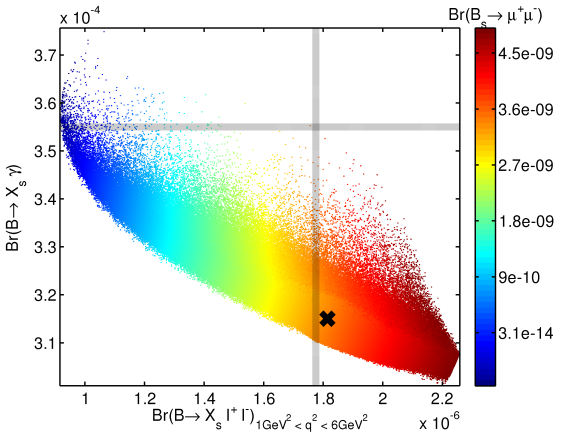


Figure 7.15: The correlation between $\mathrm{Br}(B \to X_s\gamma)$, $\mathrm{Br}(B \to X_s\ell^+\ell^-)_{1\ \mathrm{GeV}^2<q^2<6\ \mathrm{GeV}^2}$ and $\mathrm{Br}(B_s \to \mu^+\mu^-)$

cussed before, the anti-correlation between the $B_d$ and the $B_s$ system in this model is due to the constraints from rare $K$ decays. This plot serves to illustrate the strong non-MFV character of this model. In [353,354], this correlation is shown for different models such as SUSY flavour models, the LHT, and the RSc. Compared to most other models, the SM4 exhibits a very special behaviour in this correlation. This can be traced back to the fact that though the SM4 has purely LH charged currents it also introduces changes to the three-by-three sub-matrix of the CKM4 mixing matrix.

The decays $B \to X_d\nu\bar{\nu}$ and $B \to X_s\nu\bar{\nu}$ are directly correlated with $B_d \to \mu^+\mu^-$ and $B_s \to \mu^+\mu^-$, respectively. The deviations from the SM prediction can, in both modes, be either positive or negative so that either enhancements or suppressions are possible. In the right panel of figure 7.14, we show the correlation between $\mathrm{Br}(B \to X_d\nu\bar{\nu})$ and $\mathrm{Br}(B \to X_s\nu\bar{\nu})$ in dependence on $\mathrm{Re}(\lambda_{t'}^{(s)}/\lambda_t^{(s)})$ in colour. We observe the typical anti-correlation found in all $b \to s$ versus $b \to d$ transitions.
In figure 7.15, we show the correlation of $\mathrm{Br}(B \to X_s\gamma)$ and $\mathrm{Br}(B \to X_s\ell^+\ell^-)_{1\ \mathrm{GeV}^2<q^2<6\ \mathrm{GeV}^2}$ indicating the dependence on $\mathrm{Br}(B_s \to \mu^+\mu^-)$ in colour. In this plot we observe a very strong dependence of the lower limit of $\mathrm{Br}(B \to X_s\gamma)$ on the size of $\mathrm{Br}(B \to X_s\ell^+\ell^-)_{1\ \mathrm{GeV}^2<q^2<6\ \mathrm{GeV}^2}$. The upper limit on this correlation is not discernible from this plot due to the limits of our MC scan sample of the viable parameter space. We also observe a direct correlation between $\mathrm{Br}(B \to X_s\ell^+\ell^-)_{1\ \mathrm{GeV}^2<q^2<6\ \mathrm{GeV}^2}$ and $\mathrm{Br}(B_s \to \mu^+\mu^-)$ which could serve as a cross-check once $\mathrm{Br}(B_s \to \mu^+\mu^-)$ is measured. From our limited MC sample, we find that an enhancement of $\mathrm{Br}(B \to X_s\gamma)$ together with a SM like $\mathrm{Br}(B_s \to \mu^+\mu^-)$ could pose a problem in the SM4.

### Rare $K$ Decays

Turning to the very important $K$ decays, we start this section with the constraint from $\mathrm{Br}(K_L \to \mu^+\mu^-)_{\mathrm{SD}}$. As already discussed in section 4.8 and the subsequent ones, the constraints from rare $K$ decays are extremely important in the SM4. In figure 7.16, we show

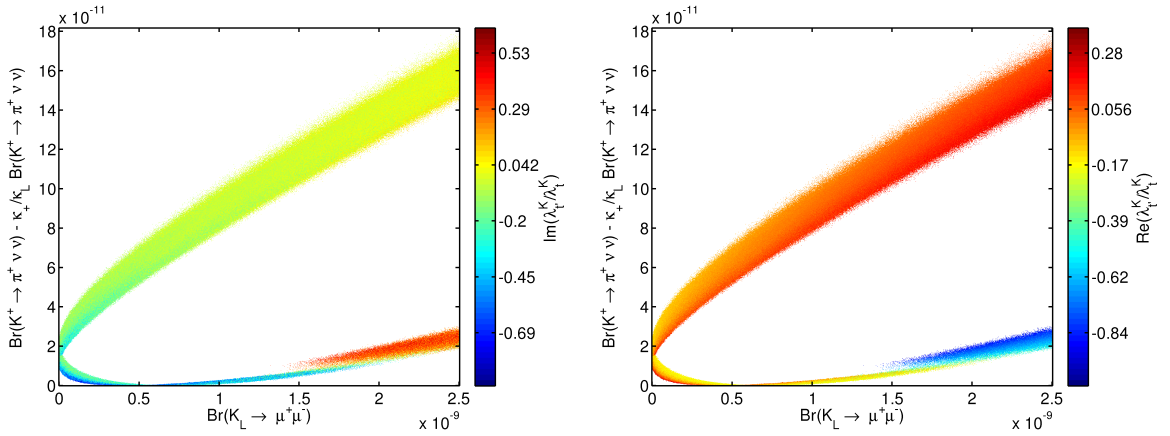


Figure 7.16: The importance of the constraint from $\mathrm{Br}(K_L \to \mu^+\mu^-)_{\mathrm{SD}}$ shown through a correlation with $\mathrm{Br}(K^+ \to \pi^+\nu\bar{\nu}) - \frac{\kappa_+}{\kappa_L}\mathrm{Br}(K_L \to \pi^0\nu\bar{\nu})$. The colour code shows the dependence on $\mathrm{Im}(\lambda_{t'}^{(K)}/\lambda_t^{(K)})$ and $\mathrm{Re}(\lambda_{t'}^{(K)}/\lambda_t^{(K)})$ in the left and right panel, respectively.

the correlation of $\mathrm{Br}(K_L \to \mu^+\mu^-)_{\mathrm{SD}}$ and $\mathrm{Br}(K^+ \to \pi^+\nu\bar{\nu}) - \frac{\kappa_+}{\kappa_L}\mathrm{Br}(K_L \to \pi^0\nu\bar{\nu})$ encoding the $\mathrm{Im}(\lambda_{t'}^{(K)}/\lambda_t^{(K)})$ dependence (left panel) and the $\mathrm{Re}(\lambda_{t'}^{(K)}/\lambda_t^{(K)})$ dependence (right panel) in colour. Because $\mathrm{Br}(K_L \to \mu^+\mu^-)_{\mathrm{SD}}$ depends on the real part of $\lambda_{t'}^{(K)}/\lambda_t^{(K)}$ and the absolute value of $\lambda_{t'}^{(K)}/\lambda_t^{(K)}$ is constrained as discussed in section 6.3. It is clear that the constraint from $\mathrm{Br}(K_L \to \mu^+\mu^-)_{\mathrm{SD}}$ imposes a cut for low values of $\mathrm{Im}(\lambda_{t'}^{(K)}/\lambda_t^{(K)})$. Interestingly, also large positive values of $\mathrm{Im}(\lambda_{t'}^{(K)}/\lambda_t^{(K)})$ get constrained. The shape of the correlation in figure 7.16 can be easily understood by comparing equations (4.83), (4.91) and (4.92) combined with the fact that $Y_0(x)$ and $X_0(x)$ have a different relative enhancement for larger values of $m_{t'}$. For a mostly real $\lambda_{t'}^{(K)}/\lambda_t^{(K)}$, the correlation is nearly linear as can be seen from the upper branch of the correlation. The cut on the lower branch of the correlation appears for large negative values of $\mathrm{Re}(\lambda_{t'}^{(K)}/\lambda_t^{(K)})$ together with large positive values of $\mathrm{Im}(\lambda_{t'}^{(K)}/\lambda_t^{(K)})$. These points are allowed due to the discrepancy between the experimental and theoretical value for $\Delta M_K$ and $\varepsilon_K$ (see section 6.1 and section 6.2). The lower values of $\mathrm{Br}(K^+ \to \pi^+\nu\bar{\nu}) - \frac{\kappa_+}{\kappa_L}\mathrm{Br}(K_L \to \pi^0\nu\bar{\nu})$ for these points can be explained by the slower increase of $X_0(x)$ as a function of $x$ when compared to $Y_0(x)$.

In figure 7.17, we show the correlations of $\mathrm{Br}(K_L \to \pi^0\nu\bar{\nu})$ and $\mathrm{Br}(K_L \to \mu^+\mu^-)$ with $\mathrm{Br}(K^+ \to \pi^+\nu\bar{\nu})$ in the left and right panel, respectively. The colour code in both plots corresponds to $\mathrm{Im}(\lambda_{t'}^{(K)}/\lambda_t^{(K)})$. The diagonal, dashed, black line in the left panel represents the model-independent Grossman-Nir bound [281]. The colour code connects both plots to the plots in figure 7.16 and thereby facilitates the understanding of the interplay between the different rare $K$ decays. In the left panel of figure 7.17, we show $\mathrm{Br}(K_L \to \pi^0\nu\bar{\nu})$ as a function of $\mathrm{Br}(K^+ \to \pi^+\nu\bar{\nu})$ with $\mathrm{Im}(\lambda_{t'}^{(K)}/\lambda_t^{(K)})$ encoded in colour. The observed two-branched structure of this correlation is a general feature of models with only LH currents [355]. In contrast to models like the LHT model [356] or a more general analysis of this correlation [357], the Grossman-Nir bound can be saturated in the SM4. The lower branch is obviously related to

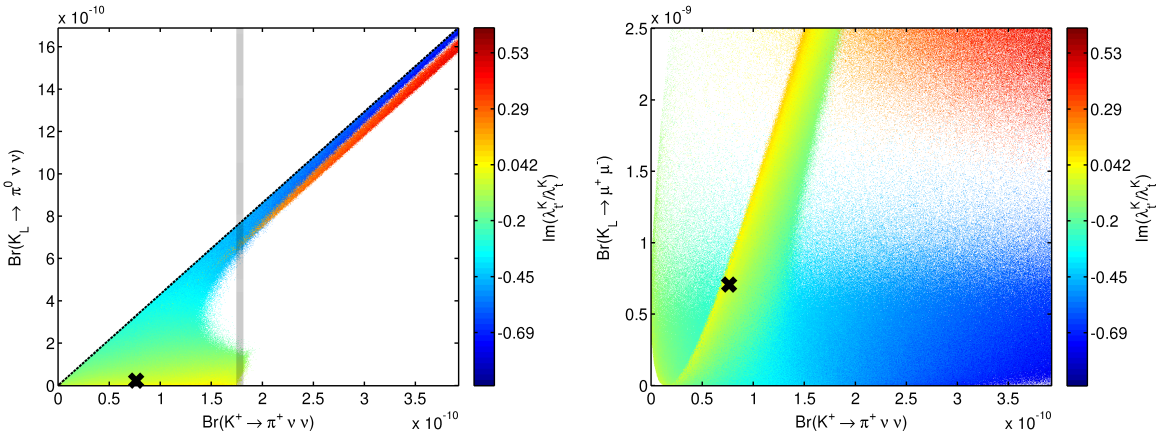


Figure 7.17: The branching ratios $\mathrm{Br}(K_L \to \pi^0\nu\bar{\nu})$ and $\mathrm{Br}(K_L \to \mu^+\mu^-)$ as functions of $\mathrm{Br}(K^+ \to \pi^+\nu\bar{\nu})$ in the left and right panel, respectively. The colour code shows the dependence on $\mathrm{Im}(\lambda_{t'}^{(K)}/\lambda_t^{(K)})$. The diagonal, black, dashed line in the left panel explicitly shows the Grossman-Nir bound [281].

the upper branch in figure 7.16, which explains the sharp cut close to the experimental central value. The upper branch of the correlation between $\mathrm{Br}(K_L \to \pi^0\nu\bar{\nu})$ and $\mathrm{Br}(K^+ \to \pi^+\nu\bar{\nu})$ corresponds to the lower branch in figure 7.16. By inspecting equation (4.97), we can easily understand the lower and the upper branch. In the upper branch, as is clear from the colour code, the imaginary part of $\lambda_{t'}^{(K)}/\lambda_t^{(K)}$ is large and therefore the first term in equation (4.91) dominates the branching ratio. In this case, $\mathrm{Br}(K_L \to \pi^0\nu\bar{\nu})$ is also enhanced as is obvious from equation (4.92). On the lower branch, $\mathrm{Im}(\lambda_{t'}^{(K)}/\lambda_t^{(K)})$ is close to zero. In this case, the second term in equation (4.91) dominates the branching ratio while $\mathrm{Br}(K_L \to \pi^0\nu\bar{\nu})$ is small. This correlation has also been studied in [297, 298, 357]. In [297], the authors derived model independent bounds on this correlation, while in [357] the structure of the correlation was studied in more detail. Interestingly, the SM4 while exhibiting the two-branched structure studied in [357], still violates the bounds and structures found in both studies. The violation of the bounds found in [297] can be traced back to the violation of three-by-three unitarity and a much larger allowed range for $\mathrm{Im}(\lambda_t^{(K)})$ than assumed in that particular study. The effect of the constraint induced by $\varepsilon'/\varepsilon$ is discussed below. In [357], it was argued that in the case of correlated phases between $\Delta F = 1$ and $\Delta F = 2$ operators, the observed correlation between $\mathrm{Br}(K^+ \to \pi^+\nu\bar{\nu})$ and $\mathrm{Br}(K_L \to \pi^0\nu\bar{\nu})$ can be explained naturally. Even if the connection between $\Delta F = 1$ and $\Delta F = 2$ was relaxed, the presence of only additive NP contributions to $\varepsilon_K$ would imply

$$\arg\left(X_0(x_t) + \frac{\lambda_{t'}^{(K)}}{\lambda_t^{(K)}} X_0(x_{t'})\right) \neq \bar{\beta} - \bar{\beta}_s \pm \frac{\pi}{2}\,, \tag{7.14}$$

and due to this the Grossman-Nir bound could not be reached by the upper branch. However, as already discussed in section 3.3, the SM4 not only introduces additional terms to $\varepsilon_K$ but also changes the SM contributions. Most importantly, the SM4 introduces an imaginary part to $\lambda_c^{(K)}$ which is potentially much larger than the SM expectation. This new contribution has the potential to compensate for some of the additional effects introduced by the $t'$. Ef-

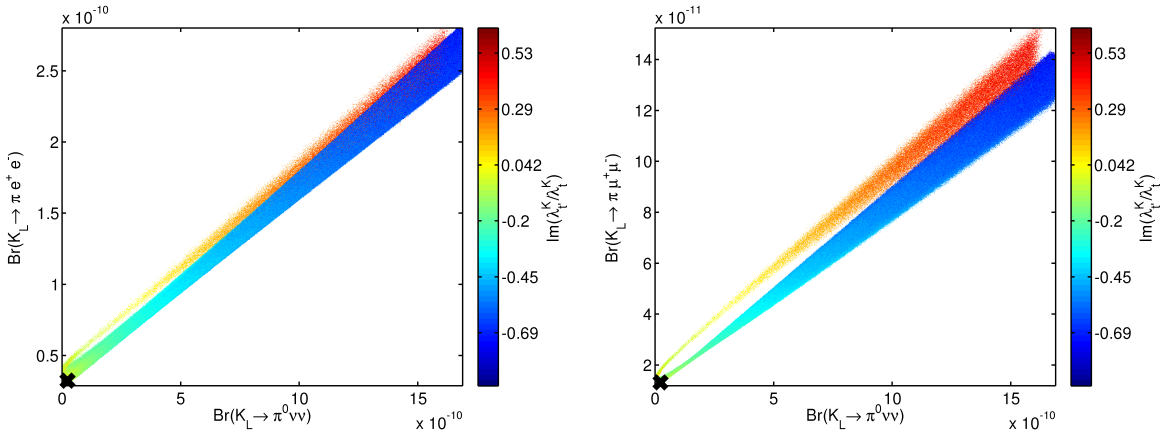


Figure 7.18: The branching ratios $\mathrm{Br}(K_L \to \pi^0 e^+ e^-)$ and $\mathrm{Br}(K_L \to \pi^0 \mu^+ \mu^-)$ as functions of $\mathrm{Br}(K_L \to \pi^0 \nu\bar{\nu})$ in the left and right panel, respectively. The colour code shows the dependence on $\mathrm{Im}(\lambda_{t'}^{(K)}/\lambda_t^{(K)})$.

fectively, the SM4 is able to maximally violate the assumptions made in [357] and therefore the Grossman-Nir bound can be reached in this model. We have verified explicitly that the new effects in $\lambda_c^{(K)}$ do not introduce significant effects in $\mathrm{Br}(K_L \to \pi^0 \nu\bar{\nu})$ and can therefore be neglected in (4.91) and (4.92).

In the right panel of figure 7.17, we show the correlation between $\mathrm{Br}(K^+ \to \pi^+ \nu\bar{\nu})$ and $\mathrm{Br}(K_L \to \mu^+ \mu^-)$. The colour code shows the dependence on $\mathrm{Im}(\lambda_{t'}^{(K)}/\lambda_t^{(K)})$. The structure of this correlation is not very clear and is in fact hardly visible without the colour code. For a mostly real $\lambda_{t'}^{(K)}/\lambda_t^{(K)}$ we observe a very steep linear correlation between the two branching ratios. This could be expected as in this case the second term in (4.91) dominates $\mathrm{Br}(K^+ \to \pi^+ \nu\bar{\nu})$ and because of the sign of the new contribution the SM and NP effects are added constructively (see figure 7.16 and the corresponding discussion for details). The red and blue clouds in this plot correspond to the points close to the Grossman-Nir bound in the left panel of figure 7.17 and the lower branch in figure 7.16. In this case the imaginary part of $\lambda_{t'}^{(K)}/\lambda_t^{(K)}$ is big and the first term in (4.91) becomes important. This enhances $\mathrm{Br}(K^+ \to \pi^+ \nu\bar{\nu})$ while having no effect on $\mathrm{Br}(K_L \to \mu^+ \mu^-)$. Therefore, the constraint from $\mathrm{Br}(K^+ \to \pi^+ \nu\bar{\nu})$ becomes important in this case.

In figure 7.18, we show the correlations between $\mathrm{Br}(K_L \to \pi^0 \ell^+ \ell^-)$ and $\mathrm{Br}(K_L \to \pi^0 \nu\bar{\nu})$ together with $\mathrm{Im}(\lambda_{t'}^{(K)}/\lambda_t^{(K)})$ in colour. These plots illustrate the constraint introduced by all three observables. In both plots, we observe a two-branched structure, which separates the points with large negative and positive $\mathrm{Im}(\lambda_{t'}^{(K)}/\lambda_t^{(K)})$. The correlation for large negative $\mathrm{Im}(\lambda_{t'}^{(K)}/\lambda_t^{(K)})$ is constrained mostly by $\mathrm{Br}(K_L \to \pi^0 \nu\bar{\nu})$ through the bound on $\mathrm{Br}(K^+ \to \pi^+ \nu\bar{\nu})$ by means of equation (4.97). However, for large positive $\mathrm{Im}(\lambda_{t'}^{(K)}/\lambda_t^{(K)})$ the branching ratio $\mathrm{Br}(K_L \to \pi^0 \nu\bar{\nu})$ does not pose a constraint. In both cases of $e$ or $\mu$ in the final state, the branching ratio $\mathrm{Br}(K_L \to \pi^0 \ell^+ \ell^-)$ has a potential for constraining points with large posi-

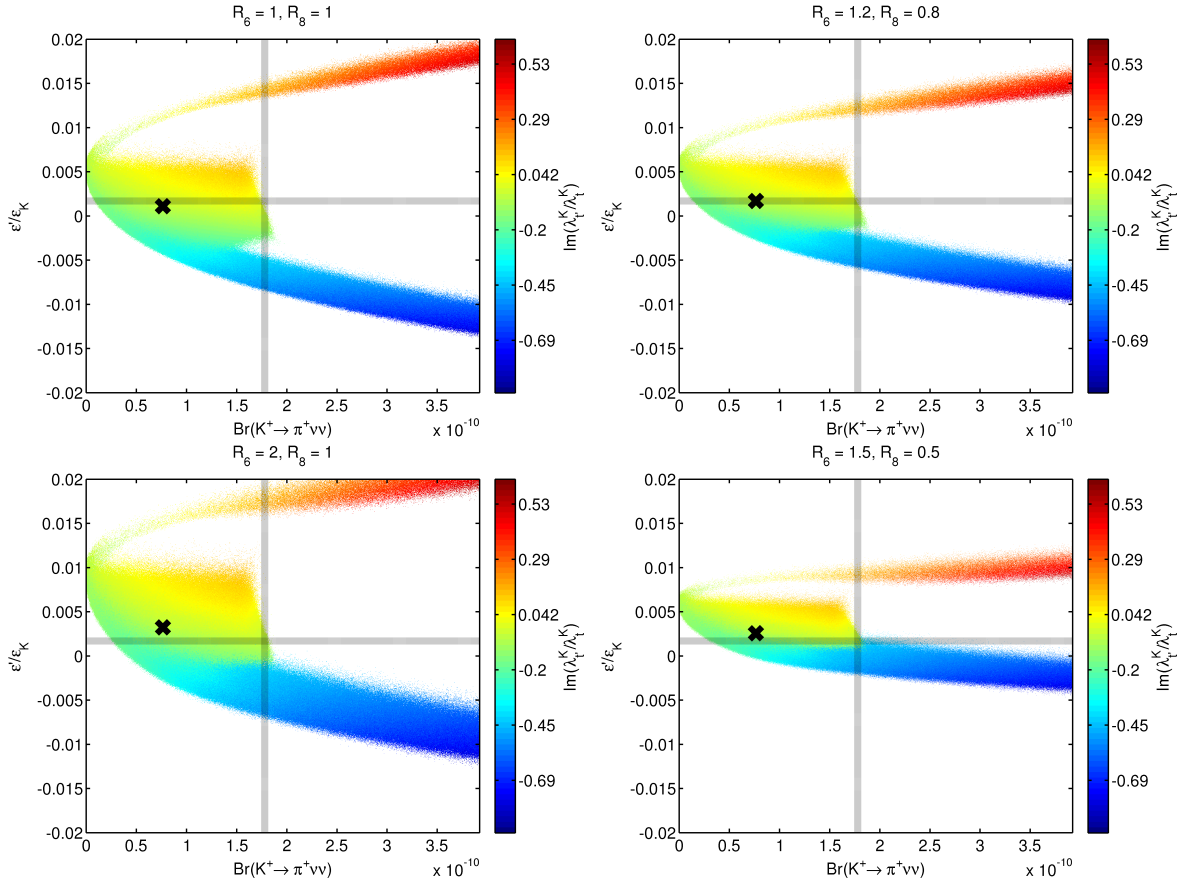


Figure 7.19: The direct CP violation $\varepsilon'/\varepsilon_K$ as a function of $\mathrm{Br}(K^+ \to \pi^+\nu\bar{\nu})$ for different values of $(R_6, R_8)$ as listed in table 4.5. The colour code shows the dependence on $\mathrm{Im}(\lambda_{t'}^{(K)}/\lambda_t^{(K)})$.

tive $\mathrm{Im}(\lambda_{t'}^{(K)}/\lambda_t^{(K)})$ that were previously missed by the other constraints like $\mathrm{Br}(K_L \to \mu^+\mu^-)$ or $\mathrm{Br}(K^+ \to \pi^+\nu\bar{\nu})$. In the left panel of figure 7.18, we also find a small region where $\mathrm{Br}(K_L \to \pi^0 e^+ e^-)$ poses a more stringent constraint than $\mathrm{Br}(K_L \to \pi^0\nu\bar{\nu})$ for points with large negative $\mathrm{Im}(\lambda_{t'}^{(K)}/\lambda_t^{(K)})$. This illustrates how every rare $K$ decay becomes important for constraining the SM4.

In figure 7.19, we show the correlation between $\varepsilon'/\varepsilon_K$ and $\mathrm{Br}(K^+ \to \pi^+\nu\bar{\nu})$ for different scenarios for the hadronic parameters $R_6$ and $R_8$ as listed in table 4.5. As before, the colour code corresponds to $\mathrm{Im}(\lambda_{t'}^{(K)}/\lambda_t^{(K)})$. From figure 7.19, we can immediately see the potential constraining power of $\varepsilon'/\varepsilon_K$ in this model. However, as we already discussed in section 4.11, this power can currently not be harnessed due to the large uncertainty on $R_8$ and, more importantly, due to lack of reliable data on $R_6$. The potentially huge effects in $\varepsilon'/\varepsilon_K$ can be explained by the new $Z$ penguins with a virtual $t'$. These new contributions upset the delicate balance between the QCD and electroweak penguins in the SM with its near perfect cancellation. As can be seen from figure 7.19 the SM4 benefits from $R_8 < 1$ and a simultaneously enhanced $R_6 > 1$. However, even in this case the red points with large positive $\mathrm{Im}(\lambda_{t'}^{(K)}/\lambda_t^{(K)})$ can probably be ruled out by $\varepsilon'/\varepsilon_K$. Eliminating these points would have profound consequences as can be

directly seen from the previous figures.

# 8

# Conclusions

In this work, we have presented a comparative numerical analysis of two well established models of physics beyond the Standard Model (SM). In the context of the Standard Model with a sequential fourth generation (SM4) and the left-right symmetric Standard Model (LRM), we have analysed the constraints imposed by the most relevant $\Delta F = 2$ processes, $\mathrm{Br}(B \to X_s\gamma)$ and $\langle \mathrm{Br}(B \to X_d\gamma) \rangle$. In our analysis, we have taken the constraints from electroweak precision tests, direct searches and tree-level determinations of CKM matrix elements into account. In the context of the SM4, we have also studied the constraints from rare $K$ and $B$ decays and have shown their important impact on the structure of the four-by-four CKM matrix. In preparation of our analysis of the models of new physics, we have performed a fit including the most important constraints in the Standard Model. We have, furthermore, studied the constraints imposed by $\Delta F = 2$ observables on generic models of new physics.

The status quo of the Standard Model including constraints on models of new physics can be summarised as follows:

- In the SM fit, we use only $\Delta F = 2$ processes together with $|V_{us}|$, $|V_{ub}/V_{cb}|$ and $\gamma$ as inputs and find a good agreement between the different measurements. However, in this case $|V_{ub}|$ and $|V_{cb}|$ are predicted to have very low values of $3.3 \cdot 10^{-3}$ and $39.7 \cdot 10^{-3}$, respectively. This corresponds to the exclusive value of $|V_{cb}|$ and the exclusive value of $|V_{ub}|$ determined by semi-leptonic decays. From this point of view, our Standard Model fit shows a tension in $\mathrm{Br}(B \to \tau\nu_\tau)$ as has also been found in [31–33].

- We do not find a clear sign for a tension in $\varepsilon_K$. The theoretical value of $\varepsilon_K$ though significantly smaller than its experimental value is still in agreement with the experiment due to the large error on $\hat{\eta}_{cc}$.

- The LHCb data on $\phi_s$ and $\Delta\Gamma_s$ together with $\Delta M_s$ efficiently constrain new physics in $B_s$. The relative amplitude of new effects in $M_{12}^{B_s}$ is constrained to be below 20% with a small correlation to the relative phase of new physics in $M_{12}^{B_s}$.

- The constraints from $\Delta M_d$ and $\sin 2\beta$ have a strong impact on possible new physics in $B_d$. The relative amplitude of new effects in $M_{12}^{B_d}$ is constrained to below $10 - 20\%$ depending on the relative phase of new physics in $M_{12}^{B_d}$.

In our analysis of the SM4 and the LRM, we have followed a strict policy of not assuming anything beyond the correctness of the imposed constraints. In our comparison of the two models, we have found that the structure of the new mixing elements/matrix in the SM4 and the LRM is impacted quite differently by the constraints. Using Monte Carlo methods to estimate the viable parameter space in the SM4 and the LRM, we find that:

- The small tension between $\varepsilon_K$ and $\sin 2\beta$ can be resolved in the SM4 as well as in the LRM. Both models introduce enough additional CP violation to fully remove the tension and still provide uncorrelated effects in $S_{\psi\phi}$. Moreover, any of the three values for $V_{ub}$ is in principle compatible with the SM4. In the LRM, we are forced to choose the inclusive value of $|V_{ub}^{\mathrm{L}}|$ as long as we believe in the experimental results.

- The structure of the right-handed mixing matrix of the LRM can be categorised by three distinct scenarios: a hierarchy similar to the one found in the Standard Model CKM matrix, an inverted hierarchy in the mixing between second and third generation or an inverted hierarchy in the mixing between the first and the second generation. The fine-tuning in the inverted scenarios is typically higher than the fine-tuning in the normal hierarchy scenario. For moderate to high values of the fine-tuning the value of $|V_{ub}^{\mathrm{R}}|$ is allowed to approach unity if $|V_{cb}^{\mathrm{R}}|$ is small.

- In the LRM, as shown in chapter 3, the contribution of the FCNC Higgs particle introduces large corrections to $\varepsilon_K$, $\Delta M_K$ and to a smaller extent to the observables in the $B$ system. The very distinct structure of the RH mixing matrix is a direct consequence of this fact.

- The LHCb data on $S_{\psi\phi}$ and $\Delta\Gamma_s$ efficiently constrain the LRM effects in the $B_s$ mixing. In the normal hierarchy scenario the LR top contribution dominates the NP effects while in other scenarios the charm-top contribution is more important.

- The mixing between the fourth and the first three generations in the Standard Model with a sequential fourth generation is tightly constrained by the rare $K$ decays. The anti-correlation between $B_d$ and $B_s$ system expressed as an anti-correlation between $\lambda_{t'}^{(d)}$ and $\lambda_{t'}^{(s)}$ is a very distinct feature of the SM4.

- The correlation between $\mathrm{Br}(B \to X_s\gamma)$ and $\langle \mathrm{Br}(B \to X_d\gamma)\rangle$ is very different in the SM4 and the LRM.

  - In the LRM, $\mathrm{Br}(B \to X_s\gamma)$ shows a very strong dependence on the electroweak parameter $s$ and a linear dependence on $\mathrm{Re}(V_{tb}^{\mathrm{R}})$. On the other hand $\langle \mathrm{Br}(B \to X_d\gamma)\rangle$ does only show a very weak correlation with $\mathrm{Br}(B \to X_s\gamma)$, $\mathrm{Re}(V_{tb}^{\mathrm{R}})$ or $s$.
  - In the SM4, $\mathrm{Br}(B \to X_s\gamma)$ strongly depends on $\mathrm{Re}(\lambda_{t'}^{(s)})$ while the new contributions to $\langle \mathrm{Br}(B \to X_d\gamma)\rangle$ are dominated by $\mathrm{Re}(\lambda_{t'}^{(d)})$. The correlation between both branching ratios shows the typical anti-correlation between $b \to d$ and $b \to s$ transitions.
  - While the LRM effects do generally not show correlations between the $b \to q\gamma$ decays and $\Delta F = 2$ observables, the SM4 effects show an interesting correlation between $\Delta M_s$ and $\mathrm{Br}(B \to X_s\gamma)$. This is due to the fact that the changes in $V_{ts}$ are correlated with new contributions introduces by $\lambda_{t'}^{(s)}$.

- The direct CP violation in $b \to q\gamma$ decays receives only marginal contributions in both models. However, in the SM4, these new contributions are correlated with $S_{\psi\phi}$ and $S_{\psi K_s}$ for $b \to s\gamma$ and $b \to d\gamma$, respectively. In the LRM on the other hand, we do not observe such a correlation due to the huge number of new CP violating phases introduced by the RH mixing matrix $V^{\mathrm{R}}$.

- For the mass of the heavy Higgs particles we find a lower limit of 2.4 TeV $\leq M_H$. Even in the case of very low Higgs mass, the fine-tuning is not necessarily high and we still find two different structures for the RH mixing matrix.

- Due to the lower limit on the mass of the heavy $W'$ boson, the $V_{ub}$ problem cannot be fully solved in the LRM. Moreover, if we were to require only a small to moderate amount of fine-tuning, the tension could not even be softened as the correction to $|V_{ub}|_{V,A}$ would be too small by one order of magnitude.

In our analysis of rare decays and CP violation in the SM4, we have identified the connections between different observables by explicitly showing the dependence on combinations of CKM4 elements in colour. The new contributions to rare decays in the SM4 introduce interesting effects in the decays of $B$ mesons always showing the SM4-typical anti-correlation between $B_d$ and $B_s$ system. The new effects in rare decays of Kaons are truly spectacular as the constraints from $\varepsilon_K$ and $\Delta M_K$ are not as strong as in most other models of NP. The most important features of rare decays in the SM4 are:

- The branching ratios $\mathrm{Br}(B_q \to \mu^+\mu^-)$ can be enhanced or suppressed in the SM4. However, the constraints from rare $K$ decays enforce a strong anti-correlation between $B_d$ and $B_s$ decays. This leads to SM like values for one branching ratio if the other is enhanced or suppressed. Simultaneous deviations from the SM predictions are only possible if they are small.

- For a suppressed branching ratio of either $B_d \to \mu^+\mu^-$ or $B_s \to \mu^+\mu^-$, the mixing induced CP asymmetry $S_{\psi\phi}$ has to be close to the SM expectation.

- The experimental upper limit on $\mathrm{Br}(B_s \to \mu^+\mu^-)$ introduces a lower limit on the branching ratio $\mathrm{Br}(B \to X_s\gamma)$. This allows for only small suppressions but still for arbitrary enhancements of $\mathrm{Br}(B \to X_s\gamma)$ (within the uncertainties on this measurement).

- The rare $K$ decays introduce very important constraints on the combination $V^*_{t's}V_{t'd}$ of CKM matrix elements. This leads to the already highlighted anti-correlation between $b \to d$ and $b \to s$ transition. For different regions of the parameter space, any rare decay could pose the most important constraint and therefore all rare decays have to be taken into account.

- The correlation between $\mathrm{Br}(K^+ \to \pi^+\nu\bar{\nu})$ and $\mathrm{Br}(K_L \to \pi^0\nu\bar{\nu})$ shows possible small enhancements of $\mathrm{Br}(K^+ \to \pi^+\nu\bar{\nu})$ for $\mathrm{Br}(K_L \to \pi^0\nu\bar{\nu}) \leq 6 \cdot 10^{-10}$ or equivalently mostly real $\lambda^{(K)}_{t'}$. For mostly imaginary $\lambda^{(K)}_{t'}$, both branching ratios are drastically enhanced simultaneously. Interestingly, in contrast to other models, the Grossman-Nir bound can be saturated in the SM4.

- The constraint from $\varepsilon'/\varepsilon$ could be very important once reliable data on the hadronic parameters $R_6$ and $R_8$ becomes available. We have shown explicitly that, in the case of $R_6$ and $R_8$ close to the large N expectation, large values for the imaginary part of $\lambda^{(K)}_{t'}$ can be drastically restricted.

- The strong dependence of all rare $K$ decays on $\lambda^{(K)}_{t'}$ makes the SM4 very predictive. If one CP violating and one CP conserving decay is measured with a decent accuracy, then all other decays as well as $\varepsilon'/\varepsilon$ would be fixed.

It is evident from our analysis that even though the SM4 and the LRM are models conceived more than thirty years ago, the constraints from most recent measurements can still not exclude them on the basis of flavour changing processes. However, the SM4 is under serious pressure due to the lower limits on the masses of the additional fermions as well as the implications of the current Higgs searches. The LRM, although it cannot be excluded for arbitrary high masses of the additional gauge bosons, has lost some of its attractiveness as it cannot explain the discrepancies in the $V_{ub}$ determinations. Furthermore, the extremely restricted ranges for the elements of the RH mixing matrix together with the heaviness of the additional gauge bosons lead us to the expection of only small effects in rare decays, especially in the absence of strong QCD enhancements in $\Delta F = 1$ processes.

However, even though the SM4 is nearly ruled out and FCNC processes in the LRM prove to be tightly constrained, there is still room for large effects in rare $K$ decays. Furthermore, even a suppression of certain branching ratios e.g. $\mathrm{Br}(B_q \to \mu^+\mu^-)$ is conceivable. In this regard the SM4 proves to be a very interesting extension of the SM as it provides possible effects in the $K$ system as well as in the $B_d$ and the $B_s$ system. This shows that models with only left-handed charged currents are very interesting in the light of the strong constraints on possible effects in $\Delta\Gamma_s$ and $S_{\psi\phi}$. In this spirit, our analysis of the SM4 might serve as an inspiration for a model independent analysis of left-handed charged currents.

# LRM Details

## Higgs Potential

The most general renormalisable Higgs potential invariant under parity is given by [129, 138, 358, 359]

$$
\begin{aligned}
V(\phi,\Delta_L,\Delta_R) = &-\mu_1^2\mathrm{Tr}(\phi^\dagger\phi) - \mu_2^2\left[\mathrm{Tr}(\tilde{\phi}\phi^\dagger)+\mathrm{Tr}(\tilde{\phi}^\dagger\phi)\right] - \mu_3^2\left[\mathrm{Tr}(\Delta_L\Delta_L^\dagger)+\mathrm{Tr}(\Delta_R\Delta_R^\dagger)\right] \\
&+ \lambda_1\left[\mathrm{Tr}(\phi^\dagger\phi)\right]^2 + \lambda_2\left\{\left[\mathrm{Tr}(\tilde{\phi}\phi^\dagger)\right]^2+\left[\mathrm{Tr}(\tilde{\phi}^\dagger\phi)\right]^2\right\} \\
&+ \lambda_3\mathrm{Tr}(\tilde{\phi}\phi^\dagger)\mathrm{Tr}(\tilde{\phi}^\dagger\phi) + \lambda_4\mathrm{Tr}(\phi^\dagger\phi)\left[\mathrm{Tr}(\tilde{\phi}\phi^\dagger)+\mathrm{Tr}(\tilde{\phi}^\dagger\phi)\right] \\
&+ \rho_1\left\{\left[\mathrm{Tr}(\Delta_L\Delta_L^\dagger)\right]^2+\left[\mathrm{Tr}(\Delta_R\Delta_R^\dagger)\right]^2\right\} \\
&+ \rho_2\left[\mathrm{Tr}(\Delta_L\Delta_L)\mathrm{Tr}(\Delta_L^\dagger\Delta_L^\dagger)+\mathrm{Tr}(\Delta_R\Delta_R)\mathrm{Tr}(\Delta_R^\dagger\Delta_R^\dagger)\right] \\
&+ \rho_3\mathrm{Tr}(\Delta_L\Delta_L^\dagger)\mathrm{Tr}(\Delta_R\Delta_R^\dagger) + \rho_4\left[\mathrm{Tr}(\Delta_L\Delta_L)\mathrm{Tr}(\Delta_R^\dagger\Delta_R^\dagger)+\mathrm{Tr}(\Delta_L^\dagger\Delta_L^\dagger)\mathrm{Tr}(\Delta_R\Delta_R)\right] \\
&+ \alpha_1\mathrm{Tr}(\phi^\dagger\phi)\left[\mathrm{Tr}(\Delta_L\Delta_L^\dagger)+\mathrm{Tr}(\Delta_R\Delta_R^\dagger)\right] \\
&+ \left\{\alpha_2 e^{i\delta_2}\left[\mathrm{Tr}(\tilde{\phi}\phi^\dagger)\mathrm{Tr}(\Delta_L\Delta_L^\dagger)+\mathrm{Tr}(\tilde{\phi}^\dagger\phi)\mathrm{Tr}(\Delta_R\Delta_R^\dagger)\right]+\mathrm{h.c.}\right\} \\
&+ \alpha_3\left[\mathrm{Tr}(\phi\phi^\dagger\Delta_L\Delta_L^\dagger)+\mathrm{Tr}(\phi^\dagger\phi\Delta_R\Delta_R^\dagger)\right] + \beta_1\left[\mathrm{Tr}(\phi\Delta_R\phi^\dagger\Delta_L^\dagger)+\mathrm{Tr}(\phi^\dagger\Delta_L\phi\Delta_R^\dagger)\right] \\
&+ \beta_2\left[\mathrm{Tr}(\tilde{\phi}\Delta_R\phi^\dagger\Delta_L^\dagger)+\mathrm{Tr}(\tilde{\phi}^\dagger\Delta_L\phi\Delta_R^\dagger)\right] + \beta_3\left[\mathrm{Tr}(\phi\Delta_R\tilde{\phi}^\dagger\Delta_L^\dagger)+\mathrm{Tr}(\phi^\dagger\Delta_L\tilde{\phi}\Delta_R^\dagger)\right] .
\end{aligned}
\tag{1}
$$

In this form of the potential, it introduces 17 real parameters $\mu^2_{1,2,3}$, $\lambda_{1,2,3,4}$, $\rho_{1,2,3,4}$, $\alpha_{1,2,3}$, and $\beta_{1,2,3}$. Due to the $P$ symmetry, only $\alpha_2$ is allowed to be complex which introduces the phase $\delta_2$. We have also studied a more general Higgs potential without $P$ symmetry. However, as only a limited number of parameters of the Higgs potential affect our analysis, we chose to employ the simpler $P$ symmetric version of the potential.

## Gauge Boson Masses and Mixing

The gauge boson mass matrices can be obtained from the relevant terms of equations (2.24) and (2.25). Diagonalising the resulting mass matrix for the charged gauge bosons yields the

mass eigenstates including terms of $\mathcal{O}(\varepsilon^2)$

$$W^{\pm} = W_L^{\pm} + sce^{\mp i\alpha}\frac{s_R c_W}{s_W}\epsilon^2 W_R^{\pm}\,, \tag{2}$$

$$W'^{\pm} = W_R^{\pm} - sce^{\pm i\alpha}\frac{s_R c_W}{s_W}\epsilon^2 W_L^{\pm}\,, \tag{3}$$

where we used the notation introduced in section 2.2. We also introduced the mixing angles

$$s_R = \frac{g'}{\sqrt{g'^2 + g_R^2}}\,, \quad c_R = \sqrt{1-s_R^2}\,, \quad s_W = \frac{s_R}{\sqrt{(g_L/g_R)^2 + s_R^2}}\,, \quad c_W = \sqrt{1-s_W^2}\,. \tag{4}$$

To leading order in $\varepsilon$, the corresponding masses are given by

$$(M_W)^2 = \frac{e^2 v^2}{2s_W^2}\left(1 - 2s^2c^2\epsilon^2\right)\,, \tag{5}$$

$$(M_{W'})^2 = \frac{e^2\kappa_R^2}{c_W^2 s_R^2}\left(1 + \frac{1}{2}\epsilon^2\right)\,. \tag{6}$$

The mixing between $W_L$ and $W_R$ is often defined as $\zeta$ in the literature. In our notation this parameter is given by

$$\zeta = sce^{\mp i\alpha}\frac{s_R c_W}{s_W}\epsilon^2\,. \tag{7}$$

After EWSB, the neutral gauge bosons can be written in terms of the fundamental fields as

$$A = s_W W_L^3 + s_R c_W W_R^3 + c_R c_W B\,, \tag{8}$$

$$Z = c_W W_L^3 - s_R s_W\left(1 - \frac{c_R^4}{4s_W^2}\epsilon^2\right)W_R^3 - c_R s_W\left(1 + \frac{s_R^2 c_R^2}{4s_W^2}\epsilon^2\right)B\,, \tag{9}$$

$$Z' = -\frac{s_R c_R^3 c_W}{4s_W}\epsilon^2 W_L^3 + c_R\left(1 + \frac{s_R^2 c_R^2}{4}\epsilon^2\right)W_R^3 - s_R\left(1 - \frac{c_R^4}{4}\epsilon^2\right)B\,. \tag{10}$$

Their corresponding masses are given by

$$(M_A)^2 = 0\,, \tag{11}$$

$$(M_Z)^2 = \frac{e^2 v^2}{2s_W^2 c_W^2}\left(1 - \frac{c_R^4}{4}\epsilon^2\right)\,, \tag{12}$$

$$(M_{Z'})^2 = \frac{2e^2\kappa_R^2}{s_R^2 c_R^2 c_W^2}\left(1 + \frac{c_R^4}{4}\epsilon^2\right)\,. \tag{13}$$

## Goldstone Boson and Higgs Mass Eigenstates

The doubly charged components $\delta_{L,R}^{++}$ of $\Delta_{L,R}$ introduce to two physical doubly charged Higgs particles with masses proportional to $\kappa_R$ and no couplings to quarks. The singly charged fields $\phi_{1,2}^{\pm}$ and $\delta_{L,R}^{\pm}$ contribute to the Goldstone bosons of $W^{\pm}$ and $W'^{\pm}$ and to two charged Higgses. The Goldstone bosons of $W^{\pm}$ and $W'^{\pm}$ are given by

$$G^{\pm} = \pm i\left[c\left(1 - s^4\epsilon^2\right)\phi_1^{\pm} - se^{\mp i\alpha}\left(1 - c^4\epsilon^2\right)\phi_2^{\pm} - \sqrt{2}cse^{\mp i\alpha}\epsilon\delta_R^{\pm}\right]\,, \tag{14}$$

$$G'^{\pm} = \mp i\left[\left(1 - \frac{\epsilon^2}{4}\right)\delta_R^{\pm} + \frac{se^{\pm i\alpha}}{\sqrt{2}}\epsilon\phi_1^{\pm} - \frac{c}{\sqrt{2}}\epsilon\phi_2^{\pm}\right]\,. \tag{15}$$

The physical charged Higgs with $\mathcal{O}(1)$ couplings to the quarks is given by the orthogonal combination

$$h^\pm = se^{\pm i\alpha}\left(1-\frac{(c^2-s^2)^2}{4}\epsilon^2\right)\phi_1^\pm + c\left(1-\frac{(c^2-s^2)^2}{4}\epsilon^2\right)\phi_2^\pm + \frac{c^2-s^2}{\sqrt{2}}\epsilon\delta_R^\pm\,, \tag{16}$$

which is no mass eigenstates of the diagonalised Higgs potential. Finally the neutral Goldstone boson and Higgs fields are built out of $\phi^0_{1,2}$ and $\delta^0_{L,R}$. Defining $\pi^0 = c\,\mathrm{Im}\phi_1^0 - s\,\mathrm{Im}(e^{-i\alpha}\phi_2^0)$, the Goldstone bosons of $Z$ and $Z'$ read

$$G^0 = \sqrt{2}\left(1-\frac{c_R^4}{8}\epsilon^2\right)\pi^0 - \frac{c_R^2}{\sqrt{2}}\epsilon\,\mathrm{Im}\delta_R^0\,, \tag{17}$$

$$G'^0 = -\sqrt{2}\left(1-\frac{c_R^4}{8}\epsilon^2\right)\mathrm{Im}\delta_R^0 - \frac{c_R^2}{\sqrt{2}}\epsilon\pi^0\,. \tag{18}$$

In addition there are six neutral Higgs fields in the spectrum, that are linear combinations of $s\,\mathrm{Im}\phi_1^0 + c\,\mathrm{Im}(e^{-i\alpha}\phi_2^0)$, $\mathrm{Re}\phi_1^0$, $\mathrm{Re}(e^{-i\alpha}\phi_2^0)$, $\mathrm{Re}\delta_R^0$, $\mathrm{Re}\delta_L^0$ and $\mathrm{Im}\delta_L^0$.

In order to make a more detailed statement about the Higgs mass eigenstates one has to diagonalise the Higgs potential (1). The eight-by-eight mass matrix for the neutral scalar particles can be diagonalised in perturbation theory. While in [138], a further hierarchy, namely $\kappa' \ll \kappa$, has been assumed, we do not restrict ourselves to this case but determine the Higgs mass eigenstates to leading order for arbitrary $s = \kappa'/v$. It turns out that the leading order Higgs couplings are not sensitive to the detailed structure of the potential and in particular the parity invariant potential yields the same result. The leading order mass eigenstates of the Higgs fields with substantial couplings to quarks are given by

$$h^0 = \sqrt{2}\left(c\,\mathrm{Re}\phi_1^0 + s\,\mathrm{Re}(e^{-i\alpha}\phi_2^0)\right) \tag{19}$$

$$H_1^0 = \sqrt{2}\left(-s\,\mathrm{Re}\phi_1^0 + c\,\mathrm{Re}(e^{-i\alpha}\phi_2^0)\right) \tag{20}$$

$$H_2^0 = \sqrt{2}\left(s\,\mathrm{Im}\phi_1^0 + c\,\mathrm{Im}(e^{-i\alpha}\phi_2^0)\right) \tag{21}$$

where $h_0$ can be identified as the light Higgs with a mass of $\mathcal{O}(v)$, while $H_1^0$ and $H_2^0$ are two new flavour-violating neutral scalar particles with masses $\mathcal{O}(\kappa_R)$. To leading order their masses are equal to each other

$$M_H^2 \equiv M_{H_1^0}^2 = M_{H_2^0}^2 = \frac{\alpha_3\kappa_R^2}{1-2s^2} = \alpha_3\kappa_R^2\sqrt{u(s)}\,. \tag{22}$$

In the course of the numerical analysis we regard $M_H$ as a free parameter. These results agree with the ones given by the authors of [138] in the limit of small $s \ll 1$. A more explicit analysis of the Higgs sector of this class of models can be also found in [129, 138, 359]. Charged Higgs effects in LR models are often neglected in the literature with the argument that they have to be small in FCNC processes as they have to take place at one loop order [360]. This is in fact true for the $\Delta F = 2$ processes but not for $B \to X_{s,d}\gamma$. This has already been pointed out in [212, 213, 216, 217, 219, 221] in LR models. As in the case of the neutral Higgs sector we are only interested in leading order couplings and masses. We find that the mass of the lightest charged Higgs,

$$H^\pm = se^{\pm i\alpha}\phi_1^\pm + c\phi_2^\pm\,, \tag{23}$$

is given to a very good approximation by

$$M_{H^+} = M_H \tag{24}$$

and hence cannot be chosen to be as light as 1 TeV as done sometimes in the literature.

## Numerical Details for $\Delta F = 2$ Processes in the LRM

In this section we provide values for $R_{ij}$ as defined in (3.71) and used in our discussion on $\Delta F = 2$ constraints in the context of the LRM in section 3.4. Including all contributions we find for $\epsilon = 0.03$, $s_R = 0.8$ and $s = 0.1$

$$\hat{R}(K) = \begin{pmatrix} -4.3236 \cdot 10^{-9} & -1.2585 \cdot 10^{-6} & -7.8924 \cdot 10^{-5} \\ -1.2585 \cdot 10^{-6} & -6.5793 \cdot 10^{-4} & -4.1333 \cdot 10^{-2} \\ -7.8924 \cdot 10^{-5} & -4.1333 \cdot 10^{-2} & -9.1112 \end{pmatrix}, \tag{25}$$

$$\hat{R}(B) = \begin{pmatrix} -2.7079 \cdot 10^{-10} & -7.8847 \cdot 10^{-8} & -4.9574 \cdot 10^{-6} \\ -7.8847 \cdot 10^{-8} & -4.1217 \cdot 10^{-5} & -2.5958 \cdot 10^{-3} \\ -4.9574 \cdot 10^{-6} & -2.5958 \cdot 10^{-3} & -0.5727 \end{pmatrix}. \tag{26}$$

For $s = 0.5$ the Higgs contributions get enhanced and the calculation of the $R_{ij}$ yields

$$\hat{R}(K) = \begin{pmatrix} -4.6987 \cdot 10^{-9} & -1.4447 \cdot 10^{-6} & -1.3159 \cdot 10^{-4} \\ -1.4447 \cdot 10^{-6} & -7.5036 \cdot 10^{-4} & -6.7475 \cdot 10^{-2} \\ -1.3159 \cdot 10^{-4} & -6.7475 \cdot 10^{-2} & -16.546 \end{pmatrix}, \tag{27}$$

$$\hat{R}(B) = \begin{pmatrix} -2.9439 \cdot 10^{-10} & -9.0565 \cdot 10^{-8} & -8.2716 \cdot 10^{-6} \\ -9.0565 \cdot 10^{-8} & -4.7034 \cdot 10^{-5} & -4.2408 \cdot 10^{-3} \\ -8.2716 \cdot 10^{-6} & -4.2408 \cdot 10^{-3} & -1.0406 \end{pmatrix}. \tag{28}$$

Keeping only gauge boson contributions we find (no $s$ dependence)

$$\hat{R}(K, \text{gauge}) = \begin{pmatrix} -3.9343 \cdot 10^{-9} & -1.0653 \cdot 10^{-6} & -2.4264 \cdot 10^{-5} \\ -1.0653 \cdot 10^{-6} & -5.6199 \cdot 10^{-4} & -1.4200 \cdot 10^{-2} \\ -2.4264 \cdot 10^{-5} & -1.4200 \cdot 10^{-2} & -1.3954 \end{pmatrix}, \tag{29}$$

$$\hat{R}(B, \text{gauge}) = \begin{pmatrix} -2.4630 \cdot 10^{-10} & -6.6689 \cdot 10^{-8} & -1.5190 \cdot 10^{-6} \\ -6.6689 \cdot 10^{-8} & -3.5182 \cdot 10^{-5} & -8.8898 \cdot 10^{-4} \\ -1.5190 \cdot 10^{-6} & -8.8898 \cdot 10^{-4} & -8.7355 \cdot 10^{-2} \end{pmatrix}. \tag{30}$$

The $H^{\pm}$ contributions are significantly smaller than gauge contributions.

# Masterfunctions

## Relevant Functions

The master functions for $\Delta F = 1$ processes in the SM and SM4 are given by [203]

$$X_0(x_i) = \frac{x_i}{8}\left[\frac{x_i+2}{x_i-1} + \frac{3x_i-6}{(x_i-1)^2}\,\log x_i\right], \tag{31}$$

$$Y_0(x_i) = \frac{x_i}{8}\left[\frac{x_i-4}{x_i-1} + \frac{3x_i}{(x_i-1)^2}\log x_i\right], \tag{32}$$

$$\begin{aligned} Z_0(x_i) &= -\frac{1}{9}\log x_i + \frac{18x_i^4-163x_i^3+259x_i^2-108x_i}{144(x_i-1)^3} \\ &\quad + \frac{32x_i^4-38x_i^3-15x_i^2+18x_i}{72(x_i-1)^4}\log x_i\,. \end{aligned} \tag{33}$$

$$C_0(x_i) = \frac{x_i}{8}\left[\frac{x_i-6}{x_i-1} + \frac{3x_i+2}{(x_i-1)^2}\log x_i\right], \tag{34}$$

$$D_0(x_i) = -\frac{4}{9}\log x_i + \frac{-19x_i^3+25x_i^2}{36(x_i-1)^3} + \frac{x_i^2(5x_i^2-2x_i-6)}{18(x_i-1)^4}\log x_i\,, \tag{35}$$

$$E_0(x_i) = -\frac{2}{3}\log x_i + \frac{x_i^2(15-16x_i+4x_i^2)}{6(x_i-1)^4}\log x_i + \frac{x_i(18-11x_i-x_i^2)}{12(1-x_i)^3}\,, \tag{36}$$

$$D_0'(x_i) = -\frac{(3x_i^3-2x_i^2)}{2(x_i-1)^4}\log x_i + \frac{(8x_i^3+5x_i^2-7x_i)}{12(x_i-1)^3}\,, \tag{37}$$

$$E_0'(x_i) = \frac{3x_i^2}{2(x_i-1)^4}\log x_i + \frac{(x_i^3-5x_i^2-2x_i)}{4(x_i-1)^3}\,. \tag{38}$$

$$B^{\mu\bar{\mu}}(x_i,y_j) = \frac{1}{4}\left[U(x_i,y_j) + \frac{x_iy_j}{4}U(x_i,y_j) - 2x_iy_j\tilde{U}(x_i,y_j)\right], \tag{39}$$

$$B^{\nu\bar{\nu}}(x_i,y_j) = \frac{1}{4}\left[U(x_i,y_j) + \frac{x_iy_j}{16}U(x_i,y_j) + \frac{x_iy_j}{2}\tilde{U}(x_i,y_j)\right], \tag{40}$$

with

$$U(x_1,x_2) = \frac{x_1^2\log x_1}{(x_1-x_2)(1-x_1)^2} + \frac{x_2^2\log x_2}{(x_2-x_1)(1-x_2)^2} + \frac{1}{(1-x_1)(1-x_2)}\,, \tag{41}$$

$$\tilde{U}(x_1,x_2) = \frac{x_1\log x_1}{(x_1-x_2)(1-x_1)^2} + \frac{x_2\log x_2}{(x_2-x_1)(1-x_2)^2} + \frac{1}{(1-x_1)(1-x_2)}\,. \tag{42}$$

The function $S_0(x_i, x_j)$ relevant for $\Delta F = 2$ processes in the SM and SM4 is, for arbitrary $x_i, x_j$, given by [361]

$$S_0(x_i,x_j) = x_i x_j \left( \frac{(4-8x_j+x_j^2)\log x_j}{4(x_j-1)^2(x_j-x_i)} + (i \leftrightarrow j) - \frac{3}{4(x_i-1)(x_j-1)} \right) . \quad (43)$$

In the limit of $\varepsilon \to 0$ in $S_0(x_i+\varepsilon, x_i-\varepsilon)$ one recovers the SM3 version of $S_0(x_i)$,

$$S_0(x_i) = \frac{x_i}{4} \frac{-4+15x_i-(12-6\log x_i)x_i^2+x_i^3}{(x_i-1)^3} . \quad (44)$$

For the LRM, the $\Delta F = 2$ loop functions are given as by [118, 138, 191–193]

$$S_{\rm LL}(x_i,x_j) = F(x_i,x_j)+F(x_u,x_u)-F(x_i,x_u)-F(x_j,x_u) , \quad (45)$$
$$S_{\rm LR}(x_i,x_j,\beta) = 2\beta r\sqrt{x_i x_j}\left[(4+x_i x_j\beta)I_1(x_i,x_j,\beta)-(1+\beta)I_2(x_i,x_j,\beta)\right] , \quad (46)$$
$$S_{\rm RR}(\tilde{x}_i,\tilde{x}_j) = \beta r^2 S_{LL}(\tilde{x}_i,\tilde{x}_j) , \quad (47)$$
$$F(x_i,x_j) = \frac{1}{4}\left[(4+x_i x_j)I_2(x_i,x_j,1)-8x_i x_j I_1(x_i,x_j,1)\right] , \quad (48)$$

with

$$I_1(x_i,x_j,\beta) = \frac{x_i\ln(x_i)}{(1-x_i)(1-x_i\beta)(x_i-x_j)} + (i \leftrightarrow j) - \frac{\beta\ln(\beta)}{(1-\beta)(1-x_i\beta)(1-x_j\beta)} , \quad (49)$$
$$I_2(x_i,x_j,\beta) = \frac{x_i^2\ln(x_i)}{(1-x_i)(1-x_i\beta)(x_i-x_j)} + (i \leftrightarrow j) - \frac{\ln(\beta)}{(1-\beta)(1-x_i\beta)(1-x_j\beta)} . \quad (50)$$

The master function for the charged Higgs contribution reads

$$S^H_{\rm LR}(x_i,x_j,\beta_H) = 2u(s)\beta_H\sqrt{x_i(\mu_H)x_j(\mu_H)}\left[x_i x_j I_1(x_i,x_j,\beta_H)-I_2(x_i,x_j,\beta_H)\right] . \quad (51)$$

The relevant functions for the LR contribution to $b \to q\gamma$ are given by

$$A^1_{H^+}(y) = \left[\frac{3y^2-2y}{3(1-y)^3}\ln y + \frac{5y^2-3y}{6(1-y)^2}\right] , \quad (52)$$
$$A^2_{H^+}(y) = \frac{1}{3}A_{\rm SM}(y) - A^1_{H^+}(y) , \quad (53)$$
$$A_{\rm SM}(y) = -2C^{\rm SM}_{7\gamma}(y) , \quad y = \frac{m_t^2}{M_H^2} . \quad (54)$$

# Individual Lattice Inputs

| |
|---|
| $\hat{B}_K = 0.7674 \pm 0.0099$ [163–167] |
| $\kappa_\varepsilon = 0.94 \pm 0.01$ [178] |
| $f_B = (190.6 \pm 4.6)$ MeV [362, 363] |
| $f_{B_s} = (227.6 \pm 4.1)$ MeV [362–364] |
| $f_{B_s}/f_{B_d} = 1.201 \pm 0.017$ [362, 363, 365] |
| $\hat{B}_d = 1.26 \pm 0.11$ [169] |
| $\hat{B}_s = 1.33 \pm 0.06$ [169] |
| $\hat{B}_s/\hat{B}_d = 1.05 \pm 0.07$ [169] |
| $f_{B_d}\sqrt{\hat{B}_{B_d}} = (227 \pm 17)$ MeV [168, 169] |
| $f_{B_s}\sqrt{\hat{B}_{B_s}} = (279 \pm 13)$ MeV [168, 169] |
| $\xi \equiv f_{B_s}\sqrt{\hat{B}_s}/(f_{B_d}\sqrt{\hat{B}_d}) = 1.237 \pm 0.032$ [169, 365, 366] |

Table 1: Lattice-QCD and other inputs to the unitarity triangle analysis. Details on the lattice-QCD averages are given in the "Note on the correlations between the various lattice calculations" at `www.latticeaverages.org` [33, 170, 367].

| |
|---|
| $m_s^{\overline{MS}}(2\text{ GeV}) = (93.4 \pm 1.1)$ MeV [165, 166, 368–371] |
| $m_{ud}^{\overline{MS}}(2\text{ GeV}) = (3.408 \pm 0.048)$ MeV [165, 166, 368–371] |
| $m_u^{\overline{MS}}(2\text{ GeV}) = (2.079 \pm 0.094)$ MeV [165, 368–371] |
| $m_d^{\overline{MS}}(2\text{ GeV}) = (3.408 \pm 0.048)$ MeV [165, 368–371] |
| $m_s/m_{ud} = 27.56 \pm 0.14$ [165, 368, 370–373] |
| $m_u/m_d = 0.444 \pm 0.044$ [165, 370, 371] |

Table 2: Lattice-QCD and other inputs to the unitarity triangle analysis. Details on the lattice-QCD averages are given in the "Note on the correlations between the various lattice calculations" at `www.latticeaverages.org` [33, 170, 367].

| |
|---|
| $\lvert V_{ub}\rvert_{\text{excl}} = (3.12 \pm 0.26) \times 10^{-3}$ [50–52, 374] |
| $\lvert V_{cb}\rvert_{\text{excl}} = (39.5 \pm 1.0) \times 10^{-3}$ [54, 333, 334] |
| $\lvert V_{ub}\rvert_{\text{incl}} = (4.34 \pm 0.16^{+0.15}_{-0.22}) \times 10^{-3}$ [54] |
| $\lvert V_{cb}\rvert_{\text{incl}} = (41.68 \pm 0.44 \pm 0.09 \pm 0.58) \times 10^{-3}$ [54] |
| $\lvert V_{ub}\rvert_{\text{avg}} = (3.74 \pm 0.59) \times 10^{-3}$ |
| $\lvert V_{cb}\rvert_{\text{avg}} = (40.77 \pm 0.81) \times 10^{-3}$ |

Table 3: Lattice-QCD and other inputs to the unitarity triangle analysis. Details on the lattice-QCD averages are given in the "Note on the correlations between the various lattice calculations" at `www.latticeaverages.org` [33, 170, 367].

# List of Figures

# List of Tables

# Bibliography


[1] **ATLAS Collaboration** Collaboration, G. Aad *et. al.*, *Combined search for the Standard Model Higgs boson using up to 4.9 $fb^{-}1$ of pp collision data at $\sqrt{s} = 7$ TeV with the ATLAS detector at the LHC*, *Phys.Lett.* **B710** (2012) 49–66, [arXiv:1202.1408].

[2] **CMS Collaboration** Collaboration, S. Chatrchyan *et. al.*, *Combined results of searches for the standard model Higgs boson in pp collisions at $\sqrt{s} = 7$ TeV*, arXiv:1202.1488.

[3] **TEVNPH (Tevatron New Phenomina and Higgs Working Group), CDF Collaboration, D0 Collaboration** Collaboration, *Combined CDF and D0 Search for Standard Model Higgs Boson Production with up to 10.0 $fb^{-1}$ of Data*, arXiv:1203.3774. Preliminary results prepared for the Winter 2012 Conferences.

[4] E. Accomando, D. Becciolini, S. De Curtis, D. Dominici, L. Fedeli, *et. al.*, *Interference effects in heavy $W'$-boson searches at the LHC*, arXiv:1110.0713.

[5] **CMS** Collaboration, "Search for a heavy neutrino and right-handed $W$ of the left-right symmetric model in $pp$ collisions at $\sqrt{s} = 7\,\text{TeV}$." http://cdsweb.cern.ch/record/1369255?ln=en, 2011.

[6] **CMS** Collaboration, "Search for $W'$ in the leptonic channels in pp Collisions at $\sqrt{s} = 7\,\text{TeV}$." http://cdsweb.cern.ch/record/1369201?ln=en, 2011.

[7] **ATLAS** Collaboration, G. Aad *et. al.*, *Search for a heavy gauge boson decaying to a charged lepton and a neutrino in $1\,fb^{-1}$ of pp collisions at $\sqrt{s} = 7$ TeV using the ATLAS detector*, arXiv:1108.1316.

[8] **CMS Collaboration** Collaboration, S. Chatrchyan *et. al.*, *Search for leptonic decays of $W'$ bosons in pp collisions at $\sqrt{s} = 7$ TeV*, arXiv:1204.4764. Submitted to the Journal of High Energy Physics.

[9] **ATLAS Collaboration** Collaboration, G. Aad *et. al.*, *Search for down-type fourth generation quarks with the ATLAS detector in events with one lepton and high transverse momentum hadronically decaying W bosons in $\sqrt{s} = 7$ TeV pp collisions*, arXiv:1202.6540.

[10] **ATLAS Collaboration** Collaboration, G. Aad *et. al.*, *Search for same-sign top-quark production and fourth-generation down-type quarks in pp collisions at $\sqrt{s} = 7$ TeV with the ATLAS detector*, *JHEP* **1204** (2012) 069, [arXiv:1202.5520].

[11] **CMS Collaboration** Collaboration, S. Chatrchyan *et. al.*, *Search for heavy bottom-like quarks in 4.9 inverse femtobarns of pp collisions at* $\sqrt{s} = 7$ TeV, arXiv:1204.1088.

[12] **CMS Collaboration** Collaboration, S. Chatrchyan *et. al.*, *Search for heavy, top-like quark pair production in the dilepton final state in pp collisions at* $\sqrt{s} = 7$ TeV, arXiv:1203.5410. Submitted to Physics Letters B.

[13] **ATLAS Collaboration** Collaboration, G. Aad *et. al.*, *Search for charged Higgs bosons decaying via* $H^+ \to \tau\nu$ *in top quark pair events using pp collision data at* $\sqrt{s} = 7$ TeV *with the ATLAS detector*, arXiv:1204.2760.

[14] **for the CMS Collaboration** Collaboration, A. K. N.A.Y.AK, *A search for* $H^+$ *and* $H^{++}$ *Higgs boson with the CMS detector*, arXiv:1112.4748.

[15] **CMS Collaboration** Collaboration, S. Chatrchyan *et. al.*, *Search for a Higgs boson in the decay channel* $H \to ZZ^{(*)} \to q\bar{q}l^-l^+$ *in pp collisions at* $\sqrt{s} = 7$ TeV, *JHEP* **1204** (2012) 036, [arXiv:1202.1416].

[16] **ATLAS Collaboration** Collaboration, N. Vranjes, *Exotic Searches in ATLAS*, arXiv:1202.3171.

[17] **for the ATLAS Collaboration, for the CDF Collaboration, for the CMS Collaboration, for the D0 Collaboration** Collaboration, S. Rahatlou, *Exotic Searches at LHC and Tevatron*, arXiv:1201.4810.

[18] **CMS Collaboration** Collaboration, B. Dahmes, *Exotic Physics Searches at CMS*, arXiv:1202.1442.

[19] **CMS Collaboration** Collaboration, S. Chatrchyan *et. al.*, *Inclusive search for squarks and gluinos in pp collisions at* $\sqrt{s} = 7$ TeV, *Phys.Rev.* **D85** (2012) 012004, [arXiv:1107.1279]. CMS-SUS-10-009, CERN-PH-EP-2011-099.

[20] **ATLAS Collaboration** Collaboration, G. Aad *et. al.*, *Search for gluinos in events with two same-sign leptons, jets and missing transverse momentum with the ATLAS detector in pp collisions at* $\sqrt{s} = 7$ TeV, arXiv:1203.5763. Long author list - awaiting processing.

[21] **CMS Collaboration** Collaboration, F. Ratnikov, *Search for Stopped Gluinos in pp collisions at* $\sqrt{s} = 7$ TeV *at CMS*, *Conf.Proc.* **C100901** (2010) 297–300, [arXiv:1111.1635].

[22] **ATLAS Collaboration** Collaboration, G. Aad *et. al.*, *Search for squarks and gluinos using final states with jets and missing transverse momentum with the ATLAS detector in* $\sqrt{s} = 7$ TeV *proton-proton collisions*, *Phys.Lett.* **B710** (2012) 67–85, [arXiv:1109.6572].

[23] E. Lunghi and A. Soni, *Possible evidence for the breakdown of the CKM-paradigm of CP-violation*, *Phys. Lett.* **B697** (2011) 323–328, [arXiv:1010.6069].

[24] E. Lunghi and A. Soni, *Unitarity Triangle Without Semileptonic Decays*, *Phys.Rev.Lett.* **104** (2010) 251802, [arXiv:0912.0002].

[25] E. Lunghi and A. Soni, *Hints for the scale of new CP-violating physics from B-CP anomalies*, *JHEP* **0908** (2009) 051, [arXiv:0903.5059].

[26] E. Lunghi and A. Soni, *Possible Indications of New Physics in $B_d$-mixing and in $\sin(2\beta)$ Determinations*, *Phys. Lett.* **B666** (2008) 162–165, [arXiv:0803.4340].

[27] A. J. Buras and D. Guadagnoli, *Correlations among new CP violating effects in $\Delta F = 2$ observables*, *Phys. Rev.* **D78** (2008) 033005, [arXiv:0805.3887].

[28] A. J. Buras, *Minimal flavour violation and beyond: Towards a flavour code for short distance dynamics*, *Acta Phys. Polon.* **B41** (2010) 2487–2561, [arXiv:1012.1447].

[29] G. Isidori, *The challenges of flavour physics*, *PoS* **ICHEP2010** (2010) 543, [arXiv:1012.1981].

[30] A. Lenz, U. Nierste, J. Charles, S. Descotes-Genon, A. Jantsch, *et. al.*, *Anatomy of New Physics in $B - \bar{B}$ mixing*, *Phys.Rev.* **D83** (2011) 036004, [arXiv:1008.1593].

[31] A. Bevan, M. Bona, M. Ciuchini, D. Derkach, A. Stocchi, *et. al.*, *The unitarity triangle analysis within and beyond the standard model*, *PoS* **HQL2010** (2011) 019. Updates available on http://www.utfit.org.

[32] A. Lenz and U. Nierste, *Numerical updates of lifetimes and mixing parameters of B mesons*, arXiv:1102.4274.

[33] J. Laiho, E. Lunghi, and R. Van De Water, *Lessons for new physics from CKM studies*, *PoS* **FPCP2010** (2010) 040, [arXiv:1102.3917].

[34] E. Lunghi and A. Soni, *Demise of CKM and its aftermath*, arXiv:1104.2117.

[35] A. J. Buras and J. Girrbach, *BSM models facing the recent LHCb data: A first look*, arXiv:1204.5064.

[36] **BELLE** Collaboration, Y. Nakahama *et. al.*, *Measurement of CP violating asymmetries in $B^0 \to K^+K^-K^0_S$ decays with a time-dependent Dalitz approach*, *Phys. Rev.* **D82** (2010) 073011, [arXiv:1007.3848].

[37] **The BABAR Collaboration** Collaboration, J. Lees, *Study of CP violation in Dalitz-plot analyses of $B^0 \to K^+K^-K^0_S$, $B^+ \to K^+K^-K^+$, and $B^+ \to K^0_SK^0_SK^+$*, arXiv:1201.5897.

[38] *Tagged time-dependent angular analysis of $b^0_s \to j/\psi\phi$ decays at lhcb*, . Linked to LHCb-ANA-2012-004.

[39] J. Brod and M. Gorbahn, *The NNLO Charm-Quark Contribution to $\epsilon_K$ and $\Delta M_K$*, arXiv:1108.2036.

[40] F. Jegerlehner and A. Nyffeler, *The Muon g-2*, *Phys.Rept.* **477** (2009) 1–110, [arXiv:0902.3360]. 134 pages, 68 figures.

[41] M. Davier and W. Marciano, *The theoretical prediction for the muon anomalous magnetic moment*, *Ann.Rev.Nucl.Part.Sci.* **54** (2004) 115–140.

[42] A. Hoecker, *The Hadronic Contribution to the Muon Anomalous Magnetic Moment and to the Running Electromagnetic Fine Structure Constant at $M_Z$ - Overview and Latest Results*, *Nucl.Phys.Proc.Suppl.* **218** (2011) 189–200, [arXiv:1012.0055].

[43] **Muon g-2 Collaboration** Collaboration, G. Bennett *et. al.*, *Measurement of the positive muon anomalous magnetic moment to 0.7 ppm*, *Phys.Rev.Lett.* **89** (2002) 101804, [hep-ex/0208001].

[44] **Muon g-2 Collaboration** Collaboration, G. Bennett *et. al.*, *Measurement of the negative muon anomalous magnetic moment to 0.7 ppm*, *Phys.Rev.Lett.* **92** (2004) 161802, [hep-ex/0401008].
http://www.bnl.gov/bnlweb/pubaf/pr/2004/bnlpr010804.htm.

[45] **Muon G-2 Collaboration** Collaboration, G. Bennett *et. al.*, *Final Report of the Muon E821 Anomalous Magnetic Moment Measurement at BNL*, *Phys.Rev.* **D73** (2006) 072003, [hep-ex/0602035]. Summary of E821 Collaboration measurements of the muon anomalous magnetic moment, each reported earlier in Letters or Brief Reports. Revised version submitted to Phys.Rev.D.

[46] **ALEPH Collaboration, DELPHI Collaboration, L3 Collaboration, OPAL Collaboration, SLD Collaboration, LEP Electroweak Working Group, SLD Electroweak Group, SLD Heavy Flavour Group** Collaboration, *Precision electroweak measurements on the Z resonance*, *Phys.Rept.* **427** (2006) 257–454, [hep-ex/0509008]. 302 pages, v2: minor corrections and updates of references. Accepted for publication by Physics Reports, v3: further small corrections and journal version Report-no: CERN-PH-EP/2005-041, SLAC-R-774.

[47] **Particle Data Group** Collaboration, K. Nakamura *et. al.*, *Review of particle physics*, *J.Phys.G* **G37** (2010) 075021.

[48] **D0 Collaboration** Collaboration, V. M. Abazov *et. al.*, *Measurement of the anomalous like-sign dimuon charge asymmetry with* $9\text{fb}^{-1}$ *of $p\bar{p}$ collisions*, *Phys.Rev.* **D84** (2011) 052007, [arXiv:1106.6308]. Submitted to Phys. Rev. D.

[49] A. Lenz, *A simple relation for $B_s$-mixing*, arXiv:1106.3200.

[50] **BELLE Collaboration** Collaboration, H. Ha *et. al.*, *Measurement of the decay $B^0 \to \pi^- \ell^+ \nu$ and determination of $|V_{ub}|$*, *Phys.Rev.* **D83** (2011) 071101, [arXiv:1012.0090].

[51] **BABAR Collaboration** Collaboration, P. del Amo Sanchez *et. al.*, *Study of $B \to \pi \ell \nu$ and $B \to \rho \ell \nu$ Decays and Determination of $|V_{ub}|$*, *Phys.Rev.* **D83** (2011) 032007, [arXiv:1005.3288]. 47 pages, 26 postscript figures, accepted by Phys. Rev. D.

[52] J. A. Bailey, C. Bernard, C. E. DeTar, M. Di Pierro, A. El-Khadra, *et. al.*, *The $B \to \pi \ell \nu$ semileptonic form factor from three-flavor lattice QCD: A Model-independent determination of $|V_{ub}|$*, *Phys.Rev.* **D79** (2009) 054507, [arXiv:0811.3640].

[53] **BABAR Collaboration, Belle Collaboration** Collaboration, A. Petrella, *Inclusive and Exclusive $|V_{ub}|$*, arXiv:0903.5180. 5 pages, 6 figures, Heavy Quarks and Leptons, Melbourne 2008.

[54] **Heavy Flavor Averaging Group** Collaboration, D. Asner *et. al.*, *Averages of b-hadron, c-hadron, and $\tau$-lepton Properties*, arXiv:1010.1589. Long author list - awaiting processing.

[55] M. Beneke and M. Neubert, *Flavor-singlet B decay amplitudes in QCD factorization*, *Nucl. Phys.* **B651** (2003) 225–248, [hep-ph/0210085].

[56] M. Beneke and M. Neubert, *QCD factorization for $B \to PP$ and $B \to PV$ decays*, *Nucl. Phys.* **B675** (2003) 333–415, [hep-ph/0308039].

[57] e. Bertone, Gianfranco, *Particle dark matter: Observations, models and searches*, .

[58] M. Veltman, *The Infrared - Ultraviolet Connection*, *Acta Phys.Polon.* **B12** (1981) 437. Dedicated to Jacques Prentki on occasion of his sixtieth birthday.

[59] S. P. Martin, *A Supersymmetry primer*, hep-ph/9709356.

[60] L. Randall and R. Sundrum, *A Large mass hierarchy from a small extra dimension*, *Phys.Rev.Lett.* **83** (1999) 3370–3373, [hep-ph/9905221]. 9 pages, LaTex Report-no: MIT-CTP-2860, PUPT-1860, BUHEP-99-9.

[61] A. Pomarol, *Gauge bosons in a five-dimensional theory with localized gravity*, *Phys.Lett.* **B486** (2000) 153–157, [hep-ph/9911294].

[62] H. Davoudiasl, J. Hewett, and T. Rizzo, *Bulk gauge fields in the Randall-Sundrum model*, *Phys.Lett.* **B473** (2000) 43–49, [hep-ph/9911262].

[63] S. Chang, J. Hisano, H. Nakano, N. Okada, and M. Yamaguchi, *Bulk standard model in the Randall-Sundrum background*, *Phys.Rev.* **D62** (2000) 084025, [hep-ph/9912498].

[64] A. Cordero-Cid, H. Novales-Sanchez, and J. Toscano, *The Standard Model with one universal extra dimension*, arXiv:1108.2926. 51 pages.

[65] N. Arkani-Hamed, A. Cohen, E. Katz, and A. Nelson, *The Littlest Higgs*, *JHEP* **0207** (2002) 034, [hep-ph/0206021].

[66] M. Perelstein, *Little Higgs models and their phenomenology*, *Prog.Part.Nucl.Phys.* **58** (2007) 247–291, [hep-ph/0512128].

[67] M. Schmaltz and D. Tucker-Smith, *Little Higgs review*, *Ann.Rev.Nucl.Part.Sci.* **55** (2005) 229–270, [hep-ph/0502182].

[68] P. H. Frampton, P. Hung, and M. Sher, *Quarks and leptons beyond the third generation*, *Phys.Rept.* **330** (2000) 263, [hep-ph/9903387].

[69] B. Holdom *et. al.*, *Four Statements about the Fourth Generation*, arXiv:0904.4698.

[70] J. C. Pati and A. Salam, *Lepton Number as the Fourth Color*, *Phys. Rev.* **D10** (1974) 275–289.

[71] R. N. Mohapatra and J. C. Pati, *Left-Right Gauge Symmetry and an Isoconjugate Model of CP Violation*, *Phys. Rev.* **D11** (1975) 566–571.

[72] R. N. Mohapatra and J. C. Pati, *A Natural Left-Right Symmetry*, *Phys. Rev.* **D11** (1975) 2558.

[73] G. Senjanovic and R. N. Mohapatra, *Exact Left-Right Symmetry and Spontaneous Violation of Parity*, *Phys. Rev.* **D12** (1975) 1502.

[74] G. Senjanovic, *Spontaneous Breakdown of Parity in a Class of Gauge Theories*, *Nucl. Phys.* **B153** (1979) 334.

[75] P. Q. Hung, *Minimal SU(5) resuscitated by long-lived quarks and leptons*, *Phys. Rev. Lett.* **80** (1998) 3000–3003, [hep-ph/9712338].

[76] W.-S. Hou, *CP Violation and Baryogenesis from New Heavy Quarks*, *Chin. J. Phys.* **47** (2009) 134, [arXiv:0803.1234].

[77] Y. Kikukawa, M. Kohda, and J. Yasuda, *The Strongly coupled fourth family and a first-order electroweak phase transition. I. Quark sector*, *Prog.Theor.Phys.* **122** (2009) 401–426, [arXiv:0901.1962].

[78] R. Fok and G. D. Kribs, *Four Generations, the Electroweak Phase Transition, and Supersymmetry*, *Phys. Rev.* **D78** (2008) 075023, [arXiv:0803.4207].

[79] W.-S. Hou, M. Nagashima, and A. Soddu, *Enhanced $K_L \to \pi^0 \nu\bar{\nu}$ from direct CP violation in $B \to K\pi$ with four generations*, *Phys. Rev.* **D72** (2005) 115007, [hep-ph/0508237].

[80] W.-S. Hou, M. Nagashima, and A. Soddu, *Large time-dependent CP violation in $B_s^0$ system and finite $D^0$ - $\bar{D}^0$ mass difference in four generation standard model*, *Phys. Rev.* **D76** (2007) 016004, [hep-ph/0610385].

[81] A. Soni, A. K. Alok, A. Giri, R. Mohanta, and S. Nandi, *The Fourth family: A Natural explanation for the observed pattern of anomalies in B–CP asymmetries*, arXiv:0807.1971.

[82] A. Soni, A. K. Alok, A. Giri, R. Mohanta, and S. Nandi, *SM with four generations: Selected implications for rare B and K decays*, *Phys.Rev.* **D82** (2010) 033009, [arXiv:1002.0595].

[83] A. J. Buras, B. Duling, T. Feldmann, T. Heidsieck, and C. Promberger, *Lepton Flavour Violation in the Presence of a Fourth Generation of Quarks and Leptons*, *JHEP* **1009** (2010) 104, [arXiv:1006.5356].

[84] H. Lacker and A. Menzel, *Simultaneous Extraction of the Fermi constant and PMNS matrix elements in the presence of a fourth generation*, *JHEP* **1007** (2010) 006, [arXiv:1003.4532].

[85] B. Holdom, *Heavy quarks and electroweak symmetry breaking*, *Phys. Rev. Lett.* **57** (1986) 2496.

[86] C. T. Hill, M. A. Luty, and E. A. Paschos, *Electroweak symmetry breaking by fourth generation condensates and the neutrino spectrum*, *Phys.Rev.* **D43** (1991) 3011–3025.

[87] S. F. King, *Is electroweak symmetry broken by a fourth family of quarks?* , *Phys. Lett.* **B234** (1990) 108–112.

[88] G. Burdman and L. Da Rold, *Electroweak Symmetry Breaking from a Holographic Fourth Generation*, *JHEP* **12** (2007) 086, [arXiv:0710.0623].

[89] P. Hung and C. Xiong, *Renormalization Group Fixed Point with a Fourth Generation: Higgs-induced Bound States and Condensates*, *Nucl.Phys.* **B847** (2011) 160–178, [arXiv:0911.3890].

[90] P. Q. Hung and C. Xiong, *Renormalization Group Fixed Point with a Fourth Generation: Solution to the hierarchy problem*, arXiv:0911.3892.

[91] B. Holdom, *Approaching a strong fourth family*, *Phys. Lett.* **B686** (2010) 146–151, [arXiv:1001.5321].

[92] C. M. Ho, P. Q. Hung, and T. W. Kephart, *Conformal Completion of the Standard Model with a Fourth Generation*, arXiv:1102.3997. 6 pages.

[93] K. Ishiwata and M. B. Wise, *Fourth Generation Bound States*, *Phys.Rev.* **D83** (2011) 074015, [arXiv:1103.0611].

[94] J. Alwall *et. al.*, *Is $V_{tb} \simeq 1$?*, *Eur. Phys. J.* **C49** (2007) 791–801, [hep-ph/0607115].

[95] G. D. Kribs, T. Plehn, M. Spannowsky, and T. M. P. Tait, *Four generations and Higgs physics*, *Phys. Rev.* **D76** (2007) 075016, [arXiv:0706.3718].

[96] M. S. Chanowitz, *Bounding CKM Mixing with a Fourth Family*, *Phys. Rev.* **D79** (2009) 113008, [arXiv:0904.3570].

[97] V. A. Novikov, A. N. Rozanov, and M. I. Vysotsky, *Once more on extra quark-lepton generations and precision measurements*, arXiv:0904.4570.

[98] O. Eberhardt, A. Lenz, and J. Rohrwild, *Less space for a new family of fermions*, arXiv:1005.3505.

[99] O. Eberhardt, G. Herbert, H. Lacker, A. Lenz, A. Menzel, *et. al.*, *Joint analysis of Higgs decays and electroweak precision observables in the Standard Model with a sequential fourth generation*, arXiv:1204.3872.

[100] A. Arhrib and W.-S. Hou, *Effect of fourth generation CP phase on $b \to s$ transitions*, *Eur.Phys.J.* **C27** (2003) 555–561, [hep-ph/0211267].

[101] J. A. Herrera, R. H. Benavides, and W. A. Ponce, *Flavor changing neutral currents with a fourth family of quarks*, *Phys. Rev.* **D78** (2008) 073008, [arXiv:0810.3871].

[102] M. Bobrowski, A. Lenz, J. Riedl, and J. Rohrwild, *How much space is left for a new family of fermions?*, *Phys. Rev.* **D79** (2009) 113006, [arXiv:0902.4883].

[103] G. Eilam, B. Melic, and J. Trampetic, *CP violation and the 4th generation*, *Phys. Rev.* **D80** (2009) 116003, [arXiv:0909.3227].

[104] A. J. Buras, B. Duling, T. Feldmann, T. Heidsieck, C. Promberger, *et. al.*, *The Impact of a 4th Generation on Mixing and CP Violation in the Charm System*, *JHEP* **1007** (2010) 094, [arXiv:1004.4565].

[105] A. J. Buras, B. Duling, T. Feldmann, T. Heidsieck, C. Promberger, *et. al.*, *Patterns of Flavour Violation in the Presence of a Fourth Generation of Quarks and Leptons*, *JHEP* **1009** (2010) 106, [arXiv:1002.2126].

[106] W.-S. Hou, M. Kohda, and F. Xu, *Hints for a Low $B_s \to \mu^+\mu^-$ Rate and the Fourth Generation*, arXiv:1203.6896.

[107] D. Choudhury and D. K. Ghosh, *A Fourth generation, anomalous like-sign dimuon charge asymmetry and the LHC*, *JHEP* **1102** (2011) 033, [arXiv:1006.2171].

[108] P. Gerhold, K. Jansen, and J. Kallarackal, *Effects of a potential fourth fermion generation on the Higgs boson mass bounds*, arXiv:1010.6169.

[109] K. Ishiwata and M. B. Wise, *Higgs Properties and Fourth Generation Leptons*, *Phys.Rev.* **D84** (2011) 055025, [arXiv:1107.1490]. 8 pages, 8 figures, published version.

[110] M. Buchkremer, J.-M. Gerard, and F. Maltoni, *Closing in on a perturbative fourth generation*, arXiv:1204.5403.

[111] A. Djouadi and A. Lenz, *Sealing the fate of a fourth generation of fermions*, arXiv:1204.1252. 8 pages, 3 figures.

[112] A. Denner, S. Dittmaier, A. Muck, G. Passarino, M. Spira, *et. al.*, *Higgs production and decay with a fourth Standard-Model-like fermion generation*, arXiv:1111.6395.

[113] R. N. Mohapatra, F. E. Paige, and D. P. Sidhu, *Symmetry Breaking and Naturalness of Parity Conservation in Weak Neutral Currents in Left-Right Symmetric Gauge Theories*, *Phys. Rev.* **D17** (1978) 2462.

[114] D. Chang, *A Minimal Model of Spontaneous CP Violation with the Gauge Group $SU(2)_L \times SU(2)_R \times U(1)_{B-L}$*, *Nucl. Phys.* **B214** (1983) 435.

[115] G. Branco, J. Frere, and J. Gerard, *The value of $\varepsilon'/\varepsilon$ in models based on $\mathrm{SU(2)_L \times SU(2)_R \times U(1)}$*, *Nucl.Phys.* **B221** (1983) 317.

[116] H. Harari and M. Leurer, *Left-Right Symmetry and the Mass Scale of a Possible Right-Handed Weak Boson*, *Nucl. Phys.* **B233** (1984) 221.

[117] G. Beall, M. Bander, and A. Soni, *Constraint on the Mass Scale of a Left-Right Symmetric Electroweak Theory from the $K_L - K_S$ Mass Difference*, *Phys. Rev. Lett.* **48** (1982) 848.

[118] G. Ecker and W. Grimus, *$\epsilon$, $\epsilon'$ in a model with spontaneous $P$ and $CP$ violation*, *Phys. Lett.* **B153** (1985) 279–285.

[119] J. M. Frere *et. al.*, *$K^0 - \bar{K}^0$ in the $SU(2)_L \times SU(2)_R \times U(1)$ model of CP violation*, *Phys. Rev.* **D46** (1992) 337–353.

[120] G. Barenboim, J. Bernabeu, and M. Raidal, *Spontaneous CP-violation in the left-right model and the kaon system*, *Nucl. Phys.* **B478** (1996) 527–543, [hep-ph/9608450].

[121] P. Langacker and S. Uma Sankar, *Bounds on the Mass of $W_R$ and the $W_L - W_R$ Mixing Angle $\xi$ in General $SU(2)_L \times SU(2)_R \times U(1)$ Models*, *Phys. Rev.* **D40** (1989) 1569–1585.

[122] G. Barenboim, J. Bernabeu, J. Prades, and M. Raidal, *Constraints on the $W_R$ mass and CP violation in left-right models*, *Phys. Rev.* **D55** (1997) 4213–4221, [hep-ph/9611347].

[123] K. Kiers, J. Kolb, J. Lee, A. Soni, and G.-H. Wu, *Ubiquitous CP violation in a top inspired left-right model*, *Phys. Rev.* **D66** (2002) 095002, [hep-ph/0205082].

[124] P. Ball, J. M. Frere, and J. Matias, *Anatomy of Mixing-Induced CP Asymmetries in Left-Right-Symmetric Models with Spontaneous CP Violation*, *Nucl. Phys.* **B572** (2000) 3–35, [hep-ph/9910211].

[125] A. Crivellin, *Effects of right-handed charged currents on the determinations of $|V_{ub}|$ and $|V_{cb}|$*, *Phys. Rev.* **D81** (2010) 031301, [arXiv:0907.2461].

[126] C.-H. Chen and S.-h. Nam, *Left-right mixing on leptonic and semileptonic $b \to u$ decays*, *Phys.Lett.* **B666** (2008) 462–466, [arXiv:0807.0896].

[127] R. Feger, T. Mannel, V. Klose, H. Lacker, and T. Luck, *Limit on a Right-Handed Admixture to the Weak $b \to c$ Current from Semileptonic Decays*, *Phys.Rev.* **D82** (2010) 073002, [arXiv:1003.4022].

[128] A. J. Buras, K. Gemmler, and G. Isidori, *Quark flavour mixing with right-handed currents: an effective theory approach*, *Nucl.Phys.* **B843** (2011) 107–142, [arXiv:1007.1993].

[129] N. Deshpande, J. Gunion, B. Kayser, and F. I. Olness, *Left-right symmetric electroweak models with triplet Higgs*, *Phys.Rev.* **D44** (1991) 837–858.

[130] R. N. Mohapatra and G. Senjanovic, *Neutrino mass and spontaneous parity nonconservation*, *Phys. Rev. Lett.* **44** (1980) 912.

[131] R. N. Mohapatra and G. Senjanovic, *Neutrino Masses and Mixings in Gauge Models with Spontaneous Parity Violation*, *Phys. Rev.* **D23** (1981) 165.

[132] O. Khasanov and G. Perez, *On neutrino masses and a low breaking scale of left-right symmetry*, *Phys. Rev.* **D65** (2002) 053007, [hep-ph/0108176].

[133] M.-C. Chen and J. Huang, *TeV Scale Models of Neutrino Masses and Their Phenomenology*, arXiv:1105.3188.

[134] **UTfit** Collaboration, M. Bona *et. al.*, *The UTfit collaboration report on the status of the unitarity triangle beyond the standard model. I. Model-independent analysis and minimal flavor violation*, *JHEP* **0603** (2006) 080, [hep-ph/0509219].

[135] M. Blanke, A. J. Buras, B. Duling, S. Gori, and A. Weiler, *$\Delta F = 2$ Observables and Fine-Tuning in a Warped Extra Dimension with Custodial Protection*, *JHEP* **03** (2009) 001, [arXiv:0809.1073].

[136] C. Csaki, A. Falkowski, and A. Weiler, *The Flavor of the Composite Pseudo-Goldstone Higgs*, *JHEP* **0809** (2008) 008, [arXiv:0804.1954].

[137] Y. Zhang, H. An, X. Ji, and R. N. Mohapatra, *Right-handed quark mixings in minimal left-right symmetric model with general CP violation*, *Phys. Rev.* **D76** (2007) 091301, [arXiv:0704.1662].

[138] Y. Zhang, H. An, X. Ji, and R. N. Mohapatra, *General CP Violation in Minimal Left-Right Symmetric Model and Constraints on the Right-Handed Scale*, *Nucl. Phys.* **B802** (2008) 247–279, [arXiv:0712.4218].

[139] A. Maiezza, M. Nemevsek, F. Nesti, and G. Senjanovic, *Left-Right Symmetry at LHC*, *Phys. Rev.* **D82** (2010) 055022, [arXiv:1005.5160].

[140] K. Hsieh, K. Schmitz, J.-H. Yu, and C. P. Yuan, *Global Analysis of General $SU(2) \times SU(2) \times U(1)$ Models with Precision Data*, *Phys. Rev.* **D82** (2010) 035011, [arXiv:1003.3482].

[141] A. Crivellin and L. Mercolli, *$B \to X_d\gamma$ and constraints on new physics*, *Phys.Rev.* **D84** (2011) 114005, [arXiv:1106.5499].

[142] M. E. Peskin and D. V. Schroeder, *An Introduction To Quantum Field Theory (Frontiers in Physics)*. Westview Press, 1995.

[143] X.-G. He and G. Valencia, *An extended scalar sector to address the tension between a fourth generation and Higgs searches at the LHC*, *Phys.Lett.* **B707** (2012) 381–384, [arXiv:1108.0222].

[144] S. Bar-Shalom, S. Nandi, and A. Soni, *Muon g-2 and lepton flavor violation in a two Higgs doublets model for the fourth generation*, *Phys.Lett.* **B709** (2012) 207–217, [arXiv:1112.3661].

[145] S. Bar-Shalom, S. Nandi, and A. Soni, *Two Higgs doublets with 4th generation fermions - models for TeV-scale compositeness*, *Phys.Rev.* **D84** (2011) 053009, [arXiv:1105.6095].

[146] A. A. Anselm, J. L. Chkareuli, N. G. Uraltsev, and T. A. Zhukovskaya, *On the Kobayashi-Maskawa model with four generations*, *Phys. Lett.* **B156** (1985) 102–108.

[147] H. Fritzsch and J. Plankl, *The Mixing of Quark Flavors*, *Phys.Rev.* **D35** (1987) 1732.

[148] H. Harari and M. Leurer, *Recommending a Standard Choice of Cabibbo Angles and KM Phases for Any Number of Generations*, *Phys.Lett.* **B181** (1986) 123.

[149] L.-L. Chau and W.-Y. Keung, *Comments on the Parametrization of the Kobayashi-Maskawa Matrix*, *Phys.Rev.Lett.* **53** (1984) 1802.

[150] W.-S. Hou, A. Soni, and H. Steger, *Effects of a fourth generation on $b \to s\gamma$ and a useful parametrization of quark mixing for rare B decays*, *Phys.Lett.* **B192** (1987) 441.

[151] P. Langacker, *Bounds on mixing between light and heavy gauge bosons*, *Phys. Rev.* **D30** (1984) 2008.

[152] M. Blanke *et. al.*, *Particle antiparticle mixing, $\epsilon_K$, $\Delta(\Gamma(q))$, $A_{\rm SL}(q)$, $A_{\rm CP}(B_d \to \psi K_S)$, $A_{\rm CP}(B_s \to \psi\phi)$ and $B \to X_{s,d}\gamma$ in the littlest Higgs model with T-parity*, *JHEP* **12** (2006) 003, [hep-ph/0605214].

[153] M. Blanke, A. J. Buras, S. Recksiegel, and C. Tarantino, *The Littlest Higgs Model with T-Parity Facing CP-Violation in $B_s - \bar{B}_s$ Mixing*, arXiv:0805.4393.

[154] M. Blanke, A. J. Buras, B. Duling, S. Recksiegel, and C. Tarantino, *FCNC Processes in the Littlest Higgs Model with T-Parity: a 2009 Look*, *Acta Phys. Polon. B* **41** (2010) 657, [arXiv:0906.5454].

[155] A. J. Buras, M. V. Carlucci, S. Gori, and G. Isidori, *Higgs-mediated FCNCs: Natural Flavour Conservation vs. Minimal Flavour Violation*, *JHEP* **10** (2010) 009, [arXiv:1005.5310].

[156] W. Altmannshofer, A. J. Buras, S. Gori, P. Paradisi, and D. M. Straub, *Anatomy and Phenomenology of FCNC and CPV Effects in SUSY Theories*, *Nucl.Phys.* **B830** (2010) 17–94, [arXiv:0909.1333].

[157] A. J. Buras, M. Misiak, and J. Urban, *Two-loop QCD anomalous dimensions of flavour-changing four-quark operators within and beyond the standard model*, *Nucl. Phys.* **B586** (2000) 397–426, [hep-ph/0005183].

[158] A. J. Buras, S. Jager, and J. Urban, *Master formulae for $\Delta F = 2$ NLO-QCD factors in the standard model and beyond*, *Nucl. Phys.* **B605** (2001) 600–624, [hep-ph/0102316].

[159] M. Gorbahn, S. Jager, U. Nierste, and S. Trine, *The supersymmetric Higgs sector and $B - \bar{B}$ mixing for large tan $\beta$*, *Phys.Rev.* **D84** (2011) 034030, [arXiv:0901.2065].

[160] M. Ciuchini, E. Franco, V. Lubicz, G. Martinelli, I. Scimemi, *et. al.*, *Next-to-leading order QCD corrections to $\Delta F = 2$ effective Hamiltonians*, *Nucl.Phys.* **B523** (1998) 501–525, [hep-ph/9711402].

[161] R. Babich *et. al.*, *$K^0 - \bar{K}^0$ mixing beyond the standard model and CP- violating electroweak penguins in quenched QCD with exact chiral symmetry*, *Phys. Rev.* **D74** (2006) 073009, [hep-lat/0605016].

[162] D. Becirevic, V. Gimenez, G. Martinelli, M. Papinutto, and J. Reyes, *B-parameters of the complete set of matrix elements of $\Delta B = 2$ operators from the lattice*, *JHEP* **04** (2002) 025, [hep-lat/0110091].

[163] S. Durr, Z. Fodor, C. Hoelbling, S. Katz, S. Krieg, *et. al.*, *Precision computation of the kaon bag parameter*, *Phys.Lett.* **B705** (2011) 477–481, [arXiv:1106.3230].

[164] **HPQCD Collaboration, UKQCD Collaboration** Collaboration, E. Gamiz *et. al.*, *Unquenched determination of the kaon parameter $B_K$ from improved staggered fermions*, *Phys.Rev.* **D73** (2006) 114502, [hep-lat/0603023].

[165] J. Laiho and R. S. Van de Water, *Pseudoscalar decay constants, light-quark masses, and $B_K$ from mixed-action lattice QCD*, arXiv:1112.4861.

[166] C. Kelly, *Continuum Results for Light Hadronic Quantities using Domain Wall Fermions with the Iwasaki and DSDR Gauge Actions*, arXiv:1201.0706. 7 pages, 3 figures. Contribution to The XXIX International Symposium on Lattice Field Theory, July 10-16, 2011.

[167] T. Bae, Y.-C. Jang, C. Jung, H.-J. Kim, J. Kim, *et. al.*, *Kaon B-parameter from improved staggered fermions in $N_f = 2 + 1$ QCD*, arXiv:1111.5698.

[168] C. Bouchard, E. Freeland, C. Bernard, A. El-Khadra, E. Gamiz, *et. al.*, *Neutral B mixing from $2 + 1$ flavor lattice-QCD: the Standard Model and beyond*, arXiv:1112.5642. 13 pages, 6 figures. Proceedings of the XXIX International Symposium on Lattice Field Theory - Lattice 2011, July 10-16, 2011, Squaw Valley, Lake Tahoe, California. Ver 2: New Figs. 2-4 and Table 4 corrects scripting error. Table 4 now includes results for BJU as well as BBGLN choice of evanescent operators.

[169] **HPQCD Collaboration** Collaboration, E. Gamiz, C. T. Davies, G. P. Lepage, J. Shigemitsu, and M. Wingate, *Neutral B Meson Mixing in Unquenched Lattice QCD*, *Phys.Rev.* **D80** (2009) 014503, [arXiv:0902.1815]. 11 pages, 8 postscript figures.

[170] J. Laiho, E. Lunghi, and R. S. Van de Water, *Lattice QCD inputs to the CKM unitarity triangle analysis*, *Phys. Rev.* **D81** (2010) 034503, [arXiv:0910.2928]. Updates available on http://latticeaverages.org/.

[171] J. Brod and M. Gorbahn, *$\varepsilon_K$ at Next-to-Next-to-Leading Order: The Charm-Top-Quark Contribution*, *Phys. Rev.* **D82** (2010) 094026, [arXiv:1007.0684].

[172] S. Herrlich and U. Nierste, *The Complete $|\Delta S| = 2$ Hamiltonian in the Next-To-Leading Order*, *Nucl. Phys.* **B476** (1996) 27–88, [hep-ph/9604330].

[173] A. J. Buras, M. Jamin, and P. H. Weisz, *Leading and next-to-leading QCD corrections to $\varepsilon$ parameter and $B^0 - \bar{B}^0$ mixing in the presence of a heavy top quark*, *Nucl. Phys.* **B347** (1990) 491–536.

[174] J. Urban, F. Krauss, U. Jentschura, and G. Soff, *Next-to-leading order QCD corrections for the $B^0 - \bar{B}^0$ mixing with an extended Higgs sector*, *Nucl. Phys.* **B523** (1998) 40–58, [hep-ph/9710245].

[175] A. J. Buras, *Weak Hamiltonian, CP violation and rare decays*, hep-ph/9806471.

[176] J. Bijnens, J. M. Gérard, and G. Klein, *The $K_L - K_S$ mass difference*, *Phys. Lett.* **B257** (1991) 191–195.

[177] A. J. Buras, D. Guadagnoli, and G. Isidori, *On $\varepsilon_K$ beyond lowest order in the Operator Product Expansion*, *Phys. Lett.* **B688** (2010) 309–313, [arXiv:1002.3612].

[178] E. Goode and M. Lightman, *$\Delta I = 3/2$ $K \to \pi\pi$ decays with nearly physical kinematics*, arXiv:1111.4889.

[179] A. J. Buras and D. Guadagnoli, *On the consistency between the observed amount of CP violation in the $K$ and $B_d$ systems within minimal flavor violation*, *Phys.Rev.* **D79** (2009) 053010, [arXiv:0901.2056].

[180] A. J. Buras, R. Fleischer, S. Recksiegel, and F. Schwab, *Anatomy of prominent B and K decays and signatures of CP violating new physics in the electroweak penguin sector*, *Nucl.Phys.* **B697** (2004) 133–206, [hep-ph/0402112].

[181] Z. Ligeti, M. Papucci, and G. Perez, *Implications of the measurement of the $B_s^0 - \bar{B}_s^0$ mass difference*, *Phys. Rev. Lett* **97** (2006) 101801, [hep-ph/0604112].

[182] M. Beneke, G. Buchalla, C. Greub, A. Lenz, and U. Nierste, *Next-to-leading order QCD corrections to the lifetime difference of $B_s$ mesons*, *Phys.Lett.* **B459** (1999) 631–640, [hep-ph/9808385].

[183] M. Ciuchini, E. Franco, V. Lubicz, and F. Mescia, *Next-to-leading order QCD corrections to spectator effects in lifetimes of beauty hadrons*, *Nucl.Phys.* **B625** (2002) 211–238, [hep-ph/0110375].

[184] M. Beneke, G. Buchalla, C. Greub, A. Lenz, and U. Nierste, *The $B^+ - B_d^0$ lifetime difference beyond leading logarithms*, *Nucl.Phys.* **B639** (2002) 389–407, [hep-ph/0202106].

[185] M. Beneke, G. Buchalla, A. Lenz, and U. Nierste, *CP asymmetry in flavor specific B decays beyond leading logarithms*, *Phys.Lett.* **B576** (2003) 173–183, [hep-ph/0307344].

[186] A. Lenz and U. Nierste, *Theoretical update of $B_s - \bar{B}_s$ mixing*, *JHEP* **0706** (2007) 072, [hep-ph/0612167].

[187] **For the CDF** Collaboration, G. Giurgiu, *New Measurement of the $B_s$ Mixing Phase at CDF*, *PoS* **ICHEP2010** (2010) 236, [arXiv:1012.0962].

[188] **D0** Collaboration, V. M. Abazov *et. al.*, *Measurement of the CP-violating phase $\phi_s^{J/\psi\phi}$ using the flavor-tagged decay $B_s^0 \to J/\psi\phi$ in 8 $fb^{-1}$ of $p\bar{p}$ collisions*, arXiv:1109.3166.

[189] **CKMfitter** Collaboration, J. Charles *et. al.*, *CP violation and the CKM matrix: Assessing the impact of the asymmetric B factories*, *Eur. Phys. J.* **C41** (2005) 1–131, [hep-ph/0406184]. Updates available on http://ckmfitter.in2p3.fr/.

[190] **LHCb Collaboration** Collaboration, R. Aaij *et. al.*, *Determination of the sign of the decay width difference in the $B_s$ system*, arXiv:1202.4717. Long author list - awaiting processing.

[191] W.-S. Hou and A. Soni, *Gauge invariance of the $K_L - \bar{K}_S$ mass difference in left-right symmetric model*, *Phys. Rev.* **D32** (1985) 163.

[192] D. Chang, J. Basecq, L.-F. Li, and P. B. Pal, *Comment on the $K_L - K_S$ mass difference in left-right model*, *Phys. Rev.* **D30** (1984) 1601.

[193] J. Basecq, L.-F. Li, and P. B. Pal, *Gauge invariant calculation of the $K_L - K_S$ mass difference in the left-right model*, *Phys. Rev.* **D32** (1985) 175.

[194] S. L. Glashow, J. Iliopoulos, and L. Maiani, *Weak Interactions with Lepton-Hadron Symmetry*, *Phys. Rev.* **D2** (1970) 1285–1292.

[195] M. Misiak, H. Asatrian, K. Bieri, M. Czakon, A. Czarnecki, *et. al.*, *Estimate of* $\mathrm{Br}(\bar{B} \to X_s\gamma)$ *at* $\mathcal{O}(\alpha_s^2)$, *Phys.Rev.Lett.* **98** (2007) 022002, [hep-ph/0609232].

[196] P. Gambino and M. Misiak, *Quark mass effects in* $\bar{B} \to X_s\gamma$, *Nucl.Phys.* **B611** (2001) 338–366, [hep-ph/0104034].

[197] M. Misiak and M. Steinhauser, *NNLO QCD corrections to the* $\bar{B} \to X_s\gamma$ *gamma matrix elements using interpolation in* $m_c$, *Nucl.Phys.* **B764** (2007) 62–82, [hep-ph/0609241].

[198] T. G. Rizzo, $b \to s\gamma$ *in the two Higgs Doublet Model*, *Phys.Rev.* **D38** (1988) 820. Revised version.

[199] A. Buras, M. Misiak, M. Munz, and S. Pokorski, *Theoretical uncertainties and phenomenological aspects of* $B \to X_s\gamma$ *decay*, *Nucl.Phys.* **B424** (1994) 374–398, [hep-ph/9311345].

[200] M. S. Carena, D. Garcia, U. Nierste, and C. E. Wagner, $b \to s\gamma$ *and supersymmetry with large* $\tan\beta$, *Phys.Lett.* **B499** (2001) 141–146, [hep-ph/0010003].

[201] A. J. Buras, P. H. Chankowski, J. Rosiek, and L. Slawianowska, $\Delta M_{d,s}, B^0_{d,s} \to \mu^+\mu^-$ *and* $B \to X_s\gamma$ *in supersymmetry at large* $\tan\beta$, *Nucl.Phys.* **B659** (2003) 3, [hep-ph/0210145].

[202] A. J. Buras, A. Poschenrieder, M. Spranger, and A. Weiler, *The Impact of universal extra dimensions on* $B \to X_s\gamma$, $B \to X_s g$, $B \to X_s\mu^+\mu^-$, $K_L \to \pi^0 e^+ e^-$ *and* $\varepsilon'/\varepsilon$, *Nucl.Phys.* **B678** (2004) 455–490, [hep-ph/0306158].

[203] G. Buchalla, A. J. Buras, and M. E. Lautenbacher, *Weak Decays Beyond Leading Logarithms*, *Rev. Mod. Phys.* **68** (1996) 1125–1144, [hep-ph/9512380].

[204] A. J. Buras, L. Merlo, and E. Stamou, *The Impact of Flavour Changing Neutral Gauge Bosons on* $\bar{B} \to X_s\gamma$, *JHEP* **1108** (2011) 124, [arXiv:1105.5146].

[205] L. Wolfenstein, *Parametrization of the Kobayashi-Maskawa Matrix*, *Phys. Rev. Lett.* **51** (1983) 1945.

[206] J. L. Hewett, *Radiative B decays with four generations*, *Phys.Lett.* **B193** (1987) 327.

[207] T. Aliev, D. A. Demir, and N. Pak, *Constraining four generation SM with* $b \to s\gamma$ *and* $b \to s\ g$ *decays*, *Phys.Lett.* **B389** (1996) 83–88, [hep-ph/9809354].

[208] N. Deshpande and J. Trampetic, *Effect of fourth generation on* $B \to K^*\gamma$, *Phys.Rev.* **D40** (1989) 3773–3774.

[209] C.-S. Huang, W.-J. Huo, and Y.-L. Wu, *The* $B \to X_s\ell^+\ell^-$ *and* $B \to X_s\gamma$ *decays with the fourth generation*, *Mod.Phys.Lett.* **A14** (1999) 2453–2462, [hep-ph/9911203].

[210] L. Solmaz, *Constraining fourth generation with* $B \to X_s\gamma$, hep-ph/0204016.

[211] T. Aliev, A. Ozpineci, and M. Savci, *Fourth generation effects in processes induced by* $b \to s$ *transition*, *Eur.Phys.J.* **C29** (2003) 265–270, [hep-ph/0301078]. 18 pages, 8 figures, LaTeX formatted Report-no: metu-phys-hep-03-03.

[212] G. Asatrian and A. Ionnisian, *Rare B meson decays in the $SU(2)_L \times SU(2)_R \times U(1)$ model*, *Mod.Phys.Lett.* **A5** (1990) 1089–1096.

[213] G. Asatryan and A. Ioannisyan, *The $b \to s\gamma$ decay in the $SU(2)_L \times SU(2)_R \times U(1)$ model. (In Russian)*, *Sov.J.Nucl.Phys.* **51** (1990) 858–860.

[214] D. Cocolicchio, G. Costa, G. L. Fogli, J. Kim, and A. Masiero, *Rare B decays in left-right symmetric models*, *Phys.Rev.* **D40** (1989) 1477.

[215] P. L. Cho and M. Misiak, *$b \to s\gamma$ decay in $SU(2)_L \times SU(2)_R \times U(1)$ extensions of the Standard Model*, *Phys.Rev.* **D49** (1994) 5894–5903, [hep-ph/9310332].

[216] K. Babu, K. Fujikawa, and A. Yamada, *Constraints on left-right symmetric models from the process $b \to s\gamma$*, *Phys.Lett.* **B333** (1994) 196–201, [hep-ph/9312315].

[217] K. Fujikawa and A. Yamada, *Test of the chiral structure of the top - bottom charged current by the process $b \to s\gamma$*, *Phys.Rev.* **D49** (1994) 5890–5893.

[218] G. Bhattacharyya and A. Raychaudhuri, *Constraining the charged Higgs mass in the left-right symmetric model from $b \to s\gamma$*, *Phys.Lett.* **B357** (1995) 119–124, [hep-ph/9505356].

[219] G. Asatrian and A. Ioannisian, *CP violation in the decay $b \to s\gamma$ in the left-right symmetric model*, *Phys.Rev.* **D54** (1996) 5642–5646, [hep-ph/9603318].

[220] C. Kim and Y. G. Kim, *$b \to s\gamma$ decays in the left-right symmetric model*, *Phys.Rev.* **D61** (2000) 054008, [hep-ph/9905529].

[221] M. Frank, A. Hayreter, and I. Turan, *B Decays in an Asymmetric Left-Right Model*, *Phys.Rev.* **D82** (2010) 033012, [arXiv:1005.3074].

[222] C. Bobeth, M. Misiak, and J. Urban, *Matching conditions for $b \to s\gamma$ $b \to sg$ in extensions of the standard model*, *Nucl.Phys.* **B567** (2000) 153–185, [hep-ph/9904413].

[223] D. Guadagnoli, R. N. Mohapatra, and I. Sung, *Gauged Flavor Group with Left-Right Symmetry*, *JHEP* **1104** (2011) 093, [arXiv:1103.4170].

[224] M. Benzke, S. J. Lee, M. Neubert, and G. Paz, *Factorization at Subleading Power and Irreducible Uncertainties in $\bar{B} \to X_s\gamma$ Decay*, *JHEP* **1008** (2010) 099, [arXiv:1003.5012].

[225] T. Hurth, E. Lunghi, and W. Porod, *Untagged $\bar{B} \to X_{s,d}\gamma$ CP asymmetry as a probe for new physics*, *Nucl.Phys.* **B704** (2005) 56–74, [hep-ph/0312260].

[226] J. M. Soares, *CP violation in radiative b decays*, *Nucl.Phys.* **B367** (1991) 575–590.

[227] A. L. Kagan and M. Neubert, *Direct CP violation in $B \to X_s\gamma$ decays as a signature of new physics*, *Phys.Rev.* **D58** (1998) 094012, [hep-ph/9803368].

[228] A. L. Kagan and M. Neubert, *QCD anatomy of $B \to X_s\gamma$ decays*, *Eur.Phys.J.* **C7** (1999) 5–27, [hep-ph/9805303].

[229] M. Benzke, S. J. Lee, M. Neubert, and G. Paz, *Long-Distance Dominance of the CP Asymmetry in $B \to X_{s,d}\gamma$ Decays*, *Phys.Rev.Lett.* **106** (2011) 141801, [arXiv:1012.3167].

[230] Z.-Z. Xing and D.-S. Du, *Constraints on the fourth generation effect on CP violation in penguin dominated $b \to s\gamma$ decays*, *Chin.Phys.Lett.* **9** (1992) 9–12.

[231] M. Misiak, *The $b \to se^+e^-$ and $b \to s\gamma$ decays with next-to-leading logarithmic QCD corrections*, *Nucl.Phys.* **B393** (1993) 23–45.

[232] A. J. Buras and M. Munz, *Effective Hamiltonian for $B \to X_s e^+e^-$ beyond leading logarithms in the NDR and HV schemes*, *Phys.Rev.* **D52** (1995) 186–195, [hep-ph/9501281].

[233] **BABAR** Collaboration, B. Aubert *et. al.*, *Measurement of the $B \to X_s\ell^+\ell^-$ branching fraction with a sum over exclusive modes*, *Phys. Rev. Lett.* **93** (2004) 081802, [hep-ex/0404006].

[234] **Belle** Collaboration, M. Iwasaki *et. al.*, *Improved measurement of the electroweak penguin process $B \to X_s\ell^+\ell^-$*, *Phys. Rev.* **D72** (2005) 092005, [hep-ex/0503044].

[235] H. Asatryan, H. Asatrian, C. Greub, and M. Walker, *Calculation of two loop virtual corrections to $b \to s\ell^+\ell^-$ in the standard model*, *Phys.Rev.* **D65** (2002) 074004, [hep-ph/0109140].

[236] H. Asatrian, H. Asatrian, C. Greub, and M. Walker, *Two loop virtual corrections to $B \to X_s\ell^+\ell^-$ in the standard model*, *Phys.Lett.* **B507** (2001) 162–172, [hep-ph/0103087].

[237] H. Asatryan, H. Asatrian, C. Greub, and M. Walker, *Complete gluon bremsstrahlung corrections to the process $b \to s\ell^+\ell^-$*, *Phys.Rev.* **D66** (2002) 034009, [hep-ph/0204341].

[238] A. Ghinculov, T. Hurth, G. Isidori, and Y. Yao, *NNLL QCD corrections to the decay $B \to X_s\ell^+\ell^-$*, *Nucl.Phys.Proc.Suppl.* **116** (2003) 284–288, [hep-ph/0211197].

[239] A. Ghinculov, T. Hurth, G. Isidori, and Y. Yao, *The Rare decay $B \to X_s\ell^+\ell^-$ to NNLL precision for arbitrary dilepton invariant mass*, *Nucl.Phys.* **B685** (2004) 351–392, [hep-ph/0312128].

[240] C. Bobeth, P. Gambino, M. Gorbahn, and U. Haisch, *Complete NNLO QCD analysis of $\bar{B} \to X_s\ell^+\ell^-$ and higher order electroweak effects*, *JHEP* **0404** (2004) 071, [hep-ph/0312090].

[241] G. Buchalla and G. Isidori, *Nonperturbative effects in $\bar{B} \to X_s\ell^+\ell^-$ for large dilepton invariant mass*, *Nucl.Phys.* **B525** (1998) 333–349, [hep-ph/9801456].

[242] G. Buchalla, G. Isidori, and S. Rey, *Corrections of order $\Lambda^2_{QCD}/m^2_c$ to inclusive rare B decays*, *Nucl.Phys.* **B511** (1998) 594–610, [hep-ph/9705253].

[243] A. Ali, G. Hiller, L. Handoko, and T. Morozumi, *Power corrections in the decay rate and distributions in $B \to X_s\ell^+\ell^-$ in the standard model*, *Phys.Rev.* **D55** (1997) 4105–4128, [hep-ph/9609449].

[244] A. F. Falk, M. E. Luke, and M. J. Savage, *Nonperturbative contributions to the inclusive rare decays $B \to X_s\gamma$ and $B \to X_s\ell^+\ell^-$*, *Phys.Rev.* **D49** (1994) 3367–3378, [hep-ph/9308288].

[245] A. Ghinculov, T. Hurth, G. Isidori, and Y. Yao, *Forward backward asymmetry in $B \to X_s\ell^+\ell^-$ at the NNLL level*, *Nucl.Phys.* **B648** (2003) 254–276, [hep-ph/0208088].

[246] Y. Dincer, *Fourth generation effects in the $B_s \to \nu\bar{\nu}\gamma$ decay*, *Phys.Lett.* **B505** (2001) 89–93, [hep-ph/0012135].

[247] L. Solmaz, *A Simple approach to fourth generation effects in $B \to X_s\ell^+\ell^-$ decay*, *Phys.Rev.* **D69** (2004) 015003, [hep-ph/0310132].

[248] A. K. Alok, A. Dighe, and S. Ray, *CP asymmetry in the decays $B \to X_{s,d}\mu^+\mu^-$ with four generations*, *Phys.Rev.* **D79** (2009) 034017, [arXiv:0811.1186].

[249] T. G. Rizzo, *Breakdown of global fits to the Wilson coefficients in rare B decays: A Left-right model example*, *Phys.Rev.* **D58** (1998) 114014, [hep-ph/9802401].

[250] T. Rizzo, *$b \to s\ell^+\ell^-$ in the left-right symmetric model*, hep-ph/9705209.

[251] P. Colangelo, F. De Fazio, P. Santorelli, and E. Scrimieri, *Rare $B \to K^*\nu\bar{\nu}$ decays at B factories*, *Phys. Lett.* **B395** (1997) 339–344, [hep-ph/9610297].

[252] M. Bartsch, M. Beylich, G. Buchalla, and D. N. Gao, *Precision Flavour Physics with $B \to K\nu\bar{\nu}$ and $B \to K\ell^+\ell^-$*, *JHEP* **11** (2009) 011, [arXiv:0909.1512].

[253] **UTfit** Collaboration, M. Bona *et. al.*, *An Improved Standard Model Prediction Of $Br(B \to \tau\nu)$ And Its Implications For New Physics*, *Phys. Lett.* **B687** (2010) 61–69, [arXiv:0908.3470].

[254] T. Aushev, W. Bartel, A. Bondar, J. Brodzicka, T. Browder, *et. al.*, *Physics at Super B Factory*, arXiv:1002.5012.

[255] M. Ciuchini and A. Stocchi, *Physics Opportunities at the Next Generation of Precision Flavor Physics*, *Ann. Rev. Nucl. Part. Sci.* **61** (2011) 491–517, [arXiv:1110.3920].

[256] G. Buchalla, G. Hiller, and G. Isidori, *Phenomenology of non-standard Z couplings in exclusive semileptonic $b \to s$ transitions*, *Phys. Rev.* **D63** (2001) 014015, [hep-ph/0006136].

[257] W. Altmannshofer, A. J. Buras, D. M. Straub, and M. Wick, *New strategies for New Physics search in $B \to K^*\nu\bar{\nu}$, $B \to K\nu\bar{\nu}$ and $B \to X_s\nu\bar{\nu}$ decays*, *JHEP* **04** (2009) 022, [arXiv:0902.0160].

[258] **LHCb collaboration** Collaboration, R. Aaij *et. al.*, *Strong constraints on the rare decays $B_s \to \mu^+\mu^-$ and $B^0 \to \mu^+\mu^-$*, arXiv:1203.4493.

[259] J. Shigemitsu *et. al.*, *Recent results on B mixing and decay constants from HPQCD*, arXiv:0910.4131.

[260] A. J. Buras, *Relations between $\Delta M_{s,d}$ and $B_{s,d} \to \mu\bar{\mu}$ in models with minimal flavour violation*, *Phys. Lett.* **B566** (2003) 115–119, [hep-ph/0303060].

[261] A. Buras, P. Gambino, M. Gorbahn, S. Jager, and L. Silvestrini, *Universal unitarity triangle and physics beyond the standard model*, *Phys.Lett.* **B500** (2001) 161–167, [hep-ph/0007085].

[262] G. Buchalla, G. Hiller, Y. Nir, and G. Raz, *The pattern of CP asymmetries in $b \to s$ transitions*, *JHEP* **09** (2005) 074, [hep-ph/0503151].

[263] Y. Grossman and M. P. Worah, *CP asymmetries in B decays with new physics in decay amplitudes*, *Phys. Lett.* **B395** (1997) 241–249, [hep-ph/9612269].

[264] M. Beneke, *Corrections to* $\sin(2\beta)$ *from CP asymmetries in* $B^0 \to (\pi^0, \rho^0, \eta^0, \eta', \omega, \phi)K_S$ *decays*, *Phys. Lett.* **B620** (2005) 143–150, [hep-ph/0505075].

[265] W.-S. Hou, H.-n. Li, S. Mishima, and M. Nagashima, *Fourth generation CP violation effect on $B \to K\pi$, $\phi K$ and $\rho K$ in NLO PQCD*, *Phys. Rev. Lett.* **98** (2007) 131801, [hep-ph/0611107].

[266] W.-S. Hou, M. Nagashima, G. Raz, and A. Soddu, *Four generation CP violation in $B \to \phi K^0, \pi^0 K^0, \eta' K^0$ and hadronic uncertainties*, *JHEP* **09** (2006) 012, [hep-ph/0603097].

[267] G. Isidori and R. Unterdorfer, *On the short distance constraints from $K_{L,S} \to \mu^+\mu^-$*, *JHEP* **0401** (2004) 009, [hep-ph/0311084].

[268] **E871 Collaboration** Collaboration, D. Ambrose *et. al.*, *Improved branching ratio measurement for the decay $K_L \to \mu^+\mu^-$* , *Phys.Rev.Lett.* **84** (2000) 1389–1392.

[269] M. Gorbahn and U. Haisch, *Charm quark contribution to $K_L \to \mu^+\mu^-$ at next-to-next-to-leading order*, *Phys. Rev. Lett.* **97** (2006) 122002, [hep-ph/0605203].

[270] **E949 Collaboration** Collaboration, A. Artamonov *et. al.*, *New measurement of the $K^+ \to \pi^+\nu\bar{\nu}$ branching ratio*, *Phys.Rev.Lett.* **101** (2008) 191802, [arXiv:0808.2459].

[271] **E391a Collaboration** Collaboration, J. Ahn *et. al.*, *Experimental study of the decay $K_L \to \pi^0\nu\bar{\nu}$*, *Phys.Rev.* **D81** (2010) 072004, [arXiv:0911.4789].

[272] C. NA62, *2011 na62 status report to the cern spsc*, Tech. Rep. CERN-SPSC-2011-015. SPSC-SR-083, CERN, Geneva, Mar, 2011.

[273] J. Brod and M. Gorbahn, *Electroweak Corrections to the Charm Quark Contribution to $K^+ \to \pi^+\nu\bar{\nu}$*, *Phys. Rev.* **D78** (2008) 034006, [arXiv:0805.4119].

[274] G. Isidori, F. Mescia, and C. Smith, *Light-quark loops in $K \to \pi\nu\bar{\nu}$*, *Nucl. Phys.* **B718** (2005) 319–338, [hep-ph/0503107].

[275] A. J. Buras, M. Gorbahn, U. Haisch, and U. Nierste, *Charm quark contribution to $K^+ \to \pi^+\nu\bar{\nu}$ at next-to-next-to-leading order*, *JHEP* **11** (2006) 002, [hep-ph/0603079].

[276] G. Buchalla and A. J. Buras, *The rare decays $K \to \pi$ neutrino anti-neutrino, $B \to X_s\nu\bar{\nu}$ and $B \to \ell^+\ell^-$: An Update*, *Nucl.Phys.* **B548** (1999) 309–327, [hep-ph/9901288]. 19 pages, no figures Report-no: CERN-TH/98-369, TUM-T31-337/98.

[277] K. G. Chetyrkin *et. al.*, *Charm and Bottom Quark Masses: an Update*, *Phys. Rev.* **D80** (2009) 074010, [arXiv:0907.2110].

[278] **HPQCD** Collaboration, I. Allison *et. al.*, *High-Precision Charm-Quark Mass from Current-Current Correlators in Lattice and Continuum QCD*, *Phys. Rev.* **D78** (2008) 054513, [arXiv:0805.2999].

[279] F. Mescia and C. Smith, *Improved estimates of rare K decay matrix-elements from $K_{l3}$ decays*, *Phys. Rev.* **D76** (2007) 034017, [arXiv:0705.2025].

[280] W. Marciano and Z. Parsa, *Rare kaon decays with 'missing energy'*, *Phys.Rev.* **D53** (1996) 1–5.

[281] Y. Grossman and Y. Nir, *$K_L \to \pi^0 \nu\bar{\nu}$ beyond the Standard Model*, *Phys. Lett.* **B398** (1997) 163–168, [hep-ph/9701313].

[282] **KTEV Collaboration** Collaboration, A. Alavi-Harati *et. al.*, *Search for the Decay $K_L \to \pi^0 \mu^+ \mu^-$*, *Phys.Rev.Lett.* **84** (2000) 5279–5282, [hep-ex/0001006].

[283] **KTeV Collaboration** Collaboration, A. Alavi-Harati *et. al.*, *Search for the rare decay $K_L \to \pi^0 e^+ e^-$-*, *Phys.Rev.Lett.* **93** (2004) 021805, [hep-ex/0309072].

[284] F. Mescia, C. Smith, and S. Trine, *$K_L \to \pi^0 e^+ e^-$ and $K_L \to \pi^0 \mu^+ \mu^-$: A binary star on the stage of flavor physics*, *JHEP* **08** (2006) 088, [hep-ph/0606081].

[285] G. Buchalla, G. D'Ambrosio, and G. Isidori, *Extracting short-distance physics from $K_{L,S} \to \pi^0 e^+ e^-$ decays*, *Nucl. Phys.* **B672** (2003) 387–408, [hep-ph/0308008].

[286] S. Friot, D. Greynat, and E. De Rafael, *Rare kaon decays revisited*, *Phys. Lett.* **B595** (2004) 301–308, [hep-ph/0404136].

[287] G. Isidori, C. Smith, and R. Unterdorfer, *The rare decay $K_L \to \pi^0 \mu^+ \mu^-$ within the SM*, *Eur. Phys. J.* **C36** (2004) 57–66, [hep-ph/0404127].

[288] A. J. Buras, M. E. Lautenbacher, and G. Ostermaier, *Waiting for the top quark mass, $K^+ \to \pi^+ \nu\bar{\nu}$, $B_s^0 - \bar{B}_s^0$ mixing and CP asymmetries in B decays*, *Phys. Rev.* **D50** (1994) 3433–3446, [hep-ph/9403384].

[289] A. J. Buras and J. M. Gérard, *$\varepsilon'/\varepsilon$ in the Standard Model*, *Phys. Lett.* **B203** (1988) 272.

[290] A. J. Buras, M. Jamin, and M. E. Lautenbacher, *The Anatomy of $\varepsilon'/\varepsilon$ beyond leading logarithms with improved hadronic matrix elements*, *Nucl.Phys.* **B408** (1993) 209–285, [hep-ph/9303284].

[291] A. J. Buras, M. Jamin, and M. E. Lautenbacher, *A 1996 analysis of the CP violating ratio $\varepsilon'/\varepsilon$*, *Phys.Lett.* **B389** (1996) 749–756, [hep-ph/9608365].

[292] S. Bosch, A. Buras, M. Gorbahn, S. Jager, M. Jamin, *et. al.*, *Standard model confronting new results for $\varepsilon'/\varepsilon$*, *Nucl.Phys.* **B565** (2000) 3–37, [hep-ph/9904408].

[293] A. J. Buras and M. Jamin, *$\epsilon'/\epsilon$ at the NLO: 10 years later*, *JHEP* **01** (2004) 048, [hep-ph/0306217].

[294] **NA48** Collaboration, J. R. Batley *et. al.*, *A precision measurement of direct CP violation in the decay of neutral kaons into two pions*, *Phys. Lett.* **B544** (2002) 97–112, [hep-ex/0208009].

[295] **KTeV** Collaboration, E. Abouzaid *et. al.*, *Search for Lepton Flavor Violating Decays of the Neutral Kaon*, *Phys. Rev. Lett.* **100** (2008) 131803, [arXiv:0711.3472].

[296] M. Blanke, A. J. Buras, S. Recksiegel, C. Tarantino, and S. Uhlig, *Correlations between $\epsilon'/\epsilon$ and rare K decays in the littlest Higgs model with T–parity*, *JHEP* **06** (2007) 082, [arXiv:0704.3329].

[297] A. J. Buras and L. Silvestrini, *Upper bounds on $K \to \pi\nu\bar{\nu}$ and $K_L \to \pi^0 e^+ e^-$ from $\varepsilon'/\varepsilon$ and $K_L \to \mu^+\mu^-$*, *Nucl. Phys.* **B546** (1999) 299–314, [hep-ph/9811471].

[298] A. J. Buras, G. Colangelo, G. Isidori, A. Romanino, and L. Silvestrini, *Connections between $\varepsilon'/\varepsilon$ and rare kaon decays in supersymmetry*, *Nucl. Phys.* **B566** (2000) 3–32, [hep-ph/9908371].

[299] M. Schmidtler and K. R. Schubert, *Experimental constraints on the phase in the Cabibbo-Kobayashi-Maskawa matrix*, *Z.Phys.* **C53** (1992) 347–354.

[300] A. Hocker, H. Lacker, S. Laplace, and F. Le Diberder, *A New approach to a global fit of the CKM matrix*, *Eur.Phys.J.* **C21** (2001) 225–259, [hep-ph/0104062]. 66 pages, added figures, corrected typos, no quantitative changes Report-no: LAL 01-06.

[301] F. Parodi, P. Roudeau, and A. Stocchi, *Constraints on the parameters of the V(CKM) matrix by end 1998*, *Nuovo Cim.* **A112** (1999) 833–854, [hep-ex/9903063].

[302] M. Ciuchini, E. Franco, L. Giusti, V. Lubicz, and G. Martinelli, *Combined analysis of the unitarity triangle and CP violation in the standard model*, *Nucl.Phys.* **B573** (2000) 201–222, [hep-ph/9910236].

[303] M. Ciuchini, G. D'Agostini, E. Franco, V. Lubicz, G. Martinelli, *et. al.*, *2000 CKM triangle analysis: A Critical review with updated experimental inputs and theoretical parameters*, *JHEP* **0107** (2001) 013, [hep-ph/0012308].

[304] G. D'Agostini, *Probability and measurement uncertainty in physics: A Bayesian primer*, hep-ph/9512295. Notes from lectures in Rome, 5/95 and DESY, 9/95.

[305] G. L. Trigg, *Mathematical Tools for Physicists*. Wiley-VCH, 2005.

[306] A. A. Markov, *Rasprostranenie zakona bol'shih chisel na velichiny, zavisyaschie drug ot druga*, *Izvestiya Fiziko-matematicheskogo obschestva pri Kazanskom universitete, 2-ya seriya* **15** (1906) 135–156.

[307] A. A. Markov, *Extension of the limit theorems of probability theory to a sum of variables connected in a chain*, *reprinted in Appendix B of: R. Howard. Dynamic Probabilistic Systems, volume 1: Markov Chains. John Wiley and Sons* (1971).

[308] L. R. Izquierdo, S. S. Izquierdo, J. M. Galán, and J. I. Santos, *Techniques to understand computer simulations: Markov chain analysis*, *Journal of Artificial Societies and Social Simulation* **12** (2009), no. 1 6.

[309] G. P. Lepage, *A New Algorithm for Adaptive Multidimensional Integration*, *J.Comput.Phys.* **27** (1978) 192. Revised version.

[310] G. P. Lepage, *VEGAS: AN ADAPTIVE MULTIDIMENSIONAL INTEGRATION PROGRAM*, .

[311] R. H. Landau, M. J. Pez, and C. C. Bordeianu, *Computational Physics: Problem Solving with Computers*. Wiley-VCH, 2007.

[312] W. H. Press, S. A. Teukolsky, W. T. Vetterling, and B. P. Flannery, *Numerical Recipes 3rd Edition: The Art of Scientific Computing*. Cambridge University Press, 2007.

[313] M. Gardner, *Knotted Doughnuts and Other Mathematical Entertainments*. W.H. Freeman & Company, 1986.

[314] **UTfit Collaboration** Collaboration, A. Bevan *et. al.*, *Update of the Unitarity Triangle Analysis*, *PoS* **ICHEP2010** (2010) 270, [arXiv:1010.5089]. updated results and plots available at: http://www.utfit.org/UTfit/.

[315] M. Battaglia, A. Buras, P. Gambino, A. Stocchi, D. Abbaneo, *et. al.*, *The CKM matrix and the unitarity triangle. Workshop, CERN, Geneva, Switzerland, 13-16 Feb 2002: Proceedings*, hep-ph/0304132. To Appear as CERN Yellow Report.

[316] G. D'Agostini, *Asymmetric Uncertainties: Sources, Treatment and Potential Dangers*, *ArXiv Physics e-prints* (Mar., 2004) [physics/0].

[317] **CDF and D0 Collaboration** Collaboration, A. Ivanov, *Searches for Fourth Generation Fermions*, arXiv:1109.1025. 14 pages, 6 figures, FPCP 2011 Conference Proceedings.

[318] C. J. Flacco, D. Whiteson, and M. Kelly, *Fourth generation quark mass limits in CKM-element space*, arXiv:1101.4976.

[319] M. E. Peskin and T. Takeuchi, *Estimation of oblique electroweak corrections*, *Phys.Rev.* **D46** (1992) 381–409.

[320] **D0** Collaboration, V. Abazov *et. al.*, *Precision measurement of the ratio* $\mathrm{B}(t \to Wb)/\mathrm{B}(t \to Wq)$ *and Extraction of* $V_{tb}$, *Phys.Rev.Lett.* **107** (2011) 121802, [arXiv:1106.5436].

[321] **D0 Collaboration** Collaboration, V. M. Abazov *et. al.*, *Combination of searches for anomalous top quark couplings with* 5.4fb$^{-}$1 *of ppbar collisions*, arXiv:1204.2332. 8 pages, submitted to Phys. Lett. B.

[322] **TWIST** Collaboration, R. Bayes *et. al.*, *Experimental Constraints on Left-Right Symmetric Models from Muon Decay*, *Phys. Rev. Lett.* **106** (2011) 041804.

[323] A. Arbuzov, M. Awramik, M. Czakon, A. Freitas, M. Grunewald, *et. al.*, *ZFITTER: A Semi-analytical program for fermion pair production in e+ e- annihilation, from version 6.21 to version 6.42*, *Comput.Phys.Commun.* **174** (2006) 728–758, [hep-ph/0507146]. Updates available on http://zfitter.desy.de/.

[324] D. Y. Bardin, M. S. Bilenky, A. Chizhov, O. Fedorenko, S. N. Ganguli, *et. al.*, *ZFITTER: An Analytical program for fermion pair production in e+ e- annihilation*, hep-ph/9412201.

[325] P. Christova, M. Jack, S. Riemann, and T. Riemann, *Predictions of ZFITTER v.6 for fermion pair production with acollinearity cut*, hep-ph/9908289. Based on talks presented at ECFA/DESY Linear Collider Project Meetings at Frascati, Nov 1998 and Oxford, Mar 1999 and at LEP-2 Miniworkshop at CERN, Mar 1999 and at Workshop for a Worldwide Study on Physics and Experiments with Future Linear e+ e- Colliders at Sitges/Barcelona, Apr 1999.

[326] D. Y. Bardin, P. Christova, M. Jack, L. Kalinovskaya, A. Olchevski, *et. al.*, *ZFITTER v.6.21: A Semianalytical program for fermion pair production in e+ e- annihilation*, *Comput.Phys.Commun.* **133** (2001) 229–395, [hep-ph/9908433].

[327] H. Flacher, M. Goebel, J. Haller, A. Hocker, K. Monig, *et. al.*, *Revisiting the Global Electroweak Fit of the Standard Model and Beyond with Gfitter*, *Eur.Phys.J.* **C60** (2009) 543–583, [arXiv:0811.0009].

[328] M. Baak *et. al.*, *Updated Status of the Global Electroweak Fit and Constraints on New Physics*, arXiv:1107.0975.

[329] J. Erler, *Global fits to electroweak data using GAPP*, hep-ph/0005084. 8 pages, Contribution to the Fermilab Workshop on Q̈CD and Weak Boson Physicsät the Tevatron Run II Report-no: UPR-885-T.

[330] J. Erler, $\alpha_s$ *with GAPP*, arXiv:1102.5520.

[331] **Particle Data Group** Collaboration, K. Nakamura *et. al.*, *Review of particle physics*, *J. Phys.* **G37** (2010) 075021. Updates available on http://pdg.lbl.gov/.

[332] M. Antonelli, V. Cirigliano, G. Isidori, F. Mescia, M. Moulson, *et. al.*, *An Evaluation of* $|V_{us}|$ *and precise tests of the Standard Model from world data on leptonic and semileptonic kaon decays*, *Eur.Phys.J.* **C69** (2010) 399–424, [arXiv:1005.2323].

[333] **Fermilab Lattice and MILC** Collaboration, J. A. Bailey *et. al.*, $B \to D^* l\nu$ *at zero recoil: an update*, *PoS* **LATTICE2010** (2010) 311, [arXiv:1011.2166].

[334] M. Okamoto, C. Aubin, C. Bernard, C. E. DeTar, M. Di Pierro, *et. al.*, *Semileptonic* $D \to \pi/K$ *and* $B \to \pi/D$ *decays in 2+1 flavor lattice QCD*, *Nucl.Phys.Proc.Suppl.* **140** (2005) 461–463, [hep-lat/0409116].

[335] M. Finkemeier, *Radiative corrections to* $\pi_{l2}$ *and* $K_{l2}$ *decays*, hep-ph/9501286.

[336] E. Witten, *Dynamical Breaking of Supersymmetry*, *Nucl.Phys.* **B188** (1981) 513.

[337] A. Grinbaum, *Which fine-tuning arguments are fine?*, *Found.Phys.* **42** (2012) 615–631, [arXiv:0903.4055]. 22 pages, 2 figures.

[338] J. Koperski, *Should we care about fine-tuning?*, *Brit.J.Phil.Sci.* **56** (2005) 303–319.

[339] R. Barbieri and G. Giudice, *Upper Bounds on Supersymmetric Particle Masses*, *Nucl.Phys.* **B306** (1988) 63.

[340] J. R. Ellis, K. Enqvist, D. V. Nanopoulos, and F. Zwirner, *Observables in Low-Energy Superstring Models*, *Mod.Phys.Lett.* **A1** (1986) 57.

[341] G. W. Anderson and D. J. Castano, *Measures of fine tuning*, *Phys.Lett.* **B347** (1995) 300–308, [hep-ph/9409419].

[342] G. W. Anderson and D. J. Castano, *Naturalness and superpartner masses or when to give up on weak scale supersymmetry*, *Phys.Rev.* **D52** (1995) 1693–1700, [hep-ph/9412322].

[343] G. W. Anderson, D. J. Castano, and A. Riotto, *Naturalness lowers the upper bound on the lightest Higgs boson mass in supersymmetry*, *Phys.Rev.* **D55** (1997) 2950–2954, [hep-ph/9609463].

[344] J. A. Casas, J. R. Espinosa, and I. Hidalgo, *Implications for new physics from fine-tuning arguments. II. Little Higgs models*, *JHEP* **0503** (2005) 038, [hep-ph/0502066].

[345] J. Casas, J. Espinosa, and I. Hidalgo, *The MSSM fine tuning problem: A Way out*, *JHEP* **0401** (2004) 008, [hep-ph/0310137].

[346] J. Casas, J. Espinosa, and I. Hidalgo, *A Relief to the supersymmetric fine tuning problem*, hep-ph/0402017.

[347] J. Casas, J. Espinosa, and I. Hidalgo, *Implications for new physics from fine-tuning arguments. 1. Application to SUSY and seesaw cases*, *JHEP* **0411** (2004) 057, [hep-ph/0410298].

[348] J. Casas, J. Espinosa, and I. Hidalgo, *Expectations for LHC from naturalness: modified versus SM Higgs sector*, *Nucl.Phys.* **B777** (2007) 226–252, [hep-ph/0607279]. 37 pages, LaTeX, 13 figures Report-no: IFT-UAM/CSIC-06/36.

[349] P. Ciafaloni and A. Strumia, *Naturalness upper bounds on gauge mediated soft terms*, *Nucl.Phys.* **B494** (1997) 41–53, [hep-ph/9611204].

[350] K. L. Chan, U. Chattopadhyay, and P. Nath, *Naturalness, weak scale supersymmetry and the prospect for the observation of supersymmetry at the Tevatron and at the CERN LHC*, *Phys.Rev.* **D58** (1998) 096004, [hep-ph/9710473].

[351] P. Athron and . Miller, D.J., *A New Measure of Fine Tuning*, *Phys.Rev.* **D76** (2007) 075010, [arXiv:0705.2241].

[352] G. t Hooft *In Proc. of 1979 Cargse Institute on Recent Developments in Gauge Theories* (1979).

[353] C. Promberger, *The Fourth Generation: A Comprehensive Analysis*, . Ph.D.Thesis (Advisor: A.J. Buras).

[354] D. M. Straub, *Overview of constraints on new physics in rare B decays*, arXiv:1205.6094.

[355] M. Blanke, *Insights from the Interplay of $K \to \pi\nu\bar{\nu}$ and $\varepsilon_K$ on the New Physics Flavour Structure*, *Acta Phys.Polon.* **B41** (2010) 127, [arXiv:0904.2528].

[356] M. Blanke, A. J. Buras, A. Poschenrieder, S. Recksiegel, C. Tarantino, *et. al.*, *Rare and CP-Violating K and B Decays in the Littlest Higgs Model with $T^-$ Parity*, *JHEP* **0701** (2007) 066, [hep-ph/0610298].

[357] M. Blanke, A. J. Buras, B. Duling, K. Gemmler, and S. Gori, *Rare K and B Decays in a Warped Extra Dimension with Custodial Protection*, *JHEP* **0903** (2009) 108, [arXiv:0812.3803].

[358] G. Barenboim, M. Gorbahn, U. Nierste, and M. Raidal, *Higgs sector of the minimal left-right symmetric model*, *Phys.Rev.* **D65** (2002) 095003, [hep-ph/0107121].

[359] K. Kiers, M. Assis, and A. A. Petrov, *Higgs sector of the left-right model with explicit CP violation*, *Phys.Rev.* **D71** (2005) 115015, [hep-ph/0503115].

[360] R. N. Mohapatra, G. Senjanovic, and M. D. Tran, *STRANGENESS CHANGING PROCESSES AND THE LIMIT ON THE RIGHT-HANDED GAUGE BOSON MASS*, *Phys.Rev.* **D28** (1983) 546.

[361] A. Buras, W. Slominski, and H. Steger, *B Meson Decay, CP Violation, Mixing Angles and the Top Quark Mass*, *Nucl.Phys.* **B238** (1984) 529.

[362] **Fermilab Lattice and MILC Collaborations** Collaboration, A. Bazavov *et. al.*, *B- and D-meson decay constants from three-flavor lattice QCD*, arXiv:1112.3051. 63 pages, 13 figures.

[363] H. Na, C. J. Monahan, C. T. Davies, R. Horgan, G. P. Lepage, *et. al.*, *The B and $B_s$ Meson Decay Constants from Lattice QCD*, arXiv:1202.4914.

[364] C. McNeile, C. Davies, E. Follana, K. Hornbostel, and G. Lepage, *High-Precision $f_{B_s}$ and HQET from Relativistic Lattice QCD*, *Phys.Rev.* **D85** (2012) 031503, [arXiv:1110.4510]. 5 pages, 3 figures.

[365] C. Albertus, Y. Aoki, P. Boyle, N. Christ, T. Dumitrescu, *et. al.*, *Neutral B-meson mixing from unquenched lattice QCD with domain-wall light quarks and static b-quarks*, *Phys.Rev.* **D82** (2010) 014505, [arXiv:1001.2023].

[366] R. Evans, A. El-Khadra, and E. Gamiz, *A determination of the $B_s$ and $B_d$ mixing matrix elements in 2+1 lattice QCD*, *PoS* **LATTICE2008** (2008) 052.

[367] J. Laiho, E. Lunghi, and R. Van de Water, *Flavor Physics in the LHC era: The Role of the lattice*, arXiv:1204.0791. Lattice 2011 proceedings. 18 pages, 6 figures. References added. Error corrected in lattice-QCD results for the B-mixing matrix elements and numerical results for the UT fit changed from V1. Discussion modified slightly, but qualitative results regarding the tension in the UT fit unchanged.

[368] S. Durr, Z. Fodor, C. Hoelbling, S. Katz, S. Krieg, *et. al.*, *Lattice QCD at the physical point: light quark masses*, *Phys.Lett.* **B701** (2011) 265–268, [arXiv:1011.2403].

[369] C. McNeile, C. Davies, E. Follana, K. Hornbostel, and G. Lepage, *High-Precision c and b Masses, and QCD Coupling from Current-Current Correlators in Lattice and Continuum QCD*, *Phys.Rev.* **D82** (2010) 034512, [arXiv:1004.4285]. 16 pages, 10 figures, 3 tables.

[370] **The MILC Collaboration** Collaboration, A. Bazavov *et. al.*, *Results from the MILC collaboration's SU(3) chiral perturbation theory analysis*, *PoS* **LAT2009** (2009) 079, [arXiv:0910.3618].

[371] T. Blum, R. Zhou, T. Doi, M. Hayakawa, T. Izubuchi, *et. al.*, *Electromagnetic mass splittings of the low lying hadrons and quark masses from 2+1 flavor lattice QCD+QED*, *Phys.Rev.* **D82** (2010) 094508, [arXiv:1006.1311].

[372] C. Davies, C. McNeile, K. Wong, E. Follana, R. Horgan, *et. al.*, *Precise Charm to Strange Mass Ratio and Light Quark Masses from Full Lattice QCD*, *Phys.Rev.Lett.* **104** (2010) 132003, [arXiv:0910.3102].

[373] **RBC Collaboration, UKQCD Collaboration** Collaboration, Y. Aoki *et. al.*, *Continuum Limit Physics from 2+1 Flavor Domain Wall QCD*, *Phys.Rev.* **D83** (2011) 074508, [arXiv:1011.0892].

[374] E. Dalgic, A. Gray, M. Wingate, C. T. Davies, G. P. Lepage, *et. al.*, *B meson semileptonic form-factors from unquenched lattice QCD*, *Phys.Rev.* **D73** (2006) 074502, [hep-lat/0601021].

## Danksagung

An dieser Stelle möchte ich die Gelegenheit ergreifen um all jenen zu danken, die mir bei meiner Arbeit zur Seite gestanden haben.

- Allen voran danke ich natürlich meinem Doktorvater Prof. Andrzej Buras für seine Unterstützung und seine endlose, mitreißende Begeisterung für die Forschung. Darüber hinaus bin ich sehr dankbar für die versprochene Übergangszeit nach meiner Verteidigung.
- Ich danke dem ganzen 4G-Team: Andrzej Buras, Björn Duling, Thorsten Feldman, Christoph Promberger und Stefan Recksiegel für die produktive Zusammenarbeit deren Ergebnisse einen wichtigen Teil meiner Dissertation ausmachen.
- Ich danke dem LRM Team: Monika Blanke, Andrzej Buras und Katrin Gemmler für die Zusammenarbeit und die Möglichkeit meine Visionen in der Analyse umsetzen zu dürfen.
- Darüber hinaus danke ich Katrin Gemmler für viele interessante Diskussionen und meinem langjährigen Zimmerkollegen Christoph Promberger für die schöne, gemeinsame Zeit.
- Katrin Gemmler und Cristoforo Simonetto danke ich für das aufmerksame Lesen meiner Arbeit und für die vielen Kommentare zur Verbesserung.
- Last but not least danke ich meiner Frau Alexandra für all ihre Unterstützung und ihre Geduld.

Ich bedanke mich außerdem für die finanzielle Unterstützung durch das Graduiertenkolleg GRK 1054.